Devolatilization During the Formation of Rocky Planets: Bulk Elemental Composition

Haiyang Wang

A thesis submitted for the degree of
Doctor of Philosophy
of The Australian National University

Research School of Astronomy and Astrophysics
College of Science
The Australian National University
Canberra ACT 2611, Australia

November 2018

"Devolatilization During the Formation of Rocky Planets: Bulk Elemental Composition"

THESIS SUPERVISORS: Charles H. Lineweaver and Trevor R. Ireland
INSTITUTION: The Australian National University, Canberra, Australia

Dedicated to my parents
献给我的父母亲

"Home is a name, a word, it is a strong one;
stronger than magician ever spoke,
or spirit ever answered to, in the strongest conjuration."
— Charles Dickens

Declaration

This thesis is an account of my research undertaken between February 2014 and March 2018 at the Research School of Astronomy and Astrophysics, College of Science, the Australian National University. The material presented in this thesis is original, and has not been submitted in whole or part for a degree in any university.

This thesis is based on four papers that I published or submitted during my PhD research. I have made significant contributions to each paper. Below I describe my contributions to the research in each chapter and associated paper.

1. Chapter 1 is completely written by me. Section 1.2 is adapted from the publication Wang and Lineweaver [2016] where all the research is my work. It was written by me with comments from my coauthor.

2. Chapter 2 is adapted from Wang et al. [2018a] originally published in Icarus 299, 460-474. I conducted all the analysis and wrote the full paper collaboratively with my coauthors.

3. Chapter 3 is under review/Icarus as Wang et al. [2018b]. I conducted all the analysis and wrote the full paper collaboratively with my coauthors.

4. Chapter 4 is adapted from Wang et al. [2019] originally published in MNRAS 482, 2222-2233. I conducted all the analysis, wrote the full paper and finalized it with comments from my coauthors.

5. Chapter 5 is summarized by me from the previous chapters. The first part of the 'Future Work' is summarized from a manuscript in preparation by me, Charles H. Lineweaver, Trevor R. Ireland, and others. The future directions are independently written by me.

Haiyang Wang
30 November 2018

Acknowledgments

This thesis is being wrapped up ten years since I completed the dissertation for my first degree. Following the conferral of my second degree six years ago, I was determined to transition from being an exploration geophysicist to being an astronomer specializing in extrasolar planets and extraterrestrial habitability. Before I acknowledge the people who supported me on this new journey, I would like to thank my old friends and colleagues, who offered their help, support, and encouragement, enabling me to begin this adventure. There are too many of you to mention by name, but I thank you all from the bottom of my heart. I would also like to thank the Australian Government Department of Education and Training for awarding me the Prime Minister's Australia Asia Endeavour Scholarship, without which I would have never embarked on this journey.

For my PhD research, I would like to first express my gratitude to my primary supervisor, Charley Lineweaver, for his patient guidance, critical comments, and sharp insights. Your enthusiasm for science, breadth of knowledge, and articulation of thoughts is inspiring. The opportunity to work with you is sincerely appreciated, and the experience has been rewarding for me.

I would also like to thank Trevor Ireland, for his time and the insights he brought into all our discussions. His advice on both my PhD and career development is particularly appreciated. Thank you David Yong for your unwavering support during the late stages of my PhD as well as always being available to answer my many (often naive) questions. Mark Krumholz (my panel chair) and Gary Da Costa (school graduate convener) were invaluable in helping me sort out several administrative roadblocks that I encountered during my PhD. Thanks to Marc Norman for his continued support, encouragement, and interest in my work.

I have also benefited from discussions with other researchers such as Martin Asplund, Brent Groves, Mike Ireland, and Joao Bento from the Research School of Astronomy and Astrophysics (RSAA) as well as Yuri Amelin, Hrvoje Tkalăcić, Penelope King, and Hugh O'Neil from the Research School of Earth Sciences. I would like to acknowledge the travel support from both ANU and RSAA, which enabled me to travel to conferences and research institutes where I met and talked to many distinguished scholars including William F. McDonough, Ramon Brasser, Steve Mojzsis, Stephen Kane, Brad Carter, and Jane MacAuthor. The discussions with them have broadened my vision, enhanced my research, and inspired me to advance.

I feel very fortunate to be surrounded by a range of amazing peers throughout my graduate study at Mount Stromlo. I would like to firstly thank Aditya Chopra, my mentor and friend, for his advice whenever I felt stressed or disoriented. I would also like to specially thank Suryashree Aniyan and Thomas Nordlander, for their

kind advice during my thesis writing stage of my PhD and for dragging me out of my office to socialize, to maintain my sanity. Fan Liu, Jane Lin, Anshu Gupta, Ayan Acharyya, Soniya Sharma, Adam Rains, and many others, thank you all for having stood by me through my ups and downs at Mount Stromlo.

I am perpetually indebted to my parents, for their patience, support, and belief in me throughout my life. And to my sisters and brother, thank you for having spent more time with our parents during my absence.

Finally, thank you Yang for being my dearest partner and for the years of companionship and love.

Abstract

As the solar nebula condensed, evaporated and fractionated to form the nascent Earth, the bulk elemental composition of the Earth was established. To first order, the Earth is a devolatilized sample of the solar nebula. Similarly, rocky exoplanets are also likely devolatilized samples of the stellar nebulae out of which they and their host stars formed. If this assumption holds, we can estimate the chemical composition of rocky exoplanets by applying a devolatilization algorithm based on the elemental abundances of their host stars. This thesis is an investigation of this potentially universal devolatilization pattern, from which exoplanetary chemistry and habitability are then derived.

To quantify (in broad terms) the chemical relationships between the Earth, the Sun and other bodies in the Solar System, the elemental abundances of the bulk Earth are required. The key to comparing Earth's composition with those of other objects is to have a determination of the bulk composition with an appropriate estimate of uncertainties. We present concordance estimates (with uncertainties) of the elemental abundances of the bulk Earth, by compiling, combining, and renormalizing a large set of heterogeneous literature values of the primitive mantle and of the core. The weighting factor for the concordance estimates comes from our new estimate of the core mass fraction of the Earth: 32.5±0.3 wt% (weight percent). The uncertainties on our elemental abundances usefully calibrate the unresolved discrepancies between standard Earth models made under various geochemical and geophysical assumptions.

We then extend our assessment of terrestrial abundances to the modeling of protosolar abundances based on the latest estimates of solar photospheric abundances and primitive meteoritic abundances. We compare our new protosolar abundances with our estimates of bulk Earth composition, thereby quantifying the devolatilization of the solar nebula that led to the formation of the Earth. As a function of elemental 50% condensation temperatures (T_C), we fit the Earth-to-Sun abundance ratios f to the linear trend $\log(f) = \alpha \log(T_C) + \beta$. The best fit coefficients are: $\alpha = 3.676 \pm 0.142$ and $\beta = -11.556 \pm 0.436$. The quantification of the slope α provides an empirical observation upon which modeling of the devolatilization processes can be based. These coefficients determine a critical devolatilization temperature for the Earth $T_{\mathrm{D}}(\mathrm{E}) = 1391 \pm 15$ K. The resultant devolatilization pattern allows inferences to be made concerning the depletions of elements in the early solar system and is potentially useful for estimating the chemical composition of rocky exoplanets from their known host stellar abundances.

We apply the devolatilization pattern to nearby planetary systems to infer the bulk elemental composition of rocky exoplanets – particularly those within the circumstellar habitable zones – from the known host stellar elemental abundances. The

estimated bulk planetary composition (rather than the host stellar abundances) is then used as a principal constraint to model the interior composition and structure of such exoplanets. We apply these constraints to four planet host stars: Kepler-10, Kepler-20, Kepler-21 and Kepler-100, to model the interiors including the mantle and core compositions as well as core mass fraction for potential terrestrial exoplanets orbiting these host stars. With respect to the estimates of the interiors, we conclude that a potential terrestrial exoplanet orbiting Kepler-21 would be the most Earth-like while one orbiting Kepler-10 would be the least.

Contents

List of Figures

List of Tables

Chapter 1

Introduction

Life is only known to exist on a single planet, the Earth. For life-forms like us, the most important feature of Earth is the fact that it is habitable – i.e. suitable for life over geological time-scales. Understanding habitability and using that knowledge to search for the nearest habitable planets may be crucial for our survival as a species in the far future [Lineweaver and Chopra, 2012; Sagan, 1994]. Aside from other rocky bodies in the solar system, exoplanet detection missions have discovered and confirmed over 3700 planets[1], which likely represent a small sample of many billions of planets yet-to-be found in our Galaxy. The discussion regarding what fraction of such planets could be Earth-like and even habitable to life as we know it is intensive [e.g. Kasting et al., 2014; Bovaird et al., 2015; Kane et al., 2016; Chopra and Lineweaver, 2016; Kaltenegger, 2017]. The near-future telescopes (e.g. JWST, WFIRST, LUVOIR, GMT and ELT) will herald a new era of space-based and ground-based observations capable of characterizing close-by habitable worlds like our own.

The principal planetary characteristics that govern the potential of a planet to host a biosphere are aspects such as mass, radius, and orbital parameters ("physical characteristics") and the composition of the atmosphere, surface, and interior ("chemical characteristics") [Meadows et al., 2009; Hinkel and Unterborn, 2018]. The physical characteristics of a planet, in addition to the planet's incident flux from its parent star, can determine whether it is located in the (circumstellar) habitable zone, which is usually defined as the region around a star where a planet can support liquid water on its surface given sufficient atmospheric pressure [e.g. Huang, 1959; Hart, 1979; Kasting et al., 1993; Lineweaver and Chopra, 2012; Kopparapu et al., 2013; Kane et al., 2016]. A more definitive determination of whether a planet can support liquid water and potentially harbor life on its surface requires the characterization of the planetary atmosphere [Meadows et al., 2009; Kasting et al., 2014] and, if possible, of the surface and interior.

Unlike the spectra of stars, the sensitivity of spectroscopic techniques to the spectra of extrasolar planets is inadequate because of the much fainter luminosity of rocky planets compared with their host stars. Some successful attempts to derive the possible exoplanetary compositions from externally polluted white dwarfs have

[1] NASA Exoplanet Archive, https://exoplanetarchive.ipac.caltech.edu, accessed March 15, 2018.

been reported in recent years [e.g. Klein et al., 2011; Zuckerman et al., 2011; Xu et al., 2014], but the observable types of exoplanets and the derivable number of elements are still limited.

Promising methods have been developed to directly measure the atmospheric composition of extrasolar planets by means of transmission spectroscopy [e.g. Charbonneau et al., 2002; Swain et al., 2009; Kaltenegger, 2017]. This method is available for those extrasolar planets that eclipse their host star, so that the planetary atmosphere filters the starlight and the atmosphere's composition can thereby be measured. However, an extrasolar planet's atmospheric composition is not the same as its overall, *bulk*, composition. The *bulk* composition of extrasolar planets can be estimated, for example, by combining planetary dynamical and chemical simulations [Bond et al., 2010a,b; Carter-Bond et al., 2012], or by assuming that compositional differences relative to exoplanet host stars are similar to those found between the Sun and other solar system bodies [Lineweaver and Robles, 2009].

The chemical composition of the Earth is in some respects remarkably similar to that of the Sun. This is especially true for the rock-forming elements, which are expected to have solidified early on during the formation of the planetary system. Volatile material (e.g. hydrogen, carbon, and oxygen) on the other hand is clearly deficient in Earth's composition, and the mechanism that caused the volatile elements to become deficient is called "devolatilization". Understanding the physical processes accounting for the volatile depletion is a hot topic that has been debated for many decades. This debate initially focused on the origin and formation of chondrites starting from late 1950s through 1960s [e.g. Urey, 1957, 1961, 1964, 1967; Wood, 1958, 1961, 1962, 1963, 1967; Ringwood, 1959, 1961, 1953, 1965, 1966; Mason, 1960a,b, 1963; Fish et al., 1960; Fish and Goles, 1962; Anders, 1960, 1963, 1964]. By now, a variety of models/hypotheses – often distinct and sometimes conflicting - have been proposed to explain the mechanisms of volatile depletion observed in various meteorites and in planetary bodies. Which of these will prevail will depend heavily on our understandings of thermal histories in the early solar system (see 1.1.1 for further discussion).

A related question is, to what extent can these sampled solar system bodies be representative for the whole solar system and can the devolatilization processes in the Solar System be a template for those that occurred during the formation of other planetary systems. No one can answer this question precisely, due to our limited knowledge of a complete picture of the formation of the Solar System, let alone that of other planetary systems. However, using the samples that we have the most comprehensive and accurate information of, investigating potential relationships/patterns between these samples should be a crucial step in understanding our planetary system and, by extension, in constraining the characterization of our neighborhood systems.

The main goal of this thesis is to analyze the compositional differences between the Earth, Sun and other solar system bodies and from this comparison quantify the devolatilization of material in the solar nebula that formed the rocky planets. The resultant devolatilization pattern can act as a thermometer revealing conditions in the

early solar system and is potentially useful for estimating the chemical composition of rocky exoplanets from the spectroscopic measurements of their host stars.

This chapter provides a background overview of the topics discussed in the thesis.

Section 1.1 reviews the studies of the devolatilization from the solar nebula to the Earth, including the compositional estimates of the proto-Sun and bulk Earth.

Section 1.2 sets the context for the formation of the terrestrial planets, particularly from the perspective of chemical inheritance from the interstellar medium.

Section 1.3 discusses the prevalent studies of exoplanetary chemistry and interiors: a growing pathway to characterize exoplanets and habitability

1.1 From the Solar Nebula to the Planet Earth: Devolatilization Matters

1.1.1 A snapshot of volatile fractionation in the early solar system

Astrophysical modeling of the relatively high temperatures in the inner solar nebula (compared to the outer) [e.g. Dullemond et al., 2002; D'Alessio et al., 2006; Dullemond and Monnier, 2010; Salmeron and Ireland, 2012a], combined with observations that volatile fractionations in chondrites – the most common and primitive type of meteorites – are mostly related to volatility in some way [e.g. O'D. Alexander, 2001; Bland et al., 2005; Davis, 2006; Braukmüller et al., 2018], lead to the picture of a vaporized early inner solar system.

Over the past 70 years, numerous models have been proposed to explain volatile fractionation in planetary materials. Anders [1964] reviewed the debate that started in the 1950s regarding the formation of chondrites. He advocated the Wood model [Wood, 1958, 1961, 1962, 1963] that was further developed by him to a two-component model. In this model, all chondrites accreted (i) a fine-grained, volatile-rich material called "matrix" and (ii) a coarse-grained, refractory fraction that formed at high temperature called "chondrules". Melting and evaporative losses of volatiles during chondrule formation account for the observed carbonaceous chondrite fractionation [see Larimer and Anders, 1967; Alexander, 2005]. Localized heat sources – e.g. shock waves and massive lightning discharges [Connolly and Love, 1998; Desch and Cuzzi, 2000] – are thought to account for the evaporation [O'D. Alexander, 2001; Alexander, 2005].

However, this two-component model has been criticized by Palme and Boynton [1993] and Cassen [1996], based on the following arguments against it: (i) chondrules are, on average, too volatile rich, e.g. for Na and K [Rubin and Wasson, 1987; Spettel et al., 1989], and matrix is not sufficiently enriched in volatile elements as expected from this model; (ii) the fractionation patterns cannot be reproduced in experiments in which meteoritic material is evaporated [Bart et al., 1980; Wulf et al., 1995]; (iii) evaporative fractionation would have produced a mass-dependent isotopic fractionation, whereas, such a feature is absent in chondrites – e.g. for Si [Clayton et al., 1988] and K [Humayun and Clayton, 1995]. The third argument has been challenged by recent findings that evaporation could produce composition diversity of chondrules while it is not accompanied by mass-dependent isotopic fractionation, if it took place in a dense ambient gas [Alexander et al., 2000; Ozawa and Nagahara, 2001; Cuzzi and Alexander, 2006; Nagahara et al., 2008].

Incomplete condensation from a hot solar nebula as the cause of volatile depletion was first proposed by Wasson and Chou [1974] to explain the decreasing volatile elemental abundances with decreasing condensation temperature[2] [see also Grossman and Larimer, 1974; Wai and Wasson, 1977; Wasson, 1985]. The key to properly understanding the "incomplete" condensation is the dissipation of the solar gas during

[2]The term "condensation temperature" or "50% condensation temperature" refers to the temperature at which 50% of an element is found in solid form under a certain nebular pressure.

the progressive condensation of the gas phase containing the volatile elements (refractory elements would have been completely condensed out). The incomplete condensation model has been a popular mechanism for explaining moderately volatile element abundances observed in primitive meteorites since the 1990s [Cassen, 1996; Palme and O'Neill, 2003; Davis, 2006]. Regardless of the mechanism, elemental condensation temperatures have been widely used in meteoritics and terrestrial planetary science [e.g. Kargel and Lewis, 1993; McDonough and Sun, 1995; Palme et al., 2014; Carlson et al., 2014] and even in stellar astrophysics [e.g. Meléndez et al., 2009; Ramírez et al., 2009; Liu et al., 2016]. The calculation of condensation temperatures is of broad interest to planetary science and astrophysics and has been regularly updated over the decades [e.g. Grossman and Larimer, 1974; Ebel and Grossman, 2000; Lodders, 2003; Unterborn et al., 2016].

In spite of the popularity of the incomplete condensation model, fractionation during chondrule formation has been revived regularly or at least has not been able to be ruled out [O'D. Alexander, 2001; Bland et al., 2005; Braukmüller et al., 2018]. Huss et al. [2003] and Huss [2004] even argued that condensation from a hot solar nebula cannot be the primary mechanism for volatile element depletion, as a completely vaporized nebula would have destroyed presolar grains (see details in Section 1.2), which however are commonly found in chondrite matrices. It is noteworthy that in the scenario of incomplete condensation, volatile depletion occurred preceding chondrule formation [Bland et al., 2005]. Possibly, the incomplete condensation may be superimposed by volatile fractionation during chondrule formation, thus accounting together for the volatile depletion in the inner protoplanetary disk.

Other models proposed to explain volatile fractionation in planetary materials include the X-wind model [Shu et al., 1996, 2001], the disk-wind model [Blandford and Payne, 1982; Coffey et al., 2004; Salmeron and Ireland, 2012a,b] and the inheritance model [e.g. Yin, 2005; Wang and Lineweaver, 2016]. The X-wind model suggests that CAIs (calcium-aluminum-rich inclusions found predominately in particular types of carbonaceous chondrites – e.g. CV3 chondrites and CM2 chondrites) and chondrules formed very close to the proto-Sun ($\sim$ 0.06 AU), before being carried out by bipolar jets to fall onto a "cold" disk. As opposed to X-winds, disk winds extend to radial distances of around a few astronomical units from the central proto-Sun [Coffey et al., 2004; Salmeron and Ireland, 2012b]. In this scenario, material may be processed in a magnetically accelerated disk wind, even at distances out to the position of the proto-asteroid belt. It can explain the basic properties of chondrules and chondrites - e.g. chondrule material generally dominates the constituents of chondrites (except CI) and a relatively low initial ambient temperature (of order 400 K or less) [Krot et al., 2009; Salmeron and Ireland, 2012b]. By comparing the volatile depletion in chondritic meteorites and the refractory depletion in the interstellar medium gas phase, Yin [2005] observed the similarities of these depletions and proposed that volatile depletion in chondritic meteorites is inherited from the interstellar medium, instead of any nebula process. Wang and Lineweaver [2016] revisited this inheritance model by extending it to the volatile depletion in terrestrial planets.

Primitive meteorites are thought to be the building blocks of the solar system,

out of which the planets formed [Wood, 1962; Salmeron and Ireland, 2012b]. Mechanisms accounting for volatile depletion in undifferentiated meteorites (i.e. chondrites) should have also contributed to the volatile depletion in Earth and other differentiated terrestrial bodies. However, terrestrial planets may have also experienced volatile loss through high-energy processes during planetary accretion and subsequent planetary evolution - e.g. melting and evaporative loss during impacts [e.g. Poitrasson et al., 2004; O'Neill and Palme, 2008; Pringle et al., 2014, 2017; Hin et al., 2017; Norris and Wood, 2017; Dhaliwal et al., 2018]. Then the question is: to what extent has the volatile loss during the accretion and evolution of terrestrial planets modified the volatile depletion (due to nebular and/or pre-nebular effects) on precursor materials that were later accreted to form these planets? An approach to find the answer is to compare the *bulk* elemental composition of these terrestrial planets to the proto-nebular (or proto-Sun) composition. It is noteworthy that volatile depletion/fractionation discussed here should not be confused with the elemental fractionation/differentiation within a planet body. The "bulk" used here is particularly important, since terrestrial planets are structurally differentiated bodies, while elements are not evenly distributed in different compositional layers (e.g. crust, mantle, and core) of a terrestrial planet.

Opposite to devolatilization (or volatile depletion/fractionation), "volatile addition" through processes such as the late veneer and/or late accretion is thought to account for much of the Earth's volatile budget [Albarède, 2009; Wang and Becker, 2013]. In this scenario, Earth is thought to form "dry" and only became "wet" at the late stage of its accretion. Or it may have formed "wet" with volatiles, which were subsequently depleted immediately following the Moon-forming impact, and regained volatiles later through accretion of wet material during the final stage of accretion. Numerous studies, based on both dynamic modeling [Walsh et al., 2012; Morbidelli and Wood, 2015] and geochemical and isotopic analysis[Drake and Righter, 2002; Dauphas et al., 2004; Alexander et al., 2012; Marty, 2012; Saal et al., 2013; Dauphas, 2017; Fischer-Gödde and Kleine, 2017; Brasser et al., 2018], have argued against the possibility that a dominant fraction of Earth's volatiles could have been delivered by the late veneer or late accretion. However, a detailed investigation of "volatile addition" is beyond the scope of this thesis, while it is noted as a caveat in relevant chapters.

This brief review of volatile fractionation in the early solar system is to introduce various concepts as well as to set the context for the following discussion and subsequent, quantitative analysis of devolatilization. Therefore, this review should not be seen as a complete one covering all models/mechanisms/hypotheses related to devolatilization (or volatile depletion/fractionation). It is also worth noting that the language used in this thesis to describe the quantitative feature of volatile depletion often involves the terminology related to the incomplete condensation model, but I use this language out of convenience more than out of a conviction that this model is the correct one (and others are not). Moreover, a variety of physical processes – including both stochastic and non-stochastic ones – might have accounted for the overall devolatilization in going from the solar nebula to the formation of rocky plan-

ets like the Earth, but their average effect is often "non-random" and a pattern can usually be identified in it – as discussed thereafter.

1.1.2 Volatility trends

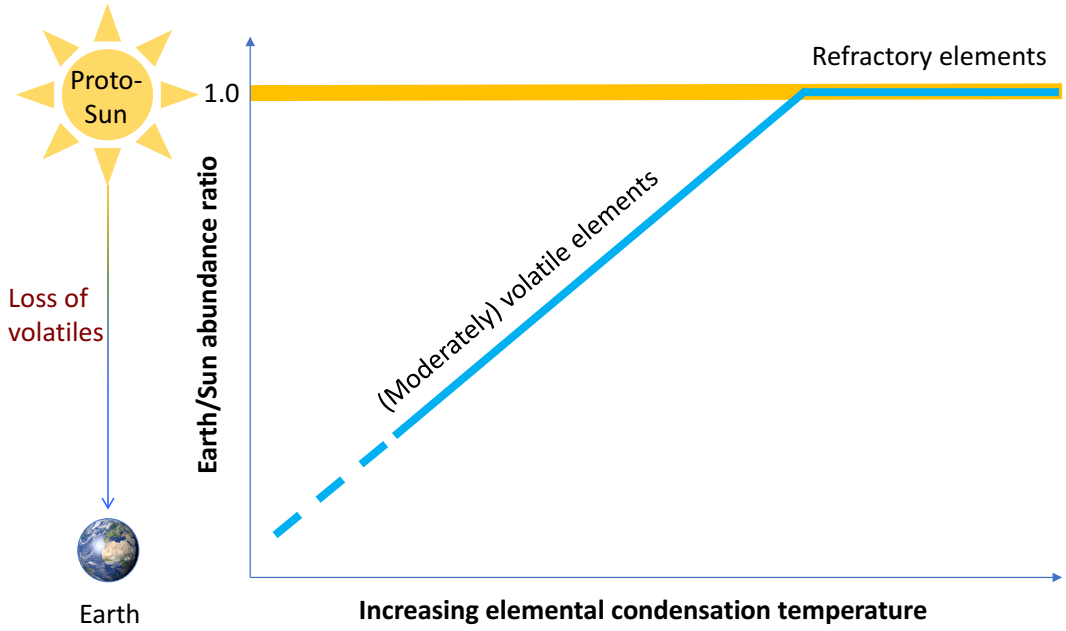

Figure 1.1: Schematic illustration of the devolatilization of the solar nebula that formed the Earth: while refractory elements above a certain threshold condensation temperature could form rocky material, volatile material was lost, with increasing depletion corresponding to lower condensation temperature.

A characteristic feature of the comparison between solar and terrestrial abundances, is the depletion of terrestrial abundances for elements with moderately low condensation temperatures. This depletion is systematic: the lower the condensation temperature, the greater the depletion, as illustrated schematically in Figure 1.1. This depletion provides quantitative insights into the processes active in the early solar system and the fractionation of elements between gas and solid phases.

This feature of volatile depletion has been previously investigated and is called the "volatility trend" of the Earth in the literature [Kargel and Lewis, 1993; McDonough, 2003, 2014; Palme and O'Neill, 2003, 2014; Carlson et al., 2014]. An example is shown in Figure 1.2, which compares the elemental compositions between the bulk silicate Earth (i.e. the bulk Earth excluding the core) and CI chondrites, as a function of the elemental 50% condensation temperature, T_C.

Previous studies on volatility trends set important constraints on the elemental abundances of the Earth's core. However, they do not give a complete picture of the devolatilization processes that led to the formation of the planet Earth from the

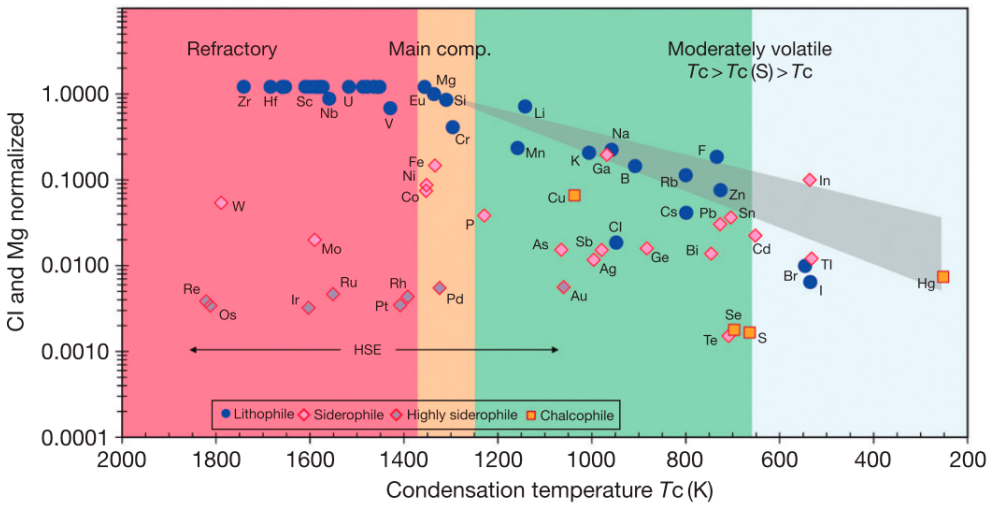

Figure 1.2: The volatility trend, illustrated by the wedge in gray, is shown as a comparison of the elemental abundances of the bulk silicate Earth (i.e. the outer part of the Earth, essentially made by silicates) to CI chondritic abundances (normalized to 1) as a function of the 50% condensation temperature [Lodders, 2003]. The figure is from Palme and O'Neill [2014]. The normalization-reference element is Mg. The legend indicates the classification of elements according to their geochemical character: lithophile (elements) preferring to be in the silicate shell/mantle rocks, siderophile tending to be in the metal phase (i.e. core), chalcophile partitioning into sulfides. Above the legend, 'HSE' is the abbreviation of 'highly siderophile elements'. 'Main comp.' near the upper x-axis denotes 'Main components', which are elements abundant in the Earth.

solar nebula, i.e., how the bulk Earth connects to the proto-Sun. First, instead of the bulk Earth, only the silicate part of the Earth (called 'bulk silicate Earth') is used, and thus the resultant trend is not appropriate to study the volatilization features of the Earth as a whole relative to the solar nebula. Second, CI chondritic abundances are used to represent the solar nebular or protosolar abundances, whereas CI chondrites are depleted in highly volatile elements (e.g., noble gases as well as H, C, N, and O) that are indispensable for fully understanding the devolatilization process that led to the formation of rocky material of our solar system. Third, Mg or Si is typically used as the reference element for normalizing the Earth to CI chondrites. However, both elements are not strictly refractory and in fact are slightly depleted in the Earth relative to CI chondrites, thus leading to the commonly misleading concept of refractory lithophile enrichment (RLE) as discussed in Lineweaver and Robles [2009]. Last but not least, these normalized abundance ratios are given without uncertainty estimates. Uncertainties are required so that we can evaluate if models fit data. Without uncertainties, such a volatility trend is essentially drawn intuitively to indicate the upper envelope of the depleted elements (relative to CI chondrites), while we do not know if residuals between models and data are due to the shortcomings in the

models, or in the data.

In order to establish a chemical relationship between the proto-Sun and the bulk Earth to the highest precision possible, we need the best elemental abundance data (with uncertainties) to compare and quantify the differences between the two bodies.

1.1.3 Elemental abundances of the proto-Sun and the bulk Earth

For decades the combination of solar photospheric abundances and CI chondritic abundances have yielded what are thought to be the best proxy for the protosolar or solar system elemental abundances [e.g. Anders and Grevesse, 1989; Grevesse and Sauval, 1998; Lodders, 2003; Lodders et al., 2009]. As an example, Figure 1.3 shows the widely used compilation of protosolar abundance estimates of Lodders et al. [2009]. However, some information in their compilations needs to be readdressed and updated. First, CI chondritic abundances have been updated since 2009, e.g., by Barrat et al. [2012], Pourmand et al. [2012], and Palme et al. [2014]. Second, the solar photospheric abundances that they compiled are outdated and based on a heterogeneous sample using different solar model atmospheres and radiative transfer calculations. In particular, their compilation does not use recent results based on 3D hydrodynamic solar models with radiative transfer calculations taking into account non-LTE (local thermodynamic equilibrium). Third, their approach of applying diffusion corrections to the combined solar abundances from both meteoritic and photospheric data is questionable, since atomic diffusion and gravitational settling affect photospheric abundances, but not meteoritic abundances. Motivated by these issues, we redetermine the protosolar abundances from the recently updated meteoritic and photospheric data with an improved approach of combining the two data sets. This work is presented in Chapter 3.

For Earth, the estimates for its elemental abundances are not straightforward and are in large part model-dependent. A major challenge to estimating the bulk chemical composition of the Earth is that we can only sample the upper part of the possibly heterogeneous mantle, and we have no direct access to its deep interior, and even less to the core [Allègre et al., 2001]. But over the decades much progress has been made in making more plausible models of both the primitive mantle and the core, though usually separately. "Primitive mantle" or "bulk silicate Earth" are synonymous referring to the mantle after core segregation but before the extraction of continental crust. Thus, it is a reservoir equivalent to the combination of the present-day mantle and crust of the Earth. Studies of primitive mantle elemental abundances have been made based on a variety of models, e.g., Kargel and Lewis [1993], McDonough and Sun [1995], Lyubetskaya and Korenaga [2007], O'Neill and Palme [2008], and Palme and O'Neill [2014]. Studies of the elemental abundances of bulk Earth include Allègre et al. [2001], McDonough [2003], and McDonough and Arevalo [2008].

Over the past decade, our knowledge of Earth's core (and therefore of the bulk Earth) has increased: high pressure experiments yield improved estimates of partition coefficients of siderophile (iron-loving) elements [Siebert et al., 2013] and affini-

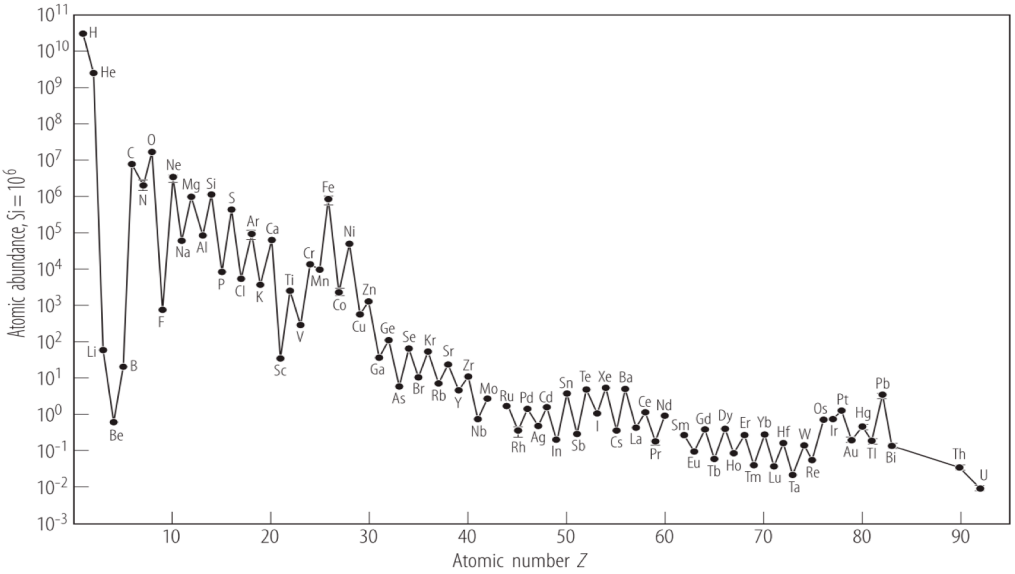

Figure 1.3: Lodders et al. [2009]'s Solar System abundances (normalized to 10^6 Si atoms), which are a combination of the elemental abundances of CI chondrites and the solar photosphere.

ties of light elements for iron [Ricolleau et al., 2011; Mookherjee et al., 2011]. Seismic velocities through the core provide increasingly precise constraints on densities and on mineral physics models [Vočadlo, 2007; Li and Fei, 2014; Badro et al., 2014]. At the same time, better subduction models [Poitrasson and Zambardi, 2015] and estimates of the degree of homogeneity of the mantle [Javoy et al., 2010; Nakajima and Stevenson, 2015; McDonough, 2016] provide new constraints that are being included in the upper and lower mantle abundance estimates. Better observations of geo-neutrinos [Bellini et al., 2010; Gando et al., 2011; Bellini et al., 2013; Gando et al., 2013] also provide new thermal constraints for the abundances of heat-producing elements in the Earth [e.g. Sramek et al., 2013; Huang et al., 2013].

Recent literature on elemental abundances of the Earth involving the analysis of the primitive mantle and core (usually separately) is increasingly important and when combined, can yield improved elemental abundances of the bulk Earth composition and more realistic uncertainties. The determination of uncertainties is essential to the quantification of elemental abundances but has been missing in previous work. Since the goal of this thesis is to analyze the compositional differences between the Earth, Sun and other solar system bodies, it requires estimates of the bulk Earth abundances *with uncertainties*. Motivated by this, we make a concordance estimate of the bulk Earth elemental abundances and their uncertainties by calibrating the discrepancies between various Earth models made under different geochemical and geophysical assumptions and we use a new estimate of the core mass fraction (with uncertainty). This work is presented in Chapter 2.

1.2 From the Interstellar Medium to Our Planetary System: A Perspective of Chemical Inheritance

While planets form from stellar nebulae – i.e. the same material as the host star forms from – the origin of that material in turn is the interstellar medium (ISM). Interestingly, the interstellar medium exhibits a depletion of certain elements compared to the chemical composition of nearby young stars. This is surprising since these stars must have formed from the nearby interstellar medium, and exhibit very homogeneous abundances. The cause of the depletion must therefore be a process that occurs in the interstellar medium.

Investigations of UV spectra of stars since the 1970s have revealed interstellar absorption features produced by atoms in their favored ionization stages in the interstellar medium [Jenkins, 2009]. Atomic abundances of heavy elements relative to that of hydrogen are found to be below the reference cosmic abundances (approximated by solar abundances in our part of the Galaxy), to varying degrees. The reduction of heavy elements represents the missing atoms in the ISM gas phase. This feature is reinforced by the correlation of the abundance deficiencies of such elements with the temperatures derived theoretically for particle condensation in stellar nebulae, suggesting that these elements have condensed into dust grains [Field, 1974]. In a study of abundances along 243 different sight lines from more than 100 papers, Jenkins [2009] characterized the systematic patterns for depletions of 17 different elements (C, N, O, Mg, Si, P, S, Cl, Ti, Cr, Mn, Fe, Ni, Cu, Zn, Ge, and Kr), from which a unified quantitative scheme was constructed to estimate dust compositions.

Similar to the interstellar medium, the chemical composition of the Sun (representing the ISM gas and solid phases) differs systematically from the composition of the Earth [Kargel and Lewis, 1993] and indeed all terrestrial planets [Warren, 2011], as well as so-called primitive meteorites [Davis, 2006]. The fact that this is seen in primitive meteorites is important, as these meteorites are thought to be remnants of the solar nebula, and indeed radioactive dating shows them to be about 4.56 billion years old. One might then ask, where the volatile material that is missing from terrestrial planets and primitive meteorites has gone– suggestions include a hypothetical volatile-rich condensate termed "mysterite" [Higuchi et al., 1977] and missing planets [Halliday and Porcelli, 2001]. It is also interesting that a search for the material that is missing from the interstellar medium initiated by [Field, 1974] eventually led to the discovery of different types of presolar grains inside carbonaceous chondrites [e.g. Lewis et al., 1987; Ireland, 1990]. These presolar grains are thought to represent the surviving condensates that are missing from the interstellar medium [Clayton, 1981; Trivedi and Larimer, 1981; Clayton, 1982; Jones and Williams, 1987]. Since these different presolar grains can be destroyed at different temperatures [Huss et al., 2003; Davis, 2006], they are quite diagnostic of nebular and parent-body thermal events. The carbonaceous chondrites wherein the presolar grains have been found are a remarkable but relatively rare type of meteorite that contains large quantities of volatile elements, e.g., water and organic compounds. Their presence indicates that this type of meteorite has not experienced significant heating (> 900 K) since its formation;

otherwise these volatiles would have considerably evaporated. These carbonaceous chondrites are subdivided into the sub-classes/groups, e.g., CI, CM, CV, CO, CR, and CK [Weisberg et al., 2004], according to their chemical and mineralogy differences.

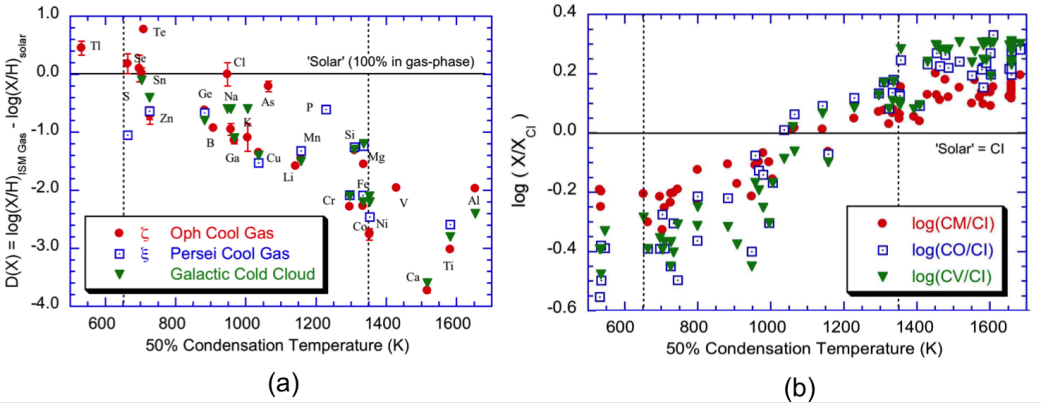

Figure 1.4: (a) Interstellar gas phase abundances relative to solar and (b) primitive meteoritic abundances relative to CI chondrites, as a function of the 50% condensation temperature [Lodders, 2003]. For these moderately volatile elements, the gas of the interstellar medium and the meteorites show opposite abundance trends. The figures are from Yin [2005].

By comparing interstellar gas and dust composition with primitive meteoritic data, Yin [2005] demonstrated a remarkable qualitative similarity in the depletion patterns between the ISM and primitive meteorites for moderately volatile elements. This similarity is further discussed in Wang and Lineweaver [2016] and shown in Figure 1.4.

Note however that the depletion scales in the ISM gas phase and the meteoritic data differ by orders of magnitude, despite the qualitatively similar (but opposite) behavior. This can be explained if the depletion pattern found in the ISM gas phase is due to the condensation of the depleted elements onto interstellar dust grains. These dust grains with the condensed layer of volatiles are processed during the collapse stage of the parent molecular cloud and in the early active solar nebula through the processes such as shock-wave compression, vaporization and recondensation, and then form the so-called primitive meteorites through further fractionation, accretion, aerodynamic heating (when passing through the Earth's atmosphere), and weathering (on the surface of the Earth). Despite this multitude of processes, it is striking how well the overall abundance pattern of the interstellar dust grains is preserved in the primitive meteorites.

The important connection between the early solar nebula and the interstellar medium was outlined in a model by Yin [2005], which explains how interstellar grains act to seed the formation of primitive meteorites. The schematic in Figure 1.5 illustrates this connection, and can be explained as follows.

(i) In the diffuse interstellar medium where elemental depletions are observed,

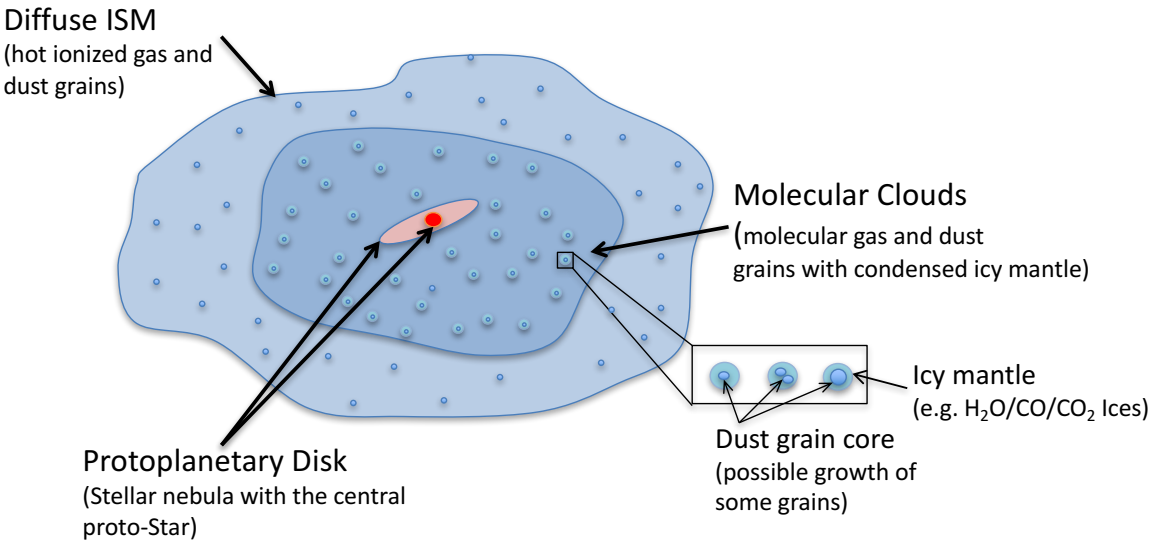

Figure 1.5: Schematic processes of dust grains inherited from the interstellar medium into the protoplanetary disk. This figure is adapted from Wang and Lineweaver [2016].

the volatile elements (i.e. elements with low condensation temperatures) are in the hot ionized gas phase, while the refractory elements (i.e. elements with high condensation temperatures) have condensed into dust grains.

(ii) In the cold and dense molecular cloud stage, the gas phase primarily consists of hydrogen molecules and helium. Carbon-rich species condense with other volatile elements onto the dust grain core. Accumulation of individual grains with icy mantles may occur at this stage, leading to the growth of dust grains.

(iii) As the gas pressure increases, the densest molecular cloud cores collapse, leading to the rapid formation of stellar nebulae. During the collapse of the cloud, the conservation of angular momentum leads to the formation of a protoplanetary disk. The disk rapidly flattens. The icy mantles (volatile compounds) on the surface of grains vaporize or sublimate if grains experience sudden heating, due to either adiabatic compression or shock waves.

In brief, the presolar grains inherited from the interstellar medium and then processed in the solar nebula constitute the primordial rocky material of our planetary system, from which terrestrial planets are formed through the progressive accretion and collisions and the accompanying volatile loss and gain.

1.3 Exoplanetary Chemistry and Interiors: A Growing Pathway to Characterize Exoplanets and Habitability

With devolatilization likely to be an essential feature of terrestrial planet formation, the bulk elemental composition of terrestrial planets orbiting other stars can be estimated by devolatilizing the observed elemental abundances of those host stars. But why and how is the planetary bulk composition important for characterizing exoplanets and their habitability?

This question is pertinent to the prevalent modeling of exoplanetary interiors including structure and mineralogy [e.g. Dorn et al., 2017b; Brugger et al., 2017; Unterborn et al., 2018]. Exoplanetary interiors can influence mantle convection and surface recycling, i.e. planet tectonics, which in turn affects the outgassing of a planet and the formation of a secondary atmosphere [Noack and Breuer, 2014], thereby, the habitability of an extrasolar planet. To model exoplanetary interiors, we need two sets of principal observational constraints. One set is the planetary mass and radius information, and the other is the host stellar abundances. With only mass and radius measurements multiple solutions of interior composition and structure are possible, thus the problem is highly underconstrained or degenerate [Seager et al., 2007; Rogers and Seager, 2010]. My study on this topic therefore focuses on the other principal constraint – the elemental abundances of host stars, by taking into account devolatilization (see the schematic in Figure 1.6).

Recent studies [e.g. Dorn et al., 2015; Santos et al., 2015] have proposed adding host stellar abundances as a principal constraint to reduce the degree of modeling degeneracy of exoplanetary interior structure and mineralogy. However, one fact that is ignored consistently in the prevalent exoplanetary interior models [e.g. Dorn et al., 2015; Santos et al., 2015; Dorn et al., 2017b; Brugger et al., 2017; Unterborn et al., 2018] is that the elemental abundances of a rocky exoplanet are *not* identical to the elemental abundances of its host star. Host stellar abundances are good proxies of planetary abundances, but *only* for refractory elements (i.e. elements with condensation temperatures $\gtrsim$ 1360 K). This is particularly true for terrestrial planets, as evidenced by the relative compositional differences between the Sun, Earth and other inner solar system bodies [Davis, 2006; Carlson et al., 2014].

Based on the quantification of the devolatilization in going from the solar nebula to the Earth (presented in Chapter 3), we know that the elemental abundance differences (on an equal basis of aluminum) between the Earth and the Sun for Si, Mg, Fe and Ni are slight, but significant (a devolatilization factor of 10-20%); those for O, S, and C are substantial and devolatilized by up to 3 orders of magnitude. The differences for Si, Mg, Fe, and Ni, in combination with the substantially devolatilized O, will have a direct and nontrivial effect on the mantle and core composition; the differences for O, S, and C will have profound impact on the atmospheric composition, including the abundances of surface water, and therefore on habitability. In Chapter 4 we discuss the inclusion of the devolatilization process into the estimates of planetary bulk composition from the host stellar abundances, to improve the modeling of exoplanetary interiors. Now we may ask to what extent the Sun-to-Earth

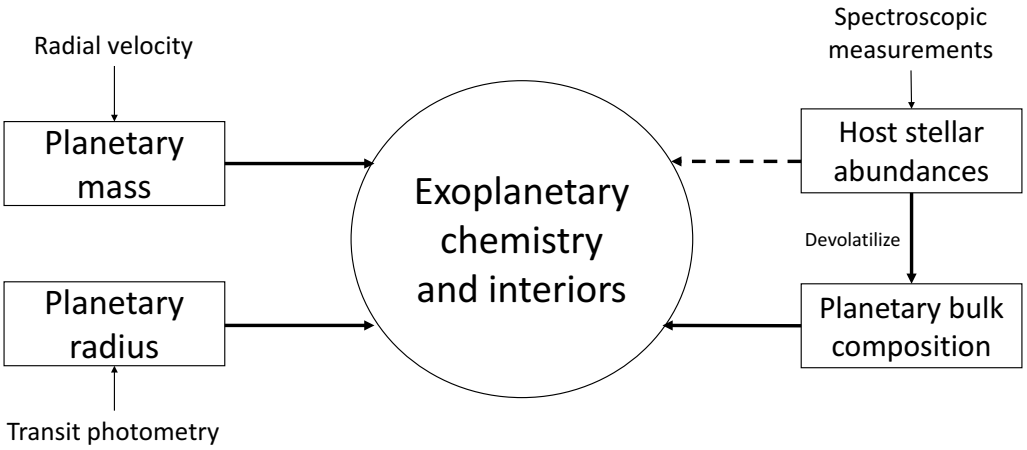

Figure 1.6: Observational information required for modeling exoplanetary chemistry and interiors. It is recommended that host stellar abundances are devolatilized first to represent the planetary bulk composition, which is then used as a principal constraint for the modeling.

devolatilization pattern applies to other planetary systems.

Composition-, location-, and timescale-dependent differences in the various fractionation processes in a stellar nebula may lead to a variety of outcomes in the composition of a rocky planet (see Figure 1.7). The compositional differences between the Earth, Mars and Venus could be a measure of these variations within our own Solar System, but the extent to which the bulk compositions of Venus and Mars are different to the Earth is still debated [Morgan and Anders, 1980; Wanke and Dreibus, 1988; Taylor, 2013; Kaib and Cowan, 2015]. We also note that the *bulk* compositions of Venus and Mars are not well determined yet and thus reliable quantitative analysis of bulk compositional differences between them and the Earth is difficult. In spite of the complexity of planet formation, an essential step to improve the study of exoplanetary chemistry is to take into account devolatilization, starting with the best constrainable trend coming from the Sun-to-Earth comparison.

An additional source of uncertainty in the studies of exoplanetary chemistry is that elements lighter than iron and nickel are rarely taken into account in estimating the core composition of a rocky exoplanet [e.g. Santos et al., 2015; Dorn et al., 2017b; Brugger et al., 2017; Unterborn et al., 2018]. These models usually simplify the core to pure iron. Light elements play a key role in compensating the 5-10% density deficit of Earth's core [Hirose et al., 2013; McDonough, 2014] (comparing to pure iron at core pressures) and in differentiating the liquid outer core from the solid inner core. The importance of light elements in a terrestrial exoplanet's core cannot be ignored, and taking them into account has direct consequences for estimates of core mass fraction and the melting temperature of an outer core (if it exists), which together have further

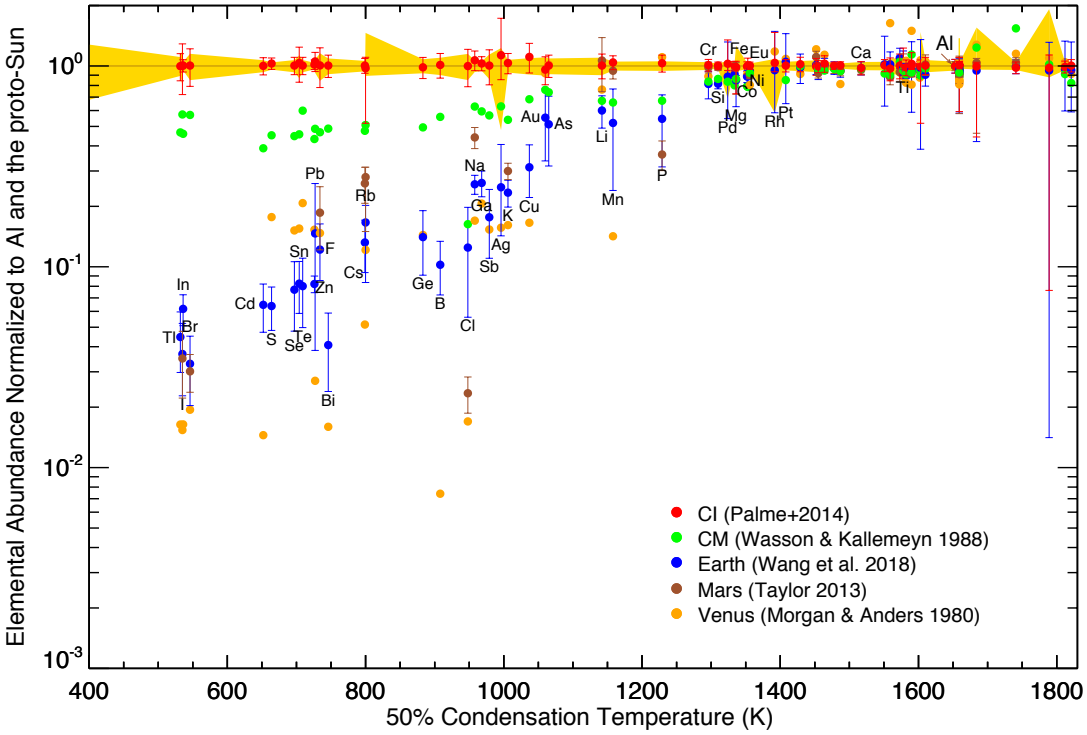

Figure 1.7: The elemental composition of solar system rocky bodies, including CI chondrites [Palme et al., 2014], CM chondrites [Wasson and Kallemeyn, 1988], Earth [Wang et al., 2018a], Mars [Taylor, 2013], and Venus [Morgan and Anders, 1980], normalized to the protosolar elemental abundances [Wang et al., 2018b], on the equal basis of 10^6 Al atoms. In Taylor [2013], the elemental composition of Mars is the primitive Martian mantle composition, so only lithophile elemental abundances are plotted here. The abundance differences between terrestrial planets are not clearly distinguishable.

implications for the generation of the planetary magnetic fields. First, nickel should be added into the constituents of a rocky planet's core, because of the strong affinity of nickel for iron. From the cosmochemical analysis of various types of chondrites [McDonough, 2017], it has been found that the Fe/Ni ratio in the rocky bodies of the Solar System is essentially fixed (17.4 ± 0.5, by mass). The variation of Fe/Ni ratios among different stars can be investigated by analyzing thousands of the solar neighborhood stars, for which the elemental abundances of Fe and Ni are typically available. Second, sulfur is increasingly recognized to be one of the major light elements in the Earth's core [Hirose et al., 2013; Li and Fei, 2014], and indeed large-scale sulfide fractionation during Earth's mantle-core differentiation has been found [Savage et al., 2015]. The fractionation of sulfur between the mantle and the core (in the form of FeS) of a terrestrial planet can be performed by using mass balance calculations and taking the oxidation state of that planet into account. It is worth

noting that sulfur abundance in a rocky exoplanet should result from devolatilizing the host star, prior to the further fractionation of sulfur within the planet body.

1.4 Thesis Outline

This thesis presents new estimates for the elemental abundances of the bulk Earth and proto-Sun. The differences quantify the devolatilization processes pertaining to the formation of the rocky planets of our Solar System. This quantification is, by extension, applicable to other planetary systems to infer the exoplanetary bulk compositions from their known host stellar abundances. We also explore constraints that can be improved to advance studies of exoplanetary interior and habitability.

Chapter 2 presents our concordance estimates for the elemental abundances with uncertainties of the primitive mantle, the core, and the bulk Earth. This work allows the comparison between the Earth and the Sun, as well as other solar system bodies, to study the accretion and fractionation processes that produce rocky planets from protoplanetary nebulae.

Chapter 3 extends our analysis of terrestrial abundances to the estimates of protosolar elemental abundances based on the latest estimates of solar photospheric abundances and primitive meteoritic abundances, and then to establish a fiducial model from the Earth-to-Sun abundance ratios as a function of elemental condensation temperatures. This model provides quantitative insights into the devolatilization processes associated with the formation of rocky planetary bodies.

Chapter 4 applies the fiducial devolatilization model to nearby planetary systems to infer the bulk elemental composition of rocky exoplanets – particularly those within the circumstellar habitable zones – from the known host stellar abundances. The estimated planetary bulk composition (rather than the host stellar abundances) is then used as a principal constraint (along with other assumptions) to model the interior composition and structure of such exoplanets, which are essential to understanding their habitability.

Chapter 5 summarizes the main results of the thesis for the bulk elemental compositions of the Earth and the Sun, the fiducial devolatilization model coming from the Sun-to-Earth comparison, as well as how this applies to rocky extrasolar planets. The limitations of these analyses are discussed, as well as prospects for future work.

Chapter 2

The Elemental Abundances (with Uncertainties) of the Most Earth-like Planet

This chapter is adapted from Wang et al. [2018a] originally published as

Wang, H. S., Lineweaver, C. H., and Ireland, T. R. 2018. The Elemental Abundances (with Uncertainties) of the Most Earth-like Planet. Icarus 299, 460-474, doi.org/10.1016/j.icarus.2017.08.024

Abstract

To first order, the Earth as well as other rocky planets in the Solar System and rocky exoplanets orbiting other stars, are refractory pieces of the stellar nebula out of which they formed. To estimate the chemical composition of rocky exoplanets based on their stellar hosts' elemental abundances, we need a better understanding of the devolatilization that produced the Earth. To quantify the chemical relationships between the Earth, the Sun and other bodies in the Solar System, the elemental abundances of the bulk Earth are required. The key to comparing Earth's composition with those of other objects is to have a determination of the bulk composition with an appropriate estimate of uncertainties. Here we present concordance estimates (*with uncertainties*) of the elemental abundances of the bulk Earth, which can be used in such studies. First we compile, combine and renormalize a large set of heterogeneous literature values of the primitive mantle (PM) and of the core. We then integrate standard radial density profiles of the Earth and renormalize them to the current best estimate for the mass of the Earth. Using estimates of the uncertainties in i) the density profiles, ii) the core-mantle boundary and iii) the inner core boundary, we employ standard error propagation to obtain a core mass fraction of 32.5 ± 0.3 wt%. Our bulk Earth abundances are the weighted sum of our concordance core abundances and concordance PM abundances. Unlike previous efforts, the uncer-

tainty on the core mass fraction is propagated to the uncertainties on the bulk Earth elemental abundances. Our concordance estimates for the abundances of Mg, Sn, Br, B, Cd and Be are significantly lower than previous estimates of the bulk Earth. Our concordance estimates for the abundances of Na, K, Cl, Zn, Sr, F, Ga, Rb, Nb, Gd, Ta, He, Ar, and Kr are significantly higher. The uncertainties on our elemental abundances usefully calibrate the unresolved discrepancies between standard Earth models under various geochemical and geophysical assumptions.

2.1 Introduction

The number of known rocky exoplanets is rapidly increasing. Transit photometry and radial velocity measurements, when combined, yield rough estimates of the densities and therefore mineralogies of these exoplanets. Independent and potentially more precise estimates of the chemical composition of these rocky planets can be made based on the known elemental abundances of their host stars combined with estimates of the devolatilization process that produced the rocky planets from their stellar nebulae. To proceed with this strategy, we need to quantify the devolatilization that produced the Earth from the solar nebula. Knowledge of the bulk elemental abundances of the Earth with uncertainties is an important part of this research. The elemental abundances of bulk Earth (including both the bulk silicate Earth and the core) can tell us a more complete story of the potentially universal accretion and fractionation processes that produce rocky planets from nebular gas during star formation. Uncertainties associated with the bulk Earth composition are needed to compare and quantify compositional differences between the Earth, Sun, and other solar system bodies. Such comparisons can lead to a more detailed understanding of devolatilization and the chemical relationship between a terrestrial planet and its host star. The bulk Earth elemental abundances will help determine what mixture of meteorites, comets and other material produced the Earth [Drake and Righter, 2002; Burbine and O'Brien, 2004] and can also help determine the width of the feeding zone of the Earth in the protoplanetary disk [Chambers, 2001; Kaib and Cowan, 2015].

There are many stages of compositional fractionation between the collapse of a stellar nebula, the evolution of a protoplanetary disk and a final rocky planet. Composition- and position-dependent differences in the duration and strength of the various fractionating processes can lead to a variety of outcomes. The different (but somewhat similar) compositions of Earth, Mars and Vesta are a measure of these variations within our own Solar System.

A major challenge to estimating the bulk chemical composition of the Earth is that we can only sample the upper part of the possibly heterogeneous mantle, and we have no direct access to its deep interior, and even less to the core [Allègre et al., 2001]. Early studies on primitive mantle (PM) elemental abundances include O'Neill [1991], Kargel and Lewis [1993], McDonough and Sun [1995], and O'Neill and Palme [1998]. Bulk elemental abundances with uncertainties [Allègre et al., 2001] were reported 16 years ago but much work on PM abundances and on core abundances (usually separately) has been done since then [e.g., Lyubetskaya and Korenaga, 2007; Palme and O'Neill, 2014; Rubie et al., 2011; Wood et al., 2013; Hirose et al., 2013]. The determination of uncertainties is central to the quantification of elemental abundances but has been a missing priority in previous work. The most recent, highly cited estimates of the elemental abundances of the bulk Earth do not include uncertainties [McDonough, 2003; McDonough and Arevalo, 2008].

Elemental abundance discrepancies are in large part model-dependent [McDonough, 2016], but over the past 15 years progress has been made in making more plau-

sible models. Our knowledge of the core (and therefore of the bulk Earth) has increased significantly: high pressure experiments yield improved partition coefficients of siderophiles [Siebert et al., 2013] and improved affinities of light elements for iron [Ricolleau et al., 2011; Mookherjee et al., 2011]. Seismic velocities through the core provide increasingly precise constraints on densities and on mineral physics models [Vočadlo, 2007; Li and Fei, 2014; Badro et al., 2014]. Better subduction models [Poitrasson and Zambardi, 2015] and estimates of the degree of homogeneity of the mantle [Javoy et al., 2010; Nakajima and Stevenson, 2015; McDonough, 2016] provide new constraints that are being included in the upper and lower mantle abundance estimates. Better observations of geo-neutrinos [Bellini et al., 2010; Gando et al., 2011; Bellini et al., 2013; Gando et al., 2013] provide new thermal constraints for the abundances of heat-producing elements in the Earth [e.g. Sramek et al., 2013; Huang et al., 2013]. The large majority of the literature on elemental abundances of the Earth, involving either the analysis of the PM or of the core, are increasingly important and when combined, yield improved elemental abundances of the bulk Earth composition and more realistic uncertainties.

Our main research goal is to analyze the compositional differences between the Earth, Sun and other solar system bodies and from this comparison quantify the devolatilization of stellar material that leads to rocky planets. This requires estimates of the bulk Earth abundances *with uncertainties*. These bulk abundances and their uncertainties are poorly constrained and often ignored in the literature. Motivated by this, we make a concordance estimate of the bulk Earth elemental abundances and their uncertainties. The words "concordance estimate" specifically mean a compositional estimate that is representative of, and concordant with previous estimates. The aim of this work therefore is not to resolve the discrepancies between competing models and assumptions but to construct a concordance model (*with uncertainties*) that represents current knowledge of bulk Earth composition and calibrates unresolved discrepancies. We envisage that if the discrepancies can be resolved, a better formulation for estimating uncertainties might be forthcoming. However, at this stage, some of the arguments concerning the derivation of models, or values resulting from these models, appear intractable. Nevertheless, there is an essential need for uncertainties in the estimates if we are to make progress in comparing planetary objects.

2.2 Composition of the Primitive Mantle

2.2.1 Data sources

Earth's primitive mantle (PM) or bulk silicate Earth (BSE) is the mantle existing after core segregation but before the extraction of continental and oceanic crust and the degassing of volatiles [Sun, 1982; Kargel and Lewis, 1993; Saal et al., 2002; McDonough, 2003; Lyubetskaya and Korenaga, 2007; Palme and O'Neill, 2014]. There are two major, and partially-overlapping modeling strategies for estimating the PM composition.

The peridotite model is based on the analysis of chemical data from basalts and

periodotite massifs. Peridotite-basalt melting trends yield an estimate of the PM composition [e.g., Ringwood, 1979; Sun, 1982; McDonough and Sun, 1995; McDonough, 2003; Lyubetskaya and Korenaga, 2007]. The peridotite model has a number of intrinsic problems, including the non-uniqueness of melting trends, large scatter in the data from mid-ocean ridge basalts (MORB) and from ocean island basalts (OIB), and the difficulty of imposing multiple cosmochemical constraints on refractory lithophile element (RLE) abundances, often resulting in model-dependent, poorly quantified uncertainties [Lyubetskaya and Korenaga, 2007].

The cosmochemical model is based on the identification of Earth with a particular class of chondritic or achondritic meteorites or their mixtures [e.g., Morgan and Anders, 1980; Javoy et al., 2010; Fitoussi et al., 2016], along with a number of assumptions on accretion and fractionation processes [Allègre et al., 2001]. The cosmochemical model uses chondritic ratios of RLEs and volatility trends [e.g., Wanke and Dreibus, 1988; Palme and O'Neill, 2003, 2014]. Palme and O'Neill [2003] and Palme and O'Neill [2014] present a core-mantle mass balance approach for calculating the primitive mantle composition. This approach requires an accurate determination of magnesium number (Mg # = molar Mg/(Mg+Fe)). A reasonable range for Mg# can be inferred from fertile mantle periodites.

Our aim is not to resolve the differences between these strategies and models but to construct a concordance model whose mean values and uncertainties adequately represent current knowledge and disagreement.

2.2.2 Concordance PM estimate

We construct our concordance PM abundances from three major papers reporting PM abundances [Lyubetskaya and Korenaga, 2007; McDonough and Arevalo, 2008; Palme and O'Neill, 2014], supplemented with noble gas abundances from Marty [2012] and Halliday [2013]. McDonough and Arevalo [2008] is an updated version of their pioneering peridotite model [McDonough and Sun, 1995; McDonough, 2003]. Updates of some abundances, for example W, K and Pb, can be found in Arevalo and McDonough [2008] and Arevalo et al. [2009]. Lyubetskaya and Korenaga [2007] performed a principal component analysis of the same peridodite database but with different model parameters. Palme and O'Neill [2014] is largely based on a cosmochemical model using mass balance and is an updated version of their pioneering earlier work [Palme and O'Neill, 2003].

Challenges to combining these three data sets are:

i) McDonough and Arevalo [2008] report no uncertainties, however the PM abundance uncertainties reported in McDonough and Sun [1995] approximately reflect current uncertainties. Thus, in our analysis, we attach them to the PM abundances reported in McDonough and Arevalo [2008].

ii) Lyubetskaya and Korenaga [2007] do not report abundances of four volatiles; C, H, N, O.

iii) Palme and O'Neill [2014] do not report uncertainties for C, N, Se, Te, In, Hg and Bi, while Lyubetskaya and Korenaga [2007] do not report uncertainties for Te,

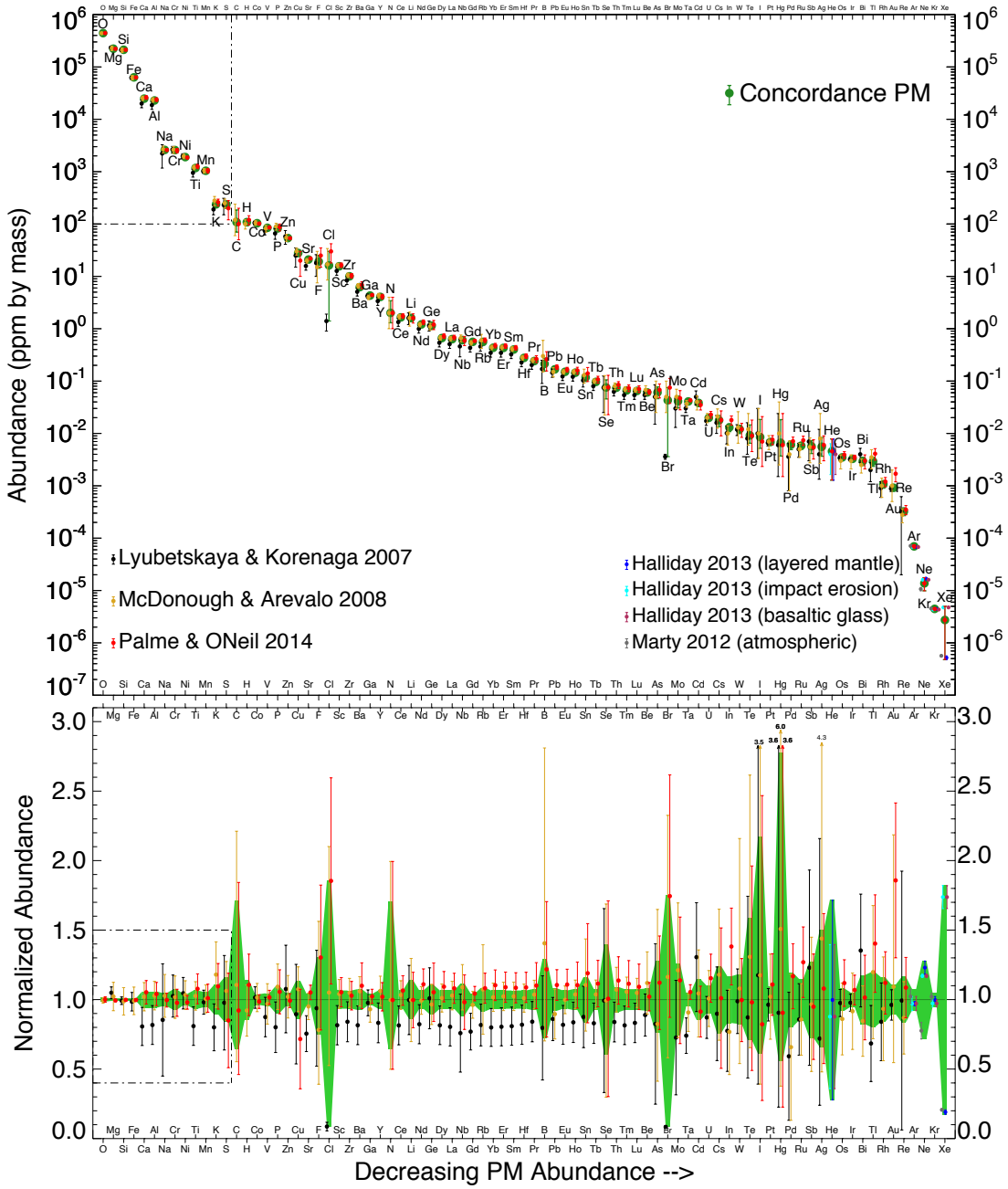

Figure 2.1: Recent literature estimates of 83 elemental abundances in the primitive mantle (PM) and our concordance estimates (green) constructed from them. Elements are plotted in order of decreasing PM abundance. The upper panel plots ppm by mass. In the lower panel, literature values have been normalized to our PM concordance estimates. Our PM concordance ppm estimates have been rescaled up by 0.3% to ensure that their sum equals 10^6. We have not rescaled the literature values (see Appendix A.3 for rescaling details). The light green band in the lower panel indicates our estimate of the uncertainties on the concordance values. 64% of the literature points fall within this band. The string of relatively low values for RLEs in the middle of the plot for the Lyubetskaya and Korenaga [2007] data set is due to its relatively high Mg abundance. Upper limits that extend beyond the plot range are labeled with their y-values. The dashed boxes on the left in both panels contain the 13 most abundant elements and are zoomed-in on in Fig. 2.2.

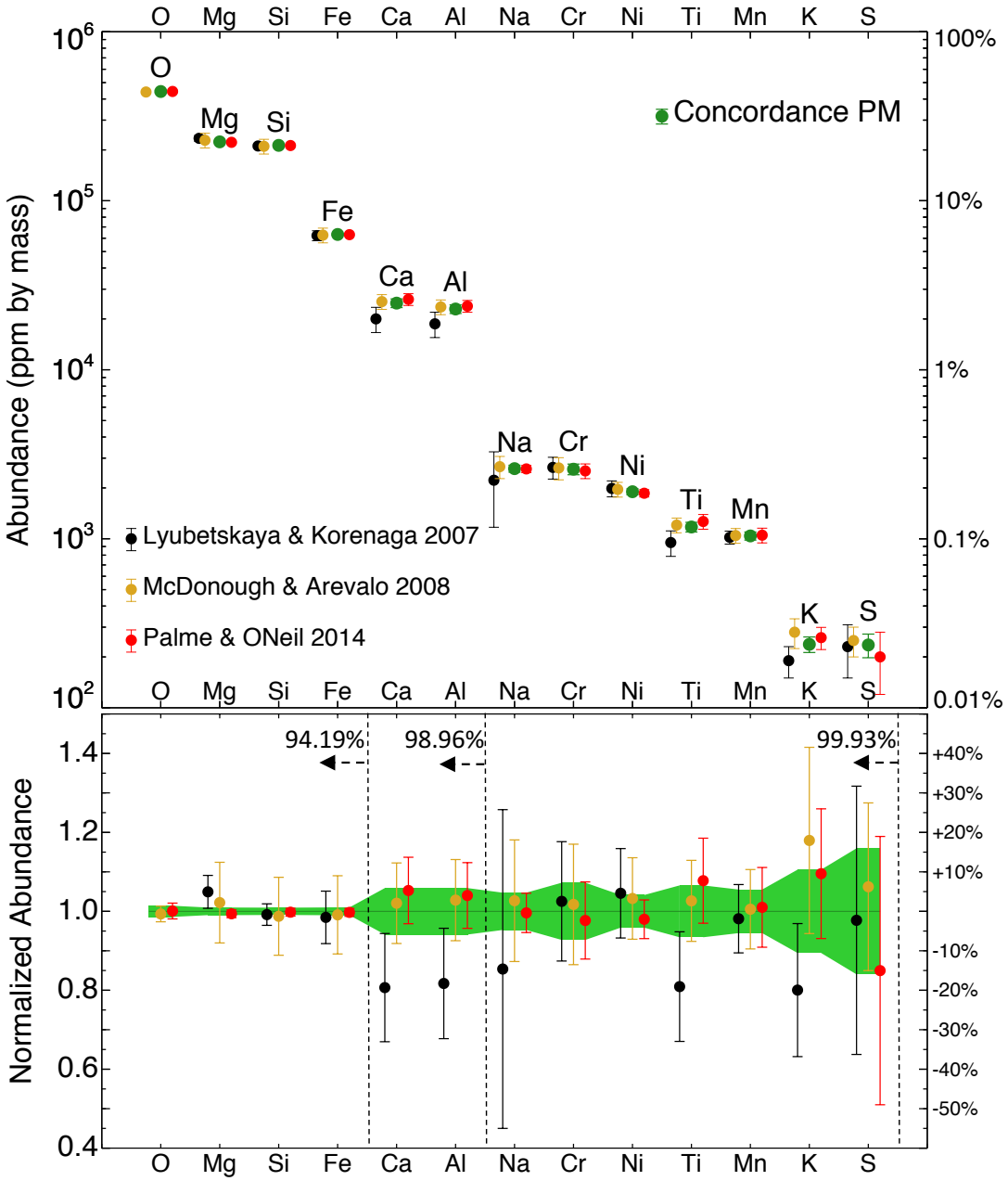

Figure 2.2: Zoom-in of the 13 most abundant elements contained in the dashed boxes in both panels of the previous figure. The sum of the abundances of the 4 most abundant elements (O, Mg, Si, Fe) make up $94.19 \pm 0.69\%$ of the total PM mass. The 6 most abundant elements (O, Mg, Si, Fe, Ca, Al) make up $98.96 \pm 0.72\%$, while the 13 most abundant elements plotted here make up $99.93^{+0.07}_{-0.72}\%$ of the total PM mass. The extra mass in Mg in the Lyubetskaya and Korenaga [2007] data set is compensated for by their low values of Ca and Al . This is a good example of the covariance or non-independence of elemental abundance estimates.

In, Hg, Bi, Ag, Cd and Tl. We assign the McDonough and Sun [1995] uncertainties to these elements.

iv) none of these three PM models include noble gas abundances. In a preliminary attempt to be more comprehensive, we supplement these three PM models with recent noble gas abundances: the atmospheric model of Marty [2012] and three different models (layered mantle, impact erosion, and basaltic glass) from Halliday [2013]. This range encompasses recent results from Dauphas and Morbidelli [2014] [Marty et al., 2016]. See Appendix A.1 for details.

The resultant concordance estimates for the PM elemental abundances and their uncertainties are listed in column 3 of Table 2.1. Our PM elemental abundances are increased by 0.3% to ensure that the sum of all the ppm values equals 10^6 (see A.3). Figs. 2.1 & 2.2 show the comparison of our concordance abundances with the literature values. The upper panel of Fig. 2.1 shows elemental abundances (ppm by mass). The literature abundances normalized to our concordance PM abundances are shown in the lower panel. For clarity, Fig. 2.2 is a zoomed-in version of the 13 most abundant elements in Fig. 2.1. The abundances of these 13 elements account for $99.93^{+0.07}_{-0.72}$ wt% of the primitive mantle.

By construction, our concordance PM abundances are consistent with the literature abundances. There are some outliers. For example, the Lyubetskaya and Korenaga [2007] abundances of Cl and Br are relatively low because they used the Cl/K ratio of 0.0075 ± 0.0025 from highly depleted MORB in Saal et al. [2002]. This ratio is $\sim$ 10 times lower than an equivalent Cl/K ratio of $\sim$ 0.07 used in McDonough and Arevalo [2008] [which came from the Cl/Rb $\sim$ 28 and K/Rb $\sim$ 400 of McDonough and Sun, 1995]. The abundances of K estimated in Lyubetskaya and Korenaga [2007] and McDonough and Arevalo [2008] are consistent (190 ± 76 ppm and 240 ± 48 ppm, respectively), resulting in the abundance of Cl in Lyubetskaya and Korenaga [2007] $\sim$ 12 times lower than that in McDonough and Arevalo [2008]. Based on a 10% partial melting MORB and the mass balance, Palme and O'Neill [2014] estimate a total Cl content of 30 ppm for PM, $\sim$ 21 times higher that that ($\sim$ 1.4 ppm) in Lyubetskaya and Korenaga [2007]. The Lyubetskaya and Korenaga [2007] abundance of Br comes from the Cl/Br ratio of $\sim 400 \pm 50$, which is the same ratio used in Palme and O'Neill [2014] and is higher than the approximate 350 [McDonough and Arevalo, 2008; McDonough and Sun, 1995]. Thus, the Lyubetskaya and Korenaga [2007] Br abundance is also low and inconsistent with that of McDonough and Arevalo [2008] and of Palme and O'Neill [2014]. Because of this inconsistency, we use an unweighted mean for Cl and Br (see Appendix A.1). As a result, the ratio of our estimated Cl and Br abundances is $\sim$ 376.

Table 2.1: Concordance estimates of the elemental abundances of primitive mantle, core, and bulk Earth. Following convention, depending on the element, we use ppm (by mass) or *wt*% or ppb (as indicated in column 2).

Z	Elem	**Concordance Primitive Mantle**		**Concordance Core**		**Bulk Earth**[d]
		abundance (ppm)[a]	Sources[b]	abundance (ppm)[a]	Sources[c]	abundance (ppm)[a]
1	H	109 ± 15	MA08, PO14	569 ± 421	W06, MA08, ZY12	258 ± 137
2	He (ppb)	4.56 ± 3.29	H13	-	-	3.08 ± 2.22
3	Li	1.60 ± 0.22	LK07, MA08, PO14	1.57 ± 0.59	KL93	1.59 ± 0.24
4	Be	0.0607 ± 0.0048	LK07	-	-	0.0410 ± 0.0033
5	B	$0.213\ ^{+0.062}_{-0.059}$	LK07, MA08, PO14	-	-	$0.144\ ^{+0.042}_{-0.040}$
6	C	$109\ ^{+77}_{-39}$	MA08, PO14	7921 ± 6820	W06, MA08, ZY12, W13, N15, LS16	2648 ± 2217
7	N	$2.01\ ^{+1.42}_{-0.71}$	MA08, PO14	$93\ ^{+77}_{-90}$	MA08, ZY12	$31.7\ ^{+24.9}_{-29.3}$
8	O (%)	44.3 ± 0.6	MA08, PO14	2.66 ± 1.82	KL93, A01, M03, J10, H11, R11, ZY12, H13, S13, B14, LS16	30.8 ± 0.7
9	F	$19.2\ ^{+5.8}_{-4.9}$	LK07, MA08, PO14	-	-	$13.0\ ^{+3.9}_{-3.3}$
10	Ne (ppb)	0.0137 ± 0.0039	M12, H13	-	-	0.00927 ± 0.00261
11	Na	2600 ± 123	LK07, MA08, PO14	1372 ± 519	KL93	2201 ± 188
12	Mg (%)	22.3 ± 0.2	LK07, MA08, PO14	$0.0588\ ^{+0.0294}_{-0.0288}$	ZY12	15.1 ± 0.2
13	Al (%)	2.29 ± 0.13	LK07, MA08, PO14	-	-	1.54 ± 0.09
14	Si (%)	21.3 ± 0.2	LK07, MA08, PO14	4.96 ± 2.34	A01, W06, MA08, J10, R11, ZY12, H13, S13, B14, LS16	16.0 ± 0.8
15	P	82.4 ± 8.0	LK07, MA08, PO14	$2774\ ^{+916}_{-1236}$	A01, MA08, KL93, ZY12	$957\ ^{+298}_{-402}$
16	S	235 ± 38	LK07, MA08, PO14	18269 ± 4497	KL93, A01, W06, MA08, R11, H13, LS16	6096 ± 1463
17	Cl	$16.2\ ^{+13.9}_{-14.8}$	LK07, MA08, PO14	$459\ ^{+278}_{-259}$	KL93, MA08	$160\ ^{+91}_{-85}$
18	Ar (ppb)	0.0697 ± 0.0054	M12, H13	-	-	0.0471 ± 0.0036
19	K	237 ± 25	LK07, MA08, PO14	206 ± 78	KL93	227 ± 30
20	Ca (%)	2.48 ± 0.15	LK07, MA08, PO14	-	-	1.67 ± 0.10
21	Sc	15.6 ± 1.0	LK07, MA08, PO14	-	-	10.5 ± 0.7
22	Ti	1174 ± 77	LK07, MA08, PO14	-	-	792 ± 52
23	V	84.6 ± 3.9	LK07, MA08, PO14	122 ± 46	KL93, MA08, R11	96.6 ± 15.2
24	Cr	2580 ± 187	LK07, MA08, PO14	6590 ± 1751	KL93, A01, MA08, J10, R11	3883 ± 583
25	Mn	1040 ± 57	LK07, MA08, PO14	$3257\ ^{+2563}_{-2903}$	KL93, A01, M03, MA08	$1760\ ^{+834}_{-944}$
26	Fe (%)	6.32 ± 0.06	LK07, MA08, PO14	82.8 ± 2.9	KL93, A01,M03, MA08, J10, R11	31.2 ± 1.0
27	Co	103 ± 4	LK07, MA08, PO14	2373 ± 141	KL93, A01, MA08, J10, R11	841 ± 46
28	Ni (%)	0.190 ± 0.008	LK07, MA08, PO14	5.06 ± 0.23	KL93, A01,M03, MA08, J10, R11	1.77 ± 0.08
29	Cu	27.9 ± 3.8	LK07, MA08, PO14	154 ± 58	MA08, KL93	69.0 ± 19.2
30	Zn	53.9 ± 2.5	LK07, MA08, PO14	29 ± 11	KL93	45.9 ± 4.0
31	Ga	4.30 ± 0.17	LK07, MA08, PO14	4.90 ± 1.85	KL93	4.49 ± 0.61
32	Ge	1.14 ± 0.12	LK07, MA08, PO14	24.0 ± 9.1	KL93, MA08	8.56 ± 2.95
33	As	$0.0606\ ^{+0.0167}_{-0.0145}$	LK07, MA08, PO14	4.89 ± 1.85	KL93, MA08	1.63 ± 0.60
34	Se	0.0755 ± 0.0300	LK07, MA08, PO14	8.63 ± 3.27	KL93, MA08	2.86 ± 1.06
35	Br	$0.0430\ ^{+0.0322}_{-0.0394}$	LK07, MA08, PO14	0.514 ± 0.195	KL93, MA08	$0.196\ ^{+0.067}_{-0.069}$
36	Kr (ppb)	0.00446 ± 0.00022	M12, H13	-	-	0.00301 ± 0.00015
37	Rb	0.559 ± 0.048	LK07, MA08, PO14	1.08 ± 0.41	KL93	0.728 ± 0.136
38	Sr	20.9 ± 0.9	LK07, MA08, PO14	-	-	14.1 ± 0.6
39	Y	4.05 ± 0.27	LK07, MA08, PO14	-	-	2.73 ± 0.18
40	Zr	10.02 ± 0.66	LK07, MA08, PO14	-	-	6.76 ± 0.44
41	Nb	0.606 ± 0.070	LK07, MA08, PO14	0.423 ± 0.160	R11	0.547 ± 0.070
42	Mo	0.0413 ± 0.0107	LK07, MA08, PO14	4.97 ± 1.88	KL93, MA08	1.64 ± 0.61
44	Ru (ppb)	5.83 ± 0.86	LK07, MA08, PO14	3939 ± 1491	KL93, MA08	1284 ± 485
45	Rh (ppb)	1.07 ± 0.17	LK07, MA08, PO14	684 ± 259	KL93, MA08	223 ± 84
46	Pd (ppb)	6.08 ± 1.18	LK07, MA08, PO14	2719 ± 1029	KL93, MA08	888 ± 335

Continued on next page

Z	Elem	**Concordance Primitive Mantle** abundance (ppm)[a]	Sources[b]	**Concordance Core** abundance (ppm)[a]	Sources[c]	**Bulk Earth**[d] abundance (ppm)[a]
47	Ag (ppb)	$5.56\ ^{+2.79}_{-1.89}$	LK07, MA08, PO14	239 ± 90	KL93, MA08	81.3 ± 29.4
48	Cd	0.0383 ± 0.0056	LK07, MA08, PO14	0.167 ± 0.063	KL93, MA08	0.0800 ± 0.0208
49	In	0.0130 ± 0.0022	LK07, MA08, PO14	-	-	0.00879 ± 0.00148
50	Sn	0.118 ± 0.019	LK07, MA08, PO14	0.490 ± 0.185	KL93, MA08	0.239 ± 0.062
51	Sb (ppb)	5.69 ± 1.57	LK07, MA08, PO14	132 ± 50	KL93, MA08	46.8 ± 16.3
52	Te (ppb)	$9.18\ ^{+5.37}_{-2.68}$	LK07, MA08, PO14	1009 ± 382	KL93, MA08	334 ± 124
53	I (ppb)	$8.51\ ^{+9.98}_{-3.33}$	LK07, MA08, PO14	92.1 ± 34.9	KL93, MA08	$35.7\ ^{+13.2}_{-11.6}$
54	Xe (ppb)	0.00274 ± 0.00226	M12, H13	-	-	0.00185 ± 0.00152
55	Cs	0.0178 ± 0.0043	LK07, MA08, PO14	0.103 ± 0.039	KL93, MA08	0.0455 ± 0.0130
56	Ba	6.23 ± 0.47	LK07, MA08, PO14	-	-	4.21 ± 0.32
57	La	0.632 ± 0.042	LK07, MA08, PO14	-	-	0.427 ± 0.028
58	Ce	1.65 ± 0.11	LK07, MA08, PO14	-	-	1.11 ± 0.07
59	Pr	0.241 ± 0.018	LK07, MA08, PO14	-	-	0.163 ± 0.012
60	Nd	1.21 ± 0.08	LK07, MA08, PO14	-	-	0.815 ± 0.054
62	Sm	0.401 ± 0.026	LK07, MA08, PO14	-	-	0.270 ± 0.018
63	Eu	0.150 ± 0.010	LK07, MA08, PO14	-	-	0.101 ± 0.007
64	Gd	0.561 ± 0.024	LK07, MA08, PO14	-	-	0.379 ± 0.017
65	Tb	0.0964 ± 0.0073	LK07, MA08, PO14	-	-	0.0651 ± 0.0049
66	Dy	0.662 ± 0.043	LK07, MA08, PO14	-	-	0.447 ± 0.029
67	Ho	0.145 ± 0.011	LK07, MA08, PO14	-	-	0.0976 ± 0.0074
68	Er	0.430 ± 0.028	LK07, MA08, PO14	-	-	0.290 ± 0.019
69	Tm	0.0663 ± 0.0050	LK07, MA08, PO14	-	-	0.0447 ± 0.0034
70	Yb	0.433 ± 0.028	LK07, MA08, PO14	-	-	0.292 ± 0.019
71	Lu	0.0649 ± 0.0049	LK07, MA08, PO14	-	-	0.0438 ± 0.0033
72	Hf	0.277 ± 0.018	LK07, MA08, PO14	-	-	0.187 ± 0.012
73	Ta	0.0408 ± 0.0019	LK07, MA08, PO14	$0.00799\ ^{+0.00407}_{-0.00399}$	R11	0.0301 ± 0.0018
74	W	$0.0120\ ^{+0.0022}_{-0.0021}$	LK07, MA08, PO14	0.502 ± 0.190	KL93, MA08, R11	0.171 ± 0.062
75	Re (ppb)	0.322 ± 0.053	LK07, MA08, PO14	214 ± 81	KL93, MA08	69.8 ± 26.4
76	Os (ppb)	3.49 ± 0.28	LK07, MA08, PO14	2719 ± 1029	KL93, MA08	886 ± 335
77	Ir (ppb)	3.27 ± 0.17	LK07, MA08, PO14	2611 ± 989	KL93, MA08	851 ± 321
78	Pt (ppb)	6.86 ± 0.67	LK07, MA08, PO14	5448 ± 2063	KL93, MA08	1775 ± 671
79	Au (ppb)	0.915 ± 0.098	LK07, MA08, PO14	481 ± 182	KL93, MA08	157 ± 59
80	Hg (ppb)	$6.63\ ^{+11.75}_{-2.94}$	LK07, MA08, PO14	$32.3\ ^{+17.7}_{-16.3}$	KL93, MA08	$15.0\ ^{+9.8}_{-5.7}$
81	Tl (ppb)	2.92 ± 0.58	LK07, MA08, PO14	29.4 ± 11.1	MA08	11.5 ± 3.6
82	Pb	0.167 ± 0.014	LK07, MA08, PO14	$1.715\ ^{+1.585}_{-1.515}$	KL93, MA08	$0.670\ ^{+0.515}_{-0.492}$
83	Bi (ppb)	2.96 ± 0.52	LK07, MA08, PO14	$19.1\ ^{+10.9}_{-10.1}$	KL93, MA08	$8.21\ ^{+3.56}_{-3.30}$
90	Th	0.0746 ± 0.0068	LK07, MA08, PO14	-	-	0.0504 ± 0.0046
92	U	0.0198 ± 0.0020	LK07, MA08, PO14	-	-	0.0134 ± 0.0013
	Total	1.00×10^6		1.00×10^6		1.00×10^6

[a] ppm (by mass) unless otherwise indicated in column 2. Values have been rescaled $\sum_{\text{ppm}} = 10^6$, see Table A.2.

[b] LK07: Lyubetskaya and Korenaga [2007] columns 4 and 5 of their Table 3; MA08: McDonough and Arevalo [2008] columns 2 and 6 of their Table 1; PO14: Palme and O'Neill [2014] columns 5 and 6 of their Table 4; H13: Halliday [2013] columns 7, 10 and 13 of their Table 2; M12: Marty [2012] last column of his Table 1. See Sect. 2.2.2 for the details of our concordance PM abundances.

[c] for the key to the literature acronyms for core abundances, see footnote a of Table 2.

[d] Weighted sum (Eqs. A.5 & A.6) of concordance estimates of the abundances of primitive mantle and core.

2.3 Composition of the Core

2.3.1 Data sources

The density deficit of the Earth's core (compared to a pure Fe-Ni composition) suggests that the core contains a significant amount of one or more light elements. The liquid outer core is thought to have a density deficit of $3-12$ wt% [e.g., Stevenson, 1981; Anderson and Ahrens, 1994; McDonough, 2003], while the solid inner core is 3-6 wt% less dense than predicted [e.g., Anderson and Ahrens, 1994; Hemley and Mao, 2001]. The candidate light elements are still controversial and have been modeled and estimated in various ways and plausibly include Si, O, S and C [e.g. Fitoussi and Bourdon, 2012; Hirose et al., 2013; Litasov and Shatskiy, 2016].

We have compiled and combined a wide variety of recent work to construct concordance core abundances. These are listed in Tables 2.1 and 2.2 and include various constraints from various core compositional models, terrestrial fractionation curves and mass balance [e.g. Kargel and Lewis, 1993; Allègre et al., 1995; McDonough, 2003; Wood et al., 2006; McDonough and Arevalo, 2008], metal-silicate equilibrium [e.g. Rubie et al., 2011], the chemistry of core formation [e.g. Javoy et al., 2010], high-pressure and high-temperature experiments [Siebert et al., 2013], experiments based on sound velocity and/or density jumps [Huang et al., 2011; Nakajima et al., 2015], and numerical simulations [e.g. Zhang and Yin, 2012; Badro et al., 2014].

2.3.2 Concordance core estimate

Since many core abundances reported in the literature are model-dependent and are given without uncertainties, our concordance abundances (Tables 2.1 and 2.2) are unweighted averages (Eq. A.3) and exclude abundances that have been set to zero. Based on mass balance between the core and the silicate Earth, McDonough [2003] proposed both Si-bearing and O-bearing core models while McDonough and Arevalo [2008] presented a Si-bearing model only. The trace elements in the McDonough [2003] O-bearing model and McDonough and Arevalo [2008] Si-bearing model are highly correlated. Therefore we only count them once in our calculations. The details of how the literature values were combined into our concordance values with uncertainties are described in A.1.2.

Fig. 2.3 shows our concordance abundances for 49 elements in the core, compared with the literature values from which they were constructed. The sum of our concordance abundances of the 49 elements is scaled to 10^6 and listed in column 5 of Table 2.1. This is the most complete compilation for the core's composition to date. Table 2.2 lists the mean concordance concentrations of the 13 most abundant elements in the core along with the literature values from which they were constructed. Fig. 2.4 is a zoom-in of the 13 most abundant elements and shows this comparison in more detail. Fe-Ni alloy accounts for 87.90 ± 2.92 wt% of the total mass of the core. The most abundant light element in the core is Si, followed by O, S, and C. The other less abundant elements include Cr, P, Mn, Co, Na, Mg and H.

Table 2.2: Concentrations (wt%) of the 13 most abundant elements in the core

Sources[a]	Fe	Ni	Si	O	S	C	Cr	Mn	P	Co	Na	Mg	H
KL93	85.55	4.88	-	5.18	2.69	-	0.45	0.41	0.347	0.218	0.14	-	-
A01/95	79.4±2.0	4.87±0.30	7.35	5.0±0.5	1.21±0.20	-	0.78	0.582	0.369	0.253	-	-	-
M03	88.3	5.4	nil	3	-	-	-	0.03	-	-	-	-	-
W06	-	-	4.5±0.5	-	1.9	0.2	-	-	-	-	-	-	0.1
MA08	85	5.2	6.4	nil	1.9	0.2	0.9	0.005	0.32	0.25	-	-	0.06
J10	85.5±1.1	5.35±0.81	6.64±0.51	1.99±0.46	-	-	0.55±0.05	-	-	0.25±0.03	-	-	-
H11	-	-	-	0.5	-	-	-	-	-	-	-	-	-
R11	83.45±0.35	5.3±0.1	8.4±0.2	0.655±0.185	2	-	0.68±0.12	-	-	0.24±0.01	-	-	-
ZY12	-	-	2.0±0.2	1.0±0.1	-	0.4±0.3	-	-	0.096±0.060	-	-	0.06±0.03	0.014±0.008
H13	-	-	6	3	1.5±0.5	-	-	-	-	-	-	-	-
W13	-	-	-	-	-	1	-	-	-	-	-	-	-
S13	-	-	1.85±0.35	5.0±0.5	-	-	-	-	-	-	-	-	-
B14	-	-	1.94±0.21	3.8±0.7	nil	nil	-	-	-	-	-	-	-
N15	-	-	-	-	-	1.05±0.15	-	-	-	-	-	-	-
LS16	-	-	5.5±0.5	0.75±0.25	1.85±0.05	2	-	-	-	-	-	-	-
Mean[b]	**82.8±2.9**	**5.06±0.23**	**4.96±2.34**	**2.66±1.82**	**1.83±0.45**	**0.79±0.68**	**0.66±0.18**	**0.326**$^{+0.256}_{-0.290}$	**0.277**$^{+0.092}_{-0.124}$	**0.237±0.014**	**0.14±0.05**[c]	**0.06±0.03**	**0.057±0.042**

[a] K93: Kargel and Lewis (1993): column 6 of Table II
A95/A01: Allègre et al. (1995) Table 2 updated with Allègre et al. (2001) for S and O to 1.21 wt% and 5 wt% respectively.
M03: McDonough (2003): contents of Fe, O, Si, and Ni in O-bearing calculations listed in Table 7.
W06: Wood et al. (2006): last paragraph of Conclusions, 4-5 wt% Si, 1.9 wt% S, 0.1 wt% H and 0.2 wt% C
MA08: McDonough and Arevalo (2008) columns 3 and 7 of Table 1
J10: Javoy et al. (2010) column 4 of Table 6
H11: Huang et al. (2011): the optimal value of 0.5 wt% oxygen in the liquid outer core
R11: Rubie et al. (2011): average of the upper and lower limits of their three heterogeneous models listed in the last three columns of Table 2
ZY12: Zhang and Yin (2012): abundances of O, Mg, and Si are from the M52 simulation results for the core listed in Table 2; abundances of H, C, P, and N are the average of the upper and lower limits of their models A and B
H13: Hirose et al. (2013): 'preferred value' listed in Table 1
W13: Wood et al. (2013): Conclusions, of $\sim$ 1 wt% of carbon in the core
S13: Siebert et al. (2013): conclusion of an oxygen-rich core with 4.5 to 5.5 wt% O and 1.5 to 2.2 wt% Si
B14: Badro et al. (2014): the best numerical fit indicated in Fig.2
N15: Nakajima et al. (2015): conclusion of 0.9-1.2 wt% carbon in the core to match sound velocity
LS16 Litasov and Shatskiy (2016): a review of the composition of Earth's core with their best estimates for Si, O, S, and C.
[b] Unweighted mean of literature values (Eq. A.3), excluding nil estimates; the reported uncertainty is the standard deviation (Eq. A.4).
[c] The uncertainty of 0.05 is assigned by the average uncertainty of 40% of the 10 most abundant elements in the core (Appendix A).

2.4 Composition of the Bulk Earth

2.4.1 The core mass fraction

The elemental abundances of bulk Earth are the weighted averages of the elemental abundances of the primitive mantle and core. The accuracy of bulk Earth abundances therefore depends on the accuracy of the core mass fraction. However, literature values of the core mass fraction (Table 2.3) vary, and none has a reported uncertainty.

Our calculation of the core mass fraction is based on the two standard Earth radial density profile models: PREM [Dziewonski and Anderson, 1981] and ak135 [Kennett et al., 1995]. We take 3480±1 km for the core-mantle boundary (CMB) and 1218±3 km for the inner core boundary (ICB) [Souriau and Calvet, 2015]. We take 5972.2±0.6 $\times 10^{21}$ kg as the total mass of the Earth[1]. This recent update of the Earth's mass is due to more precise (and accurate) estimates of Newton's constant. We renormalize the radial density profiles of core and mantle to this new lower Earth mass, which results in an overall density lower by 0.00158 g/cm^3. We assume a typical uncertainty of 1% in the density profile models (Brian Kennett, personal communication). We include the correlation between core and mantle densities, the uncertainties of the ICB and the CMB, and the fact that an increase of radius can be compensated by a lower density. Thus, we obtain estimates for the mass fraction of the inner core (f_{ic}): $f_{ic} = 1.630 \pm 0.004$ wt% and of the outer core (f_{oc}): $f_{oc} = 30.840 \pm 0.296$ wt%. The mass fraction of the total core is $f_{ic} + f_{oc} = f_{core} = 32.5 \pm 0.3$ wt%. Correspondingly, the weighting factors for estimating the bulk Earth composition are f_{core} and $1 - f_{core}$ for the core and PM respectively (Eq. A.5).

2.4.2 Concordance bulk Earth estimate

Based on our concordance estimates of the elemental abundances of the primitive mantle and core, we estimate the bulk elemental abundances of the Earth with their weighted sum (Eq. A.5). The resultant bulk Earth composition and its associated uncertainty (Eq. A.6) are listed in column 7 of Table 2.1. The construction of bulk Earth abundances from primitive mantle and core for each element is plotted in Figs. 2.5(a) and 2.5(b) to demonstrate the geochemical differentiation between PM and core. In Fig. 2.5(b) we normalize the elemental abundances of PM and core to the concordance bulk Earth abundance and plot them as a function of 50% condensation temperature [Lodders, 2003].

Our main results are shown in Fig. 2.6 which shows the comparison of our concordance estimate of bulk Earth composition and the recent bulk Earth compositional datasets of Allègre et al. [2001], McDonough [2003], and McDonough and Arevalo [2008]. The light blue band in the lower panel indicates our estimate of the uncertainties on the concordance values. 70% of the literature points fall within this band. Fig. 2.7 zooms in on the comparison of the 15 most abundant elements, which account for $99.90^{+0.10}_{-1.49}$ wt% of the bulk Earth composition.

[1] "2016 Selected Astronomical Constants" in *The Astronomical Almanac Online*, USNO-UKHO.

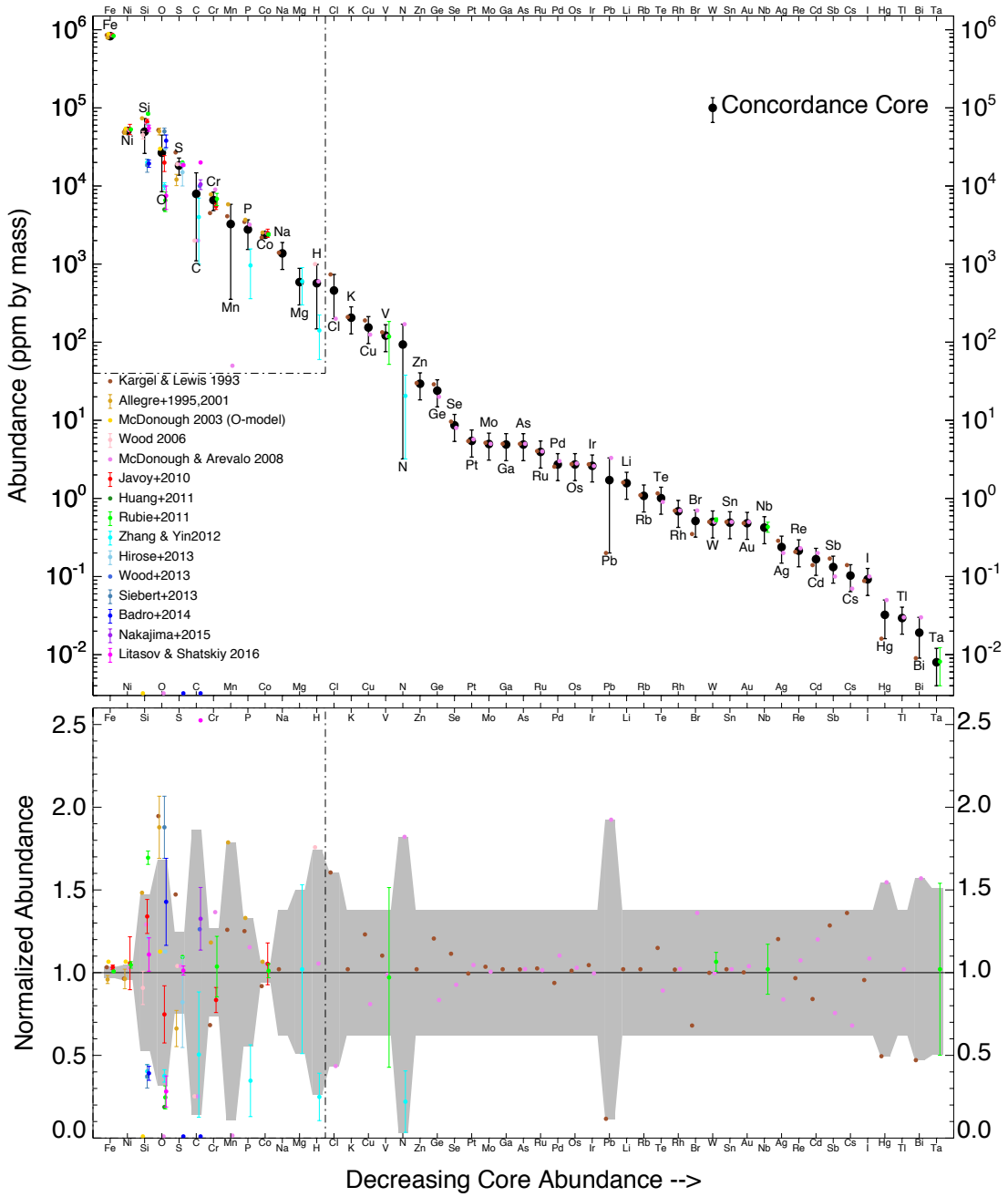

Figure 2.3: Recent literature estimates of 49 elemental abundances in the Earth's core and our concordance estimates constructed from them. Elements are plotted in order of decreasing core abundance. The upper panel plots ppm by mass. In the lower panel, literature values have been normalized to our core concordance estimates. The grey band in the lower panel indicates our estimate of the uncertainties on the concordance values. 79% of the literature points fall within this band. The dashed boxes on the left in both panels contain the 13 most abundant elements and are zoomed-in on in Fig. 2.4. Our core concordance ppm estimates have been rescaled down by 2.0% to constrain their sum to equal 10^6. We have not rescaled the literature values (see Appendix A.3, Table A.2).

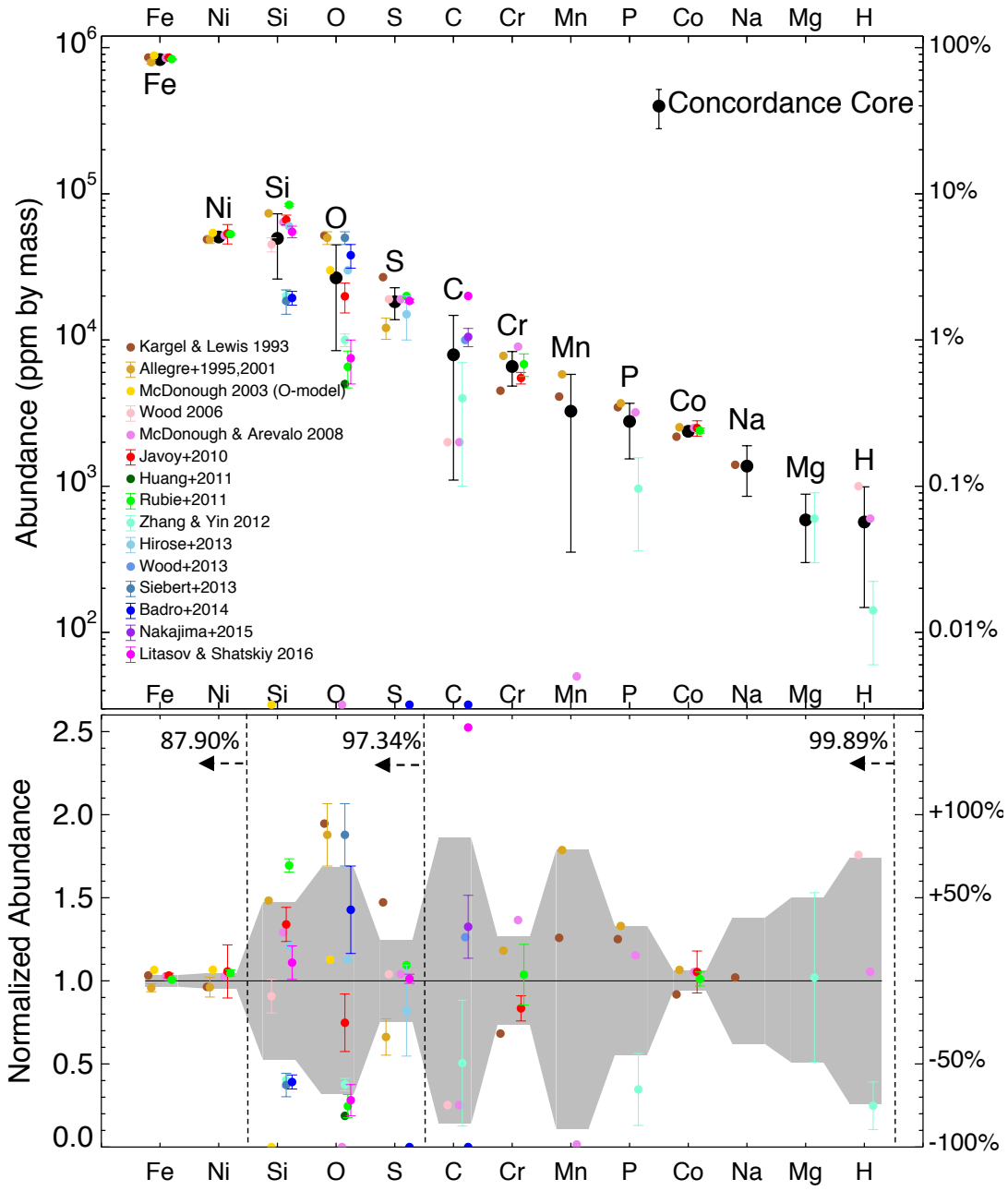

Figure 2.4: Zoom-in of the 13 most abundant elements contained in the dashed boxes in both panels of the previous figure. The sum of the Fe and Ni abundances make up $87.90 \pm 2.92\%$ of the total core mass. The 5 most abundant elements (Fe, Ni, Si, O, S) make up $97.34^{+2.66}_{-4.18}\%$, while the 13 most abundant elements plotted here make up $99.89^{+0.11}_{-4.25}\%$ of the total core mass. See Table 1 for details. The uncertainties on Si and O are not independent since to account for the density deficit in the core, high values of Si probably coincide with low values of O, and vice versa.

Table 2.3: Core mass fraction in the Earth

Reference	Core mass fraction (wt%)	Comments
Birch [1964]	32.4 and 32.7	solutions from two sets of density-velocity relations
Anderson and Kovach [1967]	32.5	see also Anderson [1989], using density profiles from Dziewonski and Anderson [1981] Preliminary Reference Earth Model (PREM model) based on seismological constraints.
Yoder [1995]	32.3	derived from estimates of the masses of inner core, outer core, and the Earth: 96.75×10^{21} kg, 1835×10^{21} kg, and 5973.6×10^{21} kg respectively; The GEM-T2 Gravitation Model [Marsh et al., 1990] and the PREM model [Dziewonski and Anderson, 1981] are cited.
Allègre et al. [1995, 2001]	32.5	derived from assumed masses of primitive mantle and core: 4090×10^{21} kg and 1967×10^{21} kg, respectively. Thus a total Earth mass of 6057×10^{21} is assumed; Anders [1977], Morgan and Anders [1980] and Wanke and Dreibus [1988] are cited.
McDonough [2003]	32.3	cites Yoder [1995]
Javoy et al. [2010]	32.4	no citations given
Hirose et al. [2013]	33	no citations given
Zeng [2015]	32.5	no citations given
This work	**32.5 $\pm$ 0.3**	seismological constraints based on the Dziewonski and Anderson [1981] PREM model, the Kennett et al. [1995] ak135 model, and the radii of inner core and outer core: 3480 ± 1 km and 1218 ± 3 km, respectively, from Souriau and Calvet [2015], along with the constraint of total mass of the Earth ($5972.2 \pm 0.6 \times 10^{21}$ kg, *the Astronomical Almanac Online, USNO-UKHO.*). See details in Section 2.4.1

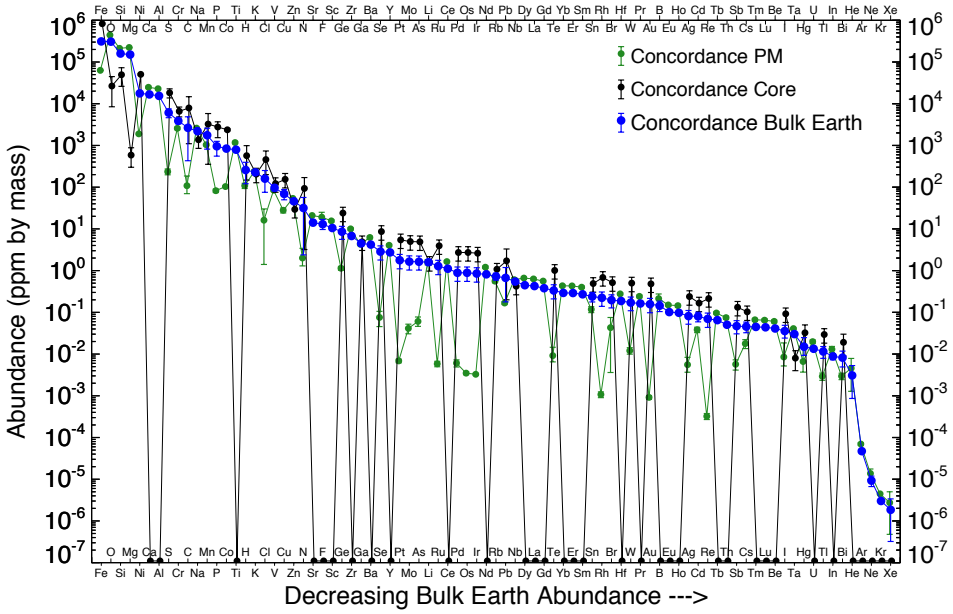

(a)

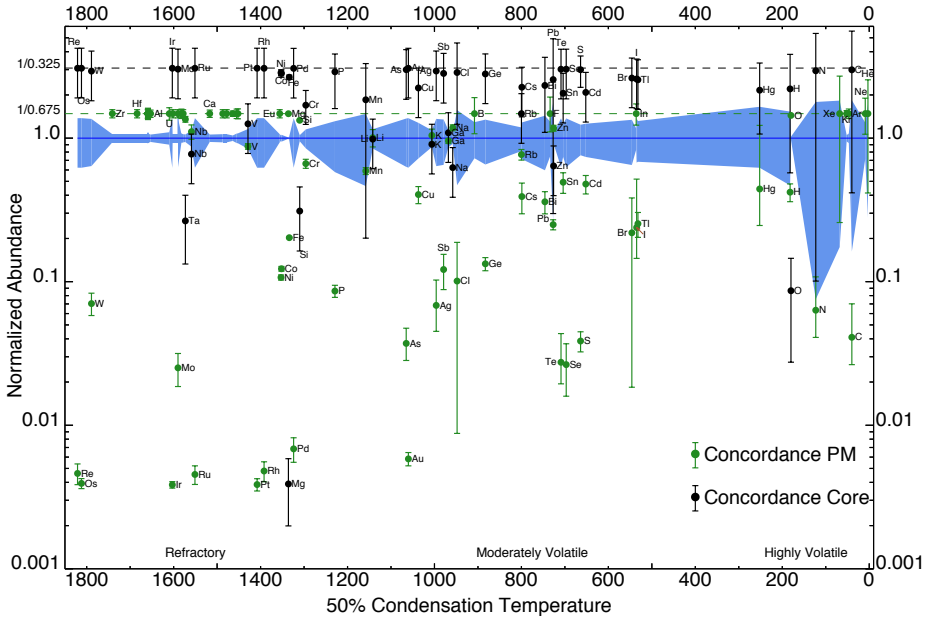

(b)

Figure 2.5: (a) The weighted sums of the concordance PM and the concordance core produce our concordance estimates of elemental abundances of the bulk Earth. The core abundances are weighted by our estimate of the core mass fraction: 32.5 ± 0.3 wt%. The PM abundances are weighted by 67.5 ± 0.3 wt% $(= 100 - 32.5)$. Elements with nil or extremely low abundance in the core are plotted on the x-axis. (b) Concordance PM and core abundances normalized to the concordance bulk Earth abundances and plotted as a function of 50% condensation temperatures [Lodders, 2003]. Refractory elements are on the left, volatiles on the right. Refractory lithophile elements are the green points at normalized abundance of ~ 1.5 $(\approx 1/0.675)$. Refractory siderophiles are the black points at a normalized abundance of ~ 3 $(\approx 1/0.325)$.

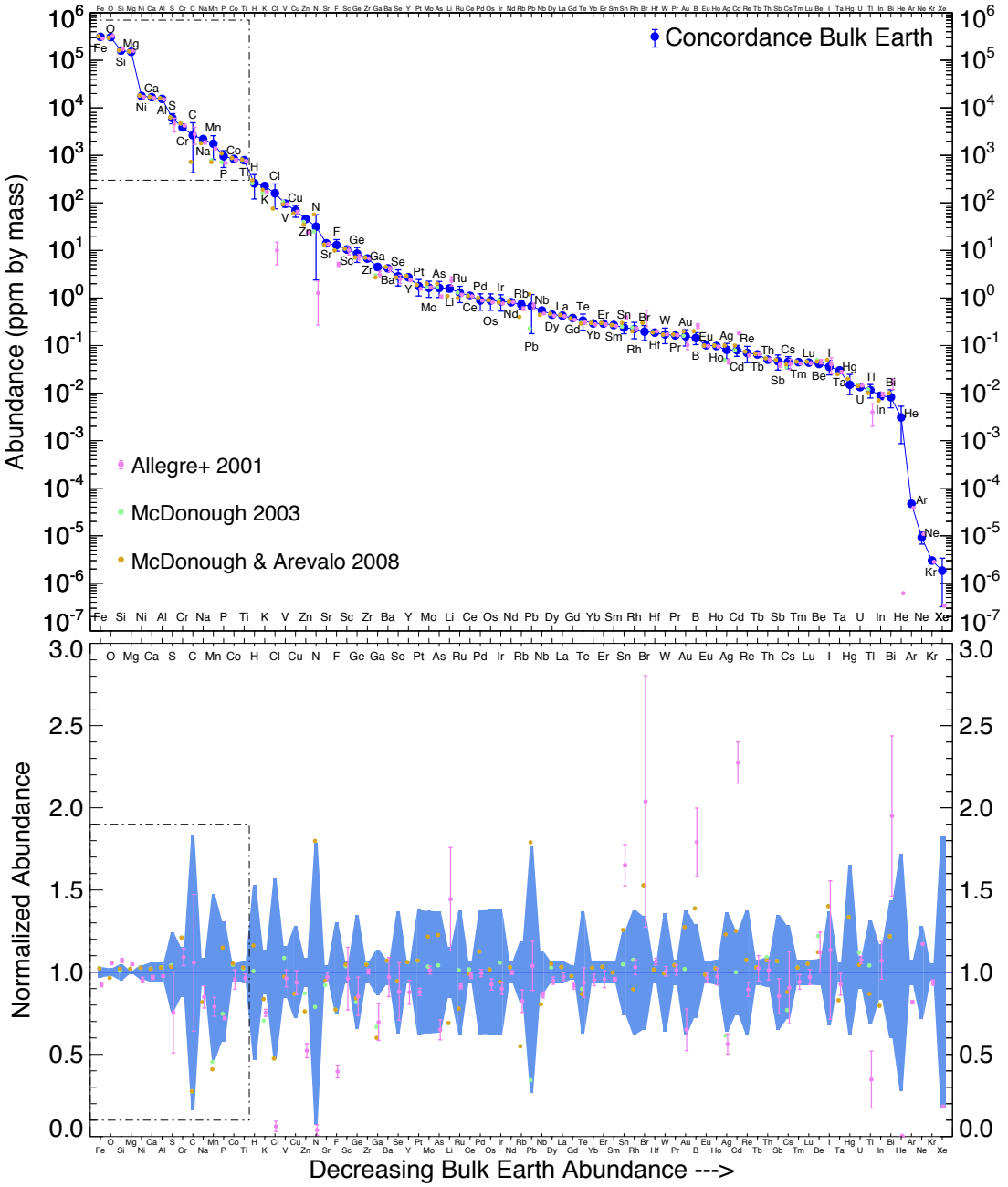

Figure 2.6: Comparison of our concordance bulk Earth elemental abundances (last column of Table 2.1) with the recent estimates of Allègre et al. [2001], McDonough [2003], and McDonough and Arevalo [2008]. Elements for which McDonough [2003] and McDonough and Arevalo [2008] reported identical values are plotted as McDonough and Arevalo [2008] points. In the lower panel the literature values from the top panel are normalized to our concordance values. The blue band in the lower panel indicates our estimate of the uncertainties on the concordance values. 70% of the literature points fall within this band. The sum of our bulk Earth abundances is 10^6 since we have rescaled the concordance PM and core abundances to 10^6 (see Appendix C). The literature abundances have not been rescaled to ensure their abundances sum to 10^6. The dashed boxes on the left in both panels contain the 15 most abundant elements and are zoomed-in on in Fig. 2.7.

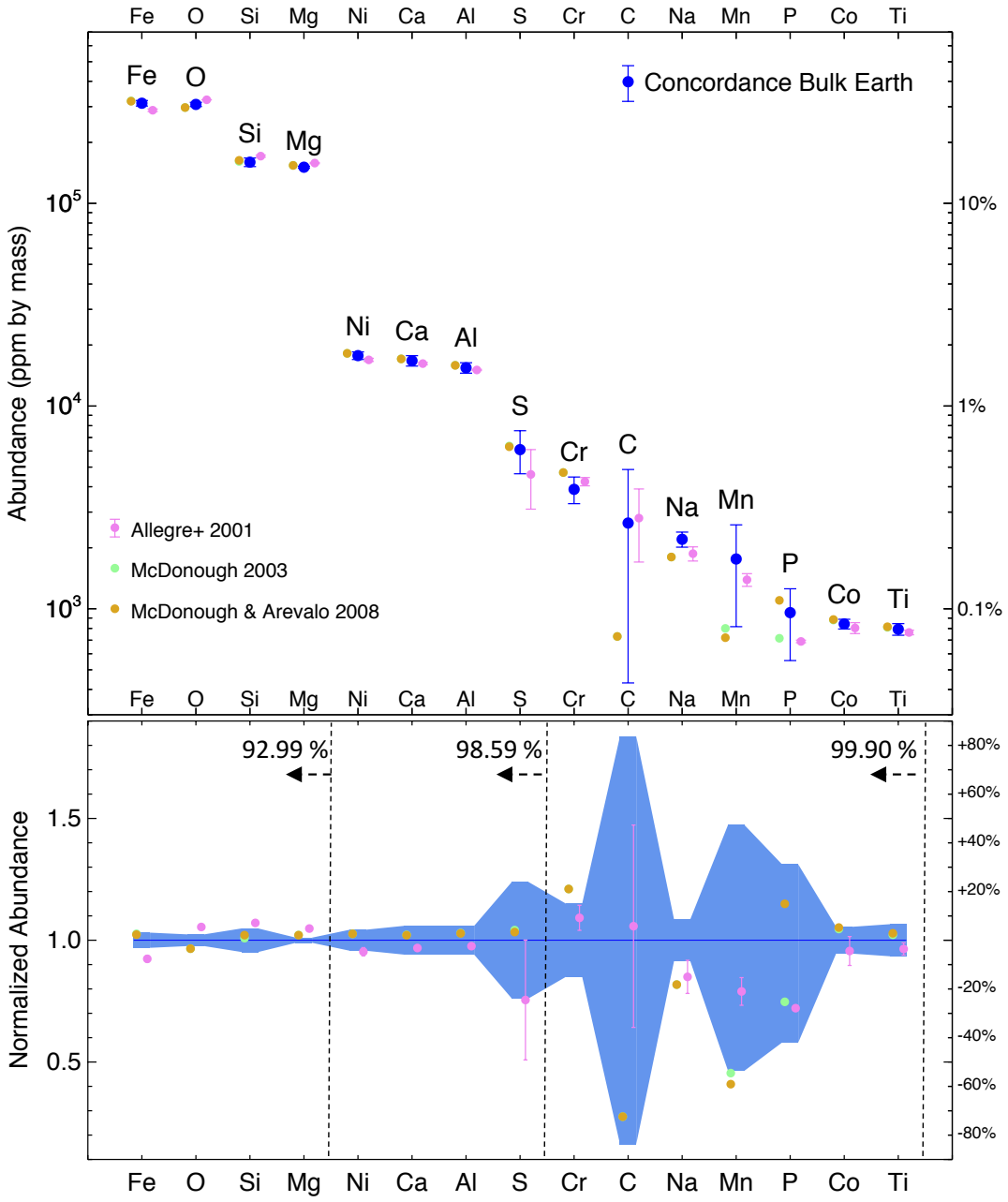

Figure 2.7: Zoom-in of the 15 most abundant elements contained in the dashed boxes in both panels of the previous figure. The sum of the abundances of the 4 most abundant elements (Fe, O, Si, Mg) make up $92.99 \pm 1.45\%$ of the total mass of the Earth. The 8 most abundant elements (Fe, O, Si, Mg, Ni, Ca, Al, S) make up $98.59^{+1.41}_{-1.47}\%$, while the 15 most abundant elements plotted here make up $99.90^{+0.10}_{-1.49}\%$ of the total mass of the Earth. Our Mg abundance is significantly lower than previous estimates. Our estimates of the uncertainties allow the evaluation of the significance of such differences. Reported values without uncertainties do not allow such a comparison.

2.5 Discussion

2.5.1 Comparison with previous estimates

Compared to our concordance values, the abundances of some elements reported by McDonough [2003] and McDonough and Arevalo [2008] are significantly different (where the significance of the difference can only be based on our reported uncertainties). Relative to our values, their abundances for Mg, Cr, Br, Sn, Cd, B and Be are significantly higher, while their abundances for O, Na, Mn, Zn, Ga, Li, Rb, Nb, Ta and In are significantly lower, where "significant" means their value is outside our estimate of the uncertainty (Figs. 2.6 & 2.7).

The bulk elemental abundances with uncertainties in Allègre et al. [2001] were determined systematically by a carbonaceous chondrite correlation line, in combination with the abundances of siderophile and chalcophile elements in Allègre et al. [1995]. These works largely depend on the accuracy of the analyses of CI, CM, CO and CV meteorites compiled in Wasson and Kallemeyn [1988]. For many elements, their mean values and/or their uncertainties are different from our results. For example, relative to our values, the Allègre et al. [2001] abundances for O, Si, Mg, Sn, Rh, B and Cd are high, while their abundances for Fe, K, Cl, Zn, N, F, Ga, Tl, He and Ar are low. One reason for these differences are the different assumptions made. For example, the estimate of nitrogen abundance in the Earth in Allègre et al. [2001] is based on the atmospheric inventories while our estimate is based on the comparison of Earth's mantle with carbonaceous chondrite data in McDonough and Arevalo [2008] and Palme and O'Neill [2014]. Allègre et al. [2001] deduced Earth's chlorine abundance from the Cl/Ba ratio in MORB, while our PM sources [Lyubetskaya and Korenaga, 2007; McDonough and Arevalo, 2008] derived Cl from the Cl/K ratio in MORB (Sect. 2.2). Other reasons for the abundance differences and differences in uncertainties are updates to PM and core abundances, and the use of slightly different core mass fractions: McDonough [2003] or McDonough and Arevalo [2008] (32.3 wt%), Allègre et al. [2001] (32.5 wt%), and this work (32.5±0.3 wt%).

Based on Eq. A.7, we quantify the significance of the deviation of our concordance bulk Earth abundances from previous estimates [Allègre et al., 2001; McDonough, 2003; McDonough and Arevalo, 2008]. Among our new bulk elemental abundances, 6 elements (Mg, Sn, Br, B, Cd and Be) are more than $\sim 1\sigma$ below previous estimates, and 14 elements (Na, K, Cl, Zn, Sr, F, Ga, Rb, Nb, Gd, Ta, He, Ar, and Kr) are more than $\sim 1\sigma$ above previous estimates (see Table A.1).

The reasons for these significant abundance differences include different assumptions and our inclusion of updated PM and core abundances. Mg and Na are the most abundant elements for which our new estimates deviate by more than $\sim 1.5\sigma$ from previous estimates. Our Mg PM abundance of 22.3±0.2 wt% is $\sim 2.5\sigma$ lower than the 22.8 wt% of McDonough and Arevalo [2008] and $\sim 5\sigma$ lower than the 23.4 wt% of Allègre et al. [2001] (deduced from their 15.8 wt% Mg bulk abundance and a 67.5 % PM mass fraction). Our lower bulk Earth Mg abundance predominantly comes from the lower PM Mg abundance in Palme and O'Neill [2014]. Our bulk

Earth Na abundance is higher than McDonough and Arevalo [2008] and Allègre et al. [2001] because unlike those authors, we have included Na in the core: 1372±519 ppm [Kargel and Lewis, 1993].

Palme and O'Neill [2014] state that the 6 most abundant elements in the PM make up 98.41 ± 0.01 wt%. We get a higher value with a much larger uncertainty: 98.96 ± 0.72 wt%. McDonough [2016] states (based on chondritic models) that Fe, O, Si and Mg make up more than 90% of the mass for the bulk Earth and the addition of Ni, Ca, Al and S accounts for more than 98% by mass. Consistent with these estimates, we find 92.99± 1.45 wt% for Fe, O, Si and Mg and $98.59^{+1.41}_{-1.47}$ wt% with the addition of Ni, Ca, Al and S.

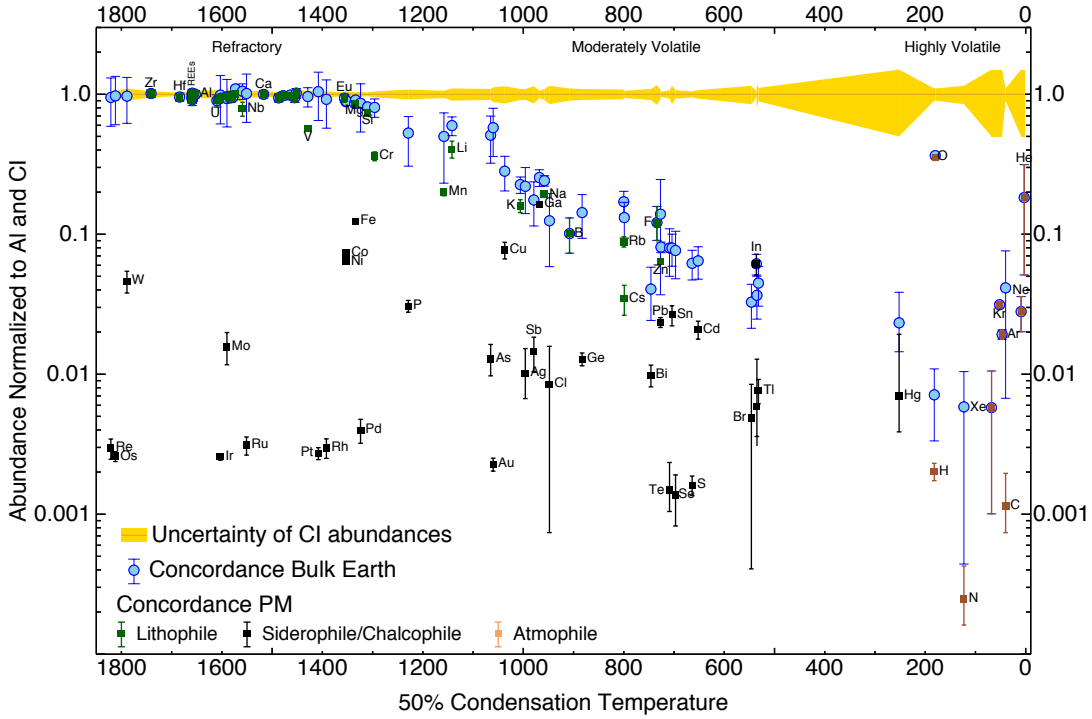

Figure 2.8: Our concordance bulk Earth and primitive mantle abundances normalized to Al and CI chondrites. Thus, for a generic element X, the bulk Earth (blue dots) we plot: $(X/\mathrm{Al})_{Earth}/(X/\mathrm{Al})_{CI}$ and analogously for the concordance PM (square points) we plot: $(X/\mathrm{Al})_{PM}/(X/\mathrm{Al})_{CI}$. Both are plotted as a function of 50% condensation temperatures [Lodders, 2003]. CI abundances and uncertainties are from Table 3 of Palme et al. [2014], except for the uncertainties of the noble gases which we have set at the same ±50% uncertainty of Hg.

Fig. 2.8 presents another way to present our PM and bulk Earth compositions (with uncertainties) in comparison with the latest compilation [Palme et al., 2014] of CI chondritic abundances. In Fig. 2.8, we have normalized both the bulk Earth and PM abundances to the highly refractory element Al and CI chondrites. More specifically, for a generic elemental abundance X, for the bulk Earth we plot:

$(X/\mathrm{Al})_{\mathrm{Earth}}/(X/\mathrm{Al})_{\mathrm{CI}}$ and for the concordance PM we plot: $(X/\mathrm{Al})_{\mathrm{PM}}/(X/\mathrm{Al})_{\mathrm{CI}}$. This figure can be directly compared with Fig. 1 of Wood et al. [2006], Fig. 1 of Carlson et al. [2014] and Fig. 21 of Palme and O'Neill [2014]. Those three figures have been normalized to Mg and CI chondrites. Because of their large abundances, Mg or Si have often been chosen as a normalization reference element [McDonough, 2003; Palme and O'Neill, 2014; Carlson et al., 2014; Litasov and Shatskiy, 2016]. However both Mg and Si are not strictly refractory elements. They both have condensation temperatures slightly lower than the transition or critical temperature ($\sim$ 1400 K), below which the devolatilization of the Earth, compared to CI, is clear. Thus, with a Mg normalization, a slight depletion of bulk Earth Mg compared to CI chondritic Mg, is misrepresented as an enrichment of refractory lithophiles.

Our PM analysis does not include estimates from Javoy et al. [2010] who only report the PM abundances of ten elements (O, Mg, Si, Fe, Al, Ca, Ti, Ni, Cr, and Co) based on their enstatite chondrite model. If these abundances were included in our analysis they would lower Al, Ca and Ti without lowering the other RLEs such as Be, Sc, Sr, Nb, REE (Rare Earth Elements), Th and U. Also, enstatite chondrites are silica-enriched (but oxygen depleted?), from which it is problematic to construct the silica-poor (peridotitic) terrestrial model [Fitoussi and Bourdon, 2012; Jellinek and Jackson, 2015].

2.5.2 Unresolved Issues

We have assumed that the bulk Earth consists of the primitive mantle and the core, and that the primitive mantle is a reservoir with the composition of the present-day Earth's mantle, crust and surface inventories taken together. Contributions of late accretion to the formation of a secondary atmosphere of the Earth introduces some ambiguity to this definition. We also neglected Earth's primary atmosphere (likely dominated by H and He) formed at the stage of solar nebula. In limiting our calculations to the prevalent standard models of the PM [Lyubetskaya and Korenaga, 2007; McDonough and Arevalo, 2008; Palme and O'Neill, 2014] we ignore the possible heterogeneity between the lower mantle and the upper mantle. Impact erosion is another issue that could have changed the PM abundances of incompatible lithophile elements. If we considered the impact erosion model of O'Neill and Palme [2008], for example, the PM abundance of K would decrease by about a factor of 2.

Recently, based on i) a high PM abundance of the chalcophile element In, ii) nucleosynthetic isotope anomalies and iii) high- and low-pressure-temperature metal-silicate partitioning data, Wang et al. [2016] suggested that Earth's moderately volatile element composition may not be chondritic.

Another concern could be that we compute weighted averages when combining the elemental abundances of the primitive mantle while we compute unweighted averages for the core. Considering the global consistency of the PM abundance datasets [i.e., Lyubetskaya and Korenaga, 2007; McDonough and Arevalo, 2008; Palme and O'Neill, 2014], computing weighted averages is appropriate. Unlike the PM, core compositional models are much more complex and mixed with experimental data.

Furthermore, uncertainties are not given in the majority of reported core compositional estimates, so computing weighted averages is not an option.

The degree to which the bulk compositions of Venus and Mars are different from the Earth [Morgan and Anders, 1980; Wanke and Dreibus, 1988] or broadly similar [Taylor, 2013; Kaib and Cowan, 2015; Fitoussi et al., 2016] is still unclear.

2.6 Summary and Conclusions

As the solar nebula condensed, evaporated and fractionated to form the early Earth [Urey, 1964; Grossman and Larimer, 1974; O'D. Alexander, 2001; Wood et al., 2006; Carlson et al., 2014], the chemical composition of the bulk Earth was essentially established. From a heterogeneous set of literature values, we present the most complete lists of the elemental abundances *with uncertainties* of the primitive mantle (PM), the core and the bulk Earth (Table 2.1, Figs. 2.1-2.4,2.6,2.7). The four most abundant elements (O, Mg, Si, and Fe) make up 94.19±0.69% of the total PM mass. Fe-Ni alloy accounts for 87.90±2.92 wt% of the total mass of the core, and the major light elements in the core are Si, O, S, C, Cr, Mn, P, Co, Na, Mg and H in order of decreasing abundance. The concordance bulk Earth abundances with uncertainties come from the weighted average of our concordance PM and core. The weighting factor for this average comes from our new estimate (with uncertainty) of the core mass fraction of the Earth: 32.5±0.3 wt%. Our concordance estimate of bulk Earth composition is largely consistent with recent bulk elemental abundance estimates; 70% of the previous bulk elemental abundances are within the uncertainties of our concordance bulk elemental abundances. Compared to previous work, the most significant differences include: 1) our abundances of Mg, Sn, Br, B, Cd and Be are more than $\sim 1\sigma$ lower, and 2) our abundances of Na, K, Cl, Zn, Sr, F, Ga, Rb, Nb, Gd, Ta, He, Ar and Kr, more than $\sim 1\sigma$ higher (Table B.4). This set of concordance estimates (*with uncertainties*) for the elemental abundances of PM, core and bulk Earth provides a reference that can be used to compare the Earth to the Sun, which will lead to a more precise devolatilization pattern, potentially applicable to exoplanets and their host stars.

Chapter 3

Protosolar Elemental Abundances and the Devolatilization that Led to the Earth

This chapter is adapted from Wang et al. [2018b] submitted to Icarus as

Wang, H. S., Lineweaver, C. H., Ireland, T. R. 2018. The Volatility Trend of Protosolar and Terrestrial Elemental Abundances. https://arxiv.org/abs/1810.12741.

Abstract

We present new estimates of protosolar elemental abundances based on an improved combination of solar photospheric abundances and CI chondritic abundances. We compare our new protosolar abundances with our recent estimates of bulk Earth composition, thereby quantifying the devolatilization of the solar nebula that led to the formation of the Earth. As a function of elemental 50% condensation temperatures (T_C) we fit the Earth-to-Sun abundance ratios f to the linear trend $\log(f) = \alpha \log(T_C) + \beta$. The best fit coefficients are: $\alpha = 3.676 \pm 0.142$ and $\beta = -11.556 \pm 0.436$. The quantification of the slope α provides an empirical observation upon which modeling of the devolatilization processes can be based. The coefficients α and β also determine a critical devolatilization temperature for the Earth $T_{\rm D}({\rm E}) = 1391 \pm 15$ K. The terrestrial abundances of elements with $T_C < T_{\rm D}({\rm E})$ are depleted compared with solar abundances, whereas the terrestrial abundances of elements with $T_C > T_{\rm D}({\rm E})$ are indistinguishable from solar abundances. The abundances of noble gases and hydrogen are depleted more than a prediction based on the extrapolation of the best-fit volatility trend. The terrestrial abundance of Hg (T_C = 252 K) appears anomalously high under the assumption that solar and CI chondrite Hg abundances are identical. To resolve this anomaly, we propose that CI chondrites have been depleted in Hg relative to the Sun by a factor of 13 ± 7. We use the best-fit volatility trend to de-

rive the fractional distribution of carbon and oxygen between volatile and refractory components ($f_{\rm vol}$, $f_{\rm ref}$). For carbon we find (0.91 ± 0.08, 0.09 ± 0.08). For oxygen we find (0.80 ± 0.04, 0.20 ± 0.04). Our preliminary estimate gives CI chondrites a critical devolatilization temperature $T_{\rm D}({\rm CI}) = 550^{+20}_{-100}$ K.

3.1 Introduction

To first order, the Earth is a devolatilized piece of the solar nebula. Similarly, rocky exoplanets are almost certainly devolatilized pieces of the stellar nebulae out of which they and their host stars formed. If this is correct, we can estimate the chemical composition of rocky exoplanets by measuring the elemental abundances of their host stars, and then applying a devolatilization algorithm. The main goal of this paper is to go beyond the usual comparison of the silicate Earth with CI chondrites. We do this by comparing the bulk elemental abundances of the Earth and Sun, and thus calibrate this potentially universal process associated with the formation of terrestrial planets.

Determining the chemical abundances of the Earth and Sun is not straightforward. For Earth, the composition must be obtained by determining the chemical abundances in primitive mantle and core, and by determining the mass fractions of these respective reservoirs. Different geochemical models make different underlying assumptions about the behavior of specific elements. However, for the purposes of this work (and for any comparative analysis), justifiable determinations of the contributions of these differences to the systematic uncertainties in the elemental abundances are required. Thus, for our analysis here, we use the bulk Earth abundances and their uncertainties from Wang et al. [2018a]. We extend our modeling of terrestrial abundances to a comparison with solar abundances. This will help quantify the processes that led to the rocky planets of our solar system, as well as by extension, to rocky exoplanets.

For the Sun, chemical abundances of a large number of elements can be determined spectroscopically, specifically by observing characteristic absorption lines in the solar photosphere. Such determinations require accurate models of the solar circulation and calibration based on radiative transfer calculations. Such calculations typically result in abundances with relatively large uncertainties, compared to the precision available from laboratory geochemical analyses. CI chondrites are therefore frequently used as a proxy in the determination of the relative abundances of many refractory elements in the Sun. Nevertheless, the abundances of some elements in CI chondrites are not representative of the abundances in the Sun. These include the most highly volatile elements (H, He and the other noble gases) as well as other elements with significant gas phase abundances (e.g. C, N, and O).

A characteristic feature of the comparison of protosolar abundances (i.e. based on photospheric and CI chondrite abundances) and terrestrial abundances, is the depletion of terrestrial abundances for elements with moderate condensation temperatures between 500 K and 1400 K. The depletion is systematic: the lower the condensation temperature, the greater the depletion. This depletion provides *quantitative* insights into the processes active in the early solar system and the fractionation of elements between gas and solid phases. Melting and vaporization experiments [Norris and Wood, 2017] and isotopic analyses [Hin et al., 2017; Pringle et al., 2017] yield complementary insights into devolatilization processes.

We organize this work as follows. In Section 2 we present estimates of protosolar

abundances based on meteoritic and photospheric data; in Section 3 we compare the Sun with the bulk Earth and quantify a devolatilization pattern. In Section 4 we compare our results to previously published volatility trends and discuss the difficulties of extrapolating the pattern to more volatile elements. We also discuss the comparison of depletion features between the Earth and CI chondrites relative to the Sun. Section 5 is our summary.

3.2 Protosolar Elemental Abundances

3.2.1 Meteoritic and photospheric elemental abundances

Analyses of CI chondrites yield abundances of 83 stable elements – many with high precision. However, not all these elemental abundances reflect protosolar abundances. Highly volatile elements, such as H, C, N, O, and the noble gases, are depleted in CI chondrites [Anders and Grevesse, 1989; Lodders, 2003]. CI chondrite abundances are good proxies of protosolar abundances only for the non-highly-volatile elements ($T_C \gtrsim 550$ K). Our analysis uses the CI chondritic abundances from the latest compilation by Palme et al. [2014] which are based on Lodders et al. [2009], Barrat et al. [2012], and Pourmand et al. [2012] (see our Table 3.2, columns 7 & 8).

Fewer elemental abundances can be inferred from spectroscopic observations of the solar photosphere. The inferences depend on the availability of spectral lines, the accuracy of atomic data, solar model atmospheres and spectral line formation calculations. For example, solar atmosphere spectral-line abundances for 13 elements are unavailable (As, Se, Br, Sb, Te, I, Cs, Ta, Re, Pt, Hg, Bi, and U). Some elements' lines (e.g. F, Cl, I and Tl) can only be identified in the spectra of sunspots because sunspot temperatures are lower than average photospheric temperatures [see Sect. 3.8 of Asplund et al., 2009]. The abundance uncertainties of these elements are correspondingly larger.

Due to lithium burning in the interior of the Sun and to mixing between the interior and the photosphere, lithium is depleted in the present-day solar photosphere. In the absence of available photospheric lines for the noble gases He, Ne, Ar, Kr, and Xe, the photospheric abundances of these elements can be estimated through helioseismology, solar winds/corona/flares, and theoretical calculations (see Sect. 3.9 of Asplund et al. [2009]). Our compilation of photospheric abundances (Table 3.2, column 3) are from Asplund et al. [2009], Scott et al. [2015a,b], and Grevesse et al. [2015]. These are based on a state-of-the-art, 3D hydrodynamic solar model atmosphere with non-LTE (= non-Local Thermodynamic Equilibrium) spectral line calculations whenever possible, in which statistical and systematic abundance uncertainties have been uniformly estimated.

Fig. 3.1 shows the comparison between solar photospheric abundances and CI chondritic abundances (columns 6 and 10 of Table 3.2 respectively). The abundances are nearly identical with some exceptions: i) 13 elements in the lower left do not have photospheric observations; ii) lithium's abundance is depleted in the photosphere but is well-preserved in CI chondrites; iii) 9 highly volatile elements are moderately or

severely depleted in CI chondrites, but their abundances can be determined through indirect observations and theoretical modeling of solar spectra. In general, the precision of meteoritic data (red) is higher than that of the photospheric data (blue).

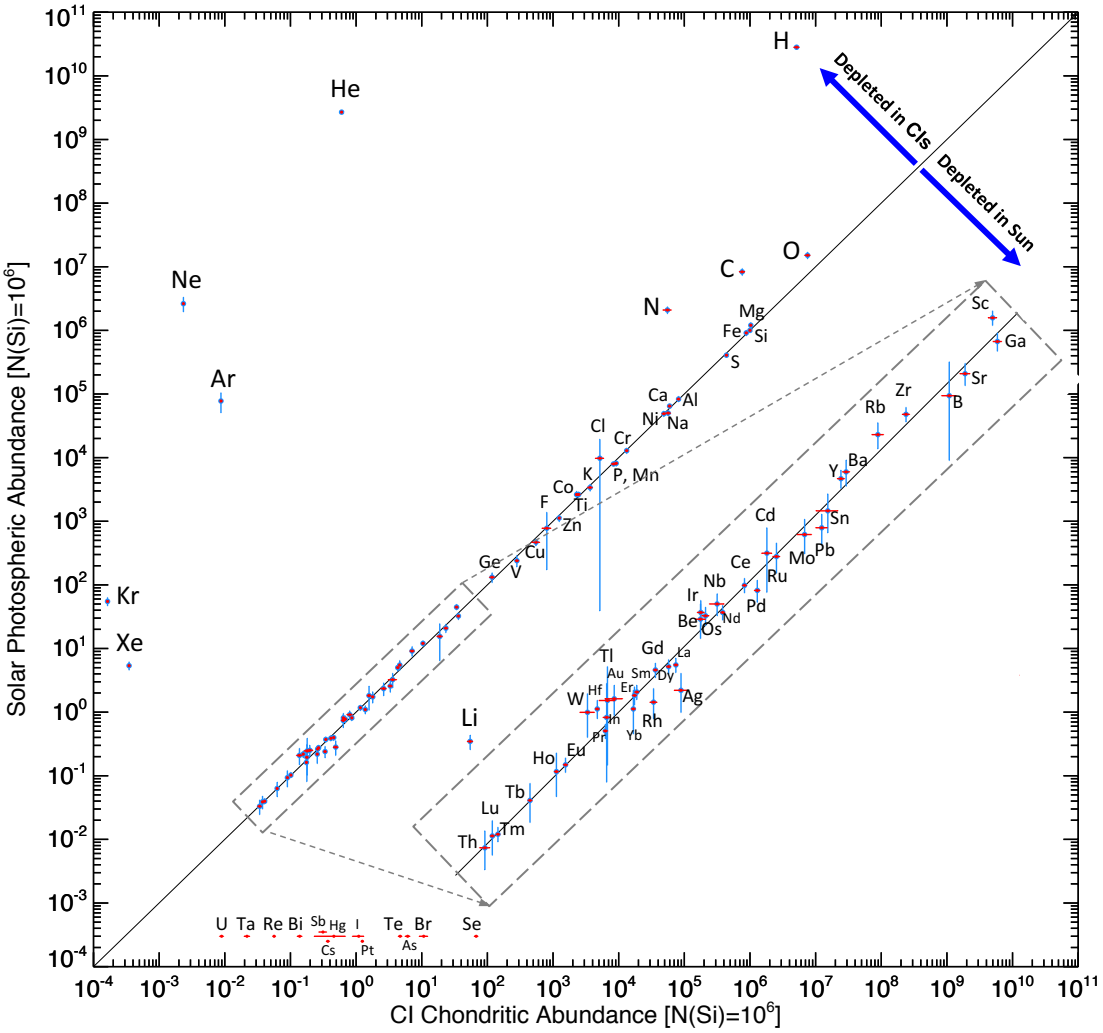

Figure 3.1: Similarity of meteoritic and photospheric abundances. Abundances have been normalized to 10^6 atoms of Si (Table 2, columns 6 and 10). Points along the diagonal have identical abundances in both data sets. Elemental abundances above the diagonal are depleted in CIs (N, C, O, H and noble gases). Elemental abundances below the diagonal are depleted in the Sun (Li). Photospheric abundances of 13 elements are unavailable. They are set arbitrarily at 3×10^{-4} and plotted on the left just above the x-axis. Uncertainties of CI chondritic abundances of noble gases are unavailable.

The observed isotopic heterogeneity of the inner Solar System [e.g. Trinquier et al., 2009; Luck et al., 2003, 2005; Pringle et al., 2014; Poitrasson et al., 2004] suggests that isotopic differences between CI and the Sun could exist. However, their effects

Table 3.1: Combining photospheric and meteoritic abundances: how our method compares with the method of Lodders et al. [2009]

SM#	This Work		Lodders et al. [2009]	
	Elements	Number	Elements	Number
p	H, C, N, O, He, Ne, Ar, Kr, Xe	9	H, C, N, O, He, Ne, Ar, Kr, Xe	9
m	Li, As, Se, Br, Sb, Te, I, Cs, Ta, Re, Pt, Hg, Bi, U	14	Li, As, Se, Br, Sb, Te, I, Cs, Ta, Re, Pt, Hg, Bi, U, Be, B, F, Si, Cl, Ca, Sc, Ti, Mn, Cu, Zn, Ga, Rb, Sr, Ru, Ag, Cd, In, Sn, La, Nd, Sm, Tb, Ho, Tm, Yb, Lu, Hf, W, Os, Au, Tl, Pb, Th	48
a	Be, B, F, Na, Al, Si, P, S, Cl, K, Ca, Ti, V, Cr, Mn, Fe, Co, Ni, Cu, Zn, Ga, Ge, Sr, Y, Zr, Nb, Mo, Ru, Cd, In, Sn, Ba, Ce, Pr, Nd, Sm, Eu, Gd, Tb, Dy, Ho, Er, Tm, Yb, Lu, Os, Au, Tl, Pb, Th, Mg*, Sc*, Rh*, Pd*, Ag*, La*, Hf*, Rb*, W*, and Ir*	60	Na, Mg, Al, P, S, K, V, Cr, Fe, Co, Ni, Ge, Y, Zr, Nb, Mo, Rh, Pd, Ba, Ce, Pr, Eu, Gd, Dy, Er, Ir	26

SM- Selection methods: 'p'- photospheric data only; 'm'- meteoritic data only; ''a'- weighted average of photospheric and meteoritic data
* for each of these 10 elements, uncertainty in the meteoritic abundance does not overlap with the uncertainty in the photospheric abundance. We compute the weighted mean in the usual way (Eq. B.8), however to be conservative, for the uncertainties, instead of using Eq. B.9, we use the upper and lower limits of the uncertainties of the photospheric and meteoritic abundances.

on estimates of the elemental abundances of the proto-Sun is not well enough understood to be included in our analysis, and such effects should be minor in comparison to the abundance uncertainties.

3.2.2 Methods used to combine photospheric and meteoritic abundances

Lodders et al. [2009] compiled and combined meteoritic and photospheric data to estimate protosolar abundances. We update this important compilation by combining photospheric-based solar abundances and CI chondritic abundances (Table 3.2 columns 6 and 10 respectively) using the following method (see Table 3.1). (1) The 9 elements in the first group labeled 'p'- are depleted in meteorites. Therefore we use only their photospheric-based solar abundances. Lodders et al. [2009] did the same. (2) 13 elements in the second group labeled 'm'- have not had their photospheric abundances measured. In addition, Li is included because its current photospheric abundance is depleted compared to its protosolar abundance. We place 14 elements in this group while Lodders et al. [2009] places 48. (3) The abundance of an element in the third group (labeled 'a') is the weighted average of its photospheric-based solar abundance and its meteoritic abundance. We place 60 elements in this category, while Lodders et al. [2009] places 26. Also, we use diffusion corrections to convert photospheric abundances to bulk solar abundances before (rather than after) they are normalized and combined with meteoritic data. This is because diffusion and settling issues affect photospheric abundances, not meteoritic abundances. For details see Appendices B.1 & B.2.

Compared with the method of Lodders et al. [2009], our method of combining meteoritic and photospheric data rejects less of the photospheric data and places more emphasis on averaging the two independent data sets. Lodders et al. [2009] has placed 48 elements in the second (meteorite-only) group either because the photospheric and meteoritic abundances are inconsistent, or because the uncertainty on the photospheric abundance is substantially larger than the uncertainty on the meteoritic abundance. Including photospheric abundances based partly on their similarity with the meteoritic evidence is not advisable [Scott et al., 2015a], since both meteoritic and photospheric data are only proxies of the bulk protosolar abundances. Both have limitations. The most primitive CI chondrite group comprises only 6 meteorites for a total mass of only 17 kg. Of these, Orgeuil is the largest with around 10 kg recovered, and this is the meteorite with the largest number of independent measurements. As such, the abundances from CI chondrites are based on an extremely small subsample of meteorites. Furthermore, these meteorites have experienced substantial fluid activity on the meteorite parent body, which could have mobilized the hydrophilic alkali metals – e.g. Na, K and Rb, as well as other elements that are mobile in fluid – e.g. S, Ca, Sr and Ba [Braukmüller et al., 2018; Bland et al., 2006]. On the other hand, photospheric measurments are limited by the precision of the extracted spectral lines, the accuracy of the solar models being applied, and the accuracy of the diffusion corrections performed. The agreement between CI chondrite abundances and solar photospheric abundances therefore needs to be reconfirmed in each analysis combining the two data sets. We therefore, where possible, have used weighted means to take advantage of the information in both sources.

3.2.3 Protosolar elemental abundance results

Fig. 3.2 shows our estimates of protosolar elemental abundances, compared with both the photospheric-based and meteoritic-based abundances, normalized to Si. The lower panel of Fig. 3.2, illustrates our selection methods and how the two data sets were combined to produce protosolar abundances. For example, the resultant Li abundance is identical to that in meteorites. The protosolar abundances of C, N and O are identical to their photospheric-based solar abundances. The weighted mean of a meteoritic abundance with a small error bar, and a photometric abundance with a large error bar, produces a result very similar to the meteoritic abundance (e.g. F and Cl). When the uncertainties from the two data sets do not overlap we assign the upper and lower limits of the two data points, as conservative error bars on the weighted mean (e.g. Rh, Pd and Ag).

From an astronomical perspective, Table 3.2 can be simplified to include only the mass fraction abundances of hydrogen (X), helium (Y) and the sum of everything else (Z), where $X + Y + Z = 1$. For the bulk protosolar elemental abundances reported here, we estimate $X = 0.7157 \pm 0.0037$, $Y = 0.2703 \pm 0.0037$, and $Z = 0.0140 \pm 0.0009$. For comparison, we compile and compute protosolar mass fractions reported in the literature over the past three decades (Table 3.3 and Fig. 3.3). There has been a steady decrease in Z from 1.89% in Anders and Grevesse [1989] to 1.40% in the present work.

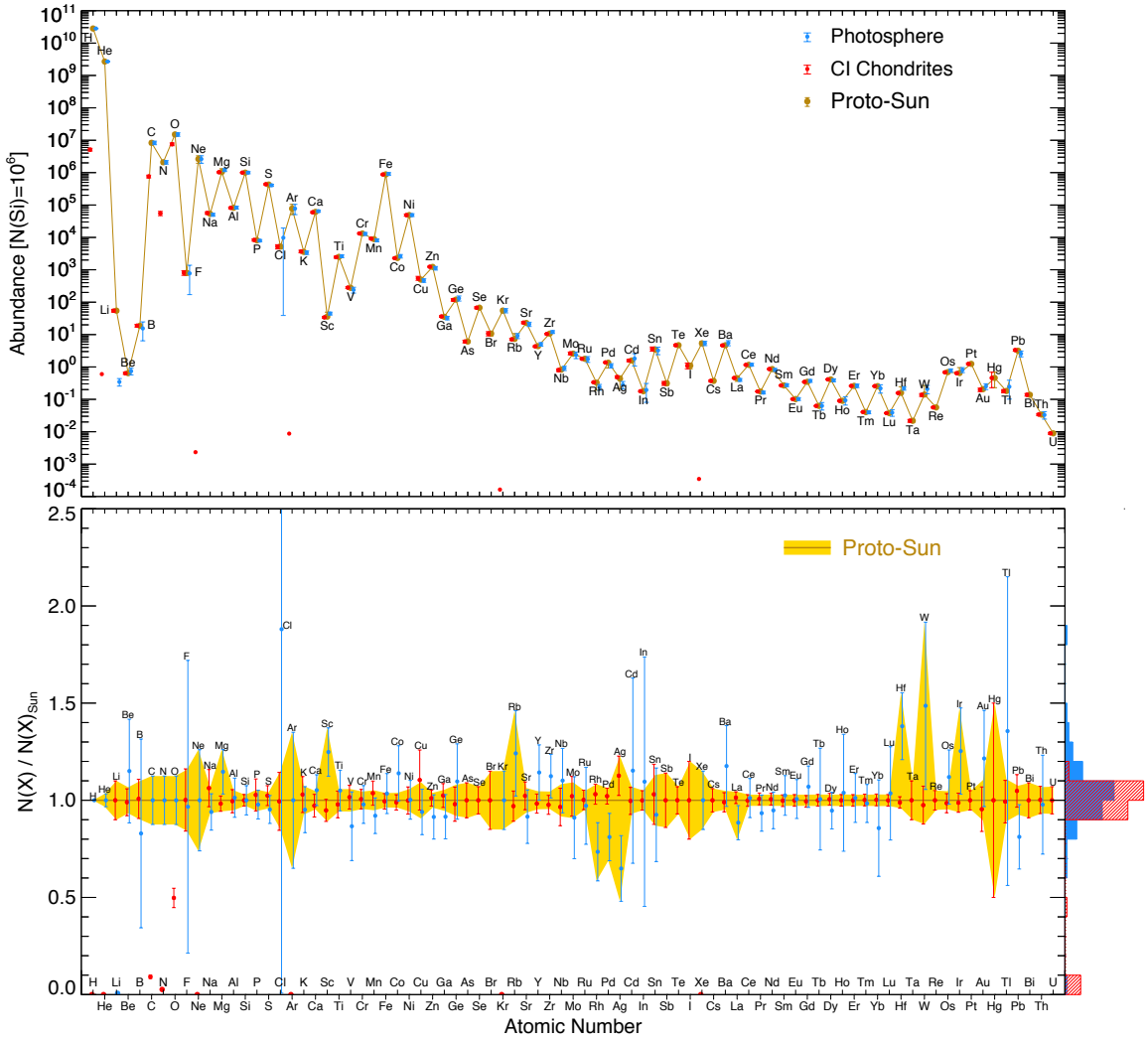

Figure 3.2: Our bulk protosolar abundances (Table 3.2, columns 13) compared with the source data: the photospheric-based solar abundances and the meteoritic abundances (Table 3.2, columns 6 and 10 respectively). In the lower panel, abundances have been normalized to our protosolar abundances. The upper limit of chlorine is off the plot at 3.76. The blue and red histograms along the right side of the lower panel show the statistical distributions of photospheric data and meteoritic data respectively.

This decrease is also reflected in the numerical factor Δ used to convert Si-normalized meteoritic abundances to H-normalized abundances, as discussed in Appendix B.2.

Table 3.2: Estimates of protosolar abundances from photospheric and CI chondritic data.

1	2	3	4	5	6	7	8	9	10	11	12	13	14
		Photosphere				**CI-Chondrites**					**Proto-Sun**		
Z	Elm	$A(\mathrm{X})_p$ [a]	Ref. [b]	$A(\mathrm{X})_{p,0}$ [c]	$N(\mathrm{X})_{p,0}$ [d]	X_{ppm} [e]	σ_X [%]	Ref. [f]	$N(\mathrm{X})_m$ [g]	$A(\mathrm{X})_m$ [h]	SM [i]	$N(\mathrm{X})_0$ [j]	$A(\mathrm{X})_0$ [k]
1	H	12.00	A09	12.00	2.82×10^{10}	19700	10	L09/P14	$5.13 \pm 0.51 \times 10^6$	8.26 ± 0.04	p	2.82×10^{10}	**12.00**
2	He	10.93 ± 0.01	A09	10.98 ± 0.01	$2.69 \pm 0.09 \times 10^9$	9.17×10^{-3}	-	L09/P14	0.60	1.33	p	$2.69 \pm 0.09 \times 10^9$	**10.98 ± 0.01**
3	Li	1.05 ± 0.10	A09	1.09 ± 0.10	0.347 ± 0.090	1.45	10	P14	54.6 ± 5.5	3.29 ± 0.04	m	54.6 ± 5.5	**3.29 ± 0.04**
4	Be	1.38 ± 0.09	A09	1.42 ± 0.09	0.741 ± 0.172	0.0219	7	P14	0.638 ± 0.045	1.36 ± 0.03	a	0.644 ± 0.043	**1.36 ± 0.03**
5	B	2.70 ± 0.20	A09	2.74 ± 0.20	15.5 ± 9.1	0.775	10	L09/P14	18.8 ± 1.9	2.83 ± 0.04	a	18.7 ± 1.8	**2.82 ± 0.04**
6	C	8.43 ± 0.05	A09	8.47 ± 0.05	$8.32 \pm 1.04 \times 10^6$	34800	10	L09/P14	$7.60 \pm 0.76 \times 10^5$	7.43 ± 0.04	p	$8.32 \pm 1.04 \times 10^6$	**8.47 ± 0.05**
7	N	7.83 ± 0.05	A09	7.87 ± 0.05	$2.09 \pm 0.26 \times 10^6$	2950	15	L09/P14	$5.53 \pm 0.83 \times 10^4$	6.30 ± 0.06	p	$2.09 \pm 0.26 \times 10^6$	**7.87 ± 0.05**
8	O	8.69 ± 0.05	A09	8.73 ± 0.05	$1.51 \pm 0.19 \times 10^7$	4.59×10^5	10	L09/P14	$7.53 \pm 0.75 \times 10^6$	8.43 ± 0.04	p	$1.51 \pm 0.19 \times 10^7$	**8.73 ± 0.05**
9	F	4.40 ± 0.25	A09	4.44 ± 0.25	776 ± 605	58.2	16	P14	804 ± 129	4.46 ± 0.06	a	803 ± 126	**4.45 ± 0.06**
10	Ne	7.93 ± 0.10	A09	7.97 ± 0.10	$2.63 \pm 0.68 \times 10^6$	1.8×10^{-4}	-	L09/P14	2.34×10^{-3}	-1.08	p	$2.63 \pm 0.68 \times 10^6$	**7.97 ± 0.10**
11	Na	6.21 ± 0.04	S15b	6.25 ± 0.04	$5.01 \pm 0.50 \times 10^4$	4962	9	P14	$5.67 \pm 0.51 \times 10^4$	6.31 ± 0.04	a	$5.33 \pm 0.36 \times 10^4$	**6.28 ± 0.03**
12	Mg	7.59 ± 0.04	S15b	7.63 ± 0.04	$1.20 \pm 0.12 \times 10^6$	95400	4	P14	$1.03 \pm 0.04 \times 10^6$	7.57 ± 0.02	a*	$1.05\ ^{+0.27}_{-0.06} \times 10^6$	**7.57** $^{+0.10}_{-0.03}$
13	Al	6.43 ± 0.04	S15b	6.47 ± 0.04	$8.32 \pm 0.83 \times 10^4$	8400	6	P14	$8.17 \pm 0.49 \times 10^4$	6.47 ± 0.03	a	$8.21 \pm 0.42 \times 10^4$	**6.46 ± 0.02**
14	Si	7.51 ± 0.03	S15b	7.55 ± 0.03	$1.00 \pm 0.08 \times 10^6$	1.07×10^5	3	L09/P14	$1.00 \pm 0.03 \times 10^6$	7.55 ± 0.01	a	$1.00 \pm 0.03 \times 10^6$	**7.55 ± 0.01**
15	P	5.41 ± 0.03	S15b	5.45 ± 0.03	7943 ± 600	985	8	P14	8347 ± 668	5.48 ± 0.03	a	8124 ± 446	**5.46 ± 0.02**
16	S	7.12 ± 0.03	S15b	7.16 ± 0.03	$4.07 \pm 0.31 \times 10^5$	53500	5	L09/P14	$4.38 \pm 0.22 \times 10^5$	7.20 ± 0.02	a	$4.28 \pm 0.18 \times 10^5$	**7.18 ± 0.02**
17	Cl	5.50 ± 0.30	S15b	5.54 ± 0.30	9772 ± 9734	698	15	L09/P14	5168 ± 775	5.27 ± 0.06	a	5197 ± 773	**5.27 ± 0.06**
18	Ar	6.40 ± 0.13	S15b	6.44 ± 0.13	$7.76 \pm 2.72 \times 10^4$	1.33×10^{-3}	-	L09/P14	8.74×10^{-3}	-0.50	p	$7.76 \pm 2.72 \times 10^4$	**6.44 ± 0.13**
19	K	5.04 ± 0.05	S15b	5.08 ± 0.05	3388 ± 422	546	9	P14	3665 ± 330	5.12 ± 0.04	a	3560 ± 260	**5.10 ± 0.03**
20	Ca	6.32 ± 0.03	S15b	6.36 ± 0.03	$6.46 \pm 0.49 \times 10^4$	9110	6	P14	$5.97 \pm 0.36 \times 10^4$	6.33 ± 0.03	a	$6.14 \pm 0.29 \times 10^4$	**6.34 ± 0.02**
21	Sc	3.16 ± 0.04	S15a	3.20 ± 0.04	44.7 ± 4.4	5.81	6	P14	33.9 ± 2.0	3.08 ± 0.03	a*	$35.8\ ^{+13.3}_{-3.9}$	**3.10** $^{+0.14}_{-0.05}$
22	Ti	4.93 ± 0.04	S15a	4.97 ± 0.04	2630 ± 262	447	7	P14	2451 ± 172	4.94 ± 0.03	a	2505 ± 144	**4.95 ± 0.02**
23	V	3.89 ± 0.08	S15a	3.93 ± 0.08	240 ± 49	54.6	6	P14	281 ± 17	4.00 ± 0.03	a	277 ± 16	**3.99 ± 0.02**
24	Cr	5.62 ± 0.04	S15a	5.66 ± 0.04	$1.29 \pm 0.13 \times 10^4$	2623	5	P14	$1.32 \pm 0.07 \times 10^4$	5.68 ± 0.02	a	$1.32 \pm 0.06 \times 10^4$	**5.67 ± 0.02**
25	Mn	5.42 ± 0.04	S15a	5.46 ± 0.04	8128 ± 810	1916	6	P14	9154 ± 549	5.52 ± 0.03	a	8831 ± 455	**5.50 ± 0.02**
26	Fe	7.47 ± 0.04	S15a	7.51 ± 0.04	$9.12 \pm 0.91 \times 10^5$	1.87×10^5	4	P14	$8.77 \pm 0.35 \times 10^5$	7.50 ± 0.02	a	$8.82 \pm 0.33 \times 10^5$	**7.50 ± 0.02**
27	Co	4.93 ± 0.05	S15a	4.97 ± 0.05	2630 ± 328	513	4	P14	2285 ± 91	4.91 ± 0.02	a	2310 ± 88	**4.91 ± 0.02**
28	Ni	6.20 ± 0.04	S15a	6.24 ± 0.04	$4.90 \pm 0.49 \times 10^4$	10910	7	P14	$4.88 \pm 0.34 \times 10^4$	6.24 ± 0.03	a	$4.89 \pm 0.28 \times 10^4$	**6.24 ± 0.02**
29	Cu	4.18 ± 0.05	G15	4.22 ± 0.05	468 ± 58	133	14	P14	549 ± 77	4.29 ± 0.06	a	498 ± 46	**4.25 ± 0.04**
30	Zn	4.56 ± 0.05	G15	4.60 ± 0.05	1122 ± 140	309	4	P14	1241 ± 50	4.65 ± 0.02	a	1227 ± 47	**4.64 ± 0.02**
31	Ga	3.02 ± 0.05	G15	3.06 ± 0.05	32.4 ± 4.0	9.62	6	P14	36.2 ± 2.2	3.11 ± 0.03	a	35.3 ± 1.9	**3.10 ± 0.02**
32	Ge	3.63 ± 0.07	G15	3.67 ± 0.07	132 ± 23	32.6	9	P14	118 ± 11	3.63 ± 0.04	a	120 ± 10	**3.63 ± 0.03**
33	As	-	-	-	-	1.74	9	L09/P14	6.10 ± 0.5	2.34 ± 0.04	m	6.10 ± 0.55	**2.34 ± 0.04**
34	Se	-	-	-	-	20.3	7	L09/P14	67.5 ± 4.7	3.38 ± 0.03	m	67.5 ± 4.7	**3.38 ± 0.03**
35	Br	-	-	-	-	3.26	15	L09/P14	10.7 ± 1.6	2.58 ± 0.06	m	10.7 ± 1.6	**2.58 ± 0.06**
36	Kr	3.25 ± 0.06	G15	3.29 ± 0.06	55.0 ± 8.3	5.22×10^{-5}	-	L09/P14	1.64×10^{-4}	-2.23	p	55.0 ± 8.3	**3.29 ± 0.06**
37	Rb	2.47 ± 0.07	G15	2.51 ± 0.07	9.12 ± 1.61	2.32	8	P14	7.12 ± 0.57	2.41 ± 0.03	a*	$7.35\ ^{+3.39}_{-0.79}$	**2.42** $^{+0.16}_{-0.05}$
38	Sr	2.83 ± 0.06	G15	2.87 ± 0.06	20.9 ± 3.1	7.79	7	P14	23.3 ± 1.6	2.92 ± 0.03	a	22.8 ± 1.4	**2.91 ± 0.03**
39	Y	2.21 ± 0.05	G15	2.25 ± 0.05	5.01 ± 0.62	1.46	5	P14	4.31 ± 0.22	2.19 ± 0.02	a	4.39 ± 0.20	**2.19 ± 0.02**
40	Zr	2.59 ± 0.04	G15	2.63 ± 0.04	12.0 ± 1.2	3.63	5	P14	10.4 ± 0.5	2.57 ± 0.02	a	10.7 ± 0.5	**2.58 ± 0.02**
41	Nb	1.47 ± 0.06	G15	1.51 ± 0.06	0.912 ± 0.137	0.283	10	P14	0.800 ± 0.080	1.46 ± 0.04	a	0.828 ± 0.069	**1.47 ± 0.03**
42	Mo	1.88 ± 0.09	G15	1.92 ± 0.09	2.34 ± 0.54	0.961	10	P14	2.63 ± 0.26	1.97 ± 0.04	a	2.57 ± 0.24	**1.96 ± 0.04**
44	Ru	1.75 ± 0.08	G15	1.79 ± 0.08	1.74 ± 0.35	0.69	5	P14	1.79 ± 0.09	1.81 ± 0.02	a	1.79 ± 0.09	**1.80 ± 0.02**
45	Rh	0.89 ± 0.08	G15	0.93 ± 0.08	0.240 ± 0.049	0.132	5	P14	0.337 ± 0.017	1.08 ± 0.02	a*	$0.326\ ^{+0.027}_{-0.135}$	**1.06** $^{+0.03}_{-0.23}$

Continued on next page

1	2	3	4	5	6	7	8	9	10	11	12	13	14
		Photosphere				**CI-Chondrites**					**Proto-Sun**		
Z	Elm	$A(X)_p$ [a]	Ref. [b]	$A(X)_{p,0}$ [c]	$N(X)_{p,0}$ [d]	X_{ppm} [e]	σ_X [%]	Ref. [f]	$N(X)_m$ [g]	$A(X)_m$ [h]	SM [i]	$N(X)_0$ [j]	$A(X)_0$ [k]
46	Pd	1.55 ± 0.06	G15	1.59 ± 0.06	1.10 ± 0.16	0.56	4	P14	1.38 ± 0.06	1.69 ± 0.02	a*	$1.352^{+0.084}_{-0.421}$	**1.68** $^{+0.03}_{-0.16}$
47	Ag	0.96 ± 0.10	G15	1.00 ± 0.10	0.282 ± 0.073	0.201	9	P14	0.489 ± 0.044	1.24 ± 0.04	a*	$0.434^{+0.099}_{-0.226}$	**1.19** $^{+0.09}_{-0.32}$
48	Cd	1.77 ± 0.15	G15	1.81 ± 0.15	1.82 ± 0.75	0.674	7	L09/P14	1.57 ± 0.11	1.75 ± 0.03	a	1.58 ± 0.11	**1.75 ± 0.03**
49	In	0.80 ± 0.20	G15	0.84 ± 0.20	0.195 ± 0.114	0.0778	5	P14	0.178 ± 0.009	0.80 ± 0.02	a	0.178 ± 0.009	**0.80 ± 0.02**
50	Sn	2.02 ± 0.10	G15	2.06 ± 0.10	3.24 ± 0.84	1.63	15	L09/P14	3.60 ± 0.54	2.11 ± 0.06	a	3.50 ± 0.46	**2.09 ± 0.05**
51	Sb	-	-	-	-	0.145	14	P14	0.313 ± 0.044	1.05 ± 0.06	m	0.313 ± 0.044	**1.04 ± 0.06**
52	Te	-	-	-	-	2.28	7	L09/P14	4.69 ± 0.33	2.23 ± 0.03	m	4.69 ± 0.33	**2.22 ± 0.03**
53	I	-	-	-	-	0.53	20	L09/P14	1.10 ± 0.22	1.59 ± 0.08	m	1.10 ± 0.22	**1.59 ± 0.08**
54	Xe	2.24 ± 0.06	G15	2.28 ± 0.06	5.37 ± 0.81	1.74×10^{-4}	-	L09/P14	3.48×10^{-4}	-1.90	p	5.37 ± 0.81	**2.28 ± 0.06**
55	Cs	-	-	-	-	0.188	6	P14	0.371 ± 0.022	1.12 ± 0.03	m	0.371 ± 0.022	**1.12 ± 0.03**
56	Ba	2.25 ± 0.07	G15	2.29 ± 0.07	5.50 ± 0.97	2.42	5	P14	4.63 ± 0.23	2.22 ± 0.02	a	4.67 ± 0.22	**2.22 ± 0.02**
57	La	1.11 ± 0.04	G15	1.15 ± 0.04	0.398 ± 0.040	0.2414	3	P14	0.456 ± 0.014	1.21 ± 0.01	a*	$0.450^{+0.020}_{-0.092}$	**1.20** $^{+0.02}_{-0.10}$
58	Ce	1.58 ± 0.04	G15	1.62 ± 0.04	1.17 ± 0.12	0.6194	3	P14	1.16 ± 0.03	1.62 ± 0.01	a	1.16 ± 0.03	**1.62 ± 0.01**
59	Pr	0.72 ± 0.04	G15	0.76 ± 0.04	0.162 ± 0.016	0.0939	3	P14	0.175 ± 0.005	0.80 ± 0.01	a	0.174 ± 0.005	**0.79 ± 0.01**
60	Nd	1.42 ± 0.04	G15	1.46 ± 0.04	0.813 ± 0.081	0.4737	3	P14	0.862 ± 0.026	1.49 ± 0.01	a	0.857 ± 0.025	**1.48 ± 0.01**
62	Sm	0.95 ± 0.04	G15	0.99 ± 0.04	0.275 ± 0.027	0.1536	3	P14	0.268 ± 0.008	0.98 ± 0.01	a	0.269 ± 0.008	**0.98 ± 0.01**
63	Eu	0.52 ± 0.04	G15	0.56 ± 0.04	0.102 ± 0.010	0.05883	3	P14	0.102 ± 0.003	0.56 ± 0.01	a	0.102 ± 0.003	**0.56 ± 0.01**
64	Gd	1.08 ± 0.04	G15	1.12 ± 0.04	0.372 ± 0.037	0.2069	3	P14	0.345 ± 0.010	1.09 ± 0.01	a	0.347 ± 0.010	**1.09 ± 0.01**
65	Tb	0.31 ± 0.10	G15	0.35 ± 0.10	0.0631 ± 0.0164	0.03797	3	P14	0.0627 ± 0.0019	0.35 ± 0.01	a	0.0627 ± 0.0019	**0.35 ± 0.01**
66	Dy	1.10 ± 0.04	G15	1.14 ± 0.04	0.389 ± 0.039	0.2558	3	P14	0.413 ± 0.012	1.17 ± 0.01	a	0.411 ± 0.012	**1.16 ± 0.01**
67	Ho	0.48 ± 0.11	G15	0.52 ± 0.11	0.0933 ± 0.0270	0.05644	3	P14	0.0898 ± 0.0027	0.51 ± 0.01	a	0.0899 ± 0.0027	**0.50 ± 0.01**
68	Er	0.93 ± 0.05	G15	0.97 ± 0.05	0.263 ± 0.033	0.1655	3	P14	0.260 ± 0.008	0.97 ± 0.01	a	0.260 ± 0.008	**0.96 ± 0.01**
69	Tm	0.11 ± 0.04	G15	0.15 ± 0.04	0.0398 ± 0.0040	0.02609	3	P14	0.0405 ± 0.0012	0.16 ± 0.01	a	0.0405 ± 0.0012	**0.16 ± 0.01**
70	Yb	0.85 ± 0.11	G15	0.89 ± 0.11	0.219 ± 0.063	0.1687	3	P14	0.256 ± 0.008	0.96 ± 0.01	a	0.255 ± 0.008	**0.96 ± 0.01**
71	Lu	0.10 ± 0.09	G15	0.14 ± 0.09	0.0389 ± 0.0090	0.02503	3	P14	0.0375 ± 0.0011	0.13 ± 0.01	a	0.0376 ± 0.0011	**0.12 ± 0.01**
72	Hf	0.85 ± 0.05	G15	0.89 ± 0.05	0.219 ± 0.027	0.1065	3	P14	0.157 ± 0.005	0.75 ± 0.01	a*	$0.158^{+0.088}_{-0.006}$	**0.75** $^{+0.19}_{-0.02}$
73	Ta	-	-	-	-	0.015	10	P14	0.0218 ± 0.0022	-0.11 ± 0.04	m	0.0218 ± 0.0022	**-0.11 ± 0.04**
74	W	0.83 ± 0.11	G15	0.87 ± 0.11	0.209 ± 0.061	0.096	10	P14	0.137 ± 0.014	0.69 ± 0.04	a*	$0.141^{+0.129}_{-0.017}$	**0.70** $^{+0.28}_{-0.06}$
75	Re	-	-	-	-	0.04	5	P14	0.056 ± 0.003	0.31 ± 0.02	m	0.0564 ± 0.0028	**0.30 ± 0.02**
76	Os	1.40 ± 0.05	G15	1.44 ± 0.05	0.776 ± 0.097	0.495	5	P14	0.683 ± 0.034	1.39 ± 0.02	a	0.693 ± 0.032	**1.39 ± 0.02**
77	Ir	1.42 ± 0.07	G15	1.46 ± 0.07	0.813 ± 0.144	0.469	5	L09/P14	0.640 ± 0.032	1.36 ± 0.02	a*	$0.649^{+0.308}_{-0.040}$	**1.36** $^{+0.17}_{-0.03}$
78	Pt	-	-	-	-	0.925	5	P14	1.24 ± 0.06	1.65 ± 0.02	m	1.24 ± 0.06	**1.65 ± 0.02**
79	Au	0.91 ± 0.08	G15	0.95 ± 0.08	0.251 ± 0.051	0.148	12	P14	0.197 ± 0.024	0.85 ± 0.05	a	0.207 ± 0.021	**0.87 ± 0.04**
80	Hg	-	-	-	-	0.35	50	P14	0.458 ± 0.229	1.21 ± 0.18	m	0.458 ± 0.229 [l]	**1.21 ± 0.18**
81	Tl	0.90 ± 0.20	G15	0.94 ± 0.20	0.245 ± 0.144	0.14	11	P14	0.180 ± 0.020	0.81 ± 0.05	a	0.181 ± 0.020	**0.81 ± 0.04**
82	Pb	1.92 ± 0.08	G15	1.96 ± 0.08	2.57 ± 0.52	2.62	8	P14	3.32 ± 0.266	2.07 ± 0.03	a	3.17 ± 0.24	**2.05 ± 0.03**
83	Bi	-	-	-	-	0.11	9	L09/P14	0.138 ± 0.012	0.69 ± 0.04	m	0.138 ± 0.012	**0.69 ± 0.04**
90	Th	0.03 ± 0.10	G15	0.07 ± 0.10	0.0331 ± 0.0086	0.03	7	P14	0.0339 ± 0.0024	0.08 ± 0.03	a	0.0339 ± 0.0023	**0.08 ± 0.03**
92	U	-	-	-	-	0.0081	7	P14	0.0089 ± 0.0006	-0.50 ± 0.03	m	0.0089 ± 0.0006	**-0.50 ± 0.03**

Continued on next page

1	2	3	4	5	6	7	8	9	10	11	12	13	14
		Photosphere				**CI-Chondrites**					**Proto-Sun**		
Z	Elm	$A(X)_p$ [a]	Ref. [b]	$A(X)_{p,0}$ [c]	$N(X)_{p,0}$ [d]	X_{ppm} [e]	σ_X [%]	Ref. [f]	$N(X)_m$ [g]	$A(X)_m$ [h]	SM [i]	$N(X)_0$ [j]	$A(X)_0$ [k]

[a] Solar photospheric abundances (in dex).
[b] References for the photosphere: A09-Columns 3 and 7 of Table 1 in Asplund et al. (2009), S15a- Column 3 of Table 5 in Scott et al. (2015a), S15b- Column 3 of Table 6 in Scott et al. (2015b), G15- Column 3 of Table 5 in Grevesse et al. (2015).
[c] Bulk solar abundances (in dex) by doing overall diffusion corrections on photospheric abundances ($A(X)_p$ in column 3) through Eq. B.2 and B.3.
[d] Bulk solar abundances per 10^6 atoms of Si, converted from $A(X)_{p,0}$ (column 5) by Eq. B.4. Uncertainties are calculated using Eq. B.5.
[e] Elemental abundances in ppm by mass.
[f] References for meteorites: L09- Columns 3 and 4 of Table 3 in Lodders et al. (2009), P14- Columns 3 and 6 of Table 3 in Palme et al. (2014).
[g] Meteoritic abundances per 10^6 atoms of Si, converted from the elemental abundances in ppm by mass (X_{ppm} and σ_X in columns 7 and 8) through Eqs. B.6 & B.7.
[h] Meteoritic abundances (in dex) converted by Eq. B.10, using $\Delta = 1.554$. See Appendix B.2 for more details.
[i] SM- Selection methods. See Table B.1.
[j] Protosolar abundance per 10^6 atoms of Si, resulted from combining $N(X)_{p,0}$ (column 6) and $N(X)_m$ (column 10) through Eqs. B.8 & B.9.
[k] Protosolar abundances (in dex), converted from $N(X_0)$ (column 13) by Eq. B.1. Uncertainties are from solving Eq. B.5 for σ_A using σ_{N_0} instead of $\sigma_{N_{p,0}}$.
[l] This meteoritic Hg abundance does not reflect the factor of 13 ± 7 increase discussed in Section 3.4.2. Including this increase yields 5.954 ± 4.375 for $N(\mathrm{Hg})_0$ and 2.325 ± 0.239 for $A(\mathrm{Hg})_0$.

Table 3.3: Protosolar mass fractions of H (X), He (Y) and metals (Z)

Source	X	Y	Z	Z/X
Anders and Grevesse [1989]	0.7068 ± 0.0177	0.2743 ± 0.0165	0.0189 ± 0.0016	0.0267 ± 0.0024
Grevesse and Sauval [1998]	0.7090 ± 0.0100	0.2750 ± 0.0100	0.0160 ± 0.0016	0.0230 ± 0.0023
Lodders [2003]	0.7110 ± 0.0040	0.2741 ± 0.0120	0.0149 ± 0.0015	0.0210 ± 0.0021
Lodders et al. [2009]	0.7112 ± 0.0033	0.2735 ± 0.0036	0.0153 ± 0.0014	0.0215 ± 0.0019
Asplund et al. [2009]	0.7154 ± 0.0037	0.2703 ± 0.0037	0.0142 ± 0.0009	0.0199 ± 0.0013
A09-S15-G15[a]	0.7156 ± 0.0037	0.2703 ± 0.0037	0.0141 ± 0.0009	0.0197 ± 0.0013
This work	0.7157 ± 0.0037	0.2703 ± 0.0037	0.0140 ± 0.0009	0.0195 ± 0.0013

Note: Mass fractions not presented in specific references are computed from the corresponding estimate of protosolar abundances in the reference and constrained by the corresponding H or He mass fraction from helioseismology used in the reference. Uncertainties not presented in a reference, associated with the mass fractions, are simulated by a standard Monte Carlo approach.
[a] A09-S15-G15 is the combination of Asplund et al. [2009], Scott et al. [2015a,b] and Grevesse et al. [2015]

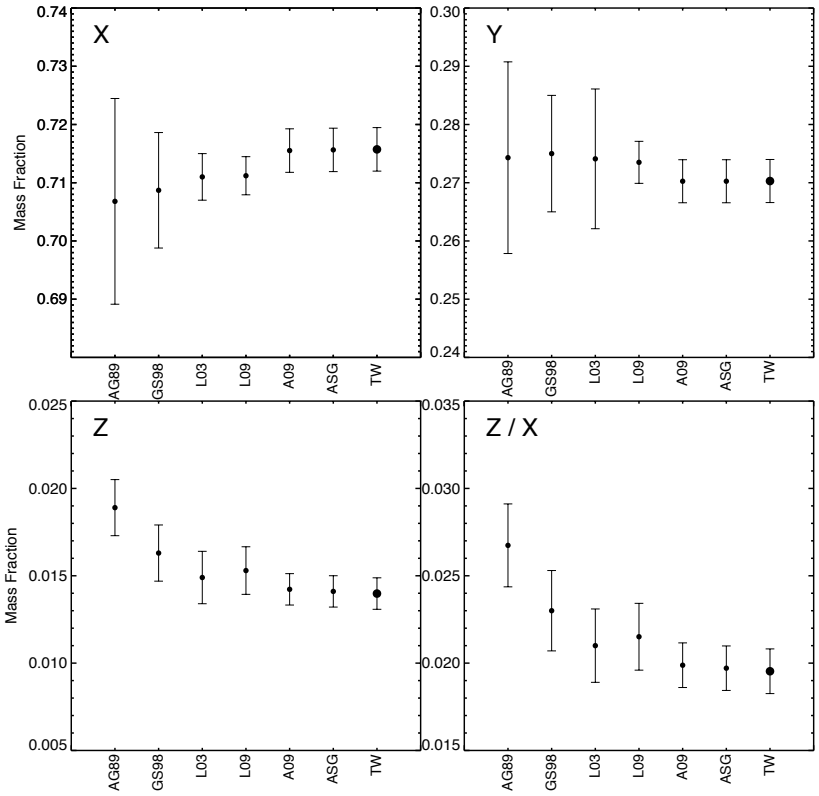

Figure 3.3: The mass fractions of H (X), He (Y) and metals (Z) for protosolar elemental abundances in the literature and this work. AG89: Anders and Grevesse [1989], GS98: Grevesse and Sauval [1998], L03: Lodders [2003], L09: Lodders et al. [2009], A09:Asplund et al. [2009], ASG: The bulk solar abundance compiled from Asplund et al. [2009], Scott et al. [2015a,b] and Grevesse et al. [2015], TW: This work.

3.3 Devolatilization and the Volatility Trend of Bulk Earth

3.3.1 Compositional comparison between the bulk Earth and the proto-Sun

Our goal is to quantify as precisely and accurately as possible the chemical relationship between the Earth and the Sun. For the Sun, we use the protosolar abundances described in the previous section. For the Earth we use our recent bulk Earth elemental abundances [Wang et al., 2018a]. To compare these two data sets, we normalize the protosolar abundances and the bulk Earth abundances to Al (i.e., $N(\mathrm{Al}) = 10^6$). A normalisation to Al is appropriate because the condensation temperature of Al is the highest of any of the major elements in a gas of solar composition. This is important since our main goal is to assess the depletion in elemental abundances as a function of condensation temperature. The abundance ratios (f) of the bulk Earth to the proto-Sun (i.e., $f = N(\mathrm{X})_{\mathrm{Earth}}/N(\mathrm{X})_{\mathrm{Sun}}$) can be plotted in order of decreasing protosolar abundance (Fig. 3.4(a)) and of increasing 50% condensation temperature (T_C) (Fig. 3.4(b)).

Fig. 3.4(a) shows that bulk Earth abundances are systematically lower than or equal to protosolar abundances. There is little correlation between abundance ratios and protosolar abundance in Fig. 3.4(a), whereas there is a definite pattern in the plot of the abundances ratios as a function of T_C in Fig. 3.4(b).

In Fig. 3.4(b) elements are split into four discrete categories. At high condensation temperatures ($T_C > 1360$ K), the abundance ratios are unity ($f \approx 1$), indicating that refractory elements have not been depleted. The abundance ratios begin to decrease for mildly refractory elements (1250 K $< T_C <$1360 K) (see the 8 grey points on the left side of the inset in Fig. 3.4(b)). The abundance ratios of moderately volatile elements (500 K $< T_C <$ 1250 K) progressively decrease in a fairly tight linear correlation with decreasing T_C. Below 500 K, the tight linear correlation weakens, but the positive correlation between decreasing condensation temperatures and decreasing abundance ratios is still strong.

3.3.2 Quantification of the devolatilization pattern

Fig. 3.5 shows the Earth-to-Sun abundance ratios (f) as a function of T_C in a log-log plot for $T_C > 500$ K. An important part of quantifying the devolatilization pattern (DP) is estimating the temperature that separates the region of undepleted terrestrial abundances on the right (i.e. $f \approx 1$) from the region on the left where f decreases with decreasing condensation temperature. A critical condensation temperature of $\approx$ 1400 K is the boundary between these two types of behavior. We call this temperature the critical condensation temperature for devolatilization $T_D(\mathrm{E})$. "E" refers to the Earth.

To quantify the dual behavior of the DP, we perform a χ^2 fit of the f values to the joint model: $\log(f) = \alpha \log(T_C) + \beta$ and $\log(f) = 0$. Details of the minimization process are given in B.3. The best-fit coefficients are $\alpha = 3.676 \pm 0.142$ and $\beta = -11.556 \pm 0.436$. The reduced χ^2 (e.g. chi-squared per degree of freedom) of

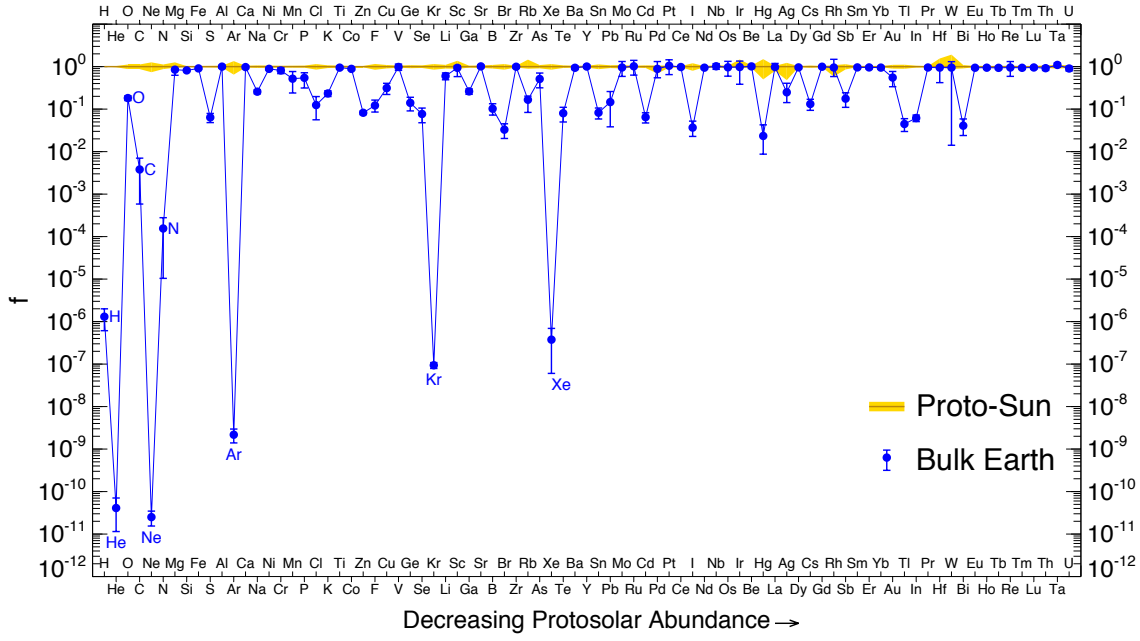

(a)

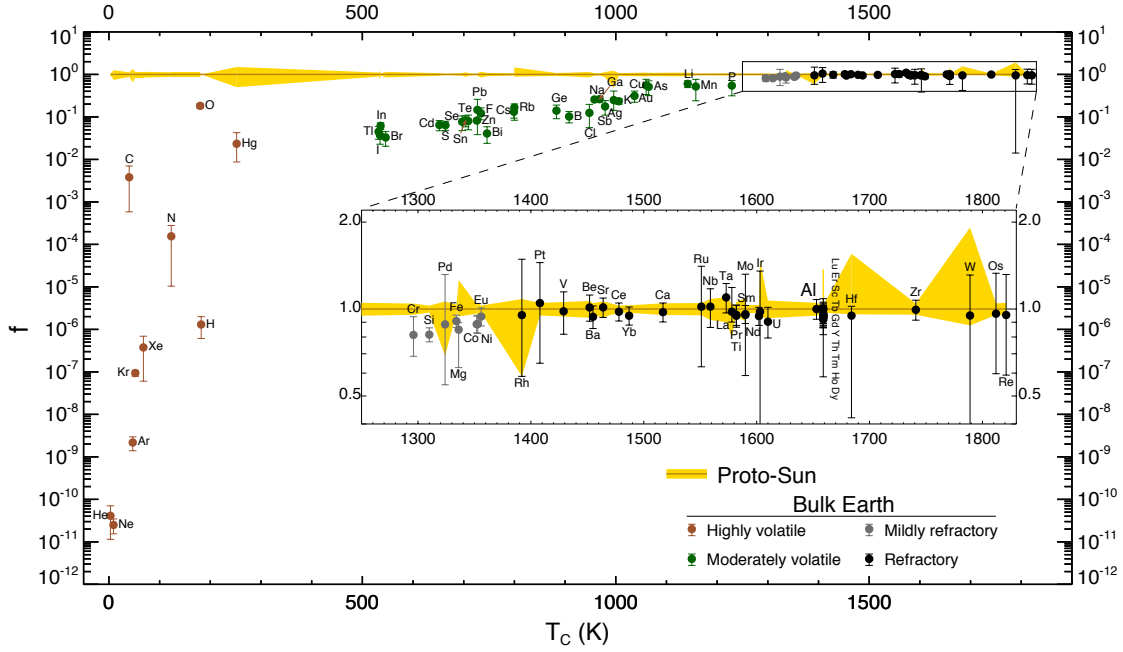

(b)

Figure 3.4: The abundance ratios f, of the bulk Earth to proto-Sun where $f = \mathrm{N(X)_{Earth}/N(X)_{Sun}}$, normalized to Al. f is plotted (a) in order of decreasing protosolar abundance and (b) in order of increasing 50% condensation temperature T_C [Lodders, 2003]. Compared with the Sun, the Earth is depleted in the most volatile elements. The abundances of the refractory elements in the Sun and Earth are indistinguishable. In the lower panel we have classified elements into four categories: *highly volatile* ($T_C < 500$ K), *moderately volatile* (500 K $< T_C <$ 1250 K), *mildly refractory* (1250 K $< T_C <$1360 K) and *refractory* ($T_C >$ 1360 K).

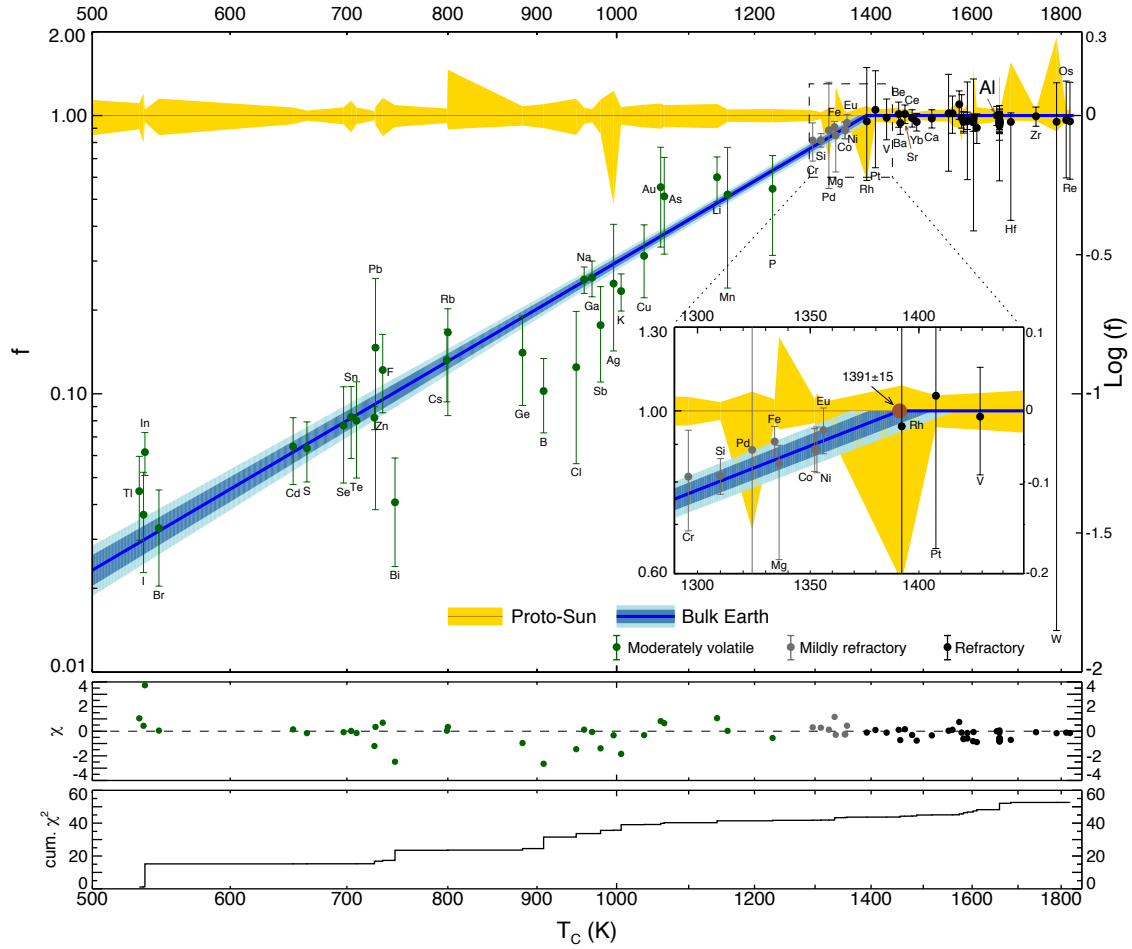

Figure 3.5: Comparison of the elemental abundances of the Earth and Sun. This plot is similar to Fig. 3.4(b) except here, we only plot elements with $T_C > 500$ K and the T_C axis is logarithmic. The diagonal dark blue line and its horizontal continuation in the upper right, is our best χ^2 fit to the data. The dark and light blue diagonal regions are the 68% and 95% confidence intervals on the fit. See Appendix B.3 for details. The diagonal dark blue line reaches $f = 1$ at the critical devolatilization temperature $T_D(E) = 1391 \pm 15$ K. The inset shows more of the details of this region. The lower two panels show the values of χ and the cumulative χ^2 as a function of T_C.

the best fit is about 1.2. Since $T_D(E) = 10^{-\beta/\alpha}$, these coefficients yield the best-fit devolatilization temperature $T_D(E) = 1391 \pm 15$ K.

The quantification of the DP provides an empirical observation upon which interpretation of the devolatilization processes can be based. The systematic depletion of moderately volatile elements versus their condensation temperatures demonstrates that the devolatilization processes are largely volatility controlled, which is consistent with a comparison of various meteorites to CI chondrites [Bland et al., 2005].

$T_D(E)$ is plausibly interpreted as the highest temperature experienced by the dominant material in the feeding zone of the proto-Earth. More specifically, at high temperatures, silicates and other mineral oxides are the dominant condensed phase and have an effective 50% condensation temperature of $\sim T_D(E)$. During repeated transient high-temperature heating events, the latent heat of vaporization of the mineral oxides could prevent the vaporization and depletion of more refractory material. Hence, producing the $f \sim 1$ region of the DP. Less refractory elements with $T_C < 1391K$ would not be protected by the latent heat of the dominant phase and would be susceptible to vaporization and depletion, depending on their T_C.

3.4 Discussion

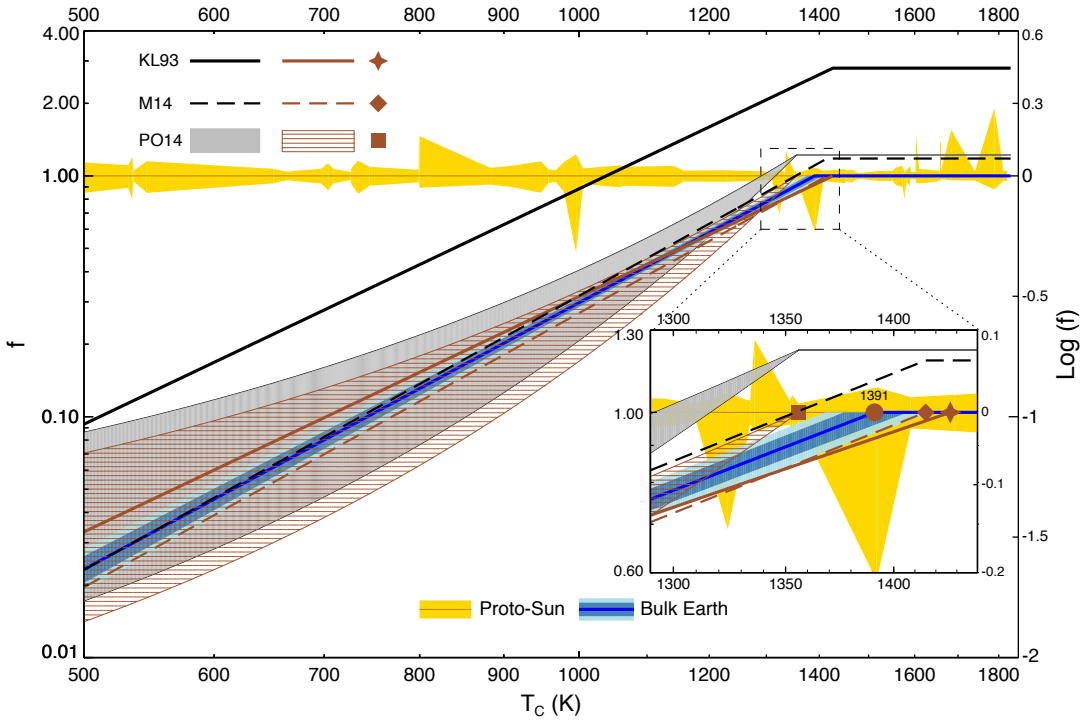

Figure 3.6: Comparison of our best-fit devolatilization pattern (DP, in blue from Fig. 3.5) with the previous analogous DPs of Kargel and Lewis [1993] (KL93), McDonough [2014] (M14) and Palme and O'Neill [2014] (PO14). These previous DPs are based on the normalization of bulk silicate Earth to CI chondrites (as a proxy for the Sun). The curved grey wedge represents the range from Fig. 21 of Palme and O'Neill [2014]. To make these previous DPs more comparable to our analysis, we renormalize them to 1 on their horizontal right hand sides. The renormalized curves are shown as brown versions of the original non-renormalized line style. For details see footnotes of Table 4. This procedure yields $T_D(E)$ values for each curve (see inset). In Table 3.4 we compare these values with our value of $T_D(E) = 1391 \pm 15$ K.

Table 3.4: Comparison of our analysis with previous studies with respect to the coefficients α and β and critical devolatilization temperatures $T_{\mathrm{D}}(\mathrm{E})$

Source	Coefficients		T_{D} (E)[a] [K]
	α	β	
Kargel and Lewis [1993][b]	3.246	-9.792 (-10.239)	1427
McDonough [2014][c]	3.78	-11.82 (-11.91)	1415
Palme and O'Neill [2014][d]	2.66 to 4.27	-8.23 to -13.30 (-8.32 to -13.38)	1356
This work	**3.676 ± 0.142**	**-11.556 ± 0.436**	**1391 ± 15**

[a] T_{D} is calculated using renormalized coefficients through $10^{-\beta/\alpha}$, except for Palme and O'Neill [2014], T_D of which is fixed at the T_C of Eu.

[b] Kargel and Lewis [1993] parameterized a DP as $\log(\mathrm{BSE/CI}) = 3.246\log(T_C) - 9.792$. This DP has a factor of refractory lithophile enrichment (RLE) ~ 2.8 in BSE relative to CI chondrites. We remove RLE, by reducing the initial β (-9.792) by $\log(2.8)$. The renormalized β is -10.239.

[c] McDonough [2014] normalized to Mg in CI chondrites (i.e., $(\mathrm{X/Mg})_{BSE}$ / $(\mathrm{X/Mg})_{CI}$), to produce an indicative DP in their Figure 4. By assuming a functional form $\log(\mathrm{BSE/CI}) = \alpha\log(T_C) + \beta$, we estimate its coefficients ($\alpha \approx 3.78$ and $\beta \approx -11.82$). This DP has a factor of RLE ~ 1.18. We renormalize by reducing the initial β by $\log(1.18)$. The renormalized β is -11.91.

[d] Palme and O'Neill [2014] normalized to Mg in CI chondrites (i.e., $(\mathrm{X/Mg})_{BSE}$ / $(\mathrm{X/Mg})_{CI}$), to produce an indicative DP in their Figure 21 (on a T_C-$\log(\mathrm{BSE/CI})$ plot). Thus, a functional form $\log(\mathrm{BSE/CI}) = aT_C + b$ is assumed. By fixing its T_D(E) at the T_C of Eu (1356 K), the ranges of a and b are $[0.00134, 0.00216]$ and $[-1.7367, -2.8460]$, respectively. In a log-log form, the corresponding α and β are in the range $[2.66, 4.27]$ and $[-8.23, -13.30]$ respectively. The corresponding DP has an RLE factor of ~ 1.22. We renormalize by reducing the initial β by $\log(1.22)$. The renormalized β is in the range $[-8.32, -13.38]$.

3.4.1 Comparison with previous devolatilization patterns (DPs)

Devolatilization Patterns (DPs) of the Earth have been presented in the literature, e.g. Kargel and Lewis [1993], McDonough [2014], and Palme and O'Neill [2014], (see Figure 3.6). In contrast to our more quantitative analysis using the elemental abundances of the bulk Earth, previous DPs use the elemental abundances of the primitive mantle without the core. Previous DPs normalize elemental abundances of silicate Earth (or primitive mantle) to CI chondrites, rather to the proto-Sun. Previous DPs were sketched or intuitively drawn to represent the upper envelope of the moderately volatile lithophiles that are depleted in the Earth's mantle relative to CI chondrites. This procedure is useful for estimating the depletion of siderophile elements from the mantle into the core, but is less useful for estimating the depletion of elements in the bulk Earth compared to their protosolar abundances.

Mg or Si have been the elements of choice for normalizing the elemental abundances of the Earth and CI chondrites. However, both Mg and Si are *mildly* refractory. Their respective T_C values are 1330 K and 1310 K, both of which are less than our calculated $T_{\mathrm{D}}(\mathrm{E}) = 1391$ K. Thus, both Mg and Si are slightly depleted in the Earth relative to CI chondrites. See for example their abundance ratios in the inset in Figure 3.5. Thus, normalizing the Earth and CI chondrites (as a proxy for the Sun) to

Mg or Si, produces the apparent enrichment of the Earth in refractory lithophiles by a factor of about $\sim$ 1.2 (normalized to Mg) or $\sim$ 1.4 (normalized to Si). Palme and O'Neill [2014] and McDonough [2014] chose Mg as the normalizing reference element. Kargel and Lewis [1993] compared the Earth's abundances (in ppm) to CI chondritic abundances (in ppm). Since the Earth is much more depleted in volatiles than are CI chondrites, this procedure elevates the abundances of refractories compared to the total mass by a factor of $\sim$ 2.8. This apparent enrichment is due to the depletion of volatiles from the total mass of the Earth [see, however, Hezel and Palme [2008]; Hezel et al. [2008] for an alternative view based on the enrichment of CAIs in carbonaceous chondrites relative to CI].

To plot these DPs and make them more comparable with our DP: (1) we estimate the coefficients α and β of DPs based on published figures in Kargel and Lewis [1993], McDonough [2014] and Palme and O'Neill [2014]; (2) we renormalize these DPs to remove apparent lithophile enrichment (see details in the footnotes of Table 3.4). Table 3.4 lists all the values of α as well as the initial and renormalized β values, along with their corresponding $T_{\mathrm{D}}(\mathrm{E})$ values. Fig. 3.6 illustrates the comparison of our DP with the previous DPs before and after renormalization.

Our analysis compared the bulk Earth and proto-Sun, using an Al-normalization. We fit the data to a joint devolatilization pattern (DP) and have improved the characterization of the devolatilization that led to the Earth. Our results yield a reference devolatilization pattern that can help resolve the first-order chemical relationship between rocky planets and their host stars with Earth as the natural example.

3.4.2 Extrapolating the DP to lower condensation temperatures

The DP has been constrained by fits to elements with $T_C > 500$ K but the linear trend can be extrapolated to lower condensation temperatures (see Fig. 3.7). Nitrogen lies on the extrapolation of the DP but the other highly volatile elements scatter around it. Hydrogen and the noble gases lie on the depleted side of the fit, while carbon and oxygen appear more enriched. Interestingly, mercury (Hg) is also significantly above the extrapolation of the DP. The implications for the behavior of these elements are discussed below.

The extra depletion of noble gases and hydrogen

Compared to the extrapolation of our DP below $T_C = 500$ K, there seems to be an extra depletion for elements with T_C less than that of water ($T_C = 182$ K). One plausible explanation for this extra depletion could be due to the latent heat of water ice which is the dominant phase at low temperatures. During repeated transient heating events, the latent heat of water ice would buffer heat excursions above $T \sim$ 182 K but not at lower temperatures. Thus, highly volatile elements with $T_C < 182K$ would be repeatedly susceptible to extra sublimation during these low temperature heating events.

It is also plausible that the transport of noble gases and hydrogen into the proto-

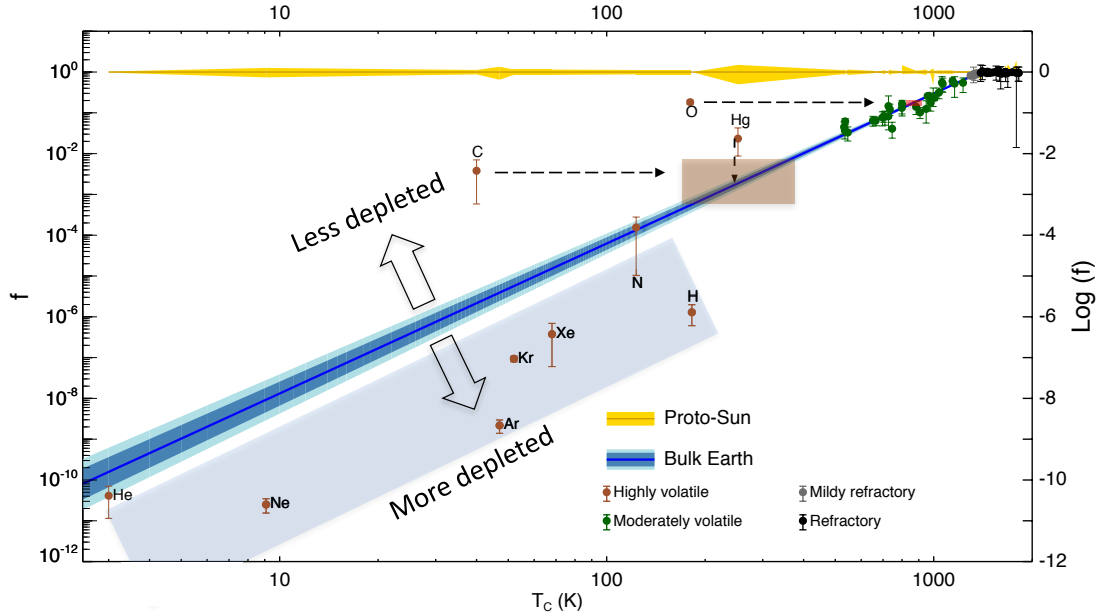

Figure 3.7: Extrapolation of our DP to the realm of highly volatile elements ($T_C <$ 500 K). Elements above the DP are depleted less than expected based on the DP; elements below the DP are depleted more than expected. The position of the light blue rectangle indicates the stronger depletion of noble gases and hydrogen. For C and O, the horizontal arrows pointing to the brown and red boxes, indicate the modification in T_C values that would bring their abundances into agreement with our best-fit DP. The vertical dashed arrow beneath Hg indicates the change in the Earth's relative abundance if the Sun's abundance of Hg were raised by a factor of 13 ± 7. For discussion see Section 3.4.2.

Sun led to the primordial depletion of these gases from the dust that coalesced to form planetesimals. H and noble gases are unreactive with cold dust, and once separated from it, their history is not associated with dust. Thus, hydrogen and the noble gases are not entrained in the solid precursors of the terrestrial planets and are subject to an extra depletion than one based solely on their condensation temperatures.

C and O

Under the assumption of equilibrium condensation from an initially hot, solar compositional gas, Lodders [2003] reported the 50% condensation temperatures of carbon ($T_C(\mathrm{C}) = T_C(\mathrm{CH_4}) \sim 40$ K) and oxygen ($T_C(\mathrm{O}) = T_C(\mathrm{H_2O}) \sim 180$ K). With these T_C values, the abundances of carbon and oxygen appear 2-3 orders of magnitude higher than the extrapolation of our DP below $T_C = 500$ K, would predict (Fig. 3.7).

We attribute these higher abundances to the significant fractions of carbon and

oxygen that are in refractory phases: kerogen and graphite for carbon; silicates and mineral oxides for oxygen. To estimate these fractions, we make the approximation that both carbon and oxygen are distributed between volatile ($f_{\rm vol}$) and refractory ($f_{\rm ref}$) components satisfying $f_{\rm vol} + f_{\rm ref} = 1$. We adopt approximate condensation temperatures for each of these components (see Table 3.5). With these two approximations, we can use the volatility trend in Fig 3.7, to estimate the fractions of these two components that are missing from the nebular composition: $f_{\rm vol,missing}$ and $f_{\rm ref,missing}$. For both carbon and oxygen we use the approximation that $f_{\rm vol,missing} = 1.00$, since in the T_C range below 200 K the Earth-to-Sun abundance ratios are less than 10^{-3}. The abundances of carbon and oxygen in the Earth tell us the total fraction of each element that has gone missing ($f_{\rm total,missing}$). Thus, we have the equation $f_{\rm total,missing} = f_{\rm vol} f_{\rm vol,missing} + f_{\rm ref} f_{\rm ref,missing}$. For both carbon and oxygen, we can now solve these two equations for the two unknowns, ($f_{\rm vol}$, $f_{\rm ref}$). For C-bearing volatile and refractory phases we find (0.91 ± 0.08, 0.09 ± 0.08). For O-bearing volatile and refractory phases we find (0.80 ± 0.04, 0.20 ± 0.04). See Table 3.5 for details.

Since both C and O have significant abundances in refractory phases, the extrapolation of our DP below 500 K yields a more appropriate proxy for "volatility" than the 50% condensation temperatures for C and O reported by Lodders [2003]. We obtain an effective condensation temperature of C and O by horizontally shifting their abundances to agree with the best fit DP. The corresponding effective T_C for C and O are illustrated by the brown and red boxes shown in Fig. 3.7. We find $T_{C,eff}$(C) = 305^{+73}_{-135} K and $T_{C,eff}$(O) = 875 ± 45 K.

Table 3.5: Fractional distribution of carbon and oxygen between volatile and refractory phases ($f_{\rm vol}$, $f_{\rm ref}$) in the solar nebular material.

	Carbon	Oxygen
$f_{\rm total,missing}$[a]	0.996 ± 0.003	0.818 ± 0.023
Volatile phases[b]	CH_4, CO_2, CO	H_2O, CO_2, CO
Adopted T_C (K)	47 ± 22	103 ± 79
$f_{\rm vol,missing}$[c]	1.00	1.00
$\boldsymbol{f_{\rm vol}}$	$\mathbf{0.91 \pm 0.08}$	$\mathbf{0.80 \pm 0.04}$
Refractory phases[b]	Kerogen, graphite	Major silicates/mineral oxides
Adopted T_C (K)	600 ± 30	1350 ± 40
$f_{\rm ref,missing}$[c]	0.955 ± 0.014	$0.106^{+0.120}_{-0.106}$
$\boldsymbol{f_{\rm ref}}$ $(= 1 - f_{\rm vol})$	$\mathbf{0.09 \pm 0.08}$	$\mathbf{0.20 \pm 0.04}$

[a] The total fraction of each element that has gone missing from the solar nebula, calculated by 1 - f of C and O as shown in Fig. 3.7 (where f is the Earth-to-Sun abundance ratio).

[b] The respective condensation temperatures (T_C) of these C- or O-bearing species refer to Lodders [2003] for CH_4 (41 K), H_2O (182 K), graphite (626 K), and major silicates/mineral oxides including enstatite (1316 K), forsterite (1354 K), diopside (1347 K), anorthite (1387 K), and spinel (1397 K); Lewis and Prinn [1980] for CO (25 K) and CO_2 (69 K); Pizzarello and Shock [2010] for kerogen (573 K).

[c] The fractions of the volatile and refractory components that have gone missing from the solar nebula, inferred from the volatility trend in Fig. 3.7, using the adopted T_C values.

Hg

There are no observable Hg photospheric lines. Mercury has a condensation temperature of 252 K. Despite this low condensation temperature, the protosolar Hg abundance is usually assumed to be identical to the Hg abundance in CI chondrites. Under this common, but dubious assumption, the ratio of the terrestrial abundance of Hg divided by the CI Hg abundance yields a point that is an order of magnitude above the extrapolation of our best-fit DP in Fig. 3.7. If the protosolar Hg abundance is 13 ± 7 times the Hg abundance in CI chondrites, the terrestrial Hg point in Fig. 7 is lowered and agrees with our best-fit DP. This lowering is indicated by the vertical dashed arrow beneath Hg in Fig. 3.7. We argue that this agreement gives a better estimate of the protosolar Hg abundance than the unmodified CI chondrite Hg abundance.

An earlier work by Lauretta et al. [1999] has shown that a large fraction of Hg can chemisorb on metal surfaces at temperatures as high as 515 K. Thermal release experiments [e.g. Lauretta et al., 2001] has also shown that Hg can be adsorbed on silicate grains in carbonaceous chondrites. Namely, the condensation temperature of Hg might be much higher than that of HgS (the major Hg-bearing phase), due to the buffer of silicate grains that have a higher condensation temperature. This may be the other plausible interpretation for the deviation of Hg from the VT. Further work however is needed to clarify this issue.

3.4.3 Comparison of volatile depletions in the Earth and CI chondrites

Comparing the compositions of the Earth and the Sun can tell us the first-order terrestrial devolatilization from the solar nebula. Comparing the Earth with other solar system rocky bodies can therefore inform a more generalized process of devolatilization that led to the rocky planets. Parent bodies of CI chondrites are from the outer regions of the asteroid belt and close to the snow line. They are less depleted in volatiles compared to the terrestrial planets.

While terrestrial elemental abundances show depletions below $T_D(\mathrm{E}) = 1391$ K, CI chondrite abundances show depletions below $T_D(\mathrm{CI}) \approx 500$ K (Figure 3.8). As shown in the inset in Figure 3.8, the photospheric-based solar abundances of both Tl and In are slightly higher than their corresponding CI chondritic abundances. This suggests that the depletion of CI chondrites (relative to the Sun) may start at the T_C values of these two elements. Without the availability of photospheric abundances of I and Br, their protosolar abundances are assumed equal to meteoritic abundances. To a first-order, therefore, the group of elements (In, Tl, I and Br) may define the boundary $T_D(\mathrm{CI})$ between the depletion and non-depletion of the parent body of CI chondrites, analogous to the group of mildly refractory elements (e.g., Mg, Si, Fe, and Ni) which define $T_D(\mathrm{E})$ for the Earth (see inset in Figure 3.8). Based on this data, we make a preliminary estimate and suggest that $T_D(\mathrm{CI}) = 550^{+20}_{-100}$ K. Below T_D(CI), the abundances of highly volatiles are depleted. It is difficult to determine a quantitative fit to the depletion pattern of the abundances of CI chondrites because of the large scatter in these elements. However, the red wedge in Fig. 3.8 represents a notional

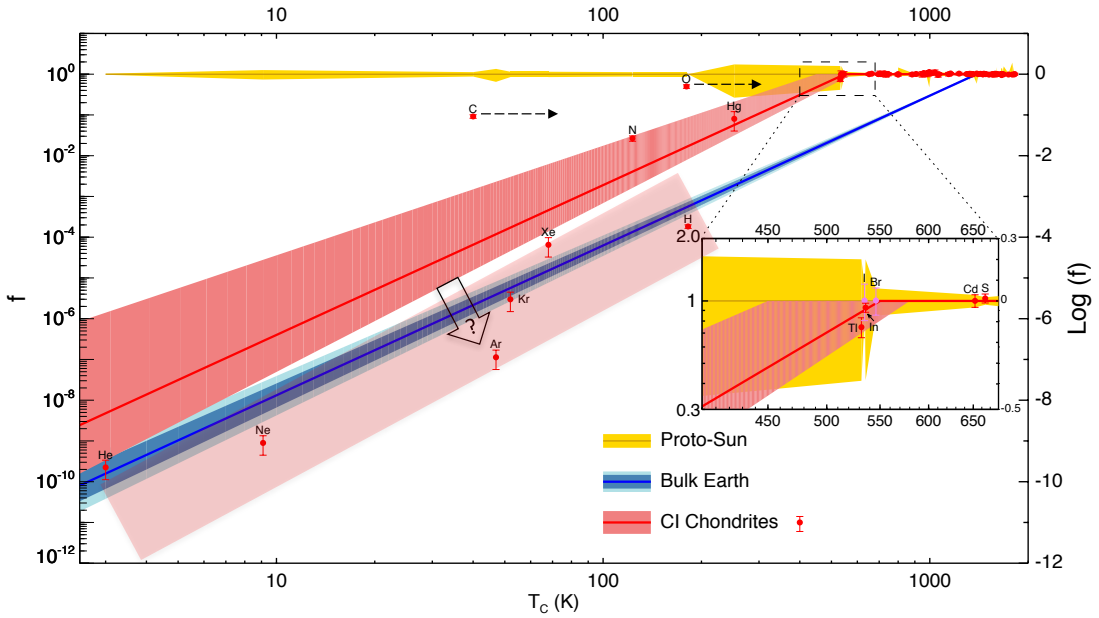

Figure 3.8: The depletion of CI chondrites relative to the Sun. The thin blue diagonal wedge represents the Earth and is taken from the previous figure. The protosolar Hg abundance has been elevated by a factor of 13 ± 7 as indicated in the previous figure. Protosolar abundances of Tl and In are not used here. Rather their photospheric-based abundances (yellow region) and their meteoritic abundances (red points) are plotted separately. Protosolar abundances of I and Br are colored in light red since they are identical to meteoritic abundances and therefore cannot help distinguish solar from meteoritic abundances. The notional volatility trend (red diagonal wedge) for CI chondrites comes from assuming the same slope as the Earth's volatility trend. The position of the light red rectangle indicates the stronger depletion of noble gases and hydrogen. For C and O, the horizontal arrows (analogous to the arrows in the previous figure) indicate modifications in their T_C values that would bring their abundances into agreement with the red wedge. The narrow upper end of the red wedge is characterized by the devolatilization temperature of $T_{\rm D}({\rm CI}) = 550^{+20}_{-100}$ K (see inset). The compositional data for CI chondrites is from Palme et al. [2014] with 50% uncertainties assigned to abundances of noble gases.

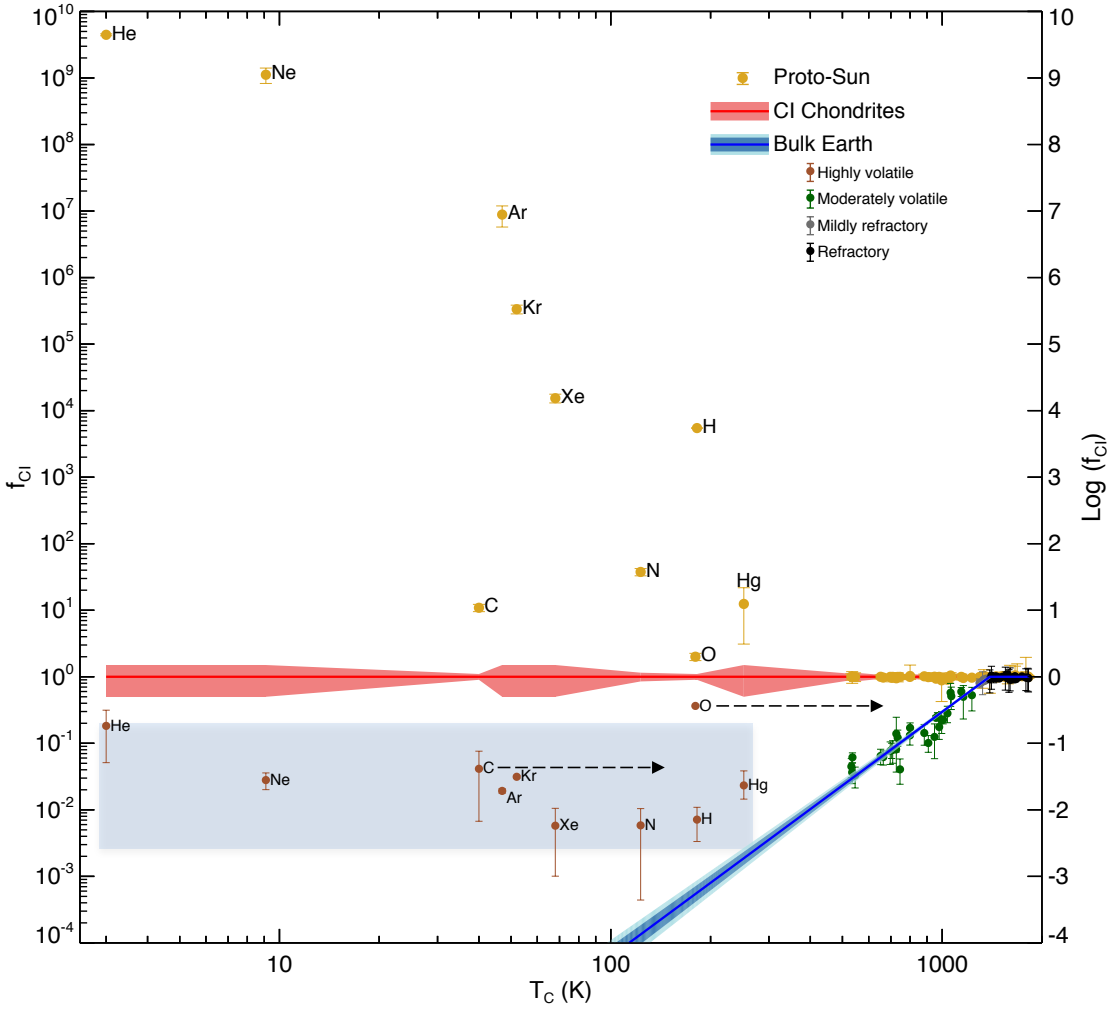

Figure 3.9: Replacing the solar normalization with a normalization to CI chondrite abundances. The depletion of the highly volatile elements from CI chondrites makes the Sun seem enriched in these elements. The light blue rectangle again represents the position of the Earth's highly volatile elements which here seem enriched compared to Earth's DP due to the depletion of these same elements in CI chondrites and the subsequent normalization to depleted CI chondritic values. The Hg protosolar abundance has been increased by a factor of 13 ± 7 relative to its abundance in CI chondrites. The horizontal arrows to the right of the Earth's C and O abundance are the same as those in Figure 3.7.

devolatilization pattern having the same slope as the terrestrial DP. The scatter of the volatile elements around this slope is very similar to that found in the Earth analysis. H and the noble gases are systematically depleted relative to the DP(CI). Carbon and oxygen lie above the DP(CI) similar to the case for Earth. In Fig. 3.9 protosolar abundances are normalized to CI chondrite abundances. Solar abundances of the most volatile elements are systematically enriched, and terrestrial abundances of the same elements are systematically depleted. This systemic behavior suggests that the cosmochemical abundances are controlled in the same way even for the most volatile elements.

3.4.4 Beyond the quantification

Throughout this paper the word “devolatilization" simply indicates the observed depletion feature of volatiles in Earth compared to Sun, with no particular reference to whether the depletion of an element happened during the collapse of the solar nebula, during accretion within the proto-planetary disk or subsequently as a result of impacts [cf. Siebert et al., 2018; Hin et al., 2017; Norris and Wood, 2017; Albarède, 2009; Palme and Boynton, 1993; Larimer, 1979; Wasson and Chou, 1974; Larimer and Anders, 1967; Anders, 1964]. Modeling the physics and chemistry of devolatilization and dust evaporation in the inner regions of protoplanetary disks is an active field of research [Dullemond and Monnier, 2010; Salmeron and Ireland, 2012a,b; Wang and Lineweaver, 2016; Brasser et al., 2017; Jin and Mordasini, 2018], ultimately with the goal of providing an appropriate context for the processes active in the formation of planetary systems.

3.5 Summary and Conclusions

Our main results can be summarized as follows:

1. We obtain improved protosolar elemental abundances by a careful combination of current estimates of CI chondritic abundances with photospheric abundances. Our estimates of the mass fraction Z of metals in the Sun is 1.40%. This value is consistent with a value of Z that has been decreasing with refinement over the past three decades from $\sim$ 1.89% to the current 1.40%.

2. We have renormalized chondritic abundances ratios to the most refractory of the major elements, Al. This results in an internally consistent normalization with all elements having abundance ratios at or below solar. This normalization removes the apparent enrichment of refractory lithophiles produced by normalization to Mg or Si.

3. The best-fit of the Earth/Sun abundance ratios f, to the joint DP model ($\log(f) = \alpha \log(T_C) + \beta$ and $\log(f) = 0$), yields $\alpha = 3.676 \pm 0.142$ and $\beta = -11.556 \pm 0.436$. These coefficients determine the critical devolatilization temperature

$T_D(E) = 1391 \pm 15$ K and represents a significant improvement on previous qualitative estimates ($\sim$ 1350–1430 K) of this important parameter.

4. Mercury (Hg) is the most volatile of all the elements for which the solar value has been assumed to be equal to the CI abundance. This leads to an expected deviation of the Earth's Hg abundance relative to the Sun. A solution to this deviation is to increase the Sun's Hg abundance by a factor of 13 ± 7 relative to the CI chondritic Hg abundance.

5. The deviations of C and O from our extrapolated volatility trend suggest that a better proxy for volatility than their T_C values based on equilibrium condensation from a hot gas, would be higher effective condensation temperatures.

6. The devolatilization processes that produced Earth's material had a similar but reduced effect on CI chondrites. Analogous to the devolatilization temperature of the Earth $T_D(E) = 1391 \pm 15$ K, we estimate the devolatization temperature of CI chondrites $T_D(CI) = 550^{+20}_{-100}$ K.

Chapter 4

Enhanced Constraints on the Interior Composition and Structure of Terrestrial Exoplanets

This chapter is adapted from Wang et al. [2019] originally published as

Wang, H. S., Liu, F., Ireland, T. R., Brasser, R., Yong, D., and Lineweaver, C. H. 2019. Enhanced Constraints on the Interior Composition and Structure of Terrestrial Exoplanets. MNRAS 482, 2222-2233, doi.org/10.1093/mnras/sty2749 (Advance Access, October 2018)

Abstract

This paper aims to enhance several important constraints that can reduce the uncertainty in the estimates of the interior composition and structure of terrestrial exoplanets. A major cause of the modeling inaccuracy is inherent in the prevalent assumption: elemental abundances of a planet are *identical* to the elemental abundances of its host star. Host stellar abundances are good proxies of planetary abundances, but *only* for refractory elements. This is particularly true for terrestrial planets, as evidenced by the relative composition differences between the Sun, Earth and other inner solar system bodies. We therefore argue that host stellar abundances should be *devolatilized* in order to correctly represent the bulk elemental composition of a terrestrial planet orbiting the host star. The modeling inaccuracy can be further reduced by considering light elements in the core of a terrestrial exoplanet. Rather than assuming pure iron, a chemical system of Fe-Ni-S is recommended in the modeling of core composition of a terrestrial exoplanet, and a value of 18 ± 4 for Fe/Ni is introduced as a constraint to this core chemical system. By applying these constraints to the Sun, it is shown that our estimates for the mantle and core compositions as well as core mass fraction of the Earth are verifiable by independent measurements/estimates.

By applying our approach to four exoplanet host stars: Kepler-10, Kepler-20, Kepler-21 and Kepler-100, we found that a potential terrestrial exoplanet orbiting Kepler-21 would be the most Earth-like while one orbiting Kepler-10 would be the least. To assess the resemblance of a rocky exoplanet to the Earth (in terms of interior composition and structure), high-precision host stellar abundances are critical. Based on our modeling approach and proposed constraints, a typical precision better than $\sim$ 0.04 dex for the host stellar abundances is necessary for such an assessment to be made.

4.1 Introduction

We are at the cusp of the golden era of discovery and characterization of exoplanets. To date, more than 3700 exoplanets have been confirmed[1] , via a wide range of observational techniques including transit photometry, radial velocity measurement, imaging, and microlensing [Winn and Fabrycky, 2015]. Continued improvements in observational and modeling techniques have led to more precise inference of planetary mass and radius [Weiss et al., 2016; Stassun et al., 2017, 2018]. High-precision and homogeneous analyses of host stellar abundances are also increasingly available [e.g. Nissen and Schuster, 2010; da Silva et al., 2015; Adibekyan et al., 2015; Brewer and Fischer, 2016; Spina et al., 2016; Kos et al., 2018]. At the same time, our knowledge of our own planet Earth and the Solar System has been enormously expanded with the efforts from the broad communities in geosciences, cosmochemistry, planet formation and star formation [e.g. Ireland and Fegley, 2000; McDonough, 2014; Wang and Lineweaver, 2016; Brasser et al., 2016; Kwok, 2016; Norris and Wood, 2017; Wang et al., 2018a]. Together these have opened the door for detailed studies of chemical composition, interior structure and habitability of rocky exoplanets.

Previous studies concerned with exoplanet interiors have generally assumed differentiated structures and molecular compositions to compute mass-radius relations [e.g. Valencia et al., 2007; Seager et al., 2007; Zeng and Sasselov, 2013; Howard et al., 2013; Dressing et al., 2015]. It has been concluded that with only mass and radius measurements an exact interior composition cannot be inferred for an exoplanet because the problem is highly underconstrained and degenerate [Rogers and Seager, 2010]. With the increasing availability of elemental abundances of planet host stars, recent studies [Dorn et al., 2015; Santos et al., 2015] have discussed the reduction of degeneracies in constraining the interior composition and structure of rocky exoplanets by adding host stellar abundances as the other principal constraint. Since then, an increasing number of updated models (with the similar principal constraints) have been proposed [e.g. Unterborn et al., 2016; Dorn et al., 2017b,a; Brugger et al., 2017; Unterborn et al., 2018], to go further in modeling exoplanetary interiors than direct conclusions that can be drawn from the observational data.

However, a major cause of modeling inaccuracy inherent in the prevalent exoplanetary interior models [e.g. Santos et al., 2015; Dorn et al., 2017b; Brugger et al., 2017; Unterborn et al., 2018; Hinkel and Unterborn, 2018] is that the elemental abundances of a rocky exoplanet are simplified to be identical to the elemental abundances of its host star. Host stellar abundances are good proxies of planetary abundances, but *only* for refractory elements[2]. This is particularly true for terrestrial planets, as evidenced by the relative differences in the bulk composition between the Sun, Earth and other inner solar system bodies [Davis, 2006; Carlson et al., 2014]. This led Dorn et al. [2017a] to conclude that further studies on solar system bodies are needed to improve our understanding of the correlation of relative bulk abundances between

[1] NASA Exoplanet Archive, `https://exoplanetarchive.ipac.caltech.edu`

[2] Elements with relatively high equilibrium condensation temperatures ($\gtrsim$ 1360 K) and they are resistant to heat/irradiation/impact. The opposite of refractory is volatile.

planets and host star and of the effect of such abundance correlations on exploring exoplanet interiors. Wang et al. [2018b] has quantified the devolatilization (i.e. depletion of volatiles) ingoing from the solar nebula to the Earth. The elemental abundance differences between the Earth and the Sun for Si, Mg, Fe and Ni are slight, but significant (a devolatilization factor of 10-20%); those for O, S, and C are substantial and devolatilized by up to 3 orders of magnitude. The former differences, in combination with the substantially devolatilized O, will have a direct and nontrivial effect on the mantle and core composition; the latter differences will have profound impact on the atmospheric composition, including importantly the abundance of surface water, and therefore habitability in general.

An additional source of modeling inaccuracy in the prevalent studies of exoplanetary interiors is that elements lighter than Fe and Ni are rarely taken into account in the core composition. Light elements play a key role in compensating the 5-10% density deficit of Earth's core [Birch, 1964; Hirose et al., 2013; McDonough, 2014; Wang et al., 2018a] (comparing to pure iron at core pressures) and in differentiating the liquid outer core from the solid inner core. The importance of light elements in a terrestrial exoplanet's core cannot be ignored, and their presence has direct consequences for estimates of core mass fraction and the melting temperature of an outer core (if it exists), and therefore the generation of exoplanetary magnetic fields.

With the goal of reducing the uncertainty in the estimates of interior composition and structure of terrestrial exoplanets, we present several important constraints and our analytical method in Sect. 4.2. Our modeling results are reported in Sect. 4.3, followed by the discussion in Sect. 4.4. We conclude in Sect. 4.5.

4.2 Constraints and Analysis

4.2.1 Bulk elemental composition of a terrestrial planet

As mentioned earlier, elemental abundances of a terrestrial planet are genetically connected to the elemental abundances of the host star, they are not identical, especially for non-refractory or volatile elements. We argue that the elemental abundances of the host star of a terrestrial planet should be devolatilized in order to infer the planetary bulk composition. Wang et al. [2018b] has established a fiducial devolatilization model (see Figure 4.1) by quantifying the compositional differences between the proto-Sun and the bulk Earth as a function of elemental condensation temperatures. This work is built upon the premise that devolatilization in a nebula may be universal and the Sun-to-Earth devolatilization pattern of Wang et al. [2018b] is applicable to infer the bulk composition of terrestrial exoplanets, particularly those within circumstellar habitable zones.

A variety of outcomes for the bulk composition of a rocky planet may result from composition-, location-, and timescale-dependent differences in various (and sometimes contrary) fractionation processes, such as incomplete condensation [e.g. Wasson and Chou, 1974; Grossman and Larimer, 1974; Cassen, 1996; Stracke et al., 2012], partial vaporization [e.g. Anders, 1964; Alexander and Wang, 2001; Huss et al.,

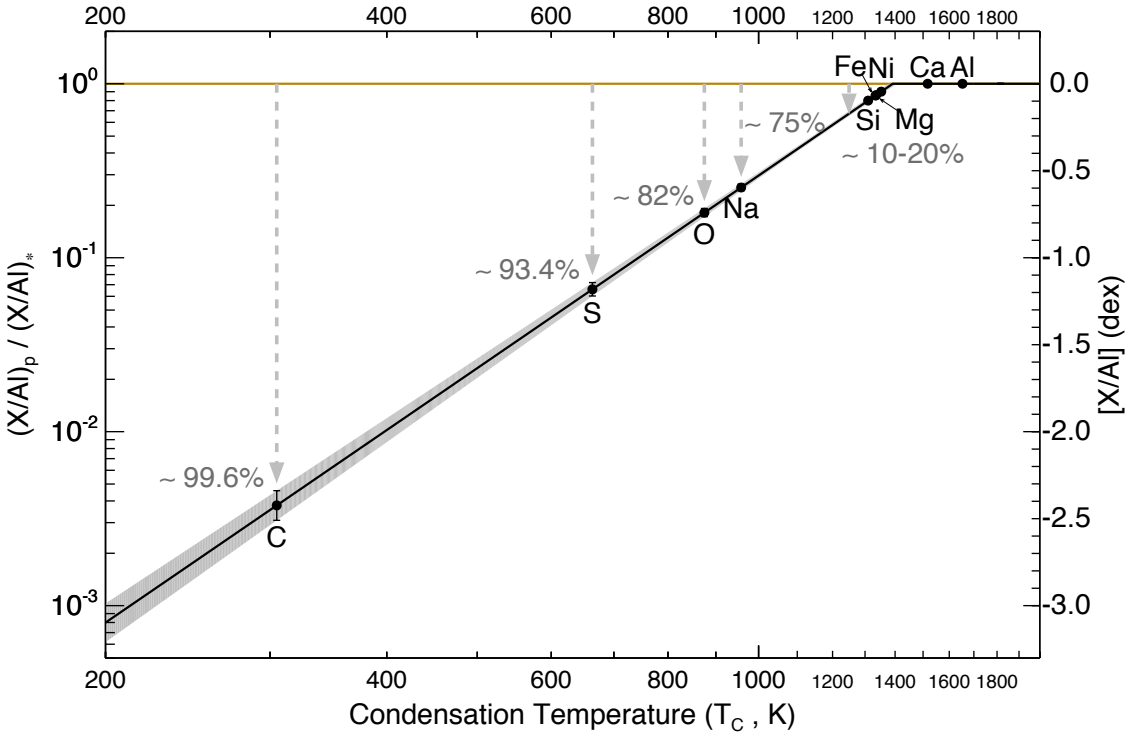

Figure 4.1: Devolatilization patterns from stellar nebulae to terrestrial exoplanets, which are drawn from the Sun-to-Earth devolatilization pattern of Wang et al. [2018b], including the best fit (the solid line in black) and its 1σ uncertainty (the wedge in grey), as well as the devolatilization factors indicated by the dashed arrows. Host stellar abundance is normalized to 1 in linear (or 0 in dex), shown as the solid horizontal line in brown. The x-axis is the elemental 50% condensation temperature (T_C) in logarithm from [Lodders, 2003], except for T_C(C) and T_C(O), which are adopted from Wang et al. [2018b] (see the text). The left-hand y-axis is in the logarithmic scale for the planet ('p')-to-star ('$*$') elemental abundance ratio (pre-normalized to Al), while the right-hand y-axis is labeled in dex for the corresponding $(X/Al)_p$ / $(X/Al)_*$. Only elements that are essential to control the mineralogy of a terrestrial planet are indicated on this plot and then employed in our subsequent analysis.

2003; Richter, 2004; Braukmüller et al., 2018], accretionary collision [e.g. O'Neill and Palme, 2008; Visscher and Fegley, 2013], and giant impacts in conjunction with magmatic differentiation [e.g. Paniello et al., 2012; Norris and Wood, 2017; Dhaliwal et al., 2018]. The compositional differences of Earth, Mars and Venus should be a measure of these variations within our own Solar System, but the degree to which the bulk compositions of Venus and Mars are different from the Earth is still debated in both the geochemical/cosmochemical community [e.g. Morgan and Anders, 1980; Wanke and Dreibus, 1988; Taylor, 2013; Wang et al., 2018a] and the planet formation community [e.g. Kaib and Cowan, 2015; Fitoussi et al., 2016; Brasser et al., 2017, 2018]. We also note that the *bulk* compositions of Venus and Mars are not well determined yet and thus reliable quantitative analysis of bulk compositional differences of them from the Sun or Earth is not warranted. We have been conservative to preclude the application of this algorithm to Mercury-orbit-like planets (e.g. warm super-Earths), as such planets may be more devolatilized than predicted due to plausibly more intensive stellar irradiation and bombardment histories. In spite of the complexity of planet formation, an essential step to improve the study of exoplanetary chemistry is to take into account devolatilization, with the best constrainable trend from the Sun to the Earth.

In Figure 4.1, we plot 10 major elements (C, S, O, Na, Si, Fe, Mg, Ni, Ca, and Al) that are essential for estimating the mineralogy of a terrestrial planet and place these on the best-fit devolatilization pattern of Wang et al. [2018b]. These 10 elements account for more than 99% of the total mass of Earth [McDonough, 2014; Wang et al., 2018a]. It should be noted that these points are not observational 'data' but indications of the model-based devolatilization scales (i.e. planet-to-host abundance ratios) of these elements versus condensation temperatures (T_C). These devolatilization scales are also numbered in the second and third columns of Table 4.1, in % (linear) and in dex (logarithmic), respectively. The normalization-reference element is Al, the most refractory major element. Normalising to other refractory elements (e.g. Ca) will not affect the analysis or results, since this normalization will not change the relative abundance ratio of other elements to oxygen that is the key to determine the redox state of a planet. It is worth noting that the T_C in Figure 4.1 refers to 50% condensation temperatures of Lodders [2003], except for C and O. As discussed in Wang et al. [2018b], an effective condensation temperature of C and O *under the assumption of non-equilibrium multiphase condensation* is a better indication of the volatility of the two elements, than 50% condensation temperature of them *under the assumption of equilibrium single-phase condensation* in Lodders [2003]. We adopt their best estimates of the effective T_C for C and O: 305 K and 875 K respectively.

4.2.2 Chemical network of the mantle of a terrestrial planet

In this study, the mantle of a terrestrial planet is limited to silicate mineralogy. This limitation is appropriate for two reasons: i) our devolatilization algorithm that is established for the Sun to a silicate-mantle terrestrial planet is unlikely to be applicable for a planetary system with C/O ratio larger than 0.8 (and thus forming carbide plan-

Table 4.1: Bulk elemental composition [X/Al][a] of potential habitable-zone terrestrial exoplanets (i.e. exoEarths) as devolatilized from their host stellar abundances[b].

X[c]	F_D (%) [d]	F_D (dex) [d]	Kepler 10 (L16)	Kepler 10 (S15)[e]	Kepler 20	Kepler 21[f]	Kepler 100b
C	99.6 ± 0.1	2.42 ± 0.09	-2.42 ± 0.09	-2.29 ± 0.10	-2.48 ± 0.10	-2.38 ± 0.10	-2.47 ± 0.12
S	93.4 ± 0.6	1.18 ± 0.04	-1.20 ± 0.04	–	–	-1.25 ± 0.06	-1.23 ± 0.07
O	82 ± 1	0.74 ± 0.02	-0.67 ± 0.03	-0.39 ± 0.08	-0.86 ± 0.08	-0.73 ± 0.07	-0.71 ± 0.10
Na	75 ± 1	0.60 ± 0.02	-0.72 ± 0.02	–	-0.65 ± 0.04	-0.62 ± 0.05	-0.57 ± 0.04
Si	20 ± 3	0.10 ± 0.02	-0.17 ± 0.02	-0.02 ± 0.03	-0.14 ± 0.03	-0.09 ± 0.03	-0.13 ± 0.04
Fe	14 ± 3	0.07 ± 0.02	-0.20 ± 0.02	-0.07 ± 0.03	-0.09 ± 0.06	-0.09 ± 0.07	-0.17 ± 0.08
Mg	14 ± 3	0.07 ± 0.02	-0.10 ± 0.02	0.09 ± 0.06	-0.05 ± 0.04	-0.07 ± 0.04	-0.10 ± 0.05
Ni	10 ± 4	0.05 ± 0.02	-0.20 ± 0.02	–	-0.07 ± 0.03	-0.12 ± 0.03	-0.11 ± 0.03
Ca	0	0	-0.05 ± 0.01	–	0.00 ± 0.04	0.00 ± 0.04	-0.06 ± 0.05
Al	0	0	0.00 ± 0.01	–	0.00 ± 0.02	–	0.00 ± 0.03

[a] $[X/Al] = \log((X/Al)_{planet}/(X/Al)_{Sun})$, where (X/Al) is the abundance ratio (by number in linear) of an element X to Al, and solar abundance refers to [Asplund et al., 2009]. Normalising to an element other than Al does not change our results. Following Wang et al. [2018b], we choose Al as the normalization element as it is the most refractory major element.
[b] Sources of host stellar abundances: Kepler 10: L16- [Column 2 of Table 2 of Liu et al., 2016]; S15- [Row 2 of Table A.1 and Row 2 of Table A.2 in Santos et al., 2015]. Kepler 20, Kepler 21 and Kepler 100: Table 3 of Schuler et al. [2015].
[c] Elements (X) are listed in order of decreasing devolatilization factor.
[d] F_D: Devolatilization factor, which refers to Figure 4.1 and Wang et al. [2018b].
[e] The elemental abundances of Kepler 10b (S15) are normalized to Fe, rather than Al, as no available Al abundance for Kepler 10 is reported in Santos et al. [2015]. This normalization difference will not change the subsequent analyses of key elemental ratios including Mg/Si, Fe/Si, and C/O.
[f] The elemental abundances of Kepler 21b are normalized to Ca, as no available Al abundance for Kepler 21 is documented in Schuler et al. [2015].

ets); ii) More recent studies [e.g. Fortney, 2012; Nissen, 2013; Teske et al., 2014; Brewer and Fischer, 2016] have suggested that prior studies [e.g. Bond et al., 2010b; Delgado Mena et al., 2010; Petigura and Marcy, 2011] overestimated C/O ratios. Thus, carbide planets may not be as abundant as previously thought.

We assume that the composition of silicate mantle varies within the chemical network of SiO_2-CaO-Na_2O-MgO-Al_2O_3-FeO-NiO-SO_3. And it is similar to to the NCFMAS (Na_2O-CaO-FeO-MgO-Al_2O_3-SiO_2) mantle model adopted in Dorn et al. [2015], but the oxides are reordered in the oxidation sequence (or ease of oxidation) [Johnson and Warr, 1999]. NiO and SO_3 are also added into the system. Due to the strong affinity of Ni with Fe, NiO is always expected if FeO is present in the mantle. SO_3 can combine with other oxides to form sulfate compounds (e.g. $CaSO_4$), which are important minerals in the silicate mantle (thought not as abundant as silicate compounds). The additions of NiO and SO_4 will also make estimates of the partition of Ni and S into the core more accurate (see Section 4.2.3). Sulfide minerals (except for FeS) are the major host of chalcophile (sulfur-loving) elements, but they are not taken into account in our mantle system since the abundances of all chalcophile elements (e.g. Cu, Zn, and Ag) are negligible in comparison with the abundances of major-rock forming elements considered here.

With regard to planetary mantle's temperature (T), pressure (P), and oxygen fugacity (fO_2, quantifying the oxidation potential of a system), the mineral host of carbon can be either oxidized carbonate species (denoted as C^{4+} or CO_2 in an ox-

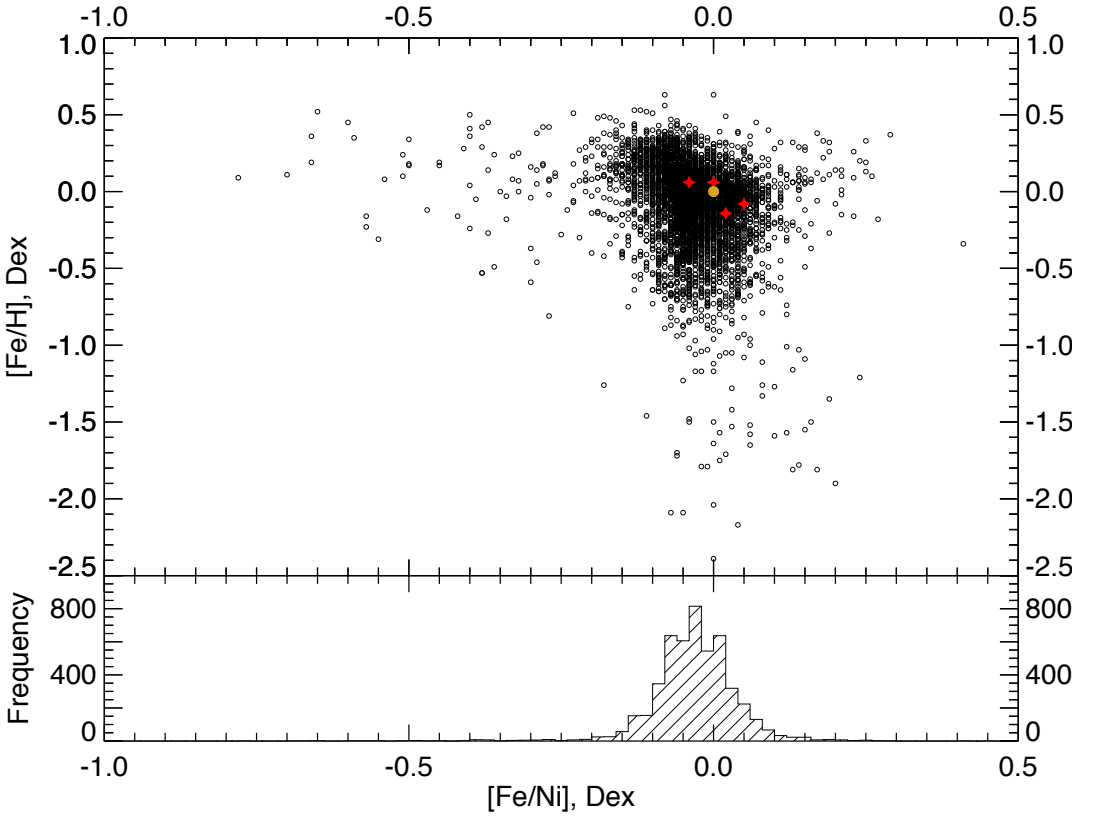

Figure 4.2: Distribution of [Fe/Ni] of more than 4900 FGK-type stars within 150 pc of the Sun. The values of [Fe/Ni] and [Fe/H] are relative to the Sun [Asplund et al., 2009], drawn from the Hypatia Catalog [Hinkel et al., 2014]. A Gaussian fit to the distribution of [Fe/Ni] gives [Fe/Ni] = -0.033 $\pm$ 0.049 dex (relative to the value of Sun = 1.28 dex). The corresponding value of Fe/Ni in linear is 17.7 ($= 10^{-0.033+1.28}$) with 1σ uncertainty of $\sim$ 2.0 (i.e. $(10^{0.049} - 1) \times 17.7 = 2.1$ for the upper error bar and $(1 - 10^{-0.049}) \times 17.7 = 1.9$ for the lower error bar). A conservative value of 18 ± 4 is adopted to constrain the Fe/Ni ratio in the core of a terrestrial exoplanet (see the main text). The yellow point represents the Sun while the red filled pluses indicate our four case stars.

idized form) [Panero and Kabbes, 2008; Boulard et al., 2011] or the reduced native element (e.g. graphite/diamond) [Walter et al., 2008; Dasgupta and Hirschmann, 2010]. Oxidized carbon is considered only when all major elements listed in the chemical network of the mantle have been oxidized, since carbon is experimentally shown to be oxidized with more difficulty than Fe (presumably Ni as well) over the entire pressure and temperature ranges of Earth's mantle [Unterborn et al., 2014]. We also assume that if oxygen fugacity is extremely limited, metals like Ca, Na, Mg and Al can be present natively in such a reduced mantle, while Fe and Ni will be all partitioned into the core.

4.2.3 Chemical network of the core of a terrestrial planet

We assume that a terrestrial planet's core consists of the Fe-Ni-S alloy. Nickel is added into the core's constituents as it has a similar siderophile tendency as iron. Sulfur is a leading candidate for the principal light element in the core because it has a strong affinity for iron [Li and Fei, 2014], and indeed evidence for large-scale sulfide fractionation during Earth's mantle-core differentiation has been found [Savage et al., 2015]. This does not preclude the existence of other light element candidates like silicon and oxygen in the core, but their fractionation between the mantle and the core is very uncertain without knowing the internal pressure and temperature of such a planet [Hirose et al., 2017]. Therefore, in this study, we limit the light element candidate in a terrestrial exoplanet's core to be sulfur only. Furthermore, sulfur is capable of reducing the core's melting temperature, density, and surface tension [Li and Fei, 2014], which may be important to the dynamo modeling of planetary magnetic field in further studies [e.g. Driscoll and Olson, 2011; Driscoll, 2016].

It is important then to put constraints on the fractionation of these elements between the mantle and core. The solar system ratio of Fe/Ni is 17.4 ± 0.5 (by mass) as drawn from a variety of chondrites in the solar system [McDonough, 2017]. This value could vary from star to star, but the variance should be small based on the common nucleosynthesis pathways of the two elements in stars. Indeed, by analysing the Fe/Ni ratios of more than 4900 FGK-type stars within 150 pc of the Sun from Hypatia Catalog [Hinkel et al., 2014], we have found that the Fe/Ni cosmic ratio is essentially fixed at 17.7 with 1σ uncertainty of ~ 2.0 (see Figure 4.2). Although their ratio in the planetary core might not be fixed, it will deviate little from the cosmic ratio considering their very similar refractory and siderophile features (William F. McDonough, personal communication). To be conservative, a value of 18 ± 4 is adopted to constrain the Fe/Ni ratio in the core of a terrestrial planet. This adoption is appropriate for this study as the upper (2σ) limit (22) of this value has covered the maximum value of Fe/Ni of our selected planet hosts. The lower limit (14) is $\sim 1.5\sigma$ lower than the Fe/Ni ratios of our selected cases, but it is a good assumption as Fe/Ni in the core of a terrestrial planet may go lower (not higher) than its value in the bulk planet [Seifert et al., 1988; McDonough and Sun, 1995; Wang et al., 2018a] Another constraint is the abundance range of Ni and S that may be present in the core. The upper limits of Ni and S in the core can be up to their abundances in the bulk planet, referring to the scenario of the Earth: $> 90\%$ of Ni and $> 95\%$ of S are in the Earth's core [McDonough, 2014]. The low limits can be assumed as nil, such as in the extreme scenario that the oxygen fugacity is too high and all metals including Fe could be fully oxidized (then a planet with no core would result) [Elkins-Tanton and Seager, 2008]. See more details in Section 4.2.4 and Appendix C.1.

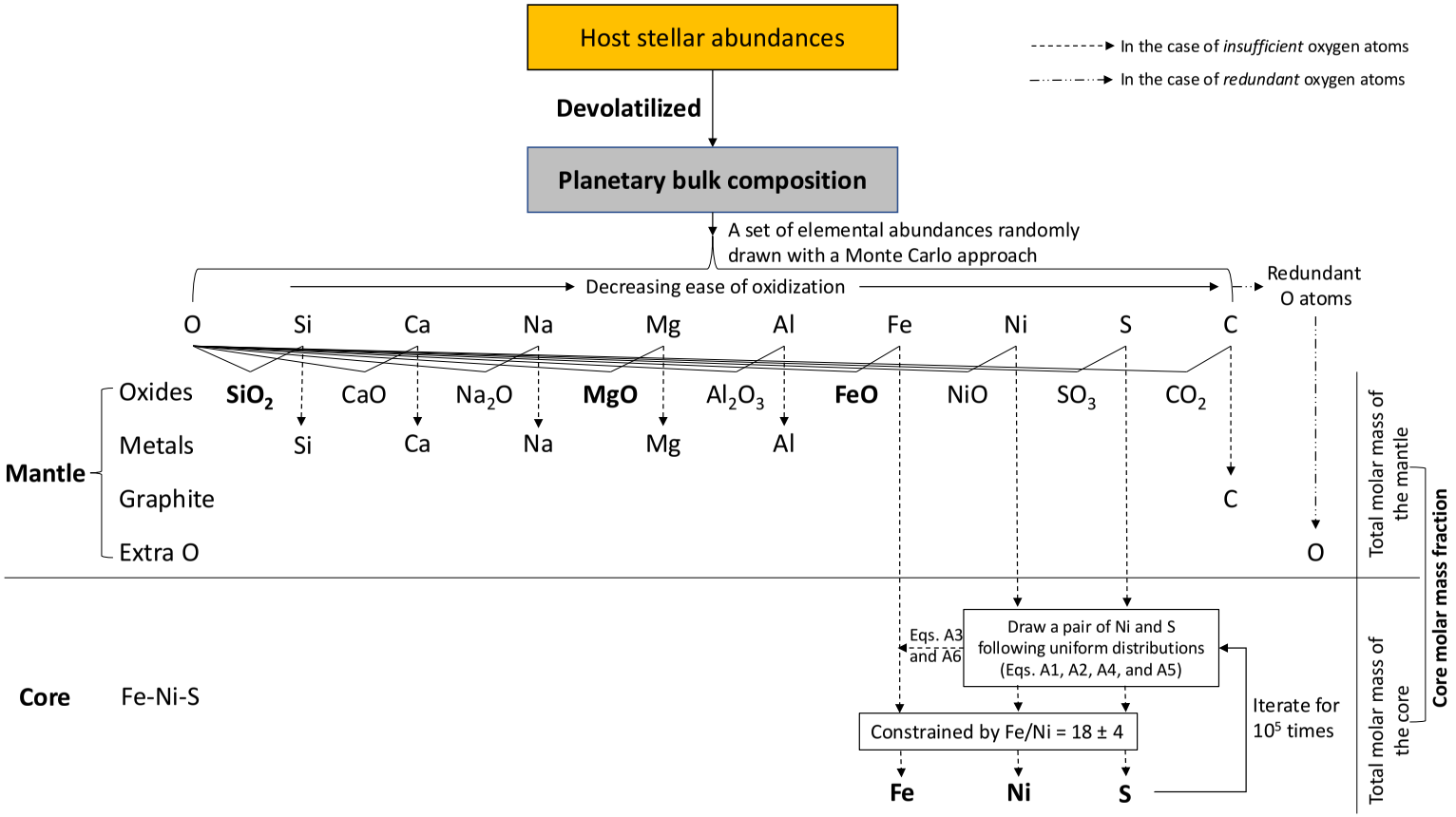

Figure 4.3: Computational procedure scheme of elemental fractionation between the mantle and the core of a terrestrial planet. The detailed descriptions of the procedure can be found in Appendix C.1.

4.2.4 Analysis

Based on the availability of high-precision stellar host abundances, we select four solar-type stars: Kepler-10 (K10), Kepler-20 (K20), Kepler-21 (K21), and Kepler 100 (K100). All four have been confirmed to be planet hosts with the discovery of at least one super-Earth (with 3-10 Earth masses) orbiting each host. If there exists terrestrial exoplanets orbitting in the habitable zone of these stars, we are interested in what the chemistry and interior structure of these postulated planets would be. For K10, we have two sets of stellar elemental abundances: Santos et al. [2015] and Liu et al. [2016]. For other selected cases, our stellar elemental abundances are from Schuler et al. [2015] (with a typical uncertainty of $\lesssim 0.04$ dex).

Following the recommended constraint on planetary bulk composition in Sect. 4.2.1, we apply the devolatilization pattern of Wang et al. [2018b] to the elemental abundances of the planet hosts of our sample. This leads to the first-order estimates of bulk elemental composition of *potential* terrestrial exoplanets that are particularly within the habitable zone around these host stars (see Table 4.1). For brevity and convenience for our subsequent descriptions, we call such an exoplanet 'exo-Earth' (or 'exoE' when it is preceded by the name of its host star). However, this term means nothing about the similarity of such a planet to the Earth, except for the connotation that this planet is derived from its host star based on the equivalent devolatilization scale from the solar nebula to the Earth (the limitation of this assumption is discussed in Section 4.4.3). The uncertainties on the bulk compositions of these exo-Earths in Table 4.1 are propagated from the 1σ uncertainty of the devolatilization pattern of Wang et al. [2018b] and the uncertainties associated with the elemental abundances of the corresponding planet hosts.

Then we analyze the key elemental ratios (e.g. Mg/Si, Fe/Si, and C/O) that modulate the primary mineralogy of a terrestrial planet. Mg/Si informs the rock types of a silicate mantle. A higher Mg/Si indicates a more olivine-dominated mantle, otherwise a more pyroxene-dominated one. Pyroxene can accommodate more water than olivine, and pyroxenites have higher capacity to hold water (if water exists on the surface or in the subsurface of a planet). Fe/Si may approximate the zero-order core mass fraction of a planet, upon the oxidation state of the planet. C/O is critical to determine the oxygen fugacity and thus the oxidation state of a planet. The errors in these key elemental ratios are calculated using a Monte Carlo approach by drawing 2×10^4 values of the estimated planetary bulk composition for each element following a Gaussian distribution around the uncertainties.

Based on the recommended chemical networks for the mantle and core of a terrestrial planet in Sects. 4.2.2 and 4.2.3, the elemental fractionation between the mantle and the core is performed using the stoichiometric balance between the budget of oxygen atoms in the bulk planet and the abundances of oxides/compounds to be considered for the planet. The computational procedure is summarised in Figure 4.3, while a detailed description can be found in Appendix C.1.

As a verification for this set of computations, we apply this procedure to the proto-Sun [Wang et al., 2018b]. The predicted interior compositions of the "model

Earth" in Table 4.2 are consistent (within uncertainties) with the independent estimates of the composition of the pyrolite silicate Earth [McDonough and Sun, 1995], the composition of Earth's core [McDonough, 2014], as well as the seismologically-constrained core mass fraction [Wang et al., 2018a].

Table 4.2: Comparison of the estimates of the interior compositions of the "model Earth" (as devolatilized from the proto-Sun[a]) with other independent estimates

	Quantity	Model Earth	McDonough and Sun [1995]
Mantle	SiO_2	50.3 ± 4.7	45.0
	CaO	3.60 ± 0.34	3.55
	Na_2O	0.44 ± 0.04	0.36
	MgO	38.0 ± 6.2	37.8
	Al_2O_3	4.40 ± 0.40	4.45
	FeO	$1.87^{+7.14}_{-1.87}$	8.05
	NiO	$0.40^{+0.45}_{-0.40}$	0.25
	SO_3	0.67 ± 0.62	–
	CO_2	–	–
	Graphite	0.39 ± 0.07	–
	Metals	–	–
	Extra O	–	–
			McDonough [2014][b]
Core	Fe	93.28 ± 1.23	92.33
	Ni	5.22 ± 0.63	5.62
	S	1.50 ± 1.05	2.05
Core mass fraction (wt% planet)		31.3 ± 5.3	32.5 ± 0.3 [c]

[a] The protosolar abundances are from Wang et al. [2018b].
[b] Mass fractions of the three elements in the core of McDonough [2014] have been renormalized under the assumption of only the three elements present in the core as practiced in this study.
[c] Refers to Wang et al. [2018a], in which the core mass fraction is integrated from Earth's radial density profiles.

4.3 Results

4.3.1 Estimates of key elemental ratios

In Figure 4.4, we compare the key elemental ratios between the host Kepler-10 and its potential exo-Earth, by using two sets of its host stellar abundances: one is with

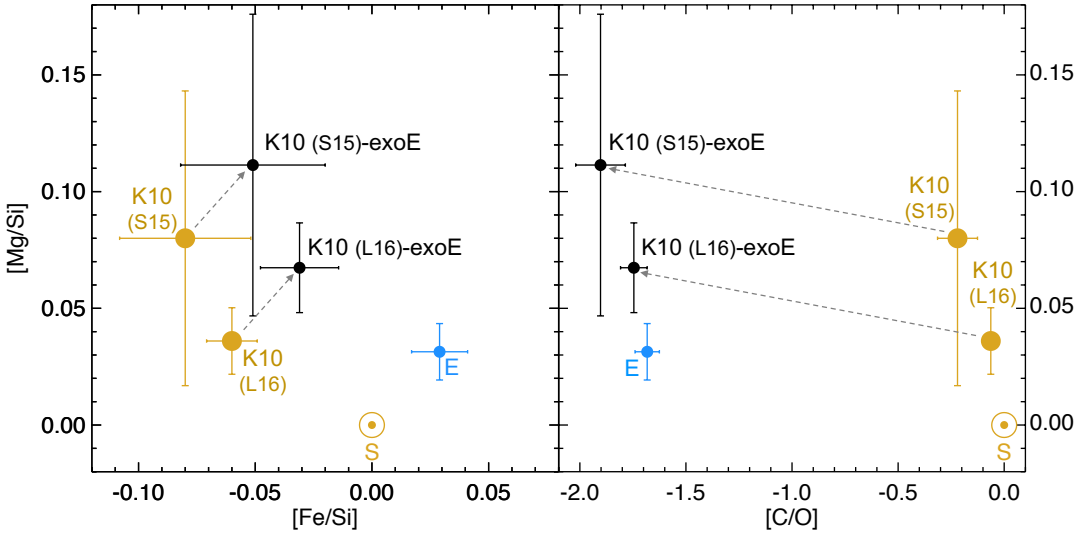

Figure 4.4: In the case of Kepler 10, the comparison of key elemental ratios ([Mg/Si], [Fe/Si], and [C/O], in dex) between the host star and its potential exo-Earth. This comparison includes two sets of host stellar abundances: Santos et al. [2015] (labeled as K10 (S15)) and Liu et al. [2016] (labeled as K10 (L16)), and their corresponding exo-Earths are potted as smaller black dots, labeled as K10 (S15)-exoE and K10 (L16)-exoE, respectively. Key elemental ratios in the Sun ('S', the symbol $\odot$ in yellow, Asplund et al. [2009]) and in Earth that is devolatilized from it ('E', the dot in blue) are plotted as references. The dashed arrows indicate the trajectories of these elemental ratios from Kepler-10 to K10-exoE due to the applied devolatilization.

a typical uncertainty of $\gtrsim 0.06$ dex [Santos et al., 2015] and the other is with a typical uncertainty of $\lesssim 0.02$ dex [Liu et al., 2016]. With the more precise host stellar abundances, the planetary elemental ratios for Mg/Si, Fe/Si, and C/O are all significantly different from the corresponding host stellar elemental ratios. Namely, they do not overlap within their uncertainties. Whereas, these significant differences are substantially dismissed with the less precise host stellar abundances, except for C/O (its difference is up to 1.7 dex, i.e., a factor of ~ 50). It is worth noting that this is the first attempt (based on theoretical models) to compare the key elemental ratio differences between a terrestrial exoplanet and its host star, rather than those differences between a star and the Sun as usually done in the literature [e.g. Bond et al., 2010b; Santos et al., 2015; Brewer and Fischer, 2016]. Nonetheless, in order to distinguish two unique terrestrial exoplanets (orbiting different stars), high-precision host stellar abundances are required, as concluded in Hinkel and Unterborn [2018] as well. In our subsequent modeling of planetary interiors, we neglect less-precise Kepler-10 abundance estimates (also available for fewer elements) of Santos et al. [2015].

We also compute the key elemental ratios for postulated exo-Earths orbiting three other planet hosts (e.g. Kepler-20, Kepler-21, and Kepler-100). The key elemental ratios of these postulated exo-Earths are plotted in Figure 4.5. When considering the

deviations of these exoplanetary key elemental ratios (including the uncertainties) from Earth's, K21-exoE is overall the most Earth-like while K10-exoE is the least. If only based on Fe/Si (i.e. indicating the plausible core/mantle mass fraction), K20-exoE is more Earth-like than K21-exoE and K100-exoE, while K10-exoE is the least. These resemblances will be refined in further by the following modeling of planetary interiors.

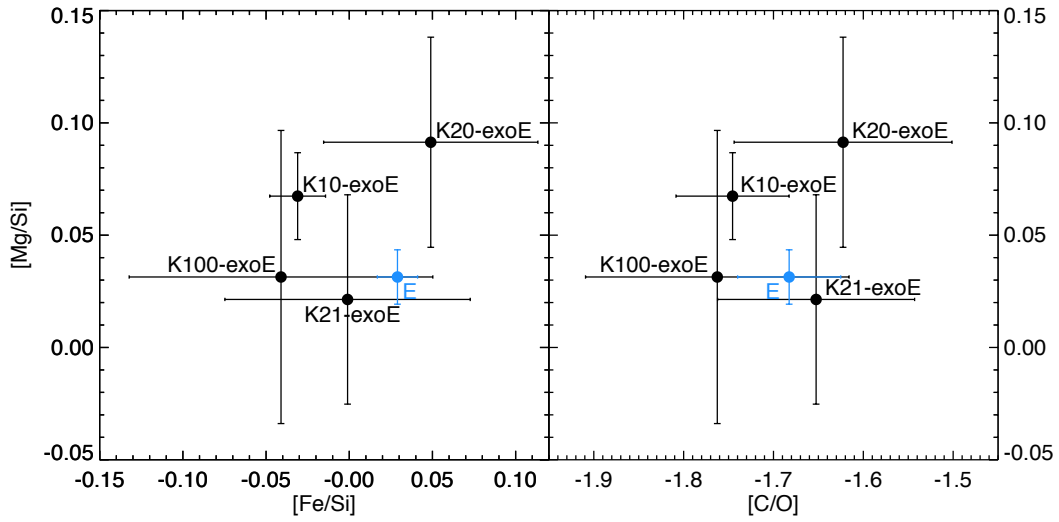

Figure 4.5: For all studied cases of planet hosts, the comparison of these key elemental ratios between their potential exo-Earths, labeled as K10-exoE, K20-exoE, K21-exoE, and K100-exoE, which are respectively corresponding to the potential habitable-zone terrestrial exoplanets orbiting the planet hosts: Kepler-10, Kepler-20, Kepler-21, and Kepler-100. Host stellar abundances are all from Schuler et al. [2015], except for Kepler-10 that is from Liu et al. [2016]. The planet Earth (same as Figure 4.4) is plotted as a reference.

4.3.2 Estimates of planetary interiors

Based on the recommended chemical systems of the mantle and core of a terrestrial planet, we estimate the mantle and core composition as well as core mass fraction for these potential exo-Earths. These estimates are listed in Table 4.3. We also extract the information of the major components (SiO_2, MgO, and FeO) in the mantle and of the core mass fraction, and then illustrate them comparatively in Figure 4.6. It should be noted that the mantle composition in the ternary diagram of Figure 4.6 has been renormalized by ignoring all minor components and assuming SiO_2 + MgO + FeO = 100 wt%.

From Table 4.3 and Figure 4.6, we can further identify that K21-exoE is the most Earth-like, in terms of all interior parameters we have modeled, including the mantle composition, core composition and core mass fraction. This similarity has been implied by the analyses of key elemental ratios above, but it is more conclusive and

Table 4.3: Estimates of the mantle and core composition as well as core mass fraction of potential habitable-zone terrestrial planets orbiting the studied host stars: Kepler-10 (K10), Kepler-20 (K20), Kepler-21 (K21), Kepler-100 (K100).

	Quantity	Potential habitable-zone terrestrial exoplanets (exo-Earths)[a]			
	(molar wt%)	K10-exoE	K20-exoE	K21-exoE	K100-exoE
Mantle	SiO_2	30.3 ± 2.6	50.7 ± 3.3	49.9 ± 4.9	40.5 ± 4.4
	CaO	2.50 ± 0.22	4.39 ± 0.34	3.85 ± 0.38	2.98 ± 0.36
	Na_2O	0.23 ± 0.02	0.43 ± 0.03	0.41 ± 0.04	0.41 ± 0.05
	MgO	29.2 ± 2.4	25.7 ± 3.6	43.3 ± 3.9	36.0 ± 4.0
	Al_2O_3	3.28 ± 0.31	–	–	4.01 ± 0.47
	FeO	31.3 ± 5.1	–	$1.53^{+8.35}_{1.53}$	13.9 ± 7.9
	NiO	1.71 ± 0.34	–	$0.15^{+0.40}_{-0.15}$	0.95 ± 0.51
	SO_3	1.25 ± 0.46	–	0.50 ± 0.48	0.90 ± 0.51
	CO_2	–	–	–	–
	Graphite	0.28 ± 0.05	0.38 ± 0.05	0.42 ± 0.06	0.30 ± 0.07
	Metals	–	18.4 ± 10.7	–	–
Core	Fe	85.7 ± 5.0	94.5 ± 0.6	94.1 ± 1.3	92.9 ± 1.9
	Ni	5.25 ± 0.73	5.49 ± 0.63	4.76 ± 0.65	5.69 ± 0.68
	S	9.07 ± 5.24	–	1.16 ± 1.14	$1.40^{+1.83}_{-1.40}$
Core mass fraction (wt% planet)		$1.4^{+5.0}_{-1.4}$	35.3 ± 5.1	31.9 ± 5.9	19.6 ± 6.3

[a] Bulk elemental compositions of these exo-Earths are from Table 4.1.

obvious here. In particular, according to the *normalized* mantle composition in the ternary diagram of Figure 4.6, K20-exoE has the highest SiO_2 (66.4 ± 4.3 wt%) and the lowest MgO (33.6 ± 4.7 wt%). The mantle rocks of K20-exoE therefore will be more enriched in pyroxene ($MgSiO_3$) compared to other planet cases studied here (including the Earth). In contrast, K10-exoE has the lowest SiO_2 (33.4 ± 2.9 wt%) and moderate MgO (32.2 ± 2.8 wt%), and thus its mantle rocks will potentially be more forsterite (Mg_2SiO_4) enriched than the others. For K21-exoE and K100-exoE, there is an overlap of their mantle compositions with that of the Earth as shown in the ternary diagram, so they would have similar mantle rocks as the Earth's. However, as shown in the bar diagram of core mass fractions (Figure 4.6b), K100-exoE has a relatively smaller core (in terms of core mass fraction) than K21-exoE and the Earth, and the latter two are comparable. This can be explained by the differences of planetary bulk compositions (Table 4.1), in which the mean of Fe abundance of K100-exoE (-0.17 ± 0.08 dex) is $\sim 1\sigma$ lower than that of K21-exoE (-0.09 ± 0.07 dex) and that of the Earth (-0.07 ± 0.02 dex) while their abundances of other major elements including O, Mg, and Si are similar.

In addition, FeO is the most enriched in the mantle of K10-exoE (while it is the least (nil) in the mantle of K20-exoE). Namely, in comparison with other planet cases studied here, the differentiation of iron into the core of K10-exoE is the least efficient, thus leading to the smallest core (0-6.4 wt %) among the studied cases. The reason is present in its distinct host stellar abundances. Comparing with other selected planet hosts, Fe abundance in Kepler 10 [refering to Liu et al., 2016] is about 1–3σ lower while its O abundance relative to Mg and Si (i.e. O - Mg - 2Si, in dex) is 1–5σ higher. As a consequence, almost all Fe in Kepler 10 is oxidized, and only a tiny amount of metallic Fe sinking into the core, thus leading to the substantially smaller core mass fraction in K10-exoE as modeled. This reveals the importance of the trade-off between oxygen and other major rock-forming elements to the exoplanetary interior modeling.

4.3.3 Conservative estimates

We also apply the upper and lower limits of the 3σ error bar of the best-fit devolatilization pattern of Wang et al. [2018b] to the respective upper and lower limits of the host stellar elemental abundances. It should be noted that the 3σ is conveniently amplified over the uncertainty associated with the coefficients of the pattern; thus, the resultant 3σ range is more conservative than a range constrained by a 3σ chi-square fit. The resultant conservative estimates A (i.e. 3σ less devolatilized compared to the Sun-Earth case) and B (i.e. 3σ more devolatilized compared to the Sun-Earth case) are listed in Table 4.4.

Though the volatile gradient of a planetary system versus the distance to its central star is still controversial [Morgan and Anders, 1980; Palme, 2000; Wang and Lineweaver, 2016; Jin and Mordasini, 2018], the dichotomy of planets from 'rocky' to 'gas/icy' or from 'warm' to 'cold' would be expected from inward to outward in a planetary system (if those planets exist around the central star). Therefore, the con-

servative estimate A might assemble the interior properties of 'cold' rocky planets (or asteroids) at or beyond the outer edge of the habitable zone but within the snow-line of a planetary system. In contrast, the conservative estimate B might be a better proxy for the interior properties of 'warm' rocky planets, such as the known planets Kepler-10b, Kepler-20b, Kepler-21b, and Kepler-100b, which are closer to their host stars.

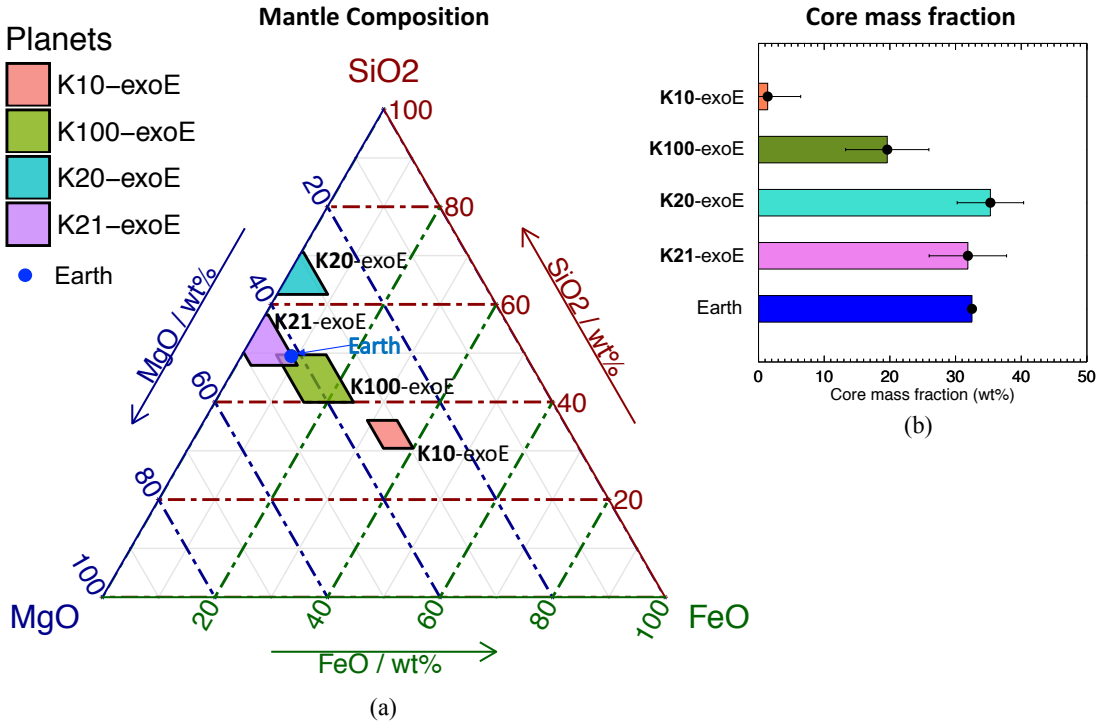

Figure 4.6: (a) A ternary diagram illustrating the estimates of the mantle composition (normalized by SiO_2 + MgO + FeO = 100 wt%, adapted from Table 4.3.) for potential exo-Earths orbiting the studied host stars. The Earth's mantle composition of SiO2, MgO, and FeO in McDonough and Sun [1995] is normalized similarly and plotted as a reference. (b) A bar graph comparing the estimates of the core molar mass fraction of these exo-Earths (see Table 4.3.). The Earth's core mass fraction (32.5 $\pm$ 0.3 wt%) in Wang et al. [2018a] is plotted as a reference.

Table 4.4: Conservative estimates of the mantle and core composition as well as core mass fraction of any rocky exoplanet orbiting the studied planet hosts

	Quantity	Conservative estimate A[a]				Conservative estimate B[b]			
	(molar wt%)	K10	K20	K21	K100	K10	K20	K21	K100
Mantle	SiO_2	23.3	26.4	25.3	24.0	51.0	47.5	61.0	59.1
	CaO	1.68	2.06	1.76	1.56	4.96	–	–	5.09
	Na_2O	0.25	0.32	0.31	0.34	0.27	–	–	0.4**1**
	MgO	22.4	27.6	22.5	21.4	26.5	–	–	**0.55**
	Al_2O_3	2.17	2.3**1**	–	2.00	–	–	–	–
	FeO	25.1	37.**2**	32.5	27.5	–	–	–	–
	NiO	1.33	1.9**0**	1.48	1.51	–	–	–	–
	SO_3	2.69	–	2.25	2.40	–	–	–	–
	CO_2	4.90	1.07	5.02	4.35	–	–	–	–
	Graphite	–	1.01	–	–	0.08	0.07	0.08	0.07
	Metals	–	–	–	–	17.2	52.4	38.9	34.8
	Extra O	16.2	–	8.90	14.9	–	–	–	–
Core	Fe	–	–	–	–	93.8	94.0	93.9	92.5
	Ni	–	–	–	–	5.28	6.05	5.39	6.68
	S	–	–	–	–	0.92	–	0.69	0.86
Core mass fraction (wt% planet)		0	0	0	0	31.7	38.3	36.1	32.8

[a] Applying the upper bound of 3σ uncertainty of the Sun-to-Earth devolatilization pattern to the upper limits of host stellar abundances.

[b] Applying the lower bound of 3σ uncertainty of the Sun-to-Earth devolatilization pattern to the lower limits of host stellar abundances.

4.4 Discussion

4.4.1 Comparison with previous studies

The diversity of planetary interiors should be expected. Neither our conservative estimates in Table 4.4 nor the estimates for habitable zone terrestrial exoplanets in Table 4.3 should be taken as an explicit interpretation of the interiors of any existing planet orbiting these studied host stars, but only the plausible ranges constrained by different scenarios as demonstrated in the paper. The previous studies [e.g. Santos et al., 2015; Weiss et al., 2016; Brugger et al., 2017] usually state that their analyses are for an explicit planet around a parent star but this statement should be taken with caution. For example, the core mass fraction (wt%) of Kepler-10b has been previously estimated to be 27.5 ± 1.7 [Santos et al., 2015], 17 ± 11 [Weiss et al., 2016], and 10-33 [Brugger et al., 2017], which seem to approximate our conservative estimate B (31.2) for a 'warm' rocky planet orbiting Kepler 10. Whereas, those previous estimates are achieved by fixing all Fe into the core [Santos et al., 2015] or relying on Mg# (= Mg/(Mg + Fe)) [Weiss et al., 2016; Brugger et al., 2017], without considering oxygen fugacity/budget that controls the oxidation state of a planet. If one generalizes those fixed assumptions to potential rocky planets in different distances to the same star, the same chemistry and interiors for these planets would result. Although taking into account planetary mass and radius, the modeling results could be more specific to such planets but those results would still be degenerate to a degree, to which that oxygen fugacity/budget would vary in the disk. When targeting a potentially habitable planet for further characterization with future missions, we should particularly be cautious with this kind of 'explicit' claim, which may only assemble one scenario of possible interior properties of rocky exoplanets orbiting in different distances to their host stars. The depletion of oxygen in Kepler-10 planets relative to the host star is not considered in Dorn et al. [2017b], but they assume $\mathrm{Fe/Si_{mantle}}$ = 0-$\mathrm{Fe/Si_{star}}$ (uniform distribution), implicitly resulting in varied differentiation of Fe into the core, which somehow assembles the consideration of oxygen fugacity/budget in determining the fractionation of Fe between the mantle and core.

Complex mineral compounds (e.g. $\mathrm{(Mg,Fe)SiO_3}$ (hypersthene), $\mathrm{(Mg,Fe)_2SiO_4}$ (olivine)) have been presumed to be present in the mantle rocks of super-Earths in the studies of Santos et al. [2015], Weiss et al. [2016], Brugger et al. [2017], and Hinkel and Unterborn [2018]. However, for exoplanets that are larger than Earth, their mineralogies may not be sensibly interpretable in using the Equation-of-State parameters measured with respect to the pressure and temperature regime of the Earth [Mazevet et al., 2015]. Therefore, we have chosen to use first-order mineral forms (i.e. oxides) for our modeling of mantle and core compositions. To first order, the planetary chemistry does not change, just the mineralogy. This practice is also in line with Dorn et al. [2015, 2017b,a]. When we would have the observational information of atmospheric thickness/composition of a terrestrial exoplanets at the era of JWST, we could know better the plausible pressure range associated with the solid regime of such a planet. With the further progress of ultrahigh pressure and

temperature experiments of the physical state and properties of minerals, we can be more confident then to model more complex exoplanetary mineralogies.

4.4.2 Requirement on the precision of host stellar abundances

Hinkel and Unterborn [2018] modeled the complex mineralogy for fictive planets around the 10 closest stars to the Sun (excluding those known to host planets), by using stellar abundances from the Hypatia Catalog [Hinkel et al., 2014]. They concluded that abundance uncertainties need to be on the order of [Fe/H] < 0.02 dex, [Si/H] < 0.01 dex, [Al/H] < 0.002 dex, [Mg/H] and [Ca/H] < 0.001 dex, in order to distinguish different planetary populations orbiting different stars. However, based on our modeling results above, we have demonstrated that the interior composition and structure of terrestrial exoplanets orbiting different stars can be distinguished between each other, by using the current high-precision host stellar abundances (with a typical uncertainty of 0.04 dex, provided with more appropriate constraints on planetary bulk composition and on mantle and core chemical networks as recommended in this work. Though it is legitimate to strive for much more precise stellar abundances (as well as planetary mass and radius measurements) and thus to improve the interior modeling accuracy, we should be more realistic however, since data precision also depends on characteristics of target stars and observation exposure time. A careful weighing of costs and benefits is crucial for the success of a space mission like TESS and follow-up observations. We hope our conclusion on the requirement of stellar abundance uncertainties could be an updated reference for the exoplanet community, which is expanding to incorporate more experts on stellar spectroscopy to join the cohort of exploring star-planet companions as an interactive system.

4.4.3 Limitations

The success of a theoretical model is subject to the limitations of premises/assumptions. Firstly, as mentioned earlier, our model is limited by how representative of the Sun-to-Earth devolatilization pattern is for terrestrial planets in general. If we had a more exhaustive devolatilization model built on the comprehensive comparisons of the compositions of all inner solar system rocky bodies, gas giants, and icy bodies (including a variety of comets), we would have more accurate modeling results for exoplanetary chemistry. However, the bulk compositions of these bodies (except for Earth) are still not well determined. Potentially, a variety of differentiated and undifferentiated meteorites would help on this. Still, such a model would be deficient in the absence of taking stochastic processes – e.g. chondrule formation and later veneer – into account. We have little knowledge of how these processes would happen in exoplanetary systems based on current observations. We have just scratched the surface of considering devolatilization in modeling exoplanetary interiors, and this issue remains degenerate. Secondly, our approach to oxidizing elements by following an oxidation sequence might be worth revisiting if the oxidation of elements is done in parallel (simultaneously), not in sequence. In the parallel case, all rock-forming

elements would compete to be oxidized to some extent. It is unclear how significant the end-member oxides resulting from this competition would be in comparison with those resulting from our assumed sequence. Thirdly, our modeling results are also limited to the current dimensionality of the model, namely, two-component overall structure (an iron alloy core and a silicate mantle), with no water layer (or oceans) or gas layer (or H/He envelopes) considered yet (also due to our currently absent consideration of planetary density). With the upcoming addition of atmosphere observations, we are expecting to expand the dimensionality of our model to be more inclusive of water/gas reservoirs in a terrestrial exoplanet by taking into account important atmospheric information, pressure and temperature associated with the actual size of the solid regime of a planetary body.

Nevertheless, we envisage that if a terrestrial planet is confirmed in the habitable zone around the host stars studied here, our modeling results of the mantle and core compositions as well as core mass fractions listed in Table 4.3 are good first-order estimates of the interior composition and structure of that planet. We also emphasize that the purpose of this work is to set more appropriate initial conditions for modeling exoplanetary interiors. These enhanced constraints can be potentially transferable to other recent models [e.g. Dorn et al., 2017b,a; Brugger et al., 2017] and thus enhance the model performance. Additional data (e.g., atmospheric information and applicable Equation-of-State parameters for all considered compositions) are required for further studies to decipher the detailed interior structure and chemistry, surface conditions and thus habitability of such terrestrial exoplanets.

4.5 Summary and Conclusions

Devolatilization (i.e. depletion of volatiles) plays an essential role in the formation of rocky planetary bodies from a stellar nebular disk [Bland et al., 2005; Norris and Wood, 2017]. The terrestrial devolatilization pattern of Wang et al. [2018b] has been applied in this study to infer the bulk elemental composition of potential terrestrial exoplanets that are presumed to exist within the circumstellar habitable zones. The inferred planetary bulk composition (rather than the host stellar abundances) provides improved principal constraints to model the interior composition and structure of such planets. Other recommended constraints include i) the mantle chemical system (SiO_2-CaO-Na_2O-MgO-Al_2O_3-FeO-NiO-SO_3, in order of the ease of oxidation); ii) the core chemical system (Fe-Ni-S alloy, with the constraint Fe/Ni = 18 $\pm$ 4).

By applying these constraints to the Sun, we show that the mantle and core compositions of our model Earth are verifiable by the independent measurements/estimates for the planet Earth in the literature. By applying our modeling approach to selected planet hosts (Kepler-10, Kepler-20, Kepler-21 and Kepler-100), we find that the interior compositions and structures of potential terrestrial exoplanets in the habitable zones around these stars are diverse. For example, the estimates of core mass fraction range from about 1.5 wt% (K10-exoE) to about 35 wt% (K20-exoE). This diversity can be explained by the differences in their host stellar abundances.

With respect to the interior estimates (i.e. mantle and core compositions as well as core mass fraction), we conclude that a potential terrestrial planet orbiting Kepler-21 would be the most Earth-like while one orbiting Kepler-10 would be the least. And the interiors of these planets can be distinguished from each other based on our modeling approach and by using the current high-precision estimates (with a typical uncertainty less than approximately ± 0.04 dex) of host stellar abundances.

In summary, for more accurate estimates of interior composition and structure of terrestrial exoplanets, it is essential to enhance the initial conditions pertinent to planetary bulk composition and interior chemical system, in addition to the increasingly higher-precision measurements of host stellar photosphere and planetary mass and radius, alongside with the progressive observations of planetary atmospheres, in the upcoming era of TESS and JWST.

Chapter 5

Summary and Future Work

As outlined in the Introduction (Chapter 1), the main goal of this thesis is to analyze the compositional differences between the Earth, Sun and other solar system bodies and from this comparison quantify the devolatilization pertaining to the formation of the rocky planets of our Solar System. The resultant pattern is then applied to estimate the chemical composition of extrasolar rocky planets from spectroscopic measurements of their host stars. The main results of this thesis are summarized in the following.

From a heterogeneous set of literature values, we present the most complete lists of the elemental abundances with uncertainties of the primitive mantle (PM), the core and the bulk Earth (Table 2.1, Figs. 2.1-2.4, 2.6, 2.7) in Chapter 2. The concordance bulk Earth abundances with uncertainties come from the weighted average of our concordance PM and core. The weighting factor for this average comes from our new estimate (with uncertainty) of the core mass fraction of the Earth: 32.5±0.3 wt%. This set of concordance estimates (with uncertainties) for the elemental abundances of the Earth provides a reference allowing terrestrial abundances to be quantitatively compared with other solar system bodies including the Sun.

A set of improved protosolar elemental abundances (Table 3.2) is obtained by a careful combination of the current best estimates of CI chondritic abundances and photospheric abundances in Chapter 3. In combination with the concordance estimates (with uncertainties) for Earth's composition, an internally consistent and well-constrained devolatilization pattern is obtained by quantifying the Earth-to-Sun abundance ratios (f) as a function of elemental condensation temperatures (T_C). This pattern consists of two joint functions:

$$\log(f) = \begin{cases} \alpha \log(T_C) + \beta & \text{when } T_C < T_D(\mathrm{E}) \\ 0 & \text{when } T_C > T_D(\mathrm{E}) \end{cases} \tag{5.1}$$

where $\alpha = 3.676 \pm 0.142$ and $\beta = -11.556 \pm 0.436$; $T_D(\mathrm{E}) = 1391 \pm 15$ K – determined by $10^{-\beta/\alpha}$ – that is the critical devolatilization temperature distinguishing the depleted and non-depleted elements in the terrestrial planet relative to the Sun. This devolatilization pattern allows inferences to be made concerning depletions of elements in the early solar system and is potentially useful for estimating the chemical

composition of rocky exoplanets from their known host stellar abundances.

Modeling the interior chemistry of extrasolar planets requires an accurate determination of their bulk composition. Based on the above analysis of the devolatilization processes of the Solar System, we recommend in Chapter 4 that the elemental abundances of extrasolar planet-host stars be devolatilized, in order to represent the exoplanetary bulk composition. After the devolatilization, the exoplanetary abundance of oxygen can be depleted relative to its host star by $\sim$ 82%, which significantly changes the oxidation state and thus mineralogy of a rocky planet. The modeling of exoplanetary interiors can be further improved by adopting a realistic chemical network for the mantle and the core. Such a network for the mantle should consider the most important mineral oxides, SiO_2-CaO-Na_2O-MgO-Al_2O_3-FeO-NiO, given here in order of the oxidation sequence. Furthermore, the modeling of the planetary core should consider a composition of not only iron, but also nickel (constrained by Fe/Ni = 18 $\pm$ 4 by number) and sulfur (an important light element). By applying these constraints to four extrasolar planetary systems: Kepler-10, Kepler-20, Kepler-21 and Kepler-100, our modeling results demonstrate that the interior composition and structure of rocky extrasolar planets can be distinguished using current high-precision stellar abundance data (with a typical uncertainty less than than $\sim$ 0.04 dex).

We note that our modeling of the chemistry and interior of extrasolar planets should be treated as first-order estimates/guidelines. The modeling is limited by the assumption that the Sun-to-Earth devolatilization pattern is similar to that of other terrestrial planets located within their circumstellar habitable zones. The modeling of the devolatilization process could be improved by including data for other rocky bodies in the inner solar system, gas giants, and icy bodies including various types of comets. Such improved modeling could be generalized to better apply to other planetary systems. However, the *bulk* compositions for such bodies other than the Earth are still not well determined. Nevertheless, if we are to make progress in the studies of exoplanetary chemistry and habitability, a devolatilization to the host star's chemical composition should be taken into account in producing the planetary bulk composition.

5.1 Future Work

5.1.1 Applying the devolatilization to the potential α Centauri planetary system

α Centauri System is the nearest stellar system to us. This system consists of two Sun-like stars (α Cen A and α Cen B) orbiting each other with an 80 year period at an average separation of 30 AU and the much less-massive, loosely bound red dwarf Proxima Centauri (α Cen C) at about 13000 AU distance. Numerical simulations have shown that stable planetary orbits are possible within the habitable zones of both α Cen A and α Cen B [Popova and Shevchenko, 2012; Andrade-Ines and Michtchenko, 2014; Quarles and Lissauer, 2016]. The supposed detection of an Earth-mass planet

orbiting α Centauri B [Dumusque et al., 2012], though not confirmed by Rajpaul et al. [2016], has brought ample attention to the possibility of finding Earth-like planets in nearby star systems [Zhao et al., 2018]. The discovery of an exoplanet (Proxima b) orbiting within the habitable zone of Proxima Centauri [Anglada-Escudé et al., 2016] – cf. Blank et al. [2018] – has increased the prospects finding extraterrestrial life and/or habitable environments, within a distance from us that future space missions, such as Breakthrough Starshot, may travel to within a few decades. Project Blue, a direct imaging survey of the habitable zones of α Cen A & B, is planned to launch by early next decade[1].

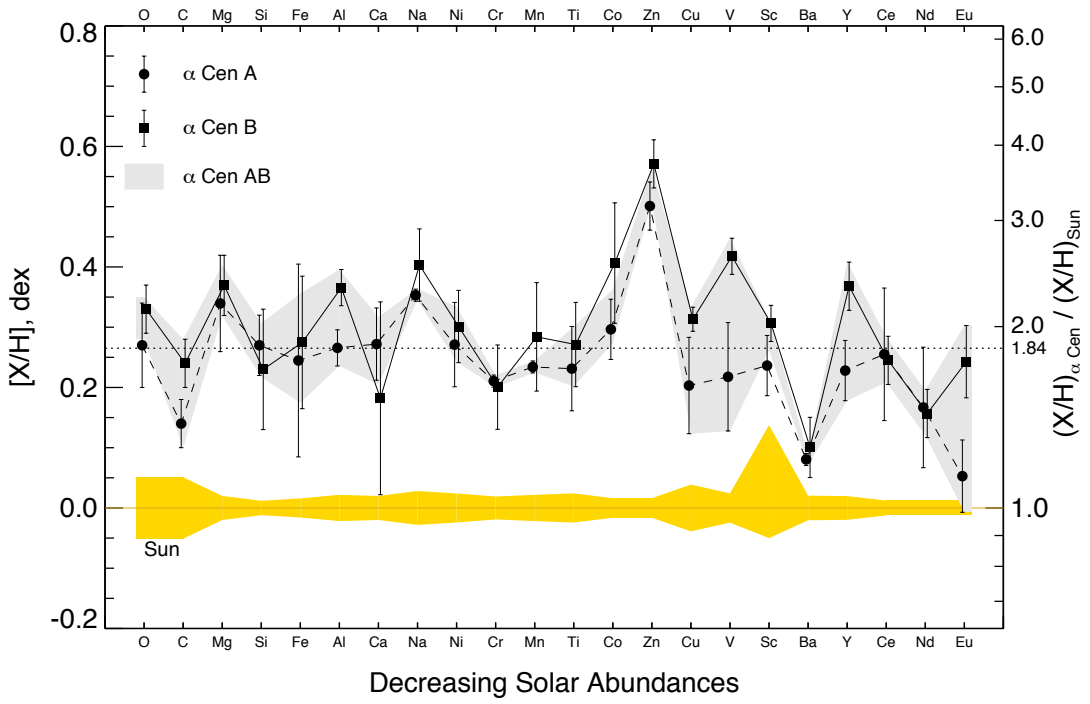

Figure 5.1: The elemental abundances (relative to hydrogen) of α Cen A & B, normalized to those of the Sun [Wang et al., 2018b]. Elements are plotted from left to right in order of decreasing solar abundance. The dotted horizontal line indicates the [Fe/H] of α AB system relative to the Sun.

Preliminarily, we have applied the analytical toolkit developed in this research to the α Centauri AB system, to estimate the chemical composition and habitability of potential terrestrial exoplanets in the circumstellar habitable zones of this binary system. Observed abundances in α Cen A and B are consistent with each other [Hinkel and Kane, 2013] and therefore consistent with the idea that they have approximately the same chemical abundances and probably formed together. We have performed

[1] http://www.projectblue.org/

the weighted average of the α Cen A and B elemental abundances from Hinkel and Kane [2013] to represent the elemental abundances of the AB system (see Figure 5.1). The AB system has $\sim 84\%$ more heavy elements than the Sun, so the protoplanetary disks around α Centauri A and B would have been more metal- or dust-rich, from which more planets or more massive planets may have formed.

If the devolatilization that led the formation of the Earth from solar material is the same as the devolatilization of α Centauri material that led to the formation of α Earths, then the abundance ratios of α Cen to the Sun are the same as α Earth to the Earth. In Figure 5.2, the overall $\sim 84\%$ higher metallicity of the α Cen AB system has been scaled away by normalizing to Al on the same amount basis between the α Cen and the Sun (or between α Earth and the Earth). Thus, only the relative abundances between elements are shown in this figure.

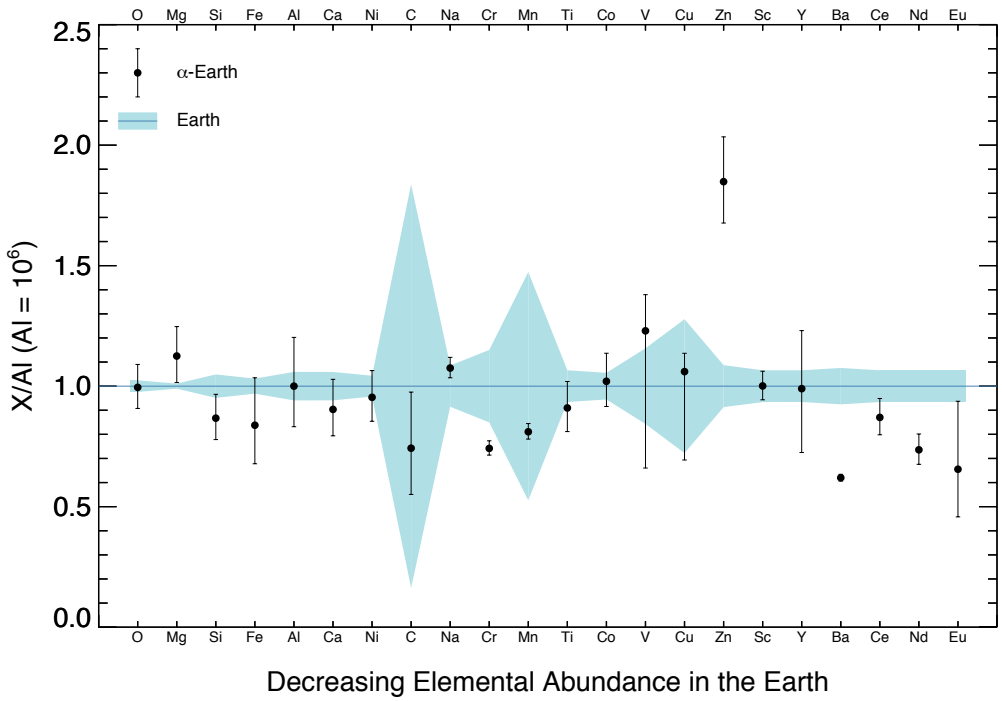

Figure 5.2: The elemental abundances of potential terrestrial planets in the habitable zones of the α Cen AB system ("α Earths"), relative to bulk Earth composition [Wang et al., 2018a] on an equal basis of Al atoms (= 10^6). Elements are ordered by decreasing elemental abundances of the Earth [Wang et al., 2018a].

To some extent we can turn these relative abundances into predictions about the nature of the terrestrial planets that may be in the habitable zone around A or B. For example, Mg in α Earth is over abundant by $13 \pm 11\%$ compared to the Earth, while Si is less abundant by $13 \pm 9\%$. With a Mg/Si of 1.26 ± 0.18 (relative to the Earth),

the ratio of olivine (Mg:Si=2:1 by number)/pyroxene (Mg:Si=1:1) in mantle rocks of α Earth increases significantly. Further, considering the hydration model, the ratio of pyroxene to olivine plays an important role because under the same upper mantle conditions, pyroxene can hold $\sim$ 25 times more water in its crystalline structure than olivine. Therefore, the higher olivine/pyroxene ratio in the mantle rocks of α Earth would possibly accommodate less water in it than the mantle on Earth. These preliminary results will be refined in the future.

5.1.2 Future directions

Extending the estimates of exoplanetary interiors to the planetary magnetic fields

A persistent, strong magnetic field and its associated magnetosphere are thought to protect a terrestrial planet's atmosphere and water from erosion by stellar winds [Heinze, 2017]. Although debated, it is possible that on long timescales such a planet could potentially be more habitable than a planet without a magnetic field. The presence of a magnetic field in a planet requires that the core be molten, neither completely liquid nor entirely solid [Labrosse, 2003; Heinze, 2017]. Inferring the presence of a magnetic field from first principles requires knowledge about the internal energy budget of the planet, which cannot be obtained from the interior geochemical modeling but could be constrained with the dynamic simulations of planetary accretion and collisions [Matsumura et al., 2016]. The magnetic field strength can then be obtained through a magnetic dynamo modeling [Driscoll, 2016; Helffrich, 2017]. For planets orbiting low-mass stars, the effect of tidal heating should also be considered, since the habitable zone around such stars overlaps with the tidal zone, where tidal dissipation is expected to be a significant heat source in the planetary interior [Driscoll and Barnes, 2015]. Radiogenic heating may also affect a planet's dynamos, though it is more important to mantle convection and crustal recycling, i.e., plate tectonics [Noack and Breuer, 2014; Frank et al., 2014]. The modeling of exoplanetary magnetic fields is complex but crucial to understanding the interaction between planetary interiors and atmospheres and thus the long-term habitability of potentially terrestrial exoplanets.

Direct observation of exoplanetary atmospheres

Although mass, density and orbital parameters help to constrain planetary habitability, a definitive determination of whether a planet can support liquid water on its surface requires characterization of the planet's atmosphere and, if possible, its surface [Meadows et al., 2009]. For transiting terrestrial planets around the closest stars, the *James Webb Space Telescope* (JWST)[2] scheduled for launch between March and June of 2019 as well as upcoming ground-based telescopes such as the *European Extremely Large Telescope* (E-ELT) [Snellen et al., 2013; Rodler and López-Morales, 2014] will be capable of measuring the atmospheric composition of such planets. Direct observation of exoplanetary atmospheres is useful not only for discovering bio-signatures

[2] https://www.nasa.gov/mission_pages/webb/about/index.html

or abio-signatures embedded in the atmospheres, but also for further reducing the degree of modeling degeneracy of exoplanetary interiors, since the radius and thus the interior pressure profile of the solid regime of a planet can be more accurately estimated with information about the atmospheres. In addition, the comparison between the observed atmospheric composition[3] and the modeled interior composition may allude to the history of late volatile delivery and/or outgassing, as well as to the activity of geological events (e.g. plate tectonics and volcanism), thus helping characterize the surface habitability of exoplanets.

An upgraded catalog of potentially habitable planets based on both physical and chemical factors

The search for exoplanets has revealed a fascinating diversity of worlds in our Solar neighborhood. Chandler et al. [2016] presented a catalog of Earth-like exoplanet survey targets in the habitable zones around 37,000 nearby stars, and Kane et al. [2016] provided a list of *Kepler* habitable zone exoplanet candidates from the *Kepler* 48-month data set (Q1-Q17 Data Release 24). Both catalogs are important as target selection tools to assist in future exoplanetary missions. These catalogs have concentrated on the observable physical properties of stars and planets, such as stellar effective temperatures, planetary radii and orbital parameters. However, planets are made habitable by both physical and chemical processes that regulate climatic and geochemical cycling between the atmosphere, surface, and interior reservoirs [Hinkel and Unterborn, 2018]. In addition to the current data in the habitable zone exoplanet catalogs, information on the planetary bulk composition, interior structure and chemistry, and atmospheric composition, would yield important constraints on habitability. Such an upgraded catalog would be crucial for future space missions such as PLATO and WFIRST, which may eventually find *real* exo-Earths that are both terrestrial and habitable – another "pale blue dot".

[3] A terrestrial planet's atmosphere is usually secondary or evolved atmosphere, which is not dominated by the primordial H/He envelope but by complex molecules that might be outsourced from late accretion of volatiles from asteroid-like material and alternatively be outgassed and evolved from the interior of the planet during the late stage of its formation and evolution.

Bibliography

Adibekyan, V. Z.; Benamati, L.; Santos, N. C.; Alves, S.; Lovis, C.; Udry, S.; Israelian, G.; Sousa, S. G.; Tsantaki, M.; Mortier, A.; Sozzett, A.; and De Medeiros, J. R., 2015. Chemical abundances and kinematics of 257 G-, K-type field giants. Setting a base for further analysis of giant-planet properties orbiting evolved stars. *Mon. Not. R. Astron. Soc.*, 450, 2 (2015), 1900–1915. doi:10.1093/mnras/stv716. 71

Albarède, F., 2009. Volatile accretion history of the terrestrial planets and dynamic implications. *Nature*, 461, 7268 (2009), 1227–1233. doi:10.1038/nature08477. 6, 66

Alexander, C. M.; Grossman, J. N.; Wang, J.; Zanda, B.; Bourot-Denise, M.; and Hewins, R. H., 2000. The lack of potassium-isotopic fractionation in Bishunpur chondrules. *Meteorit. Planet. Sci.*, 35, 4 (2000), 859–868. doi:10.1111/j.1945-5100.2000.tb01469.x. 4

Alexander, C. M. and Wang, J., 2001. Iron isotopes in chondrules: Implications for the role of evaporation during chondrule formation. *Meteorit. Planet. Sci.*, 36, 3 (2001), 419–428. doi:10.1111/j.1945-5100.2001.tb01883.x. 72

Alexander, C. M. O., 2005. From supernovae to planets: The view from meteorites and interplanetary dust particles. *Chondrites protoplanetary Disk*, 341 (2005), 972–1002. 4

Alexander, C. M. O.; Bowden, R.; Fogel, M. L.; Howard, K. T.; Herd, C. D. K.; Nittler, L. R.; Sandqvist, A.; Boissier, J.; Despois, D.; Milam, S. N.; Herbst, E.; van Dishoeck, E. F.; Crovisier, J.; Bockelée-Morvan, D.; Colom, P.; Biver, N.; Despois, D.; Lis, D. C.; Elsila, J. E.; Glavin, D. P.; Dworkin, J. P.; Bockelée-Morvan, D.; Lis, D. C.; Wink, J. E.; Despois, D.; Crovisier, J.; Bachiller, R.; Benford, D. J.; Biver, N.; Colom, P.; Davies, J. K.; Gérard, E.; Germain, B.; Houde, M.; Mehringer, D.; Moreno, R.; Paubert, G.; Phillips, T. G.; Rauer, H.; Crovisier, J.; Bockelée-Morvan, D.; Biver, N.; Colom, P.; Despois, D.; Lis, D. C.; Biver, N.; Bockelée-Morvan, D.; Debout, V.; Crovisier, J.; Boissier, J.; Lis, D. C.; Russo, N. D.; Moreno, R.; Colom, P.; Paubert, G.; Vervack, R.; Weaver, H. A.; Belloche, A.; Müller, H. S. P.; Menten, K. M.; Schilke, P.; Comito, C.; Caux, E.; Kahane, C.; Castets, A.; Coutens, A.; Ceccarelli, C.; Bacmann, A.; Bisschop, S.; Bottinelli, S.; Comito, C.; Helmich, F. P.; Lefloch, B.; Parise, B.; Schilke, P.; Tielens, A. G. G. M.; van Dishoeck, E.; Vastel, C.; Wakelam, V.; Walters, A.; Biver, N.; Bockelée-Morvan, D.; Crovisier, J.; Henry, F.; Davies, J. K.;

Matthews, H. E.; Colom, P.; Gérard, E.; Lis, D. C.; Phillips, T. G.; Rantakyrö, F.; Haikala, L.; Weaver, H. A.; Biver, N.; Bockelée-Morvan, D.; Crovisier, J.; Lis, D. C.; Moreno, R.; Colom, P.; Henry, F.; Herpin, F.; Paubert, G.; Womack, M.; Pearson, J. C.; Brauer, C. S.; Drouin, B. J.; Paganini, L.; Mumma, M. J.; Villanueva, G. L.; Keane, J. V.; Blake, G. A.; Bonev, B. P.; DiSanti, M. A.; Gibb, E. L.; Meech, K. J.; Vastel, C.; Ceccarelli, C.; Lefloch, B.; Bachiller, R.; Charnley, S. B.; Garrod, R. T.; Weaver, S. L. W.; Herbst, E.; Brouillet, N.; Despois, D.; Lu, X.-H.; Baudry, A.; Cernicharo, J.; Bockelée-Morvan, D.; Crovisier, J.; Biver, N.; Jørgensen, J. K.; Favre, C.; Bisschop, S. E.; Bourke, T. L.; van Dishoeck, E. F.; Schmalzl, M.; Taquet, V.; López-Sepulcre, A.; Ceccarelli, C.; Neri, R.; Kahane, C.; Charnley, S. B.; Dutrey, A.; Guilloteau, S.; Guélin, M.; Chapillon, E.; Dutrey, A.; Guilloteau, S.; Piétu, V.; Wakelam, V.; Hersant, F.; Gueth, F.; Henning, T.; Launhardt, R.; Schreyer, K.; Qi, C.; Öberg, K. I.; Wilner, D. J.; Rosenfeld, K. A.; Öberg, K. I.; Guzmán, V. V.; Furuya, K.; Qi, C.; Aikawa, Y.; Andrews, S. M.; Loomis, R.; Wilner, D. J.; Walsh, C.; Millar, T. J.; Nomura, H.; Herbst, E.; Weaver, S. W.; Aikawa, Y.; Laas, J. C.; Vasyunin, A. I.; Alexander, C. M.; Bowden, R.; Fogel, M. L.; Howard, K. T.; Herd, C. D.; Nittler, L. R.; Pickett, H. M.; Poynter, R. L.; Cohen, E. A.; Delitsky, M. L.; Pearson, J. C.; Müller, H. S. P.; Müller, H. S. P.; Schlöder, F.; Stutzki, J.; Winnewisser, G.; Crovisier, J.; Gérard, E.; Crovisier, J.; Colom, P.; Biver, N.; Bockelée-Morvan, D.; Rauer, H.; Bisschop, S. E.; Jørgensen, J. K.; Bourke, T. L.; Bottinelli, S.; van Dishoeck, E. F.; Fray, N.; Bénilan, Y.; Cottin, H.; and Gazeau, M.-C., 2012. The provenances of asteroids, and their contributions to the volatile inventories of the terrestrial planets. *Science*, 337, 6095 (2012), 721–3. doi:10.1126/science.1223474. 6

Allègre, C.; Manhès, G.; and Lewin, É., 2001. Chemical composition of the Earth and the volatility control on planetary genetics. *Earth Planet. Sci. Lett.*, 185, 1-2 (feb 2001), 49–69. doi:10.1016/S0012-821X(00)00359-9. 9, 21, 23, 30, 31, 34, 36, 38, 39, 127, 128

Allègre, C. J.; Poirier, J. P.; Humler, E.; and Hofmann, A. W., 1995. The chemical composition of the Earth. *Earth Planet. Sci. Lett.*, 134, 3-4 (1995), 515–526. doi:10.1016/0012-821X(95)00123-T. 29, 30, 34, 38, 128

Anders, E., 1960. The record in the meteorites - II. On the presence of aluminium-26 in meteorites and tektites. *Geochim. Cosmochim. Acta*, 19 (1960), 53–62. 2

Anders, E., 1963. Anders : Origin of Carbonaceous Chondrites. *Ann. New York Acad. Sci.*, 108 (1963), 514–533. doi:doi.org/10.1111/j.1749-6632.1963.tb13406.x. 2

Anders, E., 1964. Origin, age, and composition of meteorites. *Space Sci. Rev.*, 3 (1964), 583–714. 2, 4, 66, 72

Anders, E., 1977. Chemical compositions of the Moon , Earth , and eucrite parent body. *Phil. Trans. R. So. Lond. A*, 285, 1327 (1977), 23–40. 34

Anders, E. and Grevesse, N., 1989. Abundances of the elements: Meteoritic and solar. *Geochim. Cosmochim. Acta*, 53, 1 (1989), 197–214. doi:10.1016/0016-7037(89)90286-X. 9, 46, 49, 54, 131

Anderson, D. L., 1989. The crust and upper mantle. In *Theory of the Earth*, 3, 45–62. Blackwell Scientific Publications. ISBN 0865423350. 34

Anderson, D. L. and Kovach, R. L., 1967. The composition of the terrestrial planets. *Earth Planet. Sci. Lett.*, 3 (1967), 19–24. doi:10.1016/0012-821X(67)90005-2. 34

Anderson, W. and Ahrens, T., 1994. An equation of state for liquid iron and implications for the Earth's core. *J. Geophys. Res.*, 99 (1994), 4273–4284. 29

Andrade-Ines, E. and Michtchenko, T. A., 2014. Dynamical stability of terrestrial planets in the binary α Centauri system. *Mon. Not. R. Astron. Soc.*, 444, 3 (nov 2014), 2167–2177. doi:10.1093/mnras/stu1591. 92

Anglada-Escudé, G.; Amado, P. J.; Barnes, J.; Berdiñas, Z. M.; Butler, R. P.; Coleman, G. A. L.; de la Cueva, I.; Dreizler, S.; Endl, M.; Giesers, B.; Jeffers, S. V.; Jenkins, J. S.; Jones, H. R. A.; Kiraga, M.; Kürster, M.; López-González, M. J.; Marvin, C. J.; Morales, N.; Morin, J.; Nelson, R. P.; Ortiz, J. L.; Ofir, A.; Paardekooper, S.-J.; Reiners, A.; Rodríguez, E.; RodrÎńguez-López, C.; Sarmiento, L. F.; Strachan, J. P.; Tsapras, Y.; Tuomi, M.; and Zechmeister, M., 2016. A terrestrial planet candidate in a temperate orbit around Proxima Centauri. *Nature*, 536, 7617 (2016), 437–440. doi:10.1038/nature19106. 93

Arevalo, R. and McDonough, W. F., 2008. Tungsten geochemistry and implications for understanding the Earth's interior. *Earth Planet. Sci. Lett.*, 272, 3-4 (2008), 656–665. doi:10.1016/j.epsl.2008.05.031. 23

Arevalo, R.; McDonough, W. F.; and Luong, M., 2009. The K/U ratio of the silicate Earth: Insights into mantle composition, structure and thermal evolution. *Earth Planet. Sci. Lett.*, 278, 3-4 (2009), 361–369. doi:10.1016/j.epsl.2008.12.023. 23

Asplund, M.; Grevesse, N.; Sauval, A. J.; and Scott, P., 2009. The chemical composition of the Sun. *Annu. Rev. Astron. Astrophys.*, 47, 1 (2009), 481–522. doi:10.1146/annurev.astro.46.060407.145222. 46, 53, 54, 75, 76, 81, 129

Badro, J.; Côté, A. S.; and Brodholt, J. P., 2014. A seismologically consistent compositional model of Earth's core. *Proc. Natl. Acad. Sci. U. S. A.*, (2014), 2–5. doi:10.1073/pnas.1316708111. 10, 22, 29, 30, 128

Barrat, J.; Zanda, B.; Moynier, F.; Bollinger, C.; Liorzou, C.; and Bayon, G., 2012. Geochemistry of CI chondrites: Major and trace elements, and Cu and Zn Isotopes. *Geochim. Cosmochim. Acta*, 83 (2012), 79–92. doi:10.1016/j.gca.2011.12.011. 9, 46

Bart, G.; Ikramuddin, M.; and Lipschutz, M. E., 1980. Thermal metamorphism of primitive meteorites-IX. On the mechanism of trace element loss from Allende heated up to 1400Âř C. *Geochim. Cosmochim. Acta*, 44, 5 (1980), 719–730. doi:10.1016/0016-7037(80)90161-1. 4

Bellini, G.; Benziger, J.; Bonetti, S.; Avanzini, M. B.; Caccianiga, B.; Cadonati, L.; Calaprice, F.; Carraro, C.; Chavarria, A.; Dalnoki-Veress, F.; D'Angelo, D.; Davini, S.; de Kerret, H.; Derbin, A.; Etenko, A.; Fiorentini, G.; Fomenko, K.; Franco, D.; Galbiati, C.; Gazzana, S.; Ghiano, C.; Giammarchi, M.; Goeger-Neff, M.; Goretti, A.; Guardincerri, E.; Hardy, S.; Ianni, A.; Ianni, A.; Joyce, M.; Kobychev, V. V.; Koshio, Y.; Korga, G.; Kryn, D.; Laubenstein, M.; Leung, M.; Lewke, T.; Litvinovich, E.; Loer, B.; Lombardi, P.; Ludhova, L.; Machulin, I.; Manecki, S.; Maneschg, W.; Manuzio, G.; Meindl, Q.; Meroni, E.; Miramonti, L.; Misiaszek, M.; Montanari, D.; Muratova, V.; Oberauer, L.; Obolensky, M.; Ortica, F.; Pallavicini, M.; Papp, L.; Perasso, L.; Perasso, S.; Pocar, A.; Raghavan, R. S.; Ranucci, G.; Razeto, A.; Re, A.; Ricci, B.; Risso, P.; Romani, A.; Rountree, D.; Sabelnikov, A.; Saldanha, R.; Salvo, C.; Schönert, S.; Simgen, H.; Skorokhvatov, M.; Smirnov, O.; Sotnikov, A.; Sukhotin, S.; Suvorov, Y.; Tartaglia, R.; Testera, G.; Vignaud, D.; Vogelaar, R. B.; von Feilitzsch, F.; Winter, J.; Wojcik, M.; Wright, A.; Wurm, M.; Xu, J.; Zaimidoroga, O.; Zavatarelli, S.; and Zuzel, G., 2010. Observation of geo-neutrinos. *Phys. Lett. Sect. B Nucl. Elem. Part. High-Energy Phys.*, 687, 4-5 (2010), 299–304. doi:10.1016/j.physletb.2010.03.051. 10, 22

Bellini, G.; Ianni, A.; Ludhova, L.; Mantovani, F.; and McDonough, W. F., 2013. Geo-neutrinos. *Prog. Part. Nucl. Phys.*, 73 (2013), 1–34. doi:10.1016/j.ppnp.2013.07.001. 10, 22

Birch, F., 1964. Density and composition of mantle and core. *J. Geophys. Res.*, 69, 20 (1964), 4377. doi:10.1029/JZ069i020p04377. 34, 72

Bland, P. a.; Alard, O.; Benedix, G. K.; Kearsley, A. T.; Menzies, O. N.; Watt, L. E.; and Rogers, N. W., 2005. Volatile fractionation in the early solar system and chondrule/matrix complementarity. *Proc. Natl. Acad. Sci. U. S. A.*, 102, 39 (2005), 13755–13760. doi:10.1073/pnas.0501885102. 4, 5, 57, 89

Bland, P. a.; Zolensky, M. E.; Benedix, G. K.; and Sephton, M. a., 2006. Weathering of chondritic meteorites. *Meteorites Early Sol. Syst. II*, , January (2006), 853–867. 49

Blandford, R. D. and Payne, D. G., 1982. Hydromagnetic flows from accretion discs and the production of radio jets. *Mon. Not. R. Astron. Soc.*, 199, 4 (1982), 883–903. doi:10.1093/mnras/199.4.883. 5

Blank, D. L.; Feliz, D.; Collins, K. A.; White, G. L.; Stassun, K. G.; Curtis, I. A.; Hart, R.; Kielkopf, J. F.; Nelson, P.; Relles, H.; Stockdale, C.; Jayawardene, B.; Pennypacker, C. R.; Shankland, P.; Reichart, D. E.; Haislip, J. B.; and Kouprianov, V. V., 2018. A Multi-Year Search For Transits Of Proxima Centauri. I: Light

Curves Corresponding To Published Ephemerides. *Astron. J.*, 155, 6 (2018), 228. doi:10.3847/1538-3881/aabded. 93

Bond, J. C.; Lauretta, D. S.; and O'Brien, D. P., 2010a. Making the Earth: Combining dynamics and chemistry in the Solar System. *Icarus*, 205, 2 (2010), 321–337. doi:10.1016/j.icarus.2009.07.037. 2

Bond, J. C.; O'Brien, D. P.; and Lauretta, D. S., 2010b. The compositional diversity of extrasolar terrestrial planets. I. in situ simulations. *Astrophys. J.*, 715, 2 (jun 2010), 1050–1070. doi:10.1088/0004-637X/715/2/1050. 2, 75, 81

Boulard, E.; Gloter, A.; Corgne, A.; Antonangeli, D.; Auzende, A.-L.; Perrillat, J.-P.; Guyot, F.; and Fiquet, G., 2011. New host for carbon in the deep Earth. *Proc. Natl. Acad. Sci.*, 108, 13 (2011), 5184–5187. doi:10.1073/pnas.1016934108. 76

Bovaird, T.; Lineweaver, C. H.; and Jacobsen, S. K., 2015. Using the inclinations of Kepler systems to prioritize new titius-bode-based exoplanet predictions. *Mon. Not. R. Astron. Soc.*, 448, 4 (2015), 3608–3627. doi:10.1093/mnras/stv221. 1

Brasser, R.; Dauphas, N.; and Mojzsis, S. J., 2018. Jupiter's Influence on the Building Blocks of Mars and Earth. *Geophys. Res. Lett.*, 45, 12 (2018), 5908–5917. doi:10.1029/2018GL078011. 6, 74

Brasser, R.; Mojzsis, S.; Werner, S.; Matsumura, S.; and Ida, S., 2016. Late veneer and late accretion to the terrestrial planets. *Earth Planet. Sci. Lett.*, 455 (dec 2016), 85–93. doi:10.1016/j.epsl.2016.09.013. 71

Brasser, R.; Mojzsis, S. J.; Matsumura, S.; and Ida, S., 2017. The cool and distant formation of Mars. *Earth Planet. Sci. Lett.*, 468 (2017), 85–93. doi:10.1016/j.epsl.2017.04.005. 66, 74

Braukmüller, N.; Wombacher, F.; Hezel, D. C.; Escoube, R.; and Münker, C., 2018. The chemical composition of carbonaceous chondrites: Implications for volatile element depletion, complementarity and alteration. *Geochim. Cosmochim. Acta*, 239 (2018), 17–48. doi:10.1016/j.gca.2018.07.023. 4, 5, 49, 74

Brewer, J. M. and Fischer, D. A., 2016. C / O and Mg / Si ratios of stars in the solar neighborhood. *Astrophys. J.*, 831, 1 (2016), 1–7. doi:10.3847/0004-637X/831/1/20. 71, 75, 81

Brugger, B.; Mousis, O.; Deleuil, M.; and Deschamps, F., 2017. Constraints on super-Earths interiors from stellar abundances. *Astrophys. J.*, 850, 1 (2017), 93. doi:10.3847/1538-4357/aa965a. 14, 15, 71, 87, 89

Burbine, T. H. and O'Brien, K. M., 2004. Determining the possible building blocks of the Earth and Mars. *Meteorit. Planet. Sci.*, 39, 5 (2004), 667–681. doi:10.1111/j.1945-5100.2004.tb00110.x. 21

Carlson, R. W.; Garnero, E.; Harrison, T. M.; Li, J.; Manga, M.; McDonough, W. F.; Mukhopadhyay, S.; Romanowicz, B.; Rubie, D.; Williams, Q.; and Zhong, S., 2014. How did early Earth become our modern world? *Annu. Rev. Earth Planet. Sci.*, 42, 1 (2014), 151–178. doi:10.1146/annurev-earth-060313-055016. 5, 7, 14, 40, 41, 71

Carter-Bond, J. C.; O'Brien, D. P.; and Raymond, S. N., 2012. The compositional diversity of extrasolar terrestrial planets. II. Migration simulations. *Astrophys. J.*, 760, 1 (nov 2012), 44. doi:10.1088/0004-637X/760/1/44. 2

Cassen, 1996. Models for the fractionation of moderately volatile elements in the solar nebula. *Meteorit. Planet. Sci.*, 31 (1996), 793–806. 4, 5, 72

Chambers, J. E., 2001. Making more terrestrial planets. *Icarus*, 152 (2001), 205. doi:10.1006/icar.2001.6639. 21

Chandler, C. O.; McDonald, I.; and Kane, S. R., 2016. The catalog of Earth-like exoplanet survey targets (Celesta): A database of habitable zones around nearby stars. *Astron. J.*, 151, 3 (2016), 59. doi:10.3847/0004-6256/151/3/59. 96

Charbonneau, D.; Brown, T. M.; Noyes, R. W.; and Gilliland, R. L., 2002. Detection of an extrasolar planet atmosphere. *Astrophys. J.*, 568, 1 (mar 2002), 377–384. doi:10.1086/338770. 2

Chopra, A. and Lineweaver, C. H., 2016. The case for a Gaian bottleneck: The biology of habitability. *Astrobiology*, 16, 1 (2016), 7–22. doi:10.1089/ast.2015.1387. 1

Clayton, D. D., 1981. Origin of Ca-Al-rich inclusions. II. Sputtering and collisions in the three-phase interstellar medium. *Astrophys. J.*, 251 (1981), 374–386. 11

Clayton, D. D., 1982. Cosmic chemical memory: A new astronomy. *Q. J. R. Astr. Soc.*, 23 (1982), 174–212. 11

Clayton, R. N.; Hinton, R. W.; and Davis, A. M., 1988. Isotopic variations in the rock-forming elements in meteorites. *Phil. Trans. R. So. Lond. A*, 325 (1988), 483–501. 4

Coffey, D.; Bacciotti, F.; Woitas, J.; Ray, T. P.; and Eisloffel, J., 2004. Rotation of jets from young stars: New clues from the Hubble Space Telescope Imaging Spectrograph. *Astrophys. J.*, 604, 2 (apr 2004), 758–765. doi:10.1086/382019. 5

Connolly, H. C. and Love, S. G., 1998. The formation of chondrules: Petrologic tests of the shock wave model. *Science (80-.).*, 280, 5360 (1998), 62–67. doi:10.1126/science.280.5360.62. 4

Cuzzi, J. N. and Alexander, C. M., 2006. Chondrule formation in particle-rich nebular regions at least hundreds of kilometres across. *Nature*, 441, 7092 (2006), 483–485. doi:10.1038/nature04834. 4

da Silva, R.; Milone, A. C.; and Rocha-Pinto, H. J., 2015. Homogeneous abundance analysis of dwarf, subgiant and giant FGK stars with and without giant planets. *Astron. Astrophys.*, 580 (2015), A24. doi:10.1051/0004-6361/201525770. 71

D'Alessio, P.; Calvet, N.; Hartmann, L.; FrancoâĂŘHernandez, R.; and Servin, H., 2006. Effects of dust growth and settling in T Tauri disks. *Astrophys. J.*, 638, 1 (feb 2006), 314–335. doi:10.1086/498861. 4

Dasgupta, R. and Hirschmann, M. M., 2010. The deep carbon cycle and melting in Earth's interior. *Earth Planet. Sci. Lett.*, 298, 1-2 (2010), 1–13. doi:10.1016/j.epsl.2010.06.039. 76

Dauphas, N., 2017. The isotopic nature of the Earth's accreting material through time. *Nature*, 541, 7638 (2017), 521–524. doi:10.1038/nature20830. 6

Dauphas, N.; Davis, A. M.; Marty, B.; and Reisberg, L., 2004. The cosmic molybdenum-ruthenium isotope correlation. *Earth Planet. Sci. Lett.*, 226, 3-4 (2004), 465–475. doi:10.1016/j.epsl.2004.07.026. 6

Dauphas, N. and Morbidelli, A., 2014. Geochemical and planetary dynamical views on the origin of Earth' atmosphere and oceans. *In: Treatise Geochem.*, 6 (2014), 1–35. doi:http://dx.doi.org/10.1016/B978-0-08-095975-7.01301-2. 26

Davis, A. M., 2006. Volatile evolution and loss. *Meteorites Early Sol. Syst. II*, (2006), 295–307. 4, 5, 11, 14, 71

Delgado Mena, E.; Israelian, G.; González Hernández, J. I.; Bond, J. C.; Santos, N. C.; Udry, S.; and Mayor, M., 2010. Chemical clues on the formation of planetary systems: C/O versus Mg/Si for HARPS GTO sample. *Astrophys. J.*, 725, 2 (dec 2010), 2349–2358. doi:10.1088/0004-637X/725/2/2349. 75

Desch, S. J. and Cuzzi, J. N., 2000. The generation of lightning in the Solar Nebula. *Icarus*, 143, 1 (2000), 87–105. doi:10.1006/icar.1999.6245. 4

Dhaliwal, J. K.; Day, J. M.; and Moynier, F., 2018. Volatile element loss during planetary magma ocean phases. *Icarus*, 300 (2018), 249–260. doi:10.1016/j.icarus.2017.09.002. 6, 74

Dorn, C.; Hinkel, N. R.; and Venturini, J., 2017a. Bayesian analysis of interiors of HD 219134b, Kepler-10b, Kepler-93b, CoRoT-7b, 55 Cnc e, and HD 97658b using stellar abundance proxies. *Astron. Astrophys.*, 597 (2017), A38. doi:10.1051/0004-6361/201628749. 71, 87, 89

Dorn, C.; Khan, A.; Heng, K.; Connolly, J. A. D.; Alibert, Y.; Benz, W.; and Tackley, P., 2015. Can we constrain the interior structure of rocky exoplanets from mass and radius measurements? *Astron. Astrophys.*, 577 (2015), A83. doi:10.1051/0004-6361/201424915. 14, 71, 75, 87

Dorn, C.; Venturini, J.; Khan, A.; Heng, K.; Alibert, Y.; Helled, R.; Rivoldini, A.; and Benz, W., 2017b. A generalized Bayesian inference method for constraining the interiors of super Earths and sub-Neptunes. *Astron. Astrophys.*, 597 (2017), A37. doi:10.1051/0004-6361/201628708. 14, 15, 71, 87, 89

Drake, M. J. and Righter, K., 2002. Determining the composition of the Earth. *Nature*, 416, 6876 (2002), 39–44. doi:10.1038/416039a. 6, 21

Dressing, C. D.; Charbonneau, D.; Dumusque, X.; Gettel, S.; Pepe, F.; Collier Cameron, A.; Latham, D. W.; Molinari, E.; Udry, S.; Affer, L.; Bonomo, A. S.; Buchhave, L. A.; Cosentino, R.; Figueira, P.; Fiorenzano, A. F. M.; Harutyunyan, A.; Haywood, R. D.; Johnson, J. A.; Lopez-Morales, M.; Lovis, C.; Malavolta, L.; Mayor, M.; Micela, G.; Motalebi, F.; Nascimbeni, V.; Phillips, D. F.; Piotto, G.; Pollacco, D.; Queloz, D.; Rice, K.; Sasselov, D.; Ségransan, D.; Sozzetti, A.; Szentgyorgyi, A.; and Watson, C., 2015. The mass of Kepler-93b and the composition of terrestrial planets. *Astrophys. J.*, 800, 2 (feb 2015), 135. doi:10.1088/0004-637X/800/2/135. 71

Driscoll, P. and Barnes, R., 2015. Tidal heating of Earth-like exoplanets around M stars: Thermal, magnetic, and orbital evolutions. *Astrobiology*, 15, 9 (2015), 739–760. doi:10.1089/ast.2015.1325. 95

Driscoll, P. and Olson, P., 2011. Optimal dynamos in the cores of terrestrial exoplanets: Magnetic field generation and detectability. *Icarus*, 213, 1 (2011), 12–23. doi:10.1016/j.icarus.2011.02.010. 77

Driscoll, P. E., 2016. Simulating 2 Ga of geodynamo history. *Geophys. Res. Lett.*, 43 (2016), 5680–5687. doi:10.1002/2016GL068858. 77, 95

Dullemond, C. and Monnier, J., 2010. The inner regions of protoplanetary disks. *Annu. Rev. Astron. Astrophys.*, 48, 1 (2010), 205–239. doi:10.1146/annurev-astro-081309-130932. 4, 66

Dullemond, C. P.; van Zadelhoff, G. J.; and Natta, A., 2002. Vertical structure models of T Tauri and Herbig Ae/Be disks. *Astron. Astrophys.*, 389, 2 (jul 2002), 464–474. doi:10.1051/0004-6361:20020608. 4

Dumusque, X.; Pepe, F.; Lovis, C.; Ségransan, D.; Sahlmann, J.; Benz, W.; Bouchy, F.; Mayor, M.; Queloz, D.; Santos, N.; and Udry, S., 2012. An Earth-mass planet orbiting α Centauri B. *Nature*, 1, V (2012), 4–8. doi:10.1038/nature11572. 93

Dziewonski, A. M. and Anderson, D. L., 1981. Preliminary reference Earth model. *Phys. Earth Planet. Inter.*, 25, 4 (1981), 297–356. doi:10.1016/0031-9201(81)90046-7. 31, 34

Ebel, D. S. and Grossman, L., 2000. Condensation in dust-enriched systems. *Geochim. Cosmochim. Acta*, 64, 2 (2000), 339–366. 5

Elkins-Tanton, L. T. and Seager, S., 2008. Coreless Terrestrial Exoplanets. *Astrophys. J.*, 688 (2008), 628. doi:10.1086/592316. 77

Field, G. B., 1974. Interstellar abundances: Gas and dust. *Astrophys. J.*, 187, 1 (1974), 453–459. 11

Fischer-Gödde, M. and Kleine, T., 2017. Ruthenium isotopic evidence for an inner Solar System origin of the late veneer. *Nature*, 541, 7638 (2017), 525–527. doi:10.1038/nature21045. 6

Fish, R. A. and Goles, G. G., 1962. Ambient xenon: A key to the history of meteorites. *Nature*, 196 (1962), 27–31. 2

Fish, R. A.; Goles, G. G.; and Anders, E., 1960. The record in the meteorites. III. On the development of meteorites in asteroidal bodies. *Astrophys. J.*, 132 (1960), 243–258. 2

Fitoussi, C. and Bourdon, B., 2012. Silicon isotope evidence against an enstatite chondrite Earth. *Science (80-.).*, 335, 6075 (2012), 1477–1480. doi:10.1126/science.1219509. 29, 40

Fitoussi, C.; Bourdon, B.; and Wang, X., 2016. The building blocks of Earth and Mars: A close genetic link. *Earth Planet. Sci. Lett.*, 434 (2016), 151–160. doi:10.1016/j.epsl.2015.11.036. 23, 41, 74

Fortney, J. J., 2012. On the carbon-to-oxygen ratio measurement in nearby Sun-like stars: Implications for planet formation and the determination of stellar abundances. *Astrophys. J.*, 747, 2 (2012), L27. doi:10.1088/2041-8205/747/2/L27. 75

Frank, E. a.; Meyer, B. S.; and Mojzsis, S. J., 2014. A radiogenic heating evolution model for cosmochemically Earth-like exoplanets. *Icarus*, 243 (2014), 274–286. doi:10.1016/j.icarus.2014.08.031. 95

Gando, A.; Gando, Y.; Hanakago, H.; Ikeda, H.; Inoue, K.; Ishidoshiro, K.; Ishikawa, H.; Koga, M.; Matsuda, R.; Matsuda, S.; Mitsui, T.; Motoki, D.; Nakamura, K.; Obata, A.; Oki, A.; Oki, Y.; Otani, M.; Shimizu, I.; Shirai, J.; Suzuki, A.; Takemoto, Y.; Tamae, K.; Ueshima, K.; Watanabe, H.; Xu, B. D.; Yamada, S.; Yamauchi, Y.; Yoshida, H.; Kozlov, A.; Yoshida, S.; Piepke, A.; Banks, T. I.; Fujikawa, B. K.; Han, K.; O'Donnell, T.; Berger, B. E.; Learned, J. G.; Matsuno, S.; Sakai, M.; Efremenko, Y.; Karwowski, H. J.; Markoff, D. M.; Tornow, W.; Detwiler, J. A.; Enomoto, S.; and Decowski, M. P., 2013. Reactor on-off antineutrino measurement with KamLAND. *Phys. Rev. D - Part. Fields, Gravit. Cosmol.*, 88, 3 (2013), 1–10. doi:10.1103/PhysRevD.88.033001. 10, 22

Gando, a.; Gando, Y.; Ichimura, K.; Ikeda, H.; Inoue, K.; Kibe, Y.; Kishimoto, Y.; Koga, M.; Minekawa, Y.; Mitsui, T.; Morikawa, T.; Nagai, N.; Nakajima, K.; Nakamura, K.; Narita, K.; Shimizu, I.; Shimizu, Y.; Shirai, J.; Suekane, F.;

Suzuki, a.; Takahashi, H.; Takahashi, N.; Takemoto, Y.; Tamae, K.; Watanabe, H.; Xu, B. D.; Yabumoto, H.; Yoshida, H.; Yoshida, S.; Enomoto, S.; Kozlov, a.; Murayama, H.; Grant, C.; Keefer, G.; Piepke, a.; Banks, T. I.; Bloxham, T.; Detwiler, J. a.; Freedman, S. J.; Fujikawa, B. K.; Han, K.; Kadel, R.; O'Donnell, T.; Steiner, H. M.; Dwyer, D. a.; McKeown, R. D.; Zhang, C.; Berger, B. E.; Lane, C. E.; Maricic, J.; Miletic, T.; Batygov, M.; Learned, J. G.; Matsuno, S.; Sakai, M.; Horton-Smith, G. a.; Downum, K. E.; Gratta, G.; Tolich, K.; Efremenko, Y.; Perevozchikov, O.; Karwowski, H. J.; Markoff, D. M.; Tornow, W.; Heeger, K. M.; and Decowski, M. P., 2011. Partial radiogenic heat model for Earth revealed by geoneutrino measurements. *Nat. Geosci.*, 4, 9 (2011), 647–651. doi:10.1038/ngeo1205. 10, 22

Grevesse, N. and Sauval, A. J., 1998. Standard solar composition. *Space Sci. Rev.*, 85 (1998), 161–174. doi:10.1023/A:1005161325181. 9, 54

Grevesse, N.; Scott, P.; Asplund, M.; and Sauval, J. A., 2015. The elemental composition of the Sun. *Astron. Astrophys.*, 573 (2015), A27. doi:10.1051/0004-6361/201424111. 46, 53, 54

Grossman, L. and Larimer, J. W., 1974. Early chemical history of the solar system. *Rev. Geophys.*, 12, 1 (1974), 71–101. doi:10.1029/RG012i001p00071. 4, 5, 41, 72

Halliday, A. N., 2013. The origins of volatiles in the terrestrial planets. *Geochim. Cosmochim. Acta*, 105 (2013), 146–171. doi:10.1016/j.gca.2012.11.015. 23, 26, 28, 125

Halliday, A. N. and Porcelli, D., 2001. In search of lost planets - The paleocosmochemistry of the inner solar system. *Earth Planet. Sci. Lett.*, 192, 4 (2001), 545–559. doi:10.1016/S0012-821X(01)00479-4. 11

Hart, M. H., 1979. Habitable zones about main sequence stars. *Icarus*, 37, 1 (1979), 351–357. doi:10.1016/0019-1035(79)90141-6. 1

Heinze, W. D., 2017. A terrestrial conjecture on convection, magnetic fields, and water. In *Accretion Build. New Worlds*, 2031. https://www.hou.usra.edu/meetings/accretion2017/pdf/2031.pdf. 95

Helffrich, G., 2017. Feasibility of a magma ocean dynamo on Mars. *Prog. Earth Planet. Sci.*, 4, 1 (2017), 21. doi:10.1186/s40645-017-0135-8. 95

Hemley, R. J. and Mao, H.-K., 2001. In situ studies of iron under pressure: New windows on the Earth's core. *Int. Geol. Rev.*, 43, 1 (2001), 1–30. doi:10.2747/1938-2839.43.1.30. 29

Hezel, D. C. and Palme, H., 2008. Constraints for chondrule formation from Ca-Al distribution in carbonaceous chondrites. *Earth Planet. Sci. Lett.*, 265, 3-4 (2008), 716–725. doi:10.1016/j.epsl.2007.11.003. 60

Hezel, D. C.; Russell, S. S.; Ross, A. J.; and Kearsley, A. T., 2008. Modal abundances of CAIs: Implications for bulk chondrite element abundances and fractionations. *Meteorit. Planet. Sci.*, 43, 11 (2008), 1879–1894. doi:10.1111/j.1945-5100.2008.tb00649.x. 60

Higuchi, H.; Ganapathy, R.; Morgan, J. W.; and Anders, E., 1977. "Mysterite" : a late condensate from the solar nebula. *Geochim. Cosmochim. Acta*, 41, 7 (1977). doi:10.1016/0016-7037(77)90144-2. 11

Hin, R. C.; Coath, C. D.; Carter, P. J.; Nimmo, F.; Lai, Y.-J.; Pogge von Strandmann, P. A. E.; Willbold, M.; Leinhardt, Z. M.; Walter, M. J.; and Elliott, T., 2017. Magnesium isotope evidence that accretional vapour loss shapes planetary compositions. *Nature*, 549, 7673 (2017), 511–515. doi:10.1038/nature23899. 6, 45, 66

Hinkel, N. R. and Kane, S. R., 2013. Implications of the spectroscopic abundances in α Centauri A and B. *Mon. Not. R. Astron. Soc. Lett.*, 432, 1 (may 2013), L36–L40. doi:10.1093/mnrasl/slt032. 93, 94

Hinkel, N. R.; Timmes, F.; Young, P. A.; Pagano, M. D.; and Turnbull, M. C., 2014. Stellar abundances in the solar neighborhood: The Hypatia catalog. *Astron. J.*, 148, 3 (2014), 54. doi:10.1088/0004-6256/148/3/54. 76, 77, 88

Hinkel, N. R. and Unterborn, C. T., 2018. The star-planet connection. I. Using stellar composition to observationally constrain planetary mineralogy for the 10 closest stars. *Astrophys. J.*, 853, 1 (2018), 83. doi:10.3847/1538-4357/aaa5b4. 1, 71, 81, 87, 88, 96

Hirose, K.; Labrosse, S.; and Hernlund, J., 2013. Composition and state of the core. *Annu. Rev. Earth Planet. Sci.*, 41, 1 (2013), 657–691. doi:10.1146/annurev-earth-050212-124007. 15, 16, 21, 29, 30, 34, 72, 128

Hirose, K.; Morard, G.; Sinmyo, R.; Umemoto, K.; Hernlund, J.; Helffrich, G.; and Labrosse, S., 2017. Crystallization of silicon dioxide and compositional evolution of the Earth's core. *Nature*, 543, 7643 (2017), 99–102. doi:10.1038/nature21367. 77

Howard, A. W.; Sanchis-Ojeda, R.; Marcy, G. W.; Johnson, J. A.; Winn, J. N.; Isaacson, H.; Fischer, D. A.; Fulton, B. J.; Sinukoff, E.; and Fortney, J. J., 2013. A rocky composition for an Earth-sized exoplanet. *Nature*, 503, 7476 (2013), 381–384. doi:10.1038/nature12767. 71

Huang, H.; Fei, Y.; Cai, L.; Jing, F.; Hu, X.; Xie, H.; Zhang, L.; and Gong, Z., 2011. Evidence for an oxygen-depleted liquid outer core of the Earth. *Nature*, 479, 7374 (2011), 513–516. doi:10.1038/nature10621. 29, 30, 128

Huang, S.-S., 1959. Occurrence of life in the universe. *Am. Sci.*, 47, 3 (1959), 397–402. 1

Huang, Y.; Chubakov, V.; Mantovani, F.; Rudnick, R. L.; and McDonough, W. F., 2013. A reference Earth model for the heat-producing elements and associated geoneutrino flux. *Geochemistry, Geophys. Geosystems*, 14, 6 (2013), 2003–2029. doi:10.1002/ggge.20129. 10, 22

Humayun, M. and Clayton, R. N., 1995. Potassium isotope cosmochemistry: Genetic implications of volatile element depletion. *Geochim. Cosmochim. Acta*, 59, 10 (1995), 2131–2148. doi:10.1016/0016-7037(95)00132-8. 4

Huss, G. R., 2004. Implications of isotopic anomalies and presolar grains for the formation of the solar system. *Antarct. Meteor. Res.*, 17 (2004), 132–152. doi:10.1007/s13398-014-0173-7.2. 5

Huss, G. R.; Meshik, A. P.; Smith, J. B.; and Hohenberg, C. M., 2003. Presolar diamond, silicon carbide, and graphite in carbonaceous chondrites: Implications for thermal processing in the solar nebula. *Geochim. Cosmochim. Acta*, 67, 24 (2003), 4823–4848. doi:10.1016/j.gca.2003.07.019. 5, 11, 72

Ireland, T. R., 1990. Presolar isotopic and chemical signatures in hibonite-bearing refractory inclusions from the Murchison carbonaceous chondrite. *Geochim. Cosmochim. Acta*, 54, 11 (1990), 3219–3237. doi:10.1016/0016-7037(90)90136-9. 11

Ireland, T. R. and Fegley, B., 2000. The solar system's earliest chemistry: Systematics of refractory inclusions. *Int. Geol. Rev.*, 42, 10 (2000), 865–894. doi:10.1080/00206810009465116. 71

Javoy, M.; Kaminski, E.; Guyot, F.; Andrault, D.; Sanloup, C.; Moreira, M.; Labrosse, S.; Jambon, A.; Agrinier, P.; Davaille, A.; and Jaupart, C., 2010. The chemical composition of the Earth: Enstatite chondrite models. *Earth Planet. Sci. Lett.*, 293, 3-4 (2010), 259–268. doi:10.1016/j.epsl.2010.02.033. 10, 22, 23, 29, 30, 34, 40, 128

Jellinek, A. M. and Jackson, M. G., 2015. Connections between the bulk composition, geodynamics and habitability of Earth. *Nat. Geosci.*, 8, 8 (2015), 587–593. doi:10.1038/ngeo2488. 40

Jenkins, E. B., 2009. A unified representation of gas-phase element depletions in the interstellar medium. , Field 1974 (2009), 166. doi:10.1088/0004-637X/700/2/1299. 11

Jin, S. and Mordasini, C., 2018. Compositional imprints in density-distance-time: A rocky composition for close-in low-mass exoplanets from the location of the valley of evaporation. *Astrophys. J.*, 853, 2 (2018), 163. doi:10.3847/1538-4357/aa9f1e. 66, 84

Johnson, D. A. and Warr, K., 1999. Metals and their ease of oxidation: A hypothesis. In *Met. Chem. Chang.* (Ed. D. Johnson), 37–40. Royal Society of Chemistry, Cambridge. ISBN 9781847557919. doi:10.1039/9781847557919-00037. http://ebook.rsc.org/?DOI=10.1039/9781847557919-00037. 75

Jones, A. P. and Williams, D. A., 1987. Interplanetary material as a guide to the composition of interstllar grains. *Mon. Not. R. Astron. Soc.*, 224 (1987), 473–479. 11

Kaib, N. A. and Cowan, N. B., 2015. The feeding zones of terrestrial planets and insights into Moon formation. *Icarus*, 252 (2015), 161–174. doi:10.1016/j.icarus.2015.01.013. 15, 21, 41, 74

Kaltenegger, L., 2017. How to characterize habitable worlds and signs of life. *Annu. Rev. Astron. Astrophys.*, 55, 1 (2017), 433–485. doi:10.1146/annurev-astro-082214-122238. 1, 2

Kane, S. R.; Hill, M. L.; Kasting, J. F.; Kopparapu, R. K.; Quintana, E. V.; Barclay, T.; Batalha, N. M.; Borucki, W. J.; Ciardi, D. R.; Haghighipour, N.; Hinkel, N. R.; Kaltenegger, L.; Selsis, F.; and Torres, G., 2016. A catalog of Kepler habitable zone exoplanet candidates. *Astrophys. J.*, 830, 1 (2016), 1–10. doi:10.3847/0004-637X/830/1/1. 1, 96

Kargel, J. and Lewis, J., 1993. The composition and early evolution of Earth. *Icarus*, 105, 1 (1993), 1–25. doi:10.1006/icar.1993.1108. 5, 7, 9, 11, 21, 22, 29, 30, 39, 58, 59, 60, 126, 128

Kasting, J. F.; Kopparapu, R.; Ramirez, R. M.; and Harman, C. E., 2014. Remote life-detection criteria, habitable zone boundaries, and the frequency of Earth-like planets around M and late K stars. *Proc. Natl. Acad. Sci.*, 111, 35 (2014), 12641–12646. doi:10.1073/pnas.1309107110. 1

Kasting, J. F.; Whitmire, D. P.; and Reynolds, R. T., 1993. Habitable Zones around Main Sequence Stars. *Icarus*, 101, 1 (1993), 108–128. doi:10.1006/icar.1993.1010. 1

Kennett, B. L. N.; Engdah12, E. R.; and Buland2, R., 1995. Constraints on seismic velocities in the Earth from traveltimes. *Geophys. J. Int*, 122 (1995), 108–124. doi:10.1111/j.1365-246X.1995.tb03540.x. 31, 34

Klein, B.; Jura, M.; Koester, D.; and Zuckerman, B., 2011. Rocky extrasolar planetary compositions derived from externally-polluted white dwarfs. 64 (2011), 19. doi:10.1088/0004-637X/741/1/64. 2

Kopparapu, R. K.; Ramirez, R.; Kasting, J. F.; Eymet, V.; Robinson, T. D.; Mahadevan, S.; Terrien, R. C.; Domagal-Goldman, S.; Meadows, V.; and Deshpande, R., 2013. Habitable zones around main-sequence stars: New estimates. *Astrophys. J.*, 765, 2 (2013). doi:10.1088/0004-637X/765/2/131. 1

Kos, J.; Bland-Hawthorn, J.; Freeman, K.; Buder, S.; Traven, G.; De Silva, G. M.; Sharma, S.; Asplund, M.; Duong, L.; Lin, J.; Lind, K.; Martell, S.; Simpson, J. D.; Stello, D.; Zucker, D. B.; Zwitter, T.; Anguiano, B.; Da Costa, G.; D'Orazi, V.; Horner, J.; Kafle, P. R.; Lewis, G.; Munari, U.; Nataf, D. M.; Ness, M.; Reid, W.; Schlesinger, K.; Ting, Y.-s.; and Wyse, R., 2018. The GALAH survey: chemical

tagging of star clusters and new members in the Pleiades. *Mon. Not. R. Astron. Soc.*, 473, 4 (feb 2018), 4612–4633. doi:10.1093/mnras/stx2637. 71

Krot, A. N.; Amelin, Y.; Bland, P.; Ciesla, F. J.; Connelly, J.; Davis, A. M.; Huss, G. R.; Hutcheon, I. D.; Makide, K.; Nagashima, K.; Nyquist, L. E.; Russell, S. S.; Scott, E. R.; Thrane, K.; Yurimoto, H.; and Yin, Q. Z., 2009. Origin and chronology of chondritic components: A review. *Geochim. Cosmochim. Acta*, 73, 17 (2009), 4963–4997. doi:10.1016/j.gca.2008.09.039. http://dx.doi.org/10.1016/j.gca.2008.09.039. 5

Kwok, S., 2016. Complex organics in space from Solar System to distant galaxies. *Astron. Astrophys. Rev.*, 24, 1 (2016), 1–27. doi:10.1007/s00159-016-0093-y. 71

Labrosse, S., 2003. Thermal and magnetic evolution of the Earth's core. *Phys. Earth Planet. Inter.*, 140, 1-3 (2003), 127–143. doi:10.1016/j.pepi.2003.07.006. 95

Larimer, J. W., 1979. The condensation and fractionation of refractory lithophile elements. *Icarus*, 40, 3 (1979), 446–454. doi:10.1016/0019-1035(79)90038-1. 66

Larimer, J. W. and Anders, E., 1967. Chemical fractionations in meteorites-II. Abundance patterns and their interpretation. *Geochim. Cosmochim. Acta*, 31, 8 (1967), 1239–1270. doi:10.1016/S0016-7037(67)80014-0. 4, 66

Lauretta, D. S.; Devouard, B.; and Buseck, P. R., 1999. The cosmochemical behavior of mercury. *Earth Planet. Sci. Lett.*, 171, 1 (1999), 35–47. doi:10.1016/S0012-821X(99)00129-6. 63

Lauretta, D. S.; Klaue, B.; Blum, J. D.; and Buseck, P. R., 2001. Mercury abundances and isotopic compositions in the Murchison (CM) and Allende (CV) carbonaceous chondrites. *Geochim. Cosmochim. Acta*, 65, 16 (2001), 2807–2818. doi:10.1016/S0016-7037(01)00630-5. 63

Lewis, J. S. and Prinn, R. G., 1980. Kinetic inhibition of CO and N2 reduction in the solar nebula. *Astrophys. J.*, 238 (1980), 357–364. 62

Lewis, R. S.; Ming, T.; Wacker, J. F.; Anders, E.; and Steel, E., 1987. Interstellar diamonds in meteorites. *Nature*, 326 (1987), 160–162. 11

Li, J. and Fei, Y., 2014. Experimental constraints on core composition. In *Treatise on Geochemistry*, vol. 3, 527–557. Elsevier. ISBN 9780080983004. doi:10.1016/B978-0-08-095975-7.00214-X. 10, 16, 22, 77

Lineweaver, C. and Robles, J., 2009. Comparing the chemical compositions of the Sun and Earth. *ASP Conf. Ser.*, 420 (2009), 83–86. 2, 8

Lineweaver, C. H. and Chopra, A., 2012. The habitability of our Earth and other Earths: Astrophysical, geochemical, geophysical, and biological limits on planet habitability. *Annu. Rev. Earth Planet. Sci.*, 40, 1 (2012), 597–623. doi:10.1146/annurev-earth-042711-105531. 1

Litasov, K. D. and Shatskiy, A. F., 2016. Composition of the Earth's core: A review. *Russ. Geol. Geophys.*, 57, 1 (2016), 22–46. doi:http://dx.doi.org/10.1016/j.rgg.2016.01.003. 29, 30, 40, 128

Liu, F.; Yong, D.; Asplund, M.; Ram'Äśrez, I.; Mel'endez, J.; Gustafsson, B.; Howes, L. M.; Roederer, I. U.; Lambert, D. L.; and Bensby, T., 2016. The detailed chemical composition of the terrestrial planet host Kepler-10. *Mon. Not. R. Astron. Soc.*, 456, 3 (2016), 2636–2646. doi:10.1093/mnras/stv2821. 5, 75, 79, 81, 82, 84

Lodders, K., 2003. Solar System abundances and condensation temperatures of the elements. *Astrophys. J.*, 591, 2 (2003), 1220–1247. doi:10.1086/375492. 5, 8, 9, 12, 31, 35, 39, 46, 54, 56, 61, 62, 73, 74, 130, 131, 132

Lodders, K.; Palme, H.; and Gail, H.-P., 2009. Abundances of the elements in the Solar System. In *Landolt- Börnstein, New Ser. Vol. VI/4B* (Ed. J. E. Trümper), chap. 4.4, 560–598. Springer-Verlag. 9, 10, 46, 48, 49, 53, 54, 125, 130, 131

Luck, J. M.; Othman, D. B.; and Albarède, F., 2005. Zn and Cu isotopic variations in chondrites and iron meteorites: Early solar nebula reservoirs and parent-body processes. *Geochim. Cosmochim. Acta*, 69, 22 (2005), 5351–5363. doi:10.1016/j.gca.2005.06.018. 47

Luck, J. M.; Othman D. Ben, B.; Barrat, J. A.; and Albarède, F., 2003. Coupled 63Cu and 16O excesses in chondrites. *Geochim. Cosmochim. Acta*, 67, 1 (2003), 143–151. doi:10.1016/S0016-7037(02)01038-4. 47

Lyubetskaya, T. and Korenaga, J., 2007. Chemical composition of Earth's primitive mantle and its variance: 1. Method and results. *J. Geophys. Res.*, 112, B3 (mar 2007), B03211. doi:10.1029/2005JB004223. 9, 21, 22, 23, 24, 25, 26, 28, 38, 40, 125, 128

Marsh, J. G.; Lerch, F. J.; Putney, B. H.; Felsentreger, T. L.; Sanchez, B. V.; Klosko, S. M.; Patel, G. B.; Robbins, J. W.; Williamson, R. G.; Engelis, T. L.; Eddy, W. F.; Chandler, N. L.; Chinn, D. S.; Kapoor, S.; Rachlin, K. E.; Braatz, L. E.; and Pavlis, E. C., 1990. The GEM-T2 gravitational model. *J. Geophys. Res.*, 95, B13 (1990), 22043. doi:10.1029/JB095iB13p22043. 34

Marty, B., 2012. The origins and concentrations of water, carbon, nitrogen and noble gases on Earth. *Earth Planet. Sci. Lett.*, 313-314, 1 (2012), 56–66. doi:10.1016/j.epsl.2011.10.040. 6, 23, 26, 28, 125

Marty, B.; Avice, G.; Sano, Y.; Altwegg, K.; Balsiger, H.; Hässig, M.; Morbidelli, A.; Mousis, O.; and Rubin, M., 2016. Origins of volatile elements (H, C, N, noble gases) on Earth and Mars in light of recent results from the ROSETTA cometary mission. *Earth Planet. Sci. Lett.*, 441 (2016), 91–102. doi:10.1016/j.epsl.2016.02.031. 26

Mason, B., 1960a. Origin of chondrules and chondritic meteorites. *Nature*, 186 (1960), 230–231. 2

Mason, B., 1960b. The origin of Meteorites. *J. Geophys. Res.*, 65, 9 (1960), 2965–2970. 2

Mason, B., 1963. The carbonaceous chondrites. *Sp. Sci. Rev.*, 1, 621-646 (1963). 2

Matsumura, S.; Brasser, R.; and Ida, S., 2016. Effects of dynamical evolution of giant planets on the delivery of atmophile elements during terrestrial planet formation. *Astrophys. J.*, 818, 1 (2016), 15. doi:10.3847/0004-637X/818/1/15. 95

Mazevet, S.; Tsuchiya, T.; Taniuchi, T.; Benuzzi-Mounaix, A.; and Guyot, F., 2015. Melting and metallization of silica in the cores of gas giants, ice giants, and super Earths. *Phys. Rev. B - Condens. Matter Mater. Phys.*, 92, 1 (2015), 1–4. doi:10.1103/PhysRevB.92.014105. 87

McDonough, W., 2003. Compositional model for the Earth's core. In *Treatise on Geochemistry* (Ed. R. W. Carlson), vol. 2, 547–568. Elsevier, 1 edn. ISBN 9780080959757. doi:10.1016/B0-08-043751-6/02015-6. 7, 9, 21, 22, 23, 29, 30, 31, 34, 36, 38, 40, 127, 128

McDonough, W., 2014. Compositional model for the Earth's core. In *Treatise on Geochemistry*, vol. 3, 559–577. Elsevier, 2 edn. ISBN 9780080983004. doi:10.1016/B978-0-08-095975-7.00215-1. 7, 15, 58, 59, 60, 71, 72, 74, 77, 80

McDonough, W. F., 2016. The Composition of the lower mantle and core. In *Deep Earth Phys. Chem. Low. Mantle Core, Geophys. Monogr. Ser.* (Eds. H. Terasaki and R. A. Fischer). John Wiley & Sons, Inc., first edn. ISBN 9781118278727. 10, 21, 22, 39

McDonough, W. F., 2017. Earth's core. In *Encycl. Geochemistry* (Ed. W. White), 1–13. Springer International Publishing AG Family. ISBN 978-3-319-39193-9. doi:10.1007/978-3-319-39193-9_258-1. 16, 77

McDonough, W. F. and Arevalo, R., 2008. Uncertainties in the composition of Earth, its core and silicate sphere. *XXIII Conf. Neutrino Phys. Astrophys. J. Phys. Conf. Ser.*, 136, 2 (2008), 022006. doi:10.1088/1742-6596/136/2/022006. 9, 21, 23, 26, 28, 29, 30, 31, 36, 38, 39, 40, 126, 127, 128

McDonough, W. F. and Sun, S. S., 1995. The composition of the Earth 1. *Chem. Geol.*, 120, 3-4 (1995), 223–253. doi:10.1126/science.243.4889.367. 5, 9, 21, 23, 26, 77, 80, 85

Meadows, V. S.; Claire, M. W.; Domagal-Goldman, S. D.; Allen, M.; Anbar, A. D.; Barnes, R.; Boss, A.; Kasting, J.; Kiang, N.; and Martin-Torres, J., 2009. The search for habitable environments and life in the Universe. Technical report. 1, 95

Meléndez, J.; Asplund, M.; Gustafsson, B.; and Yong, D., 2009. The peculiar solar composition and its possible relation to planet formation. *Astrophys. J.*, 704, 1 (oct 2009), L66–L70. doi:10.1088/0004-637X/704/1/L66. 5

Mookherjee, M.; Nakajima, Y.; Steinle-Neumann, G.; Glazyrin, K.; Wu, X.; Dubrovinsky, L.; McCammon, C.; and Chumakov, A., 2011. High-pressure behavior of iron carbide (Fe7C3) at inner core conditions. *J. Geophys. Res. Solid Earth*, 116 (2011), 1–13. doi:10.1029/2010JB007819. 10, 22

Morbidelli, A. and Wood, B. J., 2015. Late accretion and the late veneer. In *Early Earth Accretion Differ.*, 71–82. ISBN 9781118860359. doi:10.1002/9781118860359.ch4. 6

Morgan, J. W. and Anders, E., 1980. Chemical composition of Earth, Venus, and Mercury. *Proc. Natl. Acad. Sci.*, 77, 12 (1980), 6973–6977. doi:10.1073/pnas.77.12.6973. 15, 16, 23, 34, 41, 74, 84

Nagahara, H.; Kita, N. T.; Ozawa, K.; and Morishita, Y., 2008. Condensation of major elements during chondrule formation and its implication to the origin of chondrules. *Geochim. Cosmochim. Acta*, 72, 5 (2008), 1442–1465. doi:10.1016/j.gca.2007.12.020. 4

Nakajima, M. and Stevenson, D. J., 2015. Melting and mixing states of the Earth's mantle after the Moon-forming impact. *Earth Planet. Sci. Lett.*, 427 (2015), 286–295. doi:10.1016/j.epsl.2015.06.023. 10, 22

Nakajima, Y.; Imada, S.; Hirose, K.; Komabayashi, T.; Ozawa, H.; Tateno, S.; Tsutsui, S.; Kuwayama, Y.; and Baron, A. Q. R., 2015. Carbon-depleted outer core revealed by sound velocity measurements of liquid iron-carbon alloy. *Nat. Commun.*, 6, May (2015), 8942. doi:10.1038/ncomms9942. 29, 30, 128

Nissen, P. E., 2013. The carbon-to-oxygen ratio in stars with planets. *Astron. Astrophys.*, 552 (2013), A73. doi:10.1051/0004-6361/201321234. 75

Nissen, P. E. and Schuster, W. J., 2010. Two distinct halo populations in the solar neighborhood. *Astron. Astrophys.*, 511 (2010), L10. doi:10.1051/0004-6361/200913877. 71

Noack, L. and Breuer, D., 2014. Plate tectonics on rocky exoplanets: Influence of initial conditions and mantle rheology. *Planet. Space Sci.*, 98 (2014), 41–49. doi:10.1016/j.pss.2013.06.020. 14, 95

Norris, C. A. and Wood, B. J., 2017. Earth's volatile contents established by melting and vaporization. *Nature*, 549, 7673 (2017), 507–510. doi:10.1038/nature23645. 6, 45, 66, 71, 74, 89

O'D. Alexander, C. M., 2001. The Early Evolution of the Inner Solar System: A Meteoritic Perspective. *Science (80-.).*, 293, 5527 (jul 2001), 64–68. doi:10.1126/science.1052872. 4, 5, 41

O'Neill, H., 1991. The origin of the moon and the early history of the earth - A chemical model. Part 2: The earth. *Geochim. Cosmochim. Acta*, 55, 4 (1991), 1159–1172. doi:10.1016/0016-7037(91)90169-6. 21

O'Neill, H. S. C. and Palme, H., 1998. Composition of the silicate Earth: Implications for accretion and core formation. In *The Earth's Mantle* (Ed. I. Jackson), 3–126. Cambridge University Press. 21

O'Neill, H. S. C. and Palme, H., 2008. Collisional erosion and the non-chondritic composition of the terrestrial planets. *Philos. Trans. A. Math. Phys. Eng. Sci.*, 366, 1883 (2008), 4205–4238. doi:10.1098/rsta.2008.0111. 6, 9, 40, 74

Ozawa, K. and Nagahara, H., 2001. Chemical and isotopic fractionations by evaporation and their cosmochemical implications. *Geochim. Cosmochim. Acta*, 65, 13 (2001), 2171–2199. doi:10.1016/S0016-7037(01)00578-6. 4

Palme, H., 2000. Are there chemical gradients in the inner solar system. *Sp. Sci. Rev.*, 92, August 1999 (2000), 237–262. doi:10.1023/a:1005247329412. 84

Palme, H. and Boynton, W. V., 1993. Meteoritic constraints on conditions in the solar nebula. In *Protostars planets III*, 979–1004. 4, 66

Palme, H.; Lodders, K.; and Jones, A., 2014. Solar System abundances of the elements. In *Treatise Geochemistry Second Ed.* (Ed. A. M. Davis), vol. 2, chap. 2, 15–36. Elsevier Ltd., 2 edn. ISBN 9780080983004. doi:10.1016/B978-0-08-095975-7.00118-2. 5, 9, 16, 39, 46, 53, 64

Palme, H. and O'Neill, H., 2014. Cosmochemical estimates of mantle composition. In *Treatise on Geochemistry* (Ed. R. W. Carlson), vol. 3, 1–39. Elsevier, 2 edn. ISBN 9780080983004. doi:10.1016/B978-0-08-095975-7.00201-1. 7, 8, 9, 21, 22, 23, 26, 28, 38, 39, 40, 58, 59, 60, 128

Palme, H. and O'Neill, H. S. C., 2003. Cosmochemical estimatess of mantle composition. In *Treatise on Geochemistry* (Ed. R. W. Carlson), vol. 2, 1–38. Elsevier, 1 edn. ISBN 9780080959757. 5, 7, 23

Panero, W. R. and Kabbes, J. E., 2008. Mantle-wide sequestration of carbon in silicates and the structure of magnesite II. *Geophys. Res. Lett.*, 35, 14 (2008), 1–5. doi:10.1029/2008GL034442. 76

Paniello, R. C.; Day, J. M.; and Moynier, F., 2012. Zinc isotopic evidence for the origin of the Moon. *Nature*, 490, 7420 (2012), 376–379. doi:10.1038/nature11507. 74

Petigura, E. a. and Marcy, G. W., 2011. Carbon and oxygen in nearby stars: Keys to protoplanetary disk chemistry. *Astrophys. J.*, 735, 1 (jul 2011), 41. doi:10.1088/0004-637X/735/1/41. 75

Pizzarello, S. and Shock, E., 2010. The organic composition of carbonaceous meteorites: the evolutionary story ahead of biochemistry. *Cold Spring Harb. Perspect. Biol.*, 2, 3 (2010), 1–19. doi:10.1101/cshperspect.a002105. 62

Poitrasson, F.; Halliday, A. N.; Lee, D. C.; Levasseur, S.; and Teutsch, N., 2004. Iron isotope differences between Earth, Moon, Mars and Vesta as possible records of contrasted accretion mechanisms. *Earth Planet. Sci. Lett.*, 223, 3-4 (2004), 253–266. doi:10.1016/j.epsl.2004.04.032. 6, 47

Poitrasson, F. and Zambardi, T., 2015. An Earth-Moon silicon isotope model to track silicic magma origins. *Geochim. Cosmochim. Acta*, 167 (2015), 301–312. doi:10.1016/j.gca.2015.07.005. 10, 22

Popova, E. A. and Shevchenko, I. I., 2012. Planetary dynamics in the system α Centauri: The stability diagrams. *Astron. Lett.*, 38, 9 (2012), 581–588. doi:10.1134/S1063773712090046. 92

Pourmand, A.; Dauphas, N.; and Ireland, T. J., 2012. A novel extraction chromatography and MC-ICP-MS technique for rapid analysis of REE, Sc and Y: Revising CI-chondrite and Post-Archean Australian Shale (PAAS) abundances. *Chem. Geol.*, 291 (2012), 38–54. doi:10.1016/j.chemgeo.2011.08.011. 9, 46

Pringle, E. A.; Moynier, F.; Beck, P.; Paniello, R.; and Hezel, D. C., 2017. The origin of volatile element depletion in early solar system material: Clues from Zn isotopes in chondrules. *Earth Planet. Sci. Lett.*, 468 (2017), 62–71. doi:10.1016/j.epsl.2017.04.002. 6, 45

Pringle, E. A.; Moynier, F.; Savage, P. S.; Badro, J.; and Barrat, J.-A., 2014. Silicon isotopes in angrites and volatile loss in planetesimals. *Proc. Natl. Acad. Sci.*, 111, 48 (2014), 17029–17032. doi:10.1073/pnas.1418889111. 6, 47

Quarles, B. and Lissauer, J. J., 2016. Long-term stability of planets in the α Centauri System. *Astron. J.*, 151, 5 (apr 2016), 111. doi:10.3847/0004-6256/151/5/111. 92

Rajpaul, V.; Aigrain, S.; and Roberts, S., 2016. Ghost in the time series: No planet for Alpha Cen B. *Mon. Not. R. Astron. Soc. Lett.*, 456, 1 (2016), L6–L10. doi:10.1093/mnrasl/slv164. 93

Ramírez, I.; Melendez, J.; and Asplund, M., 2009. Accurate abundance patterns of solar twins and analogs-Does the anomalous solar chemical composition come from planet formation? *Astron. Astrophys.*, 508, 1 (2009), L17–L20. doi:10.1051/0004-6361/200913038. 5

Richter, F. M., 2004. Timescales determining the degree of kinetic isotope fractionation by evaporation and condensation. *Geochim. Cosmochim. Acta*, 68, 23 (2004), 4971–4992. doi:10.1016/j.gca.2004.06.008. 74

Ricolleau, A.; Fei, Y.; Corgne, A.; Siebert, J.; and Badro, J., 2011. Oxygen and silicon contents of Earth's core from high pressure metal-silicate partitioning experiments. *Earth Planet. Sci. Lett.*, 310, 3-4 (2011), 409–421. doi:10.1016/j.epsl.2011.08.004. 10, 22

Ringwood, A., 1966. Chemical evolution of the terrestrial planets. *Geochim. Cosmochim. Acta*, 30, 1 (1966), 41–104. doi:10.1016/0016-7037(66)90090-1. 2

Ringwood, A., 1979. *Origin of the Earth and Moon*. Springer-Verlag New York, Inc., 1 edn. ISBN 13: 978-1-4612-6167-4. 23

Ringwood, A. E., 1953. The origin of high-temperature minerals in carbonaceous chondrites. *J. Geophys. Res.*, 68, 4 (1953), 1141–1143. 2

Ringwood, A. E., 1959. On the chemical evolution and densities of the planets. *Geochim. Cosmochim. Acta*, 15 (1959), 257–283. 2

Ringwood, A. E., 1961. Chemical and genetic relationships among meteorites. *Geochim. Cosmochim. Acta*, 24 (1961), 159–197. doi:http://dx.doi.org/10.1016/0016-7037(61)90016-3. 2

Ringwood, A. E., 1965. Origin of chondrites. *Nature*, 207 (1965), 701–704. 2

Rodler, F. and López-Morales, M., 2014. Feasibility studies for the detection of O2 in an earth-like exoplanet. *Astrophys. J.*, 781, 1 (2014). doi:10.1088/0004-637X/781/1/54. 95

Rogers, L. A. and Seager, S., 2010. A framework for quantifying the degeneracies of exoplanet interior compositions. *Astrophys. J.*, 712, 2 (2010), 974–991. doi:10.1088/0004-637X/712/2/974. 14, 71

Rubie, D. C.; Frost, D. J.; Mann, U.; Asahara, Y.; Nimmo, F.; Tsuno, K.; Kegler, P.; Holzheid, A.; and Palme, H., 2011. Heterogeneous accretion, composition and core-mantle differentiation of the Earth. *Earth Planet. Sci. Lett.*, 301, 1-2 (2011), 31–42. doi:10.1016/j.epsl.2010.11.030. 21, 29, 30, 128

Rubin, A. E. and Wasson, J. T., 1987. Chondrules, matrix and coarse-grained chondrule rims in the Allende meteorite: Origin, interrelationships and possible precursor components. *Geochim. Cosmochim. Acta*, 51, 7 (1987), 1923–1937. doi:10.1016/0016-7037(87)90182-7. 4

Saal, A. E.; Hauri, E. H.; Langmuir, C. H.; and Perfit, M. R., 2002. Vapour undersaturation in primitive mid-ocean-ridge basalt and the volatile content of Earth's upper mantle. *Nature*, 419, 6906 (2002), 451–455. doi:10.1038/nature01073. 22, 26

Saal, A. E.; Hauri, E. H.; Van Orman, J. A.; and Rutherford, M. J., 2013. Hydrogen isotopes in Lunar volcanic glasses and melt inclusions reveal a carbonaceous chondrite heritage. *Science (80-.).*, 340, 6138 (jun 2013), 1317–1320. doi:10.1126/science.1235142. 6

Sagan, C., 1994. *Pale Blue Dot*. Random House, New York. ISBN 0-679-43841-6. 1

Salmeron, R. and Ireland, T., 2012a. The role of protostellar jets in star formation and the evolution of the early solar system: Astrophysical and meteoritical perspectives. *Meteorit. Planet. Sci.*, 47, 12 (2012), 1922–1940. doi:10.1111/maps.12029. 4, 5, 66

Salmeron, R. and Ireland, T. R., 2012b. Formation of chondrules in magnetic winds blowing through the proto-asteroid belt. *Earth Planet. Sci. Lett.*, 327-328 (2012), 61–67. doi:10.1016/j.epsl.2012.01.033. 5, 6, 66

Santos, N. C.; Adibekyan, V.; Mordasini, C.; Benz, W.; Delgado-Mena, E.; Dorn, C.; Buchhave, L.; Figueira, P.; Mortier, A.; Pepe, F.; Santerne, A.; Sousa, S. G.; and Udry, S., 2015. Constraining planet structure from stellar chemistry: the cases of CoRoT-7, Kepler-10, and Kepler-93. *Astron. Astrophys.*, 580 (aug 2015), L13. doi:10.1051/0004-6361/201526850. 14, 15, 71, 75, 79, 81, 87

Savage, P.; Moynier, F.; Chen, H.; Shofner, G.; Siebert, J.; Badro, J.; and Puchtel, I., 2015. Copper isotope evidence for large-scale sulphide fractionation during Earth's differentiation. *Geochemical Perspect. Lett.*, 1 (2015), 53–64. doi:10.7185/geochemlet.1506. 16, 77

Schuler, S. C.; Vaz, Z. A.; Santrich, O. J. K.; Cunha, K.; Smith, V. V.; King, J. R.; Teske, J. K.; Ghezzi, L.; Howell, S. B.; and Isaacson, H., 2015. Detailed Abundances of Stars with Small Planets Discovered by Kepler I: The First Sample. *Astrophys. J.*, 815, 1 (2015), 5. doi:10.1088/0004-637X/815/1/5. 75, 79, 82

Scott, P.; Asplund, M.; Grevesse, N.; Bergemann, M.; and Sauval, a. J., 2015a. The elemental composition of the Sun II. The iron group elements Sc to Ni. *Astron. Astrophys.*, 573 (2015), A26(33). doi:10.1051/0004-6361/201424110. 46, 49, 53, 54

Scott, P.; Grevesse, N.; Asplund, M.; Sauval, a. J.; Lind, K.; Takeda, Y.; Collet, R.; Trampedach, R.; and Hayek, W., 2015b. The elemental composition of the Sun I. The intermediate mass elements Na to Ca. *Astron. Astrophys.*, 573 (2015), A25(19). doi:10.1051/0004-6361/201424109. 46, 53, 54

Seager, S.; Kuchner, M.; Hier-Majumder, C. A.; and Militzer, B., 2007. MassâĂŘRadius Relationships for Solid Exoplanets. *Astrophys. J.*, 669, 2 (2007), 1279–1297. doi:10.1086/521346. 14, 71

Seifert, S.; O'Neill, H. S. C.; and Brey, G., 1988. The partitioning of Fe, Ni and Co between olivine, metal, and basaltic liquid: An experimental and thermodynamic investigation, with application to the composition of the lunar core. *Geochim. Cosmochim. Acta*, 52, 3 (1988), 603–616. doi:10.1016/0016-7037(88)90322-5. 77

Shu, F. H.; Shang, H.; Gounelle, M.; Glassgold, A. E.; and Lee, T., 2001. The origin of chondrules and refractory inclusions in chondritic meteorites. *Astrophys. J.*, 548 (2001), 1029–1050. 5

Shu, F. H.; Shang, H.; and Lee, T., 1996. Toward an astrophysical theory of chondrites. *Science (80-.).*, 271, March (1996), 5255. doi:10.1126/science.271.5255.1545. 5

Siebert, J.; Badro, J.; Antonangeli, D.; and Ryerson, F. J., 2013. Terrestrial accretion under oxidizing conditions. *Science (80-.).*, 339, 6124 (2013), 1194–1197. doi:10.1126/science.1227923. 9, 22, 29, 30, 128

Siebert, J.; Sossi, P. A.; Blanchard, I.; Mahan, B.; Badro, J.; and Moynier, F., 2018. Chondritic Mn/Na ratio and limited post-nebular volatile loss of the Earth. *Earth Planet. Sci. Lett.*, 485 (2018), 130–139. doi:10.1016/j.epsl.2017.12.042. 66

Snellen, I. A.; De Kok, R. J.; Le Poole, R.; Brogi, M.; and Birkby, J., 2013. Finding extraterrestrial life using ground-based high-dispersion spectroscopy. *Astrophys. J.*, 764, 2 (2013). doi:10.1088/0004-637X/764/2/182. 95

Souriau, A. and Calvet, M., 2015. Deep Earth structure: The Earth's cores. In *Treatise Geophys.*, chap. 1.19, 725–757. Elsevier, 2 edn. doi:10.1016/B978-0-444-53802-4.00020-8. 31, 34

Spettel, B.; Palme, H.; and Kurat, G., 1989. Have different parts of Allende sampled compositionally different chondrules? In *Abstr. Progr. 52nd Annu. Meet. Meteorit. Soc.*, 326. 4

Spina, L.; Meléndez, J.; Karakas, A. I.; Ramírez, I.; Monroe, T. R.; Asplund, M.; and Yong, D., 2016. Nucleosynthetic history of elements in the Galactic disk. *Astron. Astrophys.*, 593 (sep 2016), A125. doi:10.1051/0004-6361/201628557. 71

Sramek, O.; McDonough, W. F.; Kite, E. S.; Lekic, V.; Dye, S. T.; and Zhong, S., 2013. Geophysical and geochemical constraints on geoneutrino fluxes from Earth's mantle. *Earth Planet. Sci. Lett.*, 361 (2013), 356–366. doi:10.1016/j.epsl.2012.11.001. 10, 22

Stassun, K. G.; Collins, K. A.; and Gaudi, B. S., 2017. Accurate empirical radii and masses of planets and their host stars with Gaia parallaxes. *Astron. J.*, 153, 3 (mar 2017), 136. doi:10.3847/1538-3881/aa5df3. 71

Stassun, K. G.; Corsaro, E.; Pepper, J. A.; and Gaudi, B. S., 2018. Empirical accurate masses and radii of single stars with TESS and Gaia. *Astron. J.*, 155, 1 (dec 2018), 22. doi:10.3847/1538-3881/aa998a. 71

Stevenson, D. J., 1981. Models of the Earth's Core. *Science (80-.).*, 214, 4521 (1981), 611–619. doi:10.1126/science.214.4521.611. 29

Stracke, A.; Palme, H.; Gellissen, M.; Münker, C.; Kleine, T.; Birbaum, K.; Günther, D.; Bourdon, B.; and Zipfel, J., 2012. Refractory element fractionation in the Allende meteorite: Implications for solar nebula condensation and the chondritic composition of planetary bodies. *Geochim. Cosmochim. Acta*, 85 (2012), 114–141. doi:10.1016/j.gca.2012.02.006. 72

Sun, S. S., 1982. Chemical composition and origin of the earth's primitive mantle. *Geochim. Cosmochim. Acta*, 46, 2 (1982), 179–192. doi:10.1016/0016-7037(82)90245-9. 22, 23

Swain, M. R.; Tinetti, G.; Vasisht, G.; Deroo, P.; Griffith, C.; Bouwman, J.; Chen, P.; Yung, Y.; Burrows, A.; Brown, L. R.; Matthews, J.; Rowe, J. F.; Kuschnig, R.; and Angerhausen, D., 2009. Water, methane, and carbon dioxide present in the dayside spectrum of the exoplanet HD 209458b. *Astrophys. J.*, 704, 2 (2009), 1616–1621. doi:10.1088/0004-637X/704/2/1616. 2

Taylor, G. J., 2013. The bulk composition of Mars. *Chemie der Erde - Geochemistry*, 73, 4 (2013), 401–420. doi:10.1016/j.chemer.2013.09.006. 15, 16, 41, 74

Teske, J. K.; Cunha, K.; Smith, V. V.; Schuler, S. C.; and Griffith, C. a., 2014. C/O Ratios of Stars With Transiting Hot Jupiter Exoplanets,. *Astrophys. J.*, 788, 1 (2014), 39. doi:10.1088/0004-637X/788/1/39. 75

Trinquier, A.; Elliott, T.; Ulfbeck, D.; Coath, C.; Krot, A. N.; and Bizzarro, M., 2009. Origin of Nucleosynthetic Isotope Heterogeneity in the Solar Protoplanetary Disk. *Science (80-.).*, 324, 5925 (2009), 374–376. doi:10.1126/science.1168221. 47

Trivedi, B. M. P. and Larimer, J. W., 1981. A semiempirical model for heavy element depletion in the interstellar medium. *Astrophys. J.*, 248 (1981), 563–568. 11

Unterborn, C. T.; Desch, S. J.; Hinkel, N. R.; and Lorenzo, A., 2018. Inward migration of the TRAPPIST-1 planets as inferred from their water-rich compositions. *Nat. Astron.*, 2, 4 (apr 2018), 297–302. doi:10.1038/s41550-018-0411-6. http://www.nature.com/articles/s41550-018-0411-6. 14, 15, 71

Unterborn, C. T.; Dismukes, E. E.; and Panero, W. R., 2016. Scaling the Earth: A sensitivity analysis of terrestrial exoplanetary interior models. *Astrophys. J.*, 819, 1 (2016), 32. doi:10.3847/0004-637X/819/1/32. 5, 71

Unterborn, C. T.; Kabbes, J. E.; Pigott, J. S.; Reaman, D. M.; and Panero, W. R., 2014. The role of carbon in extrasolar planetary geodynamics and habitability. *Astrophys. J.*, 793, 2 (2014), 124. doi:10.1088/0004-637X/793/2/124. 76

Urey, H. C., 1957. Boundary conditions for theories of the origin of the solar system. *Phys. Chem. Earth*, 2 (1957), 46–76. doi:0.1016/0079-1946(57)90006-X. 2

Urey, H. C., 1961. Criticism of Dr. B. Mason's paper on 'The Origin of Meteorites'. *J. Geophys. Res.*, 66, 6 (1961), 1988–1991. 2

Urey, H. C., 1964. A review of atomic abundances in chondrites and the origin of meteorites. *Rev. Geophys.*, 2, 1 (1964), 1–34. doi:10.1029/RG002i001p00001. 2, 41

Urey, H. C., 1967. Parent bodies of the meteorites and the origin of chondrules. *Icarus*, 7, 1-3 (1967), 350–359. doi:10.1016/0019-1035(67)90079-6. 2

Valencia, D.; Sasselov, D. D.; and O'Connell, R. J., 2007. Detailed Models of Super-Earths: How Well Can We Infer Bulk Properties? *Astrophys. J.*, 665, 2 (2007), 1413–1420. doi:10.1086/519554. 71

Visscher, C. and Fegley, B., 2013. Chemistry of impact-generated silicate melt-vapor debris disks. *Astrophys. J. Lett.*, 767, 1 (2013), 6–11. doi:10.1088/2041-8205/767/1/L12. 74

Vočadlo, L., 2007. Ab initio calculations of the elasticity of iron and iron alloys at inner core conditions: Evidence for a partially molten inner core? *Earth Planet. Sci. Lett.*, 254, 1-2 (2007), 227–232. doi:10.1016/j.epsl.2006.09.046. 10, 22

Wai, C. M. and Wasson, J. T., 1977. Nebular condensation of moderately volatile elements and their abundances in ordinary chondrites. *Earth Planet. Sci. Lett.*, 36, 1 (1977), 1–13. doi:10.1016/0012-821X(77)90182-0. 4

Walsh, K. J.; Morbidelli, A.; Raymond, S. N.; O'Brien, D. P.; and Mandell, A. M., 2012. Populating the asteroid belt from two parent source regions due to the migration of giant planets-"The Grand Tack". *Meteorit. Planet. Sci.*, 47, 12 (2012), 1941–1947. doi:10.1111/j.1945-5100.2012.01418.x. 6

Walter, M. J.; Bulanova, G. P.; Armstrong, L. S.; Keshav, S.; Blundy, J. D.; Gudfinnsson, G.; Lord, O. T.; Lennie, A. R.; Clark, S. M.; Smith, C. B.; and Gobbo, L., 2008. Primary carbonatite melt from deeply subducted oceanic crust. *Nature*, 454, 7204 (2008), 622–625. doi:10.1038/nature07132. 76

Wang, H. and Lineweaver, C. H., 2016. Chemical complementarity between the gas phase of the interstellar medium and the rocky material of our planetary system. In *Proc. 15th Aust. Sp. Res. Conf.*, vol. 15, 173–182. v, 5, 12, 13, 66, 71, 84

Wang, H. S.; Lineweaver, C. H.; and Ireland, T. R., 2018a. The elemental abundances (with uncertainties) of the most Earth-like planet. *Icarus*, 299 (2018), 460–474. doi:10.1016/j.icarus.2017.08.024. v, 16, 19, 45, 55, 71, 72, 74, 77, 80, 85, 94, 132

Wang, H. S.; Lineweaver, C. H.; and Ireland, T. R., 2018b. The volatility trend of protosolar and terrestrial elemental abundances. In review/Icarus, preprint (arXiv:1810.12741). (2018). v, 16, 43, 72, 73, 74, 75, 79, 80, 84, 89, 93

Wang, H. S.; Liu, F.; Ireland, T. R.; Brasser, R.; Yong, D.; and Lineweaver, C. H., 2019. Enhanced constraints on the interior composition and structure of terrestrial exoplanets. *Mon. Not. R. Astron. Soc.*, 482, 2 (2019), 2222–2233. doi:10.1093/mnras/sty2749. v, 69

Wang, Z. and Becker, H., 2013. Ratios of S, Se and Te in the silicate Earth require a volatile-rich late veneer. *Nature*, 499, 7458 (2013), 328–331. doi:10.1038/nature12285. 6

Wang, Z.; Laurenz, V.; Petitgirard, S.; and Becker, H., 2016. Earth's moderately volatile element composition may not be chondritic: Evidence from In, Cd and Zn. *Earth Planet. Sci. Lett.*, 435 (2016), 136–146. doi:10.1016/j.epsl.2015.12.012. 40

Wanke, H. and Dreibus, G., 1988. Chemical composition and accretion history of terrestrial planets. *Phil. Trans. R. So. Lond. A*, 325 (1988), 545–557. 15, 23, 34, 41, 74

Warren, P. H., 2011. Stable isotopes and the noncarbonaceous derivation of ureilites, in common with nearly all differentiated planetary materials. *Geochim. Cosmochim. Acta*, 75, 22 (2011), 6912–6926. doi:10.1016/j.gca.2011.09.011. 11

Wasson, J. T., 1985. Meteorites: Ttheir Record of Early Solar-System History. W.H. Freeman and CO., New York, NY. 4

Wasson, J. T. and Chou, C.-L., 1974. Fractionation of moderately volatile elements in ordinary chondrites. *Meteorites*, 9, 1 (1974), 69–84. 4, 66, 72

Wasson, J. T. and Kallemeyn, G. W., 1988. Compositions of chondrites. *Philos. Trans. R. Soc. A*, 325, 1587 (1988), 535–544. 16, 38

Weisberg, M. K.; Mccoy, T. J.; and Krot, A. N., 2004. Systematics and evaluation of meteorite classification. In *Meteorites Early Sol. Syst. II* (Eds. D. S. Lauretta and Y. McSween, Harold), 19–52. The University of Arizona Press. 12

Weiss, L. M.; Rogers, L. A.; Isaacson, H. T.; Agol, E.; Marcy, G. W.; Rowe, J. F.; Kipping, D.; Fulton, B. J.; Lissauer, J. J.; Howard, A. W.; and Fabrycky, D., 2016. Revised masses and densities of the planets around Kepler-10. *Astrophys. J.*, 819, 1 (2016), 83. doi:10.3847/0004-637X/819/1/83. 71, 87

Wieser, M. E.; Holden, N.; Coplen, T. B.; Böhlke, J. K.; Berglund, M.; Brand, W. A.; De Bièvre, P.; Gröning, M.; Loss, R. D.; Meija, J.; Hirata, T.; Prohaska, T.; Schoenberg, R.; O'Connor, G.; Walczyk, T.; Yoneda, S.; and Zhu, X.-K., 2013. Atomic weights of the elements 2011 (IUPAC Technical Report). *Pure Appl. Chem.*, 85, 5 (2013), 1047–1078. doi:10.1351/PAC-REP-13-03-02. 125, 130

Winn, J. N. and Fabrycky, D. C., 2015. The occurrence and architecture of exoplanetary systems. *Annu. Rev. Astron. Astrophys.*, 53, 1 (aug 2015), 409–447. doi:10.1146/annurev-astro-082214-122246. 71

Wood, B. J.; Li, J.; and Shahar, A., 2013. Carbon in the core: Its influence on the properties of core and mantle. *Rev. Mineral. Geochemistry*, 75, 1 (2013), 231–250. doi:10.2138/rmg.2013.75.8. 21, 30, 128

Wood, B. J.; Walter, M. J.; and Wade, J., 2006. Accretion of the Earth and segregation of its core. *Nature*, 441, 7095 (2006), 825–833. doi:10.1038/nature04763. 29, 30, 40, 41, 128

Wood, J. A., 1958. *Silicate Meteorite Structures and the Origin of the Meteorites*. Ph.D. thesis, Massachusetts Institute of Technology. 2, 4

Wood, J. A., 1961. Stony meteorite orbits. *Mon. Not. R. Astron. Soc.*, 122 (1961), 79–88. 2, 4

Wood, J. A., 1962. Chondrules and the origin of the terrestrial planets. *Nature*, 194 (1962), 12–130. 2, 4, 6

Wood, J. A., 1963. On the origin of chondrules and chondrites. *Icarus*, 2 (1963), 152–180. doi:10.1029/GL006i008p00677. 2, 4

Wood, J. A., 1967. Chondrites: Their metallic minerals, thermal histories, and parent planets. *Icarus*, 6, 1-3 (1967), 1–49. doi:10.1016/0019-1035(67)90002-4. 2

Wulf, A. V.; Palme, H.; and Jochum, K. P., 1995. Fractionation of volatile elements in the early solar system: evidence from heating experiments on primitive meteorites. *Planet. Space Sci.*, 43, 3-4 (1995), 451–468. doi:10.1016/0032-0633(94)00189-X. 4

Xu, S.; Jura, M.; Koester, D.; Klein, B.; and Zuckerman, B., 2014. Elemental Compositions of Two Extrasolar Rocky Planetesimals. *Astrophys. J.*, 783, 2 (2014), 79. doi:10.1088/0004-637X/783/2/79. 2

Yin, Q.-z., 2005. From dust to planets: The tale told by moderately volatile elements. *Chondrites protoplanetary Disk*, 341, Ci (2005), 632–644. http://adsabs.harvard.edu/full/2005ASPC..341..632Y. 5, 12

Yoder, C., 1995. Global earth physics : a handbook of physical constants. In *AGU Ref. shelf*, 1, 1–31. doi:10.1029/RF001. 34

Zeng, L., 2015. *Interior Structure and Chemistry of Solid Exoplanets*. Doctoral dissertation, Harvard University. 34

Zeng, L. and Sasselov, D., 2013. A detailed model grid for solid planets from 0.1 through 100 Earth masses. *Publ. Astron. Soc. Pacific*, 125, 925 (mar 2013), 227–239. doi:10.1086/669163. 71

Zhang, Y. and Yin, Q.-Z., 2012. Carbon and other light element contents in the Earth's core based on first-principles molecular dynamics. *Proc. Natl. Acad. Sci.*, 109, 48 (2012), 19579–19583. doi:10.1073/pnas.1203826109. 29, 30, 128

Zhao, L.; Fischer, D. A.; Brewer, J.; Giguere, M.; and Rojas-Ayala, B., 2018. Planet detectability in the Alpha Centauri System. *Astron. J.*, 155, 1 (dec 2018), 24. doi:10.3847/1538-3881/aa9bea. 93

Zuckerman, B.; Koester, D.; Dufour, P.; Melis, C.; Klein, B.; and Jura, M., 2011. An aluminum/calcium-rich, iron-poor, white dwarf star: Evidence for an extrasolar planetary lithosphere? *Astrophys. J.*, 739, 2 (oct 2011), 101. doi:10.1088/0004-637X/739/2/101. 2

Appendices

Appendices of Chapter 2

A.1 Concordance estimates

A.1.1 Concordance PM estimates

For a given elemental abundance X, we compute the weighted mean $\overline{X}$ and variance σ^2 from:

$$\overline{X} = \frac{\sum X_i/\sigma_i^2}{\sum 1/\sigma_i^2} \tag{A.1}$$

$$\sigma^2 = \frac{1}{\sum 1/\sigma_i^2} \tag{A.2}$$

where the index i refers to a data set and ranges from 1 to N. For most PM abundances $N = 3$. Since Lyubetskaya and Korenaga [2007] did not report abundances for C, H, N and O, $N = 2$ for these elements. Lyubetskaya and Korenaga [2007] abundances for Cl and Br are inconsistent with Cl and Br from the other two data sets. Therefore, for these 2 elements, our concordance abundance is the unweighted mean (Eq. A.3) and we take as its uncertainty the range from the highest to the lowest reported abundance.

We have treated noble gases differently. Marty [2012] using an atmospheric model and Halliday [2013] using three different models (layered mantle, impact erosion, and basaltic glass) report the molar abundances of non-radiogenic nuclides of noble gases (^{3}He, ^{20}Ne, ^{36}Ar, ^{84}Kr, ^{130}Xe). We convert these to atomic abundances (by number) by dividing by their estimated terrestrial primordial isotopic fractions [Lodders et al., 2009]. We then convert to mass ppm using the atomic weights from Wieser et al. [2013]. Our concordance PM abundances for noble gases are the median value of the highest upper limit and the lowest lower limit among the four models. We use the upper and lower limits as the uncertainty.

A.1.2 Concordance core estimates

Since the literature core abundances are more scattered and model-dependent than the PM abundances, we compute our concordance core abundances as unweighted

means and assign the standard deviations as uncertainties using:

$$\overline{X} = \frac{1}{N}\sum_{i=1}^{N} X_i \tag{A.3}$$

$$\sigma^2 = \frac{\sum (X_i - \overline{X})^2}{N-1} \tag{A.4}$$

Little work has been done on trace elements in the core. Kargel and Lewis [1993] and McDonough and Arevalo [2008] provide estimates for many trace elements but their estimates are not independent. Thus Eq. A.4 severely under-estimates the uncertainty on the abundances of these trace elements. To compensate for this underestimate, we do the following. If the standard deviation from Eq. A.4 is smaller than ±40% we assign an uncertainty of 40% (which is the average of the uncertainies of the 10 most abundant elements in the core). If the standard deviation computed from Eq. A.4 extends beyond the range of the reported values, we report the range of values as the uncertainty. For those elements with only one reported value (i.e. N=1), Eq. A.4 is undefined. For these cases, we report as an uncertainty either ±40%, or the uncertainty on the single point, whichever is larger.

A.1.3 Approach for concordance bulk Earth estimate

The concordance elemental abundances of the bulk Earth for each element are computed by

$$X = X_{core} f_{core} + X_{PM}(1 - f_{core}) \tag{A.5}$$

where, f_{core} is the core mass fraction estimated in Sect. 2.4.1. The uncertainty σ_X, associated with the bulk elemental abundance, is calculated by the error propagation of the three uncertainties: $\sigma_{X_{PM}}$, $\sigma_{X_{core}}$, and $\sigma_{f_{core}}$ of the PM elemental abundance, the core elemental abundance, and the core mass fraction, respectively:

$$\sigma_X^2 = \sigma_{X_{core}}^2 f_{core}^2 + \sigma_{X_{PM}}^2 (1 - f_{core})^2 + \sigma_{f_{core}}^2 (X_{PM} - X_{core})^2 \tag{A.6}$$

A.2 Calculation of significance of deviation

In Figs. 7 & 8 we compare our concordance bulk estimates with three previous estimates of bulk Earth abundances. For some elements, all three previous estimates are higher, or lower. For these elements we compute the significance S_X, of this difference:

$$S_X = \frac{1}{N}\sum_{i=1}^{N} \frac{X_i - X}{\sqrt{\sigma_{X_i}^2 + \sigma_X^2}} \tag{A.7}$$

where, X is our concordance estimate of the elemental abundance and σ_X^2 is its variance from Eq. A.6. X_i is the abundance reported in the i-th literature source, with N being the total number of literature sources. Identical abundances reported in

Table A.1: Significances[a] of deviations between our concordance bulk Earth abundances and previous estimates[b]

6 Elements with abundances more than $\sim 1\sigma$ *below* previous estimates					
Mg	Cd	B	Be	Br	Sn
-2.60	-1.79	-1.76	-1.71	-1.40	-1.15

14 Elements with abundances more than $\sim 1\sigma$ *above* previous estimates													
Zn	Ga	Ar	Ta	Na	K	Rb	F	He	Cl	Nb	Kr	Sr	Gd
3.04	2.36	2.34	1.82	1.75	1.75	1.64	1.63	1.39	1.38	1.30	1.20	1.19	1.11

[a] calculated by Eq. B.1.
[b] Allègre et al. [2001], McDonough [2003], and McDonough and Arevalo [2008]

McDonough [2003] and in McDonough and Arevalo [2008] have only been used once in this calculation. $\sigma^2_{X_i}$ is its variance. If the source has no reported variance, we set $\sigma^2_{X_i} = 0$.

Table A.1 lists the significances (more than $\sim 1\sigma$) of the deviations between our concordance bulk Earth abundances and previous estimates [Allègre et al., 2001; McDonough, 2003; McDonough and Arevalo, 2008].

A.3 Rescaling data

Elemental abundances are usually reported in ppm by mass. Thus, when all elements are estimated, the sum of their abundances should equal 10^6. The abundances of all elements are usually not reported. We use this $\Sigma\, ppm = 10^6$ constraint to rescale our PM, core (and thus our bulk) abundances. Our concordance PM abundances summed to 0.997×10^6 so we rescaled all of our PM abundances up by 0.3%. Our concordance core abundances summed to 1.020×10^6 so we rescaled all of our core abundances down by 2.0%. In Table C.5 we sum the literature abundances (column 3). In column 4 we supplement the sums from column 3 with our rescaled concordance abundances. Deviations from 1.000×10^6 in column 5 indicate the level of inconsistency in the literature with the $\Sigma\, ppm = 10^6$ constraint, even after the missing elements have been supplemented with our concordance abundances.

Table A.2: Rescaling the sums of elemental abundances (ppm by mass) for Earth components

Sources	Number of reported abundances	Sum of reported abundances	Sum of reported abundances after the missing elements have been supplemented using our rescaled concordance abundances
	a. Primitive mantle		
Lyubetskaya and Korenaga [2007]	74 (missing C, H, N, O, and noble gases)	0.556 $\times 10^6$	0.998 $\times 10^6$
McDonough and Arevalo [2008]	78 (missing noble gases)	1.000 $\times 10^6$	1.000 $\times 10^6$
Palme and O'Neill [2014]	78 (missing noble gases)	1.001 $\times 10^6$	1.001 $\times 10^6$
Concordance PM	**83**	**0.997 $\times$ 10^6** (pre-scaled)	-
	b. Core		
Kargel and Lewis [1993]	41	1.000 $\times 10^6$	1.058 $\times 10^6$
Allègre et al. [1995, 2001]	9 (O, Si, P, S, Cr, Mn, Fe, Co, Ni)	0.998 $\times 10^6$	1.009 $\times 10^6$
McDonough [2003]	5 (O, Si, Mn, Fe, Ni)	0.967 $\times 10^6$	1.009 $\times 10^6$
Wood et al. [2006]	4 (H, C, Si, S)	0.067 $\times 10^6$	0.990 $\times 10^6$
McDonough and Arevalo [2008]	40	1.003 $\times 10^6$	1.005 $\times 10^6$
Javoy et al. [2010]	6 (O, Si, Cr, Fe, Co, Ni)	1.003 $\times 10^6$	1.038 $\times 10^6$
Huang et al. [2011]	1 (O)	0.005 $\times 10^6$	0.978 $\times 10^6$
Rubie et al. [2011]	11 (O, Si, S, V, Cr, Fe, Co, Ni, Nb, Ta, W)	1.007 $\times 10^6$	1.024 $\times 10^6$
Zhang and Yin [2012]	7 (H, C, N, O, Mg, Si, P)	0.036 $\times 10^6$	0.947 $\times 10^6$
Hirose et al. [2013]	3 (O, Si, and S)	0.105 $\times 10^6$	1.010 $\times 10^6$
Wood et al. [2013]	1 (C)	0.010 $\times 10^6$	1.002 $\times 10^6$
Siebert et al. [2013]	2 (O and Si)	0.069 $\times 10^6$	0.992 $\times 10^6$
Badro et al. [2014]	4 (C, O, Si, S)	0.057 $\times 10^6$	0.955 $\times 10^6$
Nakajima et al. [2015]	1 (C)	0.011 $\times 10^6$	1.002 $\times 10^6$
Litasov and Shatskiy [2016]	4 (C, O, Si, S)	0.101 $\times 10^6$	0.998 $\times 10^6$
Concordance Core	**49**	**1.020 $\times$ 10^6** (pre-scaled)	-
	c. Bulk Earth		
Allègre et al. [2001]	81 (missing H and Hg)	1.007$\times 10^6$	1.007$\times 10^6$
McDonough [2003]	78 (missing noble gases)	1.002$\times 10^6$	1.002$\times 10^6$
McDonough and Arevalo [2008]	78 (missing noble gases)	1.001$\times 10^6$	1.001$\times 10^6$
Concordance Bulk Earth	**83**	**1.000 $\times$ 10^{6*}**	-

* Based on rescaled concordance PM and concordance core.

Appendices of Chapter 3

B.1 How we normalize and combine photospheric and meteoritic abundances

Let $N(X)$ be the photospheric abundance (by number of atoms) of element X. We normalize this abundance to 10^{12} atoms of hydrogen and write the abundance in dex as:

$$A(\mathrm{X})|_{A(\mathrm{H})\equiv 12} = \log[N(\mathrm{X})/N(\mathrm{H})] + 12. \tag{B.1}$$

Meteoritic abundances are often reported in parts-per-million (ppm) by mass and are denoted here as $\mathrm{X_{ppm}}$. To combine the two sets of abundances, we normalize both to 10^6 atoms of Si (i.e., $N(\mathrm{X})|_{N(Si)=10^6}$). As discussed in Section 3.2.2, we make diffusion corrections on photospheric abundances before normalizing them and before combining them with meteoritic data. Following [Asplund et al., 2009], we use the overall diffusion correction factors from Turcotte & Wimmer-Schweingruber (2002). Our diffusion correction converts photospheric abundances $A(\mathrm{X})_p$, into bulk solar abundances $A(\mathrm{X})_{p,0}$. For helium we set,

$$A(\mathrm{He})_{p,0} = A(\mathrm{He})_p + 0.05 \tag{B.2}$$

and for all elements heavier than helium we set,

$$A(\mathrm{X})_{p,0} = A(\mathrm{X})_p + 0.04. \tag{B.3}$$

The uncertainty in the overall diffusion correction is assumed to be 0.01 dex [Asplund et al., 2009]. In Table 3.2, this 0.01 uncertainty has been added in quadrature to the uncertainties of $A(\mathrm{X})_p$ (column 3) to produce the uncertainties of $A(\mathrm{X})_{p,0}$ (column 5).

After these diffusion corrections, photospheric abundances are normalized to Si using:

$$N(\mathrm{X})_{p,0} = 10^{A(\mathrm{X})_{p,0} - A(\mathrm{Si})_{p,0}} \times 10^6 \tag{B.4}$$

We convert the uncertainty σ_A (in dex) of $A(\mathrm{X})_{p,0}$ to the standard deviation, $\sigma_{N,p,0}$ (in %) of $N(\mathrm{X})_{p,0}$ by:

$$\pm\sigma_{N,p,0}(\%) = (10^{\pm\sigma_A} - 1) \times 100 \tag{B.5}$$

where the $\pm$ indicates separate upper and lower error bars. In using Eq. B.5, symmetric errors in logarithmic abundances correspond to asymmetric errors in linear abundances, and vice versa. Asymmetric errors add an extra level of complication to computing weighted averages. Following Lodders [2003] and Lodders et al. [2009], when faced with upper and lower error bars of different sizes, we conservatively choose the larger one for further analysis. That is why there are no separate upper and lower error bars in Table 3.2, column 6.

To convert meteoritic abundances by mass (i.e., X_{ppm}) to abundances by number, normalized to Si we use:

$$N(X)_m = \frac{X_{ppm}/m_a(X)}{Si_{ppm}/m_a(Si)} \times 10^6 \tag{B.6}$$

where $m_a(X)$ is the atomic mass of an element X [Wieser et al., 2013]. Let σ_X be the uncertainty (in %) on X_{ppm}. We obtain the uncertainty σ_m on $N(X)_m$ from:

$$\sigma_m = N(X)_m \times \frac{\sigma_X}{100} \tag{B.7}$$

With these conversions, the two data sets are ready to be combined to obtain protosolar abundances. For the 60 elements in Table 3.1 for which we compute the weighted average of the two sets, we use

$$N(X)_0 = \frac{N(X)_{p,0}/\sigma^2_{N,p,0} + N(X)_m/\sigma^2_m}{1/\sigma^2_{N,p,0} + 1/\sigma^2_m} \tag{B.8}$$

If the values of $N(X)_{p,0}$ and $N(X)_m$ overlap within uncertainties we compute the uncertainty on $N(X)_0$ using

$$\sigma_{N_0} = \sqrt{1/(1/\sigma^2_{N,p,0} + 1/\sigma^2_m)} \tag{B.9}$$

If the values of $N(X)_{p,0}$ and $N(X)_m$ do not overlap within uncertainties the highest upper and lowest lower limit of the two data points are taken as the error bars.

B.2 How we renormalize meteoritic abundances from a silicon to a hydrogen normalization

Due to the depletion of hydrogen in meteorites, Eq. B.1 is not used to convert Si-normalized meteoritic abundances to H-normalized abundances. Instead we write,

$$A(X)_m = \log N(X)_m + \Delta \tag{B.10}$$

where Δ is a numerical conversion factor. For refractory elements, solar abundances and CI abundances are indistinguishable. Therefore we expect,

$$A(X)_m = A(X)_p \tag{B.11}$$

Combining Eqs. B.10 and B.11 we obtain

$$\Delta = A(\mathrm{X})_p - \log N(\mathrm{X})_m \tag{B.12}$$

Following Lodders et al. [2009] we require that the elements used in Eqs B.10 - B.12, satisfy several criteria: (1) the elements must have both photospheric and meteoritic abundances, (2) uncertainties on their photospheric abundances must be less than 0.1 dex (i.e., below $\sim$ 25%), (3) no noble gases, (4) atomic numbers greater than neon. Thus, for these elements, by subtracting the logarithm of the Si-normalized meteoritic abundances ($\log N(\mathrm{X})_m$) from the logarithmic H-normalized photospheric abundances ($A(\mathrm{X})_p$) we obtain an average numerical factor Δ from Eq. B.12 that can be generallly used in Eq. B.10 to convert Si-normalized meteoritic abundances to H-normalized meteoritic abundances. Using the updated meteoritic and photospheric abundances compiled here, 46 elements satisfy the criteria above. We find $\Delta = 1.514 \pm 0.009$ where the uncertainty is the standard error of the mean: $\frac{1}{\sqrt{n}} \sum_{i=1}^{n=46} \sqrt{(x_i - \bar{x})^2/(n-1)}$. Figure B.1 shows the various values of Δ from Eq. B.12 as a function of atomic number. Over the past few decades, estimates of Δ have been decreasing. This decrease can be attributed to the updates of meteoritic and photospheric data and an increasing number of elements that can be used. For example, Anders and Grevesse [1989] used 12 elements and obtained 1.554. Lodders [2003] used 35 elements and obtained 1.540. Lodders et al. [2009] used 39 elements and obtained 1.533. We used 46 elements and obtained 1.514 ± 0.009, significantly lower than previous estimates.

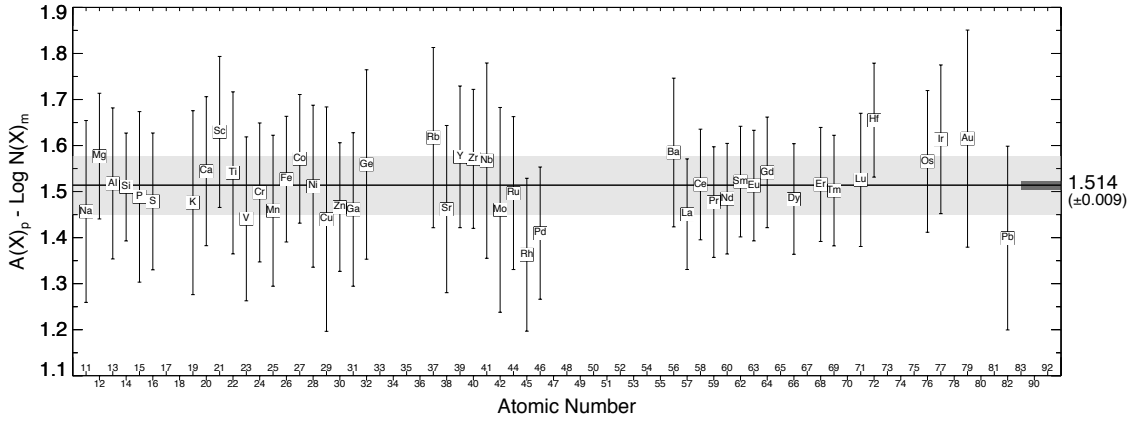

Figure B.1: Values of Δ from Eq. B.12 for 46 refractory elements. The gray band shows the 1σ standard deviation. On the far right we plot our main result: $\Delta = 1.514 \pm 0.009$.

When meteoritic abundances are taken as a proxy for protosolar abundances, a diffusion correction factor should be added to Δ to make the meteoritic abundances comparable with protosolar abundances. Because the diffusion correction factor we

applied for all elements (except helium) is 0.04 dex, the corrected conversion factor should be 1.554 ($= 1.514 + 0.04$) when taking photospheric diffusion into account.

B.3 χ^2 minimization to determine the coefficients of the devolatilization pattern

The elemental abundance ratios of bulk Earth to the proto-Sun normalized to Al are $f = N(X)_{\rm Earth}/N(X)_{\rm Sun}$. where $N(X)_{\rm Sun}$ is from column 13 of Table 3.2 after the Al normalization, and $N(X)_{\rm Earth}$ is from Wang et al. [2018a]. These ratios are plotted as a function of T_C in Fig. 5, where T_C is the elemental 50% condensation temperature for the relevant element [Lodders, 2003]. We fit all elements with $T_C > 500$ K. We simultaneously fit the two functions $\log(f) = \alpha \log(T_C) + \beta$ and $\log(f) = 0$ to the abundance data, and find the best-fit values of α and β.

Step 1: We create an array of the two parameters α and β in the ranges $2 < \alpha < 6$ and $-20 < \beta < -6$, using an increment step of 0.001 for both parameters. For each pair (α, β), we compute $T_{\rm D}(\alpha, \beta) = 10^{-\beta/\alpha}$. For each coordinate pair (α, β), elements with $T_C < T_{\rm D}(\alpha, \beta)$ are fit to $\log(f) = \alpha \log(T_C) + \beta$ while elements with $T_C > T_{\rm D}(\alpha, \beta)$ are fit to $\log(f) = 0$.

Step 2: We compute $\chi^2 = \chi^2_{\rm I} + \chi^2_{\rm II}$ using the equations:

$$\chi^2_{\rm I}(\alpha, \beta) = \sum_{i=1}^{k} \frac{[log(f_i) - (\alpha \log(T_{C_i}) + \beta)]^2}{\sigma_i^2} \tag{B.13}$$

where k is the number of the last element whose condensation temperature is less than $T_{\rm D}(\alpha, \beta)$. Thus k is a function of (α, β). For the remainder of the elements, $T_C > T_{\rm D}(\alpha, \beta)$ and we compute,

$$\chi^2_{\rm II}(\alpha, \beta) = \sum_{i=k+1}^{N} \frac{[log(f_i) - 0]^2}{\sigma_i^2} \tag{B.14}$$

where $N = 72$. This comes from 83 (the total number of elements) minus 11 (number of elements with $T_C < 500$ K). In both equations, when the error bars of an elemental abundance are asymmetric, the error bar in the direction of the model is used for σ_i.

We find $\chi^2_{\rm min} = 52.67$, which is the sum of $\chi^2_{{\rm I},min} = 43.68$ and $\chi^2_{{\rm II},min} = 8.99$. The best fit coefficient values are $\alpha = 3.676 \pm 0.142$ and $\beta = -11.556 \pm 0.436$. Therefore, the best fit devolatilization temperature $T_{\rm D}$(E) = 1391 $\pm$ 15 since $T_{\rm D} = 10^{-\beta/\alpha}$. The number of elements with $T_C < 1391$ K is 37. Thus the approximate number of degrees of freedom for the first part of the fit (Eq. B.13) is $\nu_I = 35 (= 37 - 2)$. For the second part of the fit (Eq. B.14), the number of degrees of freedom is not equal to the number of data points, since protosolar and terrestrial abundances of refractory elements are highly correlated. We approximate the number of degrees of freedom for the second part as $\nu_{II} \approx \chi^2_{\rm II} = 9$. Thus, with $\nu = \nu_I + \nu_{II}$ the reduced χ^2 of the best fit is $\chi^2_{\rm min}/\nu = 52.67/44 \approx 1.2$. The probability of having a reduced χ^2 lower than this value is $P(\chi^2 \leq \chi^2_{\rm min}, \nu) = 0.83$. Thus, our best-fit is a reasonably good fit.

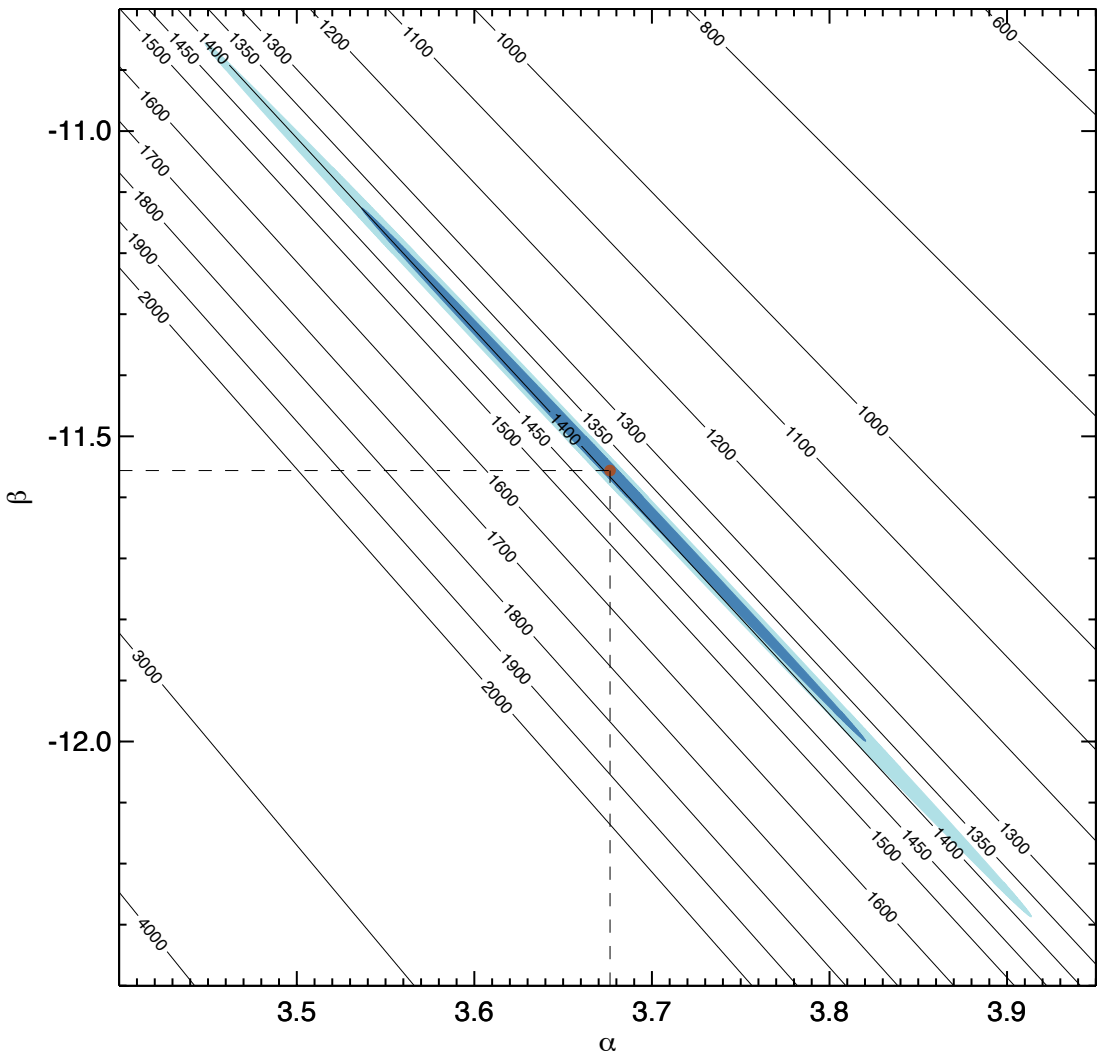

Figure B.2: Determination of the coefficients α and β and therefore of $T_{\mathrm{D}}(\mathrm{E}) = 10^{-\beta/\alpha}$. The central brown dot represents the best fit values $\alpha = 3.676$ and $\beta = -11.556$ indicated by the vertical and horizontal dash lines. The dark and light blue ellipses indicate respectively, the 68% and 95% confidence levels. These levels are computed from $\chi^2_{\mathrm{min}} + 2.3$ and $\chi^2_{\mathrm{min}} + 6.17$ respectively. The diagonal solid black lines labeled between 600 and 4000 are isothermal lines of T_D (=$10^{-\beta/\alpha}$) in units of Kelvin. The best fit devolatilization temperature $T_{\mathrm{D}}(\mathrm{E}) = 1391 \pm 15$ K.

Appendices of Chapter 4

C.1 Computational details of elemental fractionation between the mantle and core for a terrestrial planet

The elemental fractionation is based on the recommended chemical systems for the mantle and core of a terrestrial planet in Sects. 4.2.2 and 4.2.3. The computational procedure illustrated in Figure 4.3 is described in detail in the following.

First, oxidize Si, Ca, Na, Mg, and Al (in order of the decreasing ease of oxidation addressed in Section 4.2.3) to form oxides: SiO_2, CaO, Na_2O, MgO, and Al_2O_3, respectively. For each element, assess the sufficiency of O atoms: i) if the budget of (remaining) O atoms is not stoichiometrically sufficient to fully oxidize the element, then the non-oxidized part of the element's atoms and the atoms of the subsequent elements (up to Al) will be deemed as metals in the mantle; ii) otherwise (namely, all atoms of an element can be fully oxidized), the oxidation process will be performed to the subsequent elements one by one (up to Al), unless the remaining O atoms have been exhausted.

Second, fractionate Fe, Ni, and S between the mantle and the core, for two scenarios:

i) If the remaining O atoms (after having oxidized Si, Ca, Na, Mg, and Al) are still stoichiometrically sufficient to fully oxidize Fe, Ni, and S into the form of FeO, NiO, and SO_3, then there will be no Fe, Ni, or S fractionated into the core, and a coreless planet will form. The left over oxygen atoms may oxidize the stoichiometric amount of C atoms to form CO_2 in the phase of carbonates, then the remaining C atoms are present in the phase of graphite in the mantle. However, if the amount of the left over oxygen atoms is more than that of C atoms, all C atoms will be oxidized to form CO_2 and the extra O is assumed to be present in the mantle to oxidize other minor elements that are not investigated in this work.

ii) Complementarily, if the remaining O atoms are *not* sotichiometrically sufficient to fully oxidize Fe, Ni, and S, then the atoms of the three elements will be fractionated between the mantle and the core, and all C atoms will be present in the phase of graphite in the mantle. The upper limits of atomic abundances of Ni and S in the phase of NiO and SO_3 in the mantle are assumed to be equal to their respective planetary bulk abundances (devolatilized from the host stellar abundance). Their

lower limits are assumed to be 0. Assume the abundances of Ni and S in the mantle can be any value within their respective upper and lower limits, following a uniform distribution (denoted as 'u'):

$$N_{\text{Ni, mantle}} = [0, N_{\text{Ni, bulk}}]_u \tag{C.1}$$
$$N_{\text{S, mantle}} = [0, N_{\text{S, bulk}}]_u \tag{C.2}$$

The abundance of Fe in the phase of FeO (present in the mantle) can then be computed by

$$N_{\text{Fe, mantle}} = N_{\text{O, remain}} - N_{\text{Ni, mantle}} - 3N_{\text{S, mantle}} \tag{C.3}$$

where, $N_{\text{O, remain}}$ is the remaining amount of O atoms after Si, Ca, Na, Mg, and Al have been oxidized.

Then, the corresponding abundances of Fe, Ni and S in the core can be obtained by deducting the abundance of them from the respective abundances of them in the bulk planet. Namely,

$$N_{\text{Ni, core}} = N_{\text{Ni, bulk}} - N_{\text{Ni, mantle}} \tag{C.4}$$
$$N_{\text{S, core}} = N_{\text{Fe, bulk}} - N_{\text{S, mantle}} \tag{C.5}$$
$$N_{\text{Fe, core}} = N_{\text{Fe, bulk}} - N_{\text{Fe, mantle}} \tag{C.6}$$

On the basis, we use the constraint Fe/Ni = 18 $\pm$ 4 in the core (as addressed in Sect. 4.2.3) to verify the series of Fe/Ni ratios as computed from each pair of Ni and S drawn from their respective uniform distributions (here, we draw 10^5 times). Only computations matching with this constraint are deemed as valid estimates.

Then in combination with the atomic masses, these mantle and core abundances (by number) can be converted to the molar masses. The core (molar) mass fraction is the total molar mass in the core divided by the sum of the total molar masses in both the mantle and the core.

The process above is iterated for each combination of planetary elemental abundances, by 2×10^4 Monte Carlo simulations assuming that each element's abundance (within its uncertainty) follows a Gaussian distribution. The results corresponding to the best-fit pattern and the mean of each input elemental abundance are reported as the mean values of the modeling results (i.e. mantle composition, core composition, and core mass fraction) in Tables 4.2 and 4.3. The error bar associated with a mean value are corresponding to the standard deviation of the population of the modeling results for that quantity. The distribution of the modeling results for FeO, NiO, and SO_3 in the mantle and Fe, Ni, and S in the core as well as the core mass fraction may be asymmetric around their corresponding mean values. In this case, the standard deviation of the population of the modeling results for such a quantity is not an accurate but conservative estimate for the uncertainty on the mean value of the quantity. If the standard deviation may cause the lower limit of the quantity to be negative, then the lower limit is set to be zero. As such, the error bars of some quantities in Tables 4.2 and 4.3 are asymmetric.